LASER SPECKLE FROM THIN AND CASCADED DIFFUSERS

by

Lyle Gordon Shirley

Submitted in Partial Fulfillment

of the

Requirements for the Degree

DOCTOR OF PHILOSOPHY

Supervised by Professor Nicholas George

The Institute of Optics

University of Rochester

Rochester, New York

Copyright © 1988

VITAE

Lyle Shirley was born on June 8, 1956 in Rigby, Idaho. He graduated from Ricks college with an Associate degree in Physics in 1978 and from Brigham Young University with a Bachelor of Science degree in Physics in 1980. He spent one year as a graduate student in the Physics Department at Brigham Young University and began a research project in acoustics before coming to the University of Rochester in the fall of 1981. While at the University of Rochester he completed the thesis requirement, and he received a Master of Science degree in Physics from Brigham Young University in 1984. His research at the Institute of Optics was supervised by Professor Nicholas George. He was supported by an Army Research Office Fellowship from 1983 to 1988.

ii

ACKNOWLEDGMENTS

ABSTRACT

The scattering of laser light from a single diffuser and from a cascade of two diffusers is analyzed with particular emphasis on remote sensing. It is shown that diffuser surface properties and the spacing between diffuser planes can be determined remotely. Conceptually, one measures the angular distribution of the radiation pattern or the decorrelation of the far-zone speckle pattern with respect to changes in the wavelength or the angle of incidence of an input plane wave.

Models for the transmission of light through single diffusers are presented that contain a dependence on the angle of illumination. The validity of a simplified transmission function for single diffusers that does not depend on angle is examined, and it is found that the simple transmission function is adequate for treating the individual diffusers in a cascade. This is important, since the simpler transmission function leads to manageable overall expressions for the cascade.

A general expression is derived for the two-state correlation function of far-zone complex amplitude from a cascade of two diffusers, where the two states are the initial and final values of the wavelength, angle of incidence, angle of observation, and spacing. This function is then related to the two-state correlation function of intensity, which is a measure of the correlation between the initial and final speckle patterns. The two-state correlation function of intensity is evaluated for various double diffuser combinations.

The effect of surface height models on the radiation pattern is studied. Of particular interest are strong diffusers that have a normally distributed height profile and whose surface height autocorrelation functions are paraboloidal or conical for small spatial offsets. Excellent agreement is obtained between theoretical radiation patterns calculated with conical and paraboloidal autocorrelation functions and experimental radiation patterns measured from ground-glass and acid-etched diffusers, respectively.

TABLE OF CONTENTS

APPENDIX

LIST OF FIGURES

ix

Chapter 1

Introduction

1.1 Laser Speckle

Laser speckle is a granular pattern of bright and dark regions of intensity that occurs when laser light is scattered from a rough surface or a diffuser. For example, one can observe speckle by placing a piece of ground glass in the path of a laser beam and looking at the scattered light on a screen or a wall. With the advent of the visible line in the helium-neon laser in 1962, speckle became readily observable,[1-3] and many researchers became interested in this phenomenon. However, while the name "speckle" is new, the phenomenon itself is an old subject, e.g., one of the first to study the statistics of speckle was Lord Rayleigh who in 1880 derived the probability density function for the light scattered from a rough surface.[4] Extensive treatments appeared on this topic in the intervening years, as is evident in the following quotation taken from M. von Laue's paper on this subject published in 1914:[5] "The theme of our investigation is an old one; it is treated in many papers and in every optics textbook." Nevertheless, he was the first to describe an experimental observation of speckle, together with an adequate theory.

Early observers of laser speckle recognized that speckle arises from the interference of coherent diffraction patterns from different regions of the scatterer.[1] In other words, the speckle pattern occurs because the nonuniformities in the scatterer introduce phase deviations in the scattered light. Since the light that reaches the observation point is made up of contributions from different regions of the scatterer, there will be either destructive or constructive interference, depending on the sum of the various components at the observation point.

In order to observe speckle, the light must have some degree of temporal coherence, i.e., there must be a correlation between the phase of the optical wave at a

1

given point in space at two different times. The coherence time of the light source is essentially the largest time difference for which this correlation exists. A related quantity, the longitudinal coherence length, is the distance that light travels during its coherence time. There is a tremendous difference between the coherence length of white light and laser light, e.g., it is only about 1 μm for white light, but it is tens of meters or much more for a single-mode argon-ion laser beam. If the various paths that the light takes in traveling from the source to the scatterer and then on to the observation point differ by more than the coherence length, then interference effects are not appreciable, i.e., speckle is not observed. For white light it is difficult to satisfy the path length condition, however, one can observe low contrast polychromatic speckle in the sunlight reflected from the broad curved portion of one's fingernail[6]. One can also observe speckle in a microfilm viewer. For laser light, on the other hand, it is difficult to eliminate laser speckle because of the long coherence length.

Early contributions that are important to the theoretical analysis of speckle in this thesis were the introduction of the notion of a thin phase-changing screen by Booker, Ratcliffe, and Shinn[7] in treating diffraction from the ionosphere and the treatment of scattering from rough surfaces in the book by Beckmann and Spizzichino.[8] Other important contributions were the use of correlation functions and linear systems theory in the early analysis of the statistics of speckle by Goodman[9], Goldfischer,[10] Enloe,[11] Burckhardt,[12] Lowenthal and Arsenault,[13] and Dainty.[14] The first treatment of correlation functions in which space and wavelength dependence occured simultaneously was by George and Jain.[15-17] They also expressed their results in terms of the characteristic function of the density of heights and stressed that in diffraction integrals with phase retardations the characteristic function occurs in a natural way when one calculates higher order moments. Hundreds of papers have been published on the subject of speckle since 1970, and we will not attempt to review them here.

However, good compilations are found in books, conference proceedings, and special issues of journals.[18-26]

1.2 Review of Literature on Speckle from Double Diffusers

In speckle calculations it is usually assumed that light is scattered from a single rough surface or a single diffuser. However, interesting and useful new properties of speckle arise when the light is scattered from two or more objects. A major portion of this thesis, Chapters 3 and 4, is a treatment of the decorrelation of far-zone speckle from a cascade of two diffusers with changes in wavelength, angle of incidence, and spacing. Before introducing this topic in Section 1.3, we will briefly review the literature on scattering from double diffusers.

Several authors have used two diffusers in relative motion to eliminate speckle from rear-projection screens.[27,28] This phenomenon, the decorrelation of the speckle pattern from two parallel diffusers with in-pane displacement, was analyzed by Lowenthal and Joyeux.[29] Experimental measurements of the wavelength dependence of speckle from two ground-glass diffusers, whose spacing varied between 20 and 110 μm, were reported by George and Jain.[30] Interference from two identical diffusers has also been studied.[31]

Speckled speckle, which results from illuminating the second diffuser with the speckle pattern caused by the first diffuser, was studied by Fried[32] who was concerned about laser eye safety and calculated the probability that the intensity of the speckled speckle formed at a point on the retina would exceed safe levels. The statistics of doubly scattered light was studied further by O'Donnell[33] and Barakat.[34,35] Newman[36] experimentally confirmed O'Donnel's result that the intensity of doubly scattered coherent light is K-distributed.

As described above, a topic considered in this thesis is the decorrelation of far-zone speckle from a cascade of two thin diffusers with changes in the angle of

illumination. We have already published preliminary results from this thesis on angular decorrelation.[37]

As an extension of double scattering, multiple diffusers have been used in modeling atmospheric turbulence.[38-41] Another topic related to the scattering of light from double diffusers is the scattering from a regular structure such as a grating that is placed behind a diffuser.[42,43] In another related field, speckle interferometry,[20,24] speckle is used to measure displacement or vibration of a single rough surface.

1.3 Statement of Thesis Problem

The material in this thesis is divided into two major topics. In the first topic, see Fig. 1.1(a), a diffuser D is illuminated with a plane wave of wavelength λ and angle of incidence θ_0, and the radiation pattern in the far zone of the aperture a is determined as a function of the output angle θ. For the radiation pattern from a diffuser, one can consider the finest variations angularly, i.e., the speckle, or alternately the slowly changing envelope of intensity. In this thesis, we will refer to the envelope of intensity as the radiation pattern and to the fine detail as the speckle pattern.

In the second topic, see Fig. 1.1(b), two diffusers, D_1 and D_2, separated by the spacing H, are probed with a plane wave, and the decorrelation of the speckle pattern in the far zone of aperture a is observed as the wavelength λ and the angle of incidence θ_0 of the plane wave are varied. Also included in the second topic is speckle decorrelation with respect to changes in the spacing H between diffusers. We will show that these two topics are very closely related in that one can predict the decorrelation behavior from a cascade of two diffusers given the angular distribution of the radiation patterns from the single diffusers that make up the cascade.

The main questions to be answered in this thesis are: How is the angular distribution of light in the radiation pattern of diffuser D shown in Fig. 1.1(a) related to the surface statistics of the diffuser, what information about the surface statistics of
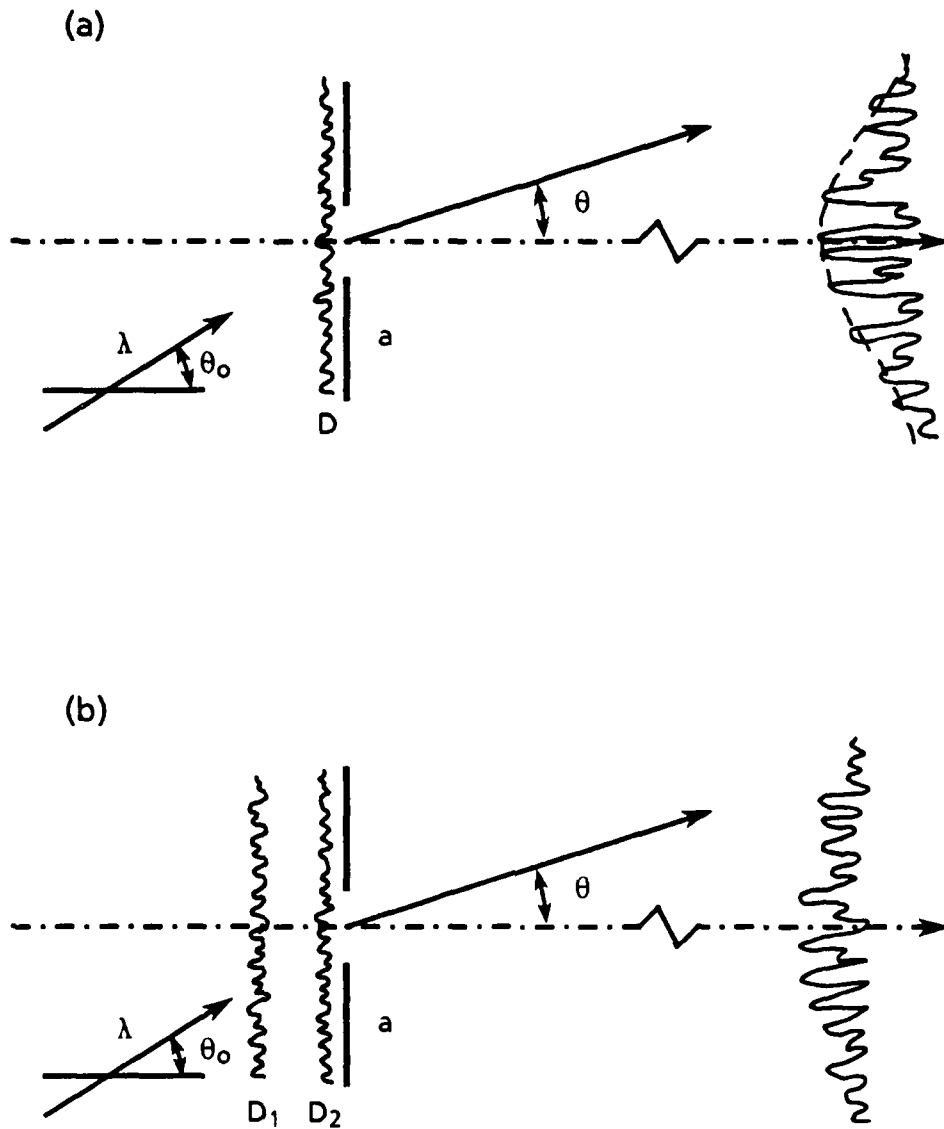
Fig. 1.1. Radiation pattern from a single diffuser (a) and speckle pattern from a cascade of two diffusers (b).

diffusers D_1 and D_2 in Fig. 1.1(b) and about the spacing H between these diffusers or changes ΔH in this spacing can be obtained by observing the speckle pattern, and what types of remote sensing experiments are necessary in order to extract this information?

We use Figs. 1.2 and 1.3 to illustrate what is meant by speckle decorrelation and to motivate its use in determining the structure of cascaded diffusers. In the experimental arrangement depicted in Fig. 1.2(a), an expanded laser beam traveling along the z-axis is incident on a single thin diffuser. A camera is placed on axis in the far zone of the aperture a, and its lens is removed so that the speckle intensity is photographed directly, i.e, the light falls directly onto the film plane. The angle of diffuser illumination is varied by rotating the diffuser about the origin by the angle $\Delta\theta$, and pictures are taken at various values of $\Delta\theta$. In this configuration the laser beam and the camera stay aligned as the diffuser rotates, and the speckle pattern stays centered on the z-axis.

The results of this experiment for a diffuser made by etching glass as described in Section 5.4.2 are shown in Figs. 1.2(b) through 1.2(d) for illumination with an argon-ion laser beam of wavelength 0.5145 μm and for various values of $\Delta\theta$. In Fig. 1.2(b) we see the speckle pattern that results from normally incident illumination of the diffuser, i.e., for $\Delta\theta = 0°$. The wire grid is used as a position reference and marks the z-axis. The other speckle patterns in the series are to be compared with this first pattern. In the second photograph, Fig. 1.2(c), the diffuser has been rotated to $\Delta\theta = 10°$, and there are only minor differences between the two speckle patterns. In the third photograph, Fig. 1.2(d), $\Delta\theta = 20°$; even for this relatively large change in angle, there is still a small degree of correlation between the two patterns. This series of photographs has illustrated the relatively slow decorrelation of the speckle pattern from a single diffuser with changes in the angle of incidence.

We contrast the slow angular decorrelation of speckle in Fig. 1.2 from a single diffuser with the rapid angular decorrelation in Fig. 1.3 from a double diffuser. In the

(a)

(b)　(c)　(d)
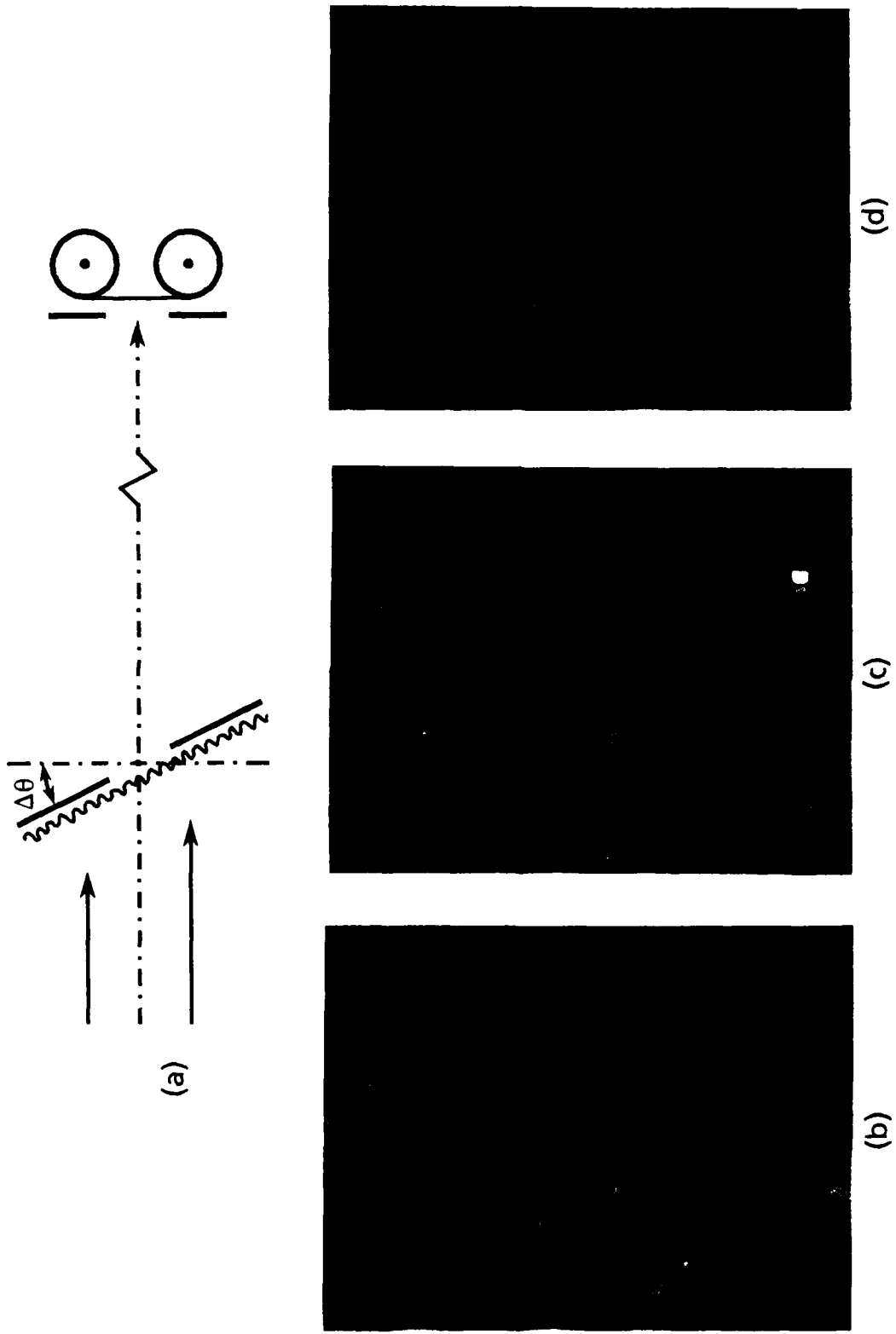
Fig. 1.2　Experimental configuration for photographing the far-zone speckle pattern from a single diffuser as a function of angular rotation $\Delta\theta$ (a) and the resulting speckle patterns for values of $\Delta\theta$ of 0° (b), 10° (c), and 20° (d).
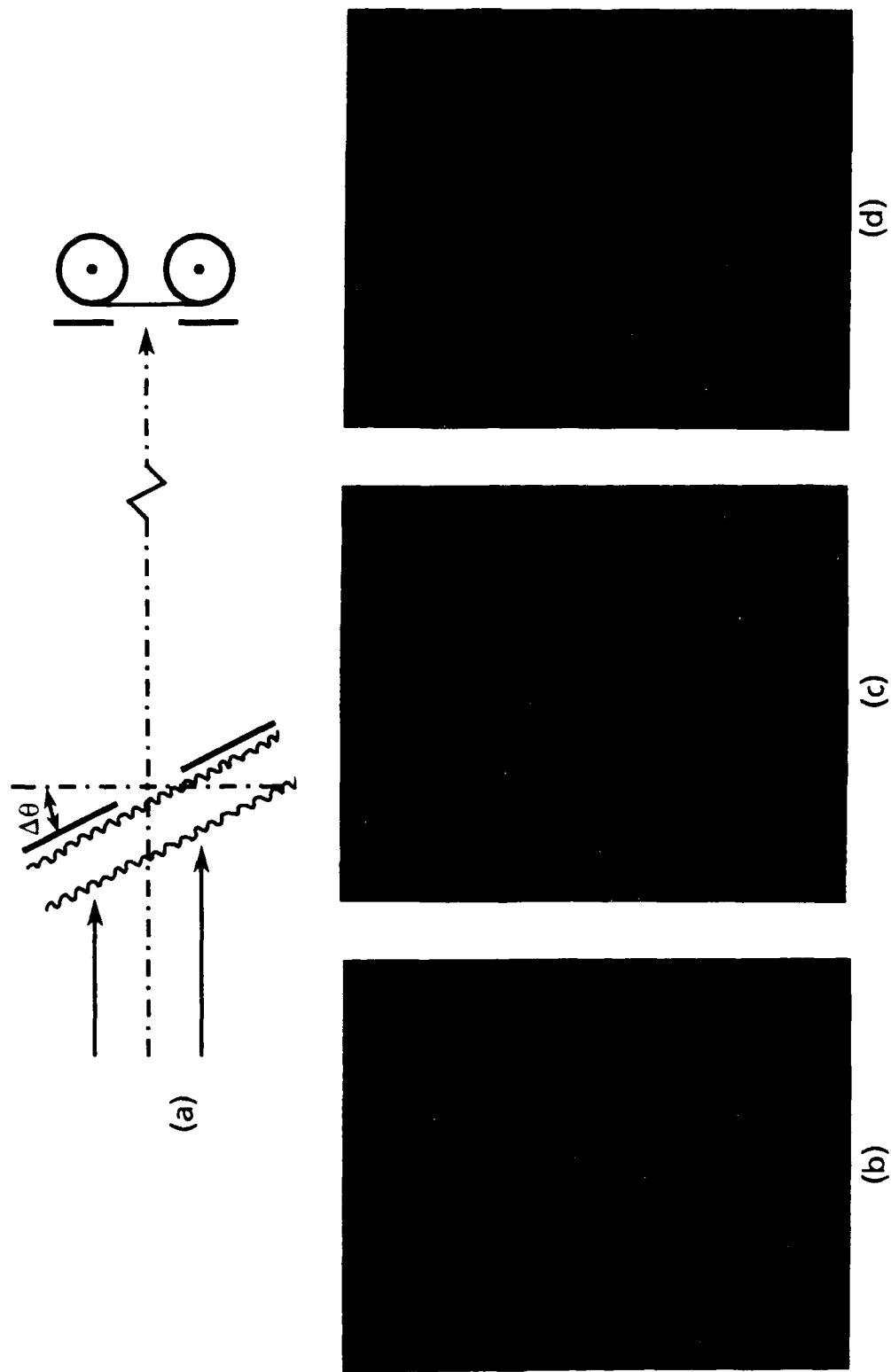
Fig 1.3. Experimental configuration for photographing the far-zone speckle pattern from a double diffuser as a function of angular rotation $\Delta\theta$ (a) and the resulting speckle patterns for values of $\Delta\theta$ of 0 (b), 2 (c), and 5 (d) minutes of arc.

experiment depicted in Fig. 1.3(a), the single diffuser is replaced by a cascade of two diffusers. In the actual experiment the cascade is made by etching both sides of an approximately 10 mm thick piece of glass. There is an inconsequential change of wavelength to the 0.4880 µm line of the argon ion laser, and a different wire grid is used. In the series of photographs in Figs. 1.3(b) through 1.3(d), $\Delta\theta$ is equal to 0, 2, and 5 minutes of arc, respectively. We see that angular decorrelation for the double diffuser occurs much more rapidly, i.e., for angular changes of arc minutes rather than degrees. This demonstrates that the magnitude of $\Delta\theta$ necessary for decorrelation decreases as diffuser thickness effects become more important, and it motivates the analysis of speckle decorrelation as a means for determining diffuser structure remotely.

1.4 Overview of Thesis

Having introduced the topics considered in this thesis, we now give an overview of the contents of the individual chapters. In Chapter 2 we consider the validity of the simple transmission function approach for analyzing the propagation of light through diffusers. A simple transmission function is a two-dimensional position-dependent function, from which the complex amplitude at the output plane is obtained by performing a point-by-point multiplication with the complex amplitude at the input plane. In Chapter 2, which is based on an earlier publication,[44] we are concerned about the validity of this transmission function because it can not account for diffuser thickness effects.

For the purpose of comparison, we introduce a generalized transmission function that does account for thickness effects through its additional dependence on the angle of incidence, and we derive approximate expressions for the generalized transmission function of rough surface and bulk diffusers. In the generalized transmission function formalism, an angular spectrum representation of the input illumination is used for non-plane-wave illumination.

Through the photographs of far-zone speckle patterns in Figs. 1.2 and 1.3, the computer simulations of speckle patterns in Chapter 2, and the analytical calculations of the decorrelation of speckle form thin diffusers in Appendix B, we show that the angular dependence of the generalized transmission function is not important compared to spacing effects for typical thin diffusers and for reasonable input angles. The simulations and calculations also predict the slow angular decorrelation of speckle from single diffusers that was illustrated in Fig. 1.2. From the above results we conclude that the simple transmission function is adequate for treating the individual diffusers in the cascade. This is important because it makes the resulting expressions for the cascade manageable.

In Chapter 3 we analyze the decorrelation of speckle from double diffusers with respect to changes in wavelength, angle of incidence, angle of observation, and spacing. In so doing we derive a general expression for the two-state correlation function u_{ab} of the far-zone complex amplitude v. The subscripts a and b represent the initial and final states of the parameters listed above that can be varied during an experiment. We also show how u_{ab} is related to the two-state correlation function $<I_a I_b>$ of far-zone intensity, which is a measure of the correlation between the initial and final speckle patterns.

The analysis in Chapter 3 applies to general diffusers; however, strong diffusers are emphasized in the applications in Chapters 4 and 5. A strong diffuser is one that introduces an rms phase delay that is large compared to one radian. Two specific types of strong diffusers are defined in Chapter 3; they are designated as paraboloidal, P, and conical, C, according to whether the autocorrelation function of the surface profile is shaped like a paraboloid or a cone for small spatial offsets. For paraboloidal diffusers, the slope parameter σ_h/w, where σ_h is the rms surface roughness and w is the lateral correlation length, determines the angular spread of the radiation pattern. For conical diffusers, the corresponding parameter is σ_h^2/w.

In Chapter 4 we apply the analysis of speckle decorrelation to the remote sensing of a *P-P* diffuser cascade. In an effort to make Chapter 4 self-contained, the pertinent results from Chapter 3 are reviewed in Section 4.2. This allows the person who wants to read about the remote sensing application first to go directly to Chapter 4. The advantage of analyzing the *P-P* diffuser cascade first is that the two-state correlation function of intensity can be calculated in closed form for arbitrary values of the state variables. The resulting solution is useful in categorizing the different speckle decorrelation phenomenon and in learning how to configure remote sensing experiments.

The corresponding analysis is presented for the *P-C* and *C-P* diffuser combinations in Appendix E and for the *C-C* diffuser cascade in Appendix F. It is shown that one can determine the values of the appropriate diffuser parameter σ_h/w or σ_h^2/w for each diffuser in the cascade, together with the spacing, by performing simple remote sensing experiments. These experiments involve measurement of the decorrelation of the speckle pattern with changes of wavelength and spacing and measurement of the angular distribution of the radiation pattern.

In Chapter 5 we compare theoretical radiation patterns with measured radiation patterns from ground-glass and acid-etched diffusers. As described above, by radiation pattern we mean the envelope of intensity, not the detail of the speckle pattern. In the theoretical analysis, the smoothing is accomplished by averaging the speckle patterns from an ensemble of diffusers having the same statistical properties, i.e., from diffusers representing different realizations of the same random process. In the laboratory, this smoothing can be accomplished with a single diffuser by spatial averaging of the speckle pattern, i.e., by using a detector whose active area is large compared to the speckle size yet small enough not to significantly affect the angular resolution of the measurement.

The ensemble average and the spatial average are very nearly equivalent, especially under the following two conditions: If the area of the diffuser being

illuminated is large compared to the wavelength of light, then the angular extent of the individual speckles will be small, and the detector will integrate over a large number of speckles. This will reduce the local variations in intensity measured by the detector. If in addition, the area of the diffuser being illuminated is large compared to the lateral scale of roughness, i.e., to the diffuser correlation length, then the light reaching an observation point in the far-zone will have come from many uncorrelated regions of the diffuser. Thus a large region of the diffuser will be sampled and this will tend to average out the effect of sample variations. In effect this is like performing an ensemble average because the number of uncorrelated contributions to the total output is increased.

Measured radiation patterns over a dynamic range of 6 to 8 orders of magnitude are presented in Chapter 5 for ground-glass and etched-glass diffusers. For ground glass, excellent agreement is obtained using an autocorrelation function that is conical for small spatial offsets; this is consistent with our physical expectation based on the need for a rapid fall-off in surface correlation due to the jagged nature of the surface relief. For etched glass, excellent agreement is obtained by assuming two scales of roughness. The upper two or three orders of magnitude of the radiation pattern is dominated by a large roughness paraboloidal component, and the scattering at wide angles is predicted by a small roughness component having a decaying exponential autocorrelation function. By varying the etching time, values of σ_h/w for the paraboloidal component between 0.02 and 0.1 are obtained. There is excellent agreement between these values as measured by light scattering and by a stylus profilometer. Preliminary results having to do with Chapter 5 have been reported in the literature.[45,46] Except for minor revisions, and the addition of the material where the effect of etch time on σ_h/w is studied, the text of Chapter 5 is identical to that in a recent publication.[47]

Chapter 1 References

1. J. D. Rigden and E. I. Gordon, "The granularity of scattered optical maser light," Proc. IRE **50**, 2367-2368 (1962).

2. B. M. Oliver, "Sparkling spots and random diffraction," Proc. IEEE **5**, 220-221 (1963).

3. R. V. Langmuir, "Scattering of Laser light," Appl. Phys. Lett. **2**, 29-30 (1963).

4. Lord Rayleigh, "On the resultant of a large number of vibrations of the same pitch and of arbitrary phase," Phil. Mag. **10**, 73-78 (1880).

5. M. von Laue, Sitzungsber. K. Preuss. Akad. Wiss. **47**,1144 (1914).

6. N. George and D. C. Sinclair, "Editorial---Topical issue on laser speckle" J. Opt. Soc. AM. **66**, 1316 (1976).

7. H. G. Booker, J. A. Ratcliffe, and D. H. Shinn, "Diffraction from an irregular screen with applications to ionospheric problems," Philos. Trans. R. Soc. London Ser. A **242**, 579-607 (1950).

8. P. Beckmann and A. Spizzichino, *The Scattering of Electromagnetic Waves from Rough Surfaces* (Pergamon Press, New York, 1962).

9. J. W. Goodman, "Statistical properties of Laser sparkle patterns," Stanford Electronics Laboratories TR2303-1 (SEL-63-140) (1963).

10. L. I. Goldfischer, "Autocorrelation function and power spectral density of laser-produced speckle patterns," J. Opt. Soc. Am. **55**, 247-253 (1965).

11. L. H. Enloe, "Noise-like structure in the image of diffusely reflecting objects in coherent illumination,"Bell System Tech. J. **46**, 1479-1489 (1967).

12. C. B. Burckhardt, "Laser speckle pattern---A narrowband noise model," Bell System Tech. J. **49**, 309-316 (1970).

13. S. Lowenthal and H. Arsenault, "Image formation for coherent diffuse objects: Statistical properties," J. Opt. Soc. Am. **60**, 1478-1483 (1970).

14. J. C. Dainty, "Some statistical properties of random speckle patterns in coherent and partially coherent illumination," Optica Acta 17, 761-772 (1970).

15. N. George and A. Jain, "Speckle reduction using multiple tones of illumination," Appl. Opt. 12, 1202-1212 (1973).

16. N. George and A. Jain, "Space and wavelength dependence of speckle intensity," Appl. Phys. 4, 201-212 (1974).

17. N. George, A. Jain, and R. D. S. Melville, Jr., "Experiments on the space and wavelength dependence of speckle," Appl. Phys. 7, 157-169 (1975).

18. J. C. Dainty, ed., *Laser Speckle and Related Phenomenon* (Springer-Verlag, Berlin, 1975).

19. Special Issue on Speckle, Opt. Soc. Am. 66, No. 11, (1976).

20. A. E. Ennos, "Speckle Interferometry," in *Progress in Optics XVI*, 235-288, E. Wolf, ed. (North-Holland, Amsterdam, 1978).

21. M. Francon, *Laser Speckle and Applications in Optics* (Academic Press, New York, 1979).

22. R. K. Erf, ed., *Speckle Metrology* (Academic Press, New York, 1979).

23. W. H. Carter, ed., *Applications of Speckle Phenomena*, Proc. SPIE 243 (1980).

24. R. Jones and C. Wykes, *Holographic and Speckle Interferometry* (Cambridge University Press, Cambridge, 1983).

25. H. H. Arsenault, ed., *International Conference on Speckle*, Proc. SPIE 556 (1985).

26. Special Issues on Speckle, Opt. Eng. 25, Nos. 5,6 (1986).

27. I. Liefer, C. J. D. Spencer, and W. T. Welford, "Grainless screens for projection microscopy," J. Opt. Soc. Am. 51, 1422-1423 (1961).

28. E. G. Rawson, A. B. Nafarrate, and R. E. Norton, "Speckle-free rear-projection screen using two close screens in slow relative motion," J. Opt. Soc. Am. 66, 1290-1294 (1976).

29. S. Lowenthal and D. Joyeux, "Speckle removal by a slowly moving diffuser associated with a motionless diffuser," J. Opt. Soc. Am. 61, 847-851 (1971).

30. N. George and A. Jain, "Speckle from a cascade of two diffusers," Opt. Commun. 15, 71-75 (1975).

31. N. Barakat, T. El Dessouki, M. El Nicklawy, and M. Abdel Sadek, "Interference from two identical diffusers," Acta Phys. Acad. Scientiarum Hungaricae 51, 341-347 (1981).

32. D. L. Fried, "Laser eye safety: the implications of ordinary speckle statistics and of speckled-speckle statistics," J. Opt. Soc. Am. 71, 914-916 (1981).

33. K. A. O'Donnell, "Speckle statistics of doubly scattered light," J. Opt. Soc. Am. 72, 1459-1463 (1982).

34. R. Barakat, "The brightness distribution of the product of two partially correlated speckle patterns," Opt. Commun. 52, 1-4 (1984).

35. R. Barakat and R. J. Salawitch, "Second- and fourth-order statistics of double scattered speckle," Opt. Acta 33, 79-89 (1986).

36. D. Newman, "K distributions from doubly scattered light," J. Opt. Soc. Am. A 2, 22-26 (1985).

37. L. G. Shirley and N. George, "Speckle from a thick diffuser," J. Opt. Soc. Am. A 3, P121 (1986).

38. H. P. Baltes, H. A. Ferwerda, A. S. Glass, and B. Steinle, "Retrieval of structural information from far-zone intensity and coherence of scattered radiation," Opt. Acta 28, 11-28 (1981).

39. J. C. Dainty and D. Newman, "Detection of gratings hidden by diffusers using photon-correlation techniques," Opt. Lett. 8, 608-610 (1983).

40. R. W. Lee and J. C. Harp, "Weak scattering in random media, with applications to remote probing," Proc. IEEE 57, 375-406 (1969).

41. F. Roddier, "The effects of atmospheric turbulence in optical astronomy," in *Progress in Optics XIX*, E. Wolf, ed. (North-Holland, Amsterdam, 1981), pp.281-376.

42. F. Roddier, J. M. Gilli, and J. Vernin, " On the isoplanatic patch size in stellar speckle interferometry," J. Optics. **13**, 63-70 (1982).

43. F. Roddier, J. M. Gilli, and G. Lund, "On the origin of speckle boiling and its effects in stellar speckle interferometry," J. Optics **13**, 263-271 (1982).

44. L. G. Shirley and N. George, "Wide-angle diffuser transmission functions and far-zone speckle," J. Opt. Soc. Am. A **4**, 734-745 (1987).

45. L. G. Shirley and N. George, "Diffuser transmission functions and far-zone speckle patterns," in *International Conference on Speckle*, H. H. Arsenault, ed., Proc. Soc. Photo-Opt. Instrum. Eng. **556**, 63-69 (1985).

46. L. G. Shirley and N. George, "Diffuser radiation patterns over a large dynamic range," J. Opt. Soc. Am. A **5**, P64 (1988).

47. L. G. Shirley and N. George, "Diffuser radiation patterns over a large dynamic range. Part I: Strong diffusers," Appl. Opt. **27**, 1850-1861 (1988).

Chapter 2

Diffuser Transmission Functions

2.1 Introduction

In many speckle calculations the diffuser is modeled as a thin phase-changing screen that introduces a position-dependent phase delay on the incident wave.[1-8] Hence the complex amplitude $v_2(\mathbf{r})$ at the output plane of the diffuser, see Fig. 2.1, can be calculated from the input complex amplitude $v_1(\mathbf{r})$ by using the simple relationship

$$v_2(\mathbf{r}) = v_1(\mathbf{r})\, t(\mathbf{r};k). \tag{2.1}$$

Here the transmission function $t(\mathbf{r};k)$ is given by

$$t(\mathbf{r};k) = \exp\left[-i\phi(\mathbf{r};k)\right], \tag{2.2}$$

and the phase retardation is denoted by $\phi(\mathbf{r};k)$. The vector $\mathbf{r}$ represents position in the diffuser plane, and the wave number k is related to the free space wavelength λ by $k = 2\pi/\lambda$. The k dependence is shown explicitly in the transmission function because the phase delay $\phi(\mathbf{r};k)$ is a function of wavelength.

One should be concerned about the range of validity of Eqs. (2.1) and (2.2) when using them to calculate diffuser radiation patterns for large angles of incidence or to analyze speckle from cascaded diffusers. Owing to thickness effects, a transmission function must have angular dependence in order to be valid over a wide range of input angles. However, since Eq. (2.1) implies a simple point-by-point multiplication, there is obviously no angular dependence in this transmission-function formalism.

In this chapter we consider the limitations imposed by Eqs. (2.1) and (2.2), and we generalize the transmission function of Eq. (2.2) to include not only dependence on the wave number k but also dependence on the direction $\mathbf{s}_0$ of the incident illumination. The unit vector $\mathbf{s}_0$ is related to the spherical-polar coordinates (θ_0, ϕ_0) and the cartesian unit vectors $\mathbf{x}$, $\mathbf{y}$, and $\mathbf{z}$ by
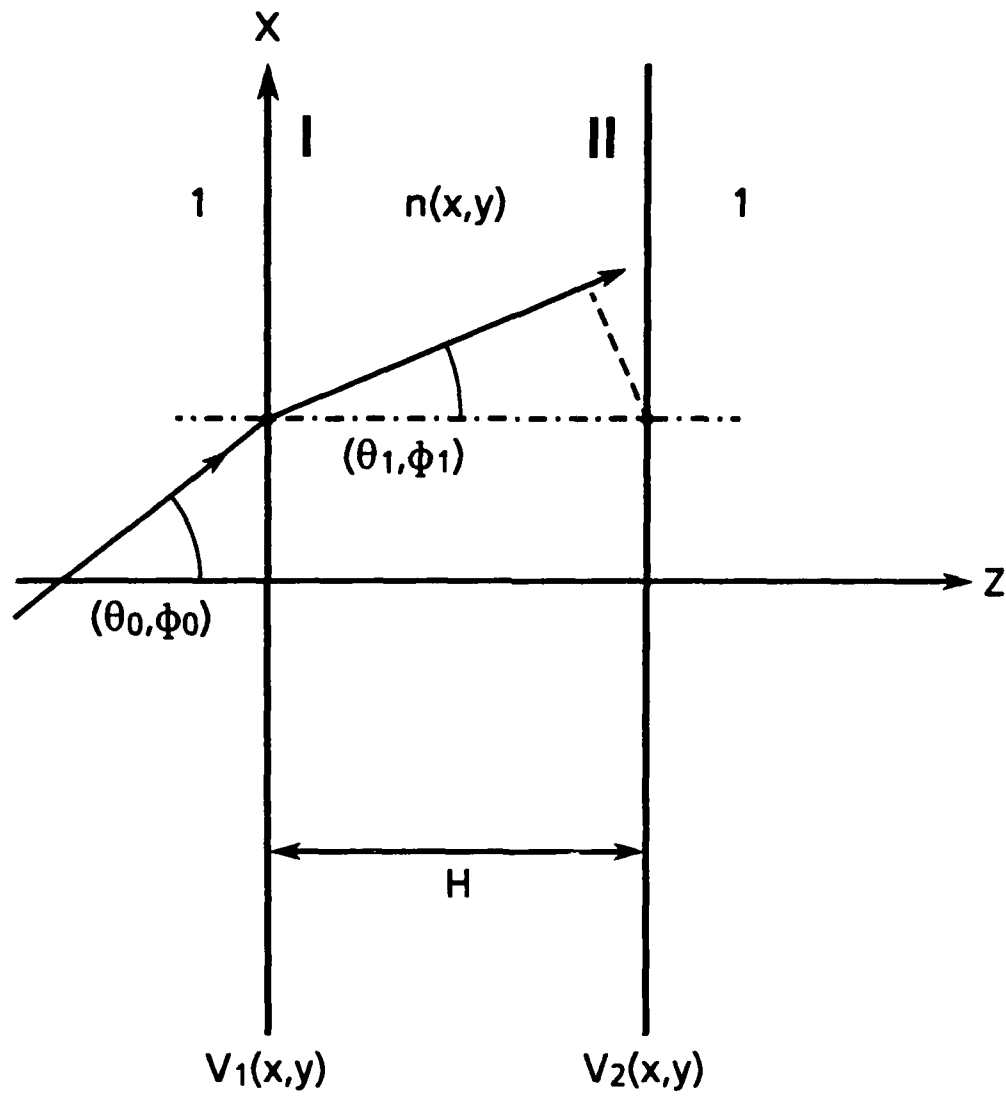
Fig. 2.1   Input and output planes for a bulk diffuser consisting of a planar slab of
thickness H with index of refraction inhomogeneous $n(r)$.

$$\mathbf{s}_0 = \mathbf{x} \sin\theta_0 \cos\phi_0 + \mathbf{y} \sin\theta_0 \sin\phi_0 + \mathbf{z} \cos\theta_0 , \qquad (2.3)$$

as illustrated in Fig. 2.2. We define the new transmission function $t(\mathbf{r};\mathbf{k}_0)$ to be valid for an input plane wave with wave vector $\mathbf{k}_0 = k\mathbf{s}_0$. We will refer to $t(\mathbf{r};\mathbf{k}_0)$ as the plane-wave transmission function for $\mathbf{k}_0$. Using this notation one can write the output $v_2(\mathbf{r};\mathbf{k}_0)$ corresponding to a unit-amplitude plane wave having wave vector $\mathbf{k}_0$ in the form

$$v_2(\mathbf{r}; \mathbf{k}_0) = \exp\left(-i\,\mathbf{k}_{0\perp} \bullet \mathbf{r}\right) t(\mathbf{r}; \mathbf{k}_0) . \qquad (2.4)$$

The meaning of the subscript $\perp$ in Eq. (2.4) is that only the transverse components, i.e., the k_x and the k_y components of the vector $\mathbf{k}_0$ are retained.

Equation (2.4) can be used directly when the input to the diffuser is a plane wave. The generalization to arbitrary illumination is presented in Section 2.2, where we represent the input $v_1(\mathbf{r})$ in terms of an angular spectrum of plane waves. Although we are mainly concerned with diffuser transmission functions in this thesis, the concept of an angle-dependent transmission function can be used to describe any linear optical system. The relationship between the plane-wave transmission function and the impulse response representations of an optical system is also given in Section 2.2.

In Section 2.3 we obtain plane-wave transmission functions for a bulk diffuser having plane parallel surfaces and a varying index of refraction $n(\mathbf{r})$ and for a rough-surface diffuser having a constant index of refraction with height profile $h(\mathbf{r})$. There is an extensive literature for scattering from rough surfaces and for propagation through random media,[9-14] and these problems can be treated at varying levels of complexity. However, we seek simple models that account for the most basic angle-dependence effects and that are convenient for use in statistical calculations. Hence we make the simplifying assumption of local plane-wave behavior within the diffuser; We also ignore reflections, multiple scattering, shadowing, and Fresnel losses.

20
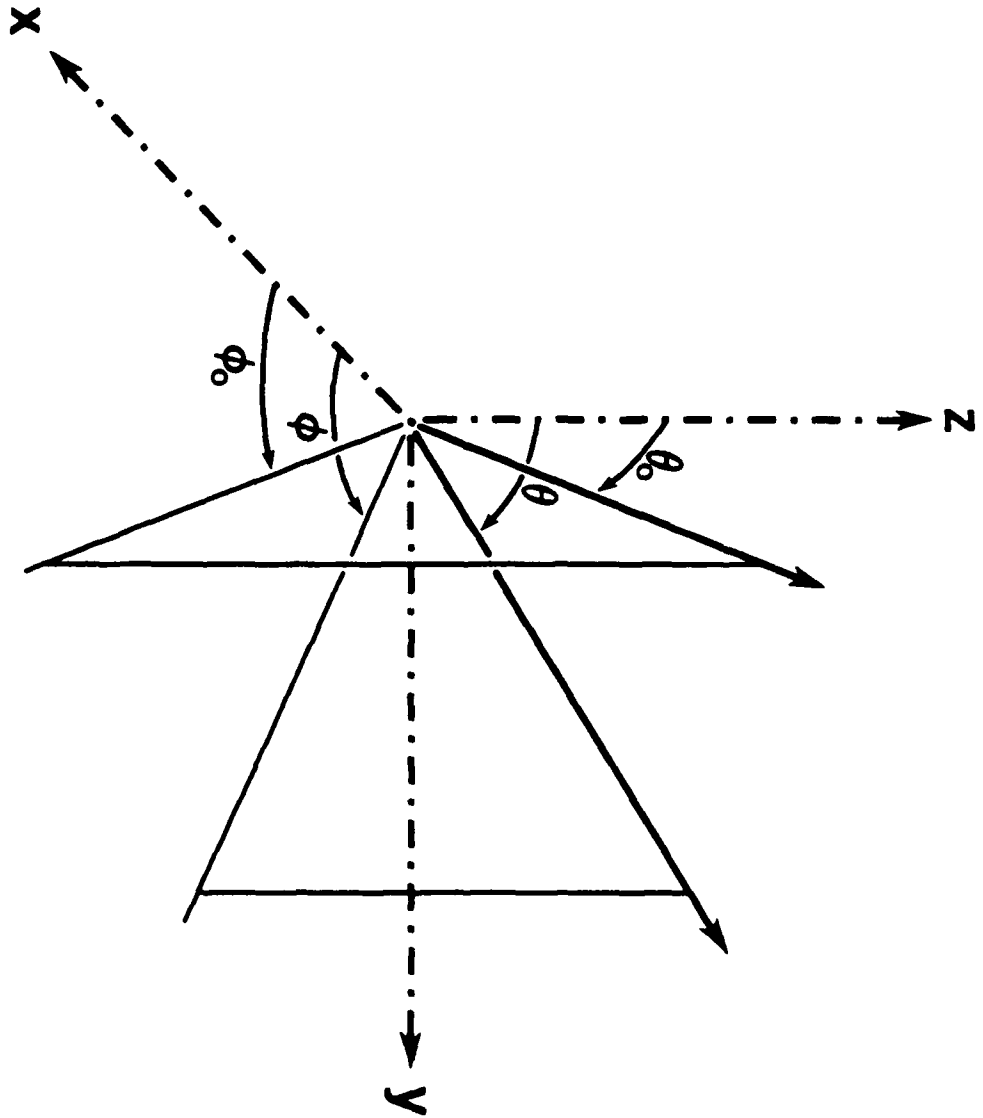
Fig. 2.2.   Coordinate system with input angles (θ_0, ϕ_0) and observation angles (θ, ϕ).   The output diffuser is located in the x-y plane of the coordinate system.

Section 2.4 contains computer simulations that illustrate how the far-zone speckle patterns, as calculated by the paraxial transmission function of Eq. (2.2) and the wide-angle transmission function of Eq. (2.4), become increasingly different as the angle of incidence increases. We use these curves as indicators of when it is important to include angle dependence in the diffuser transmission function. In particular, we are interested in the change in input angle necessary to "decorrelate" the speckle pattern. From the computer simulations in Section 2.4.2, we will see that this angle is typically quite large, i.e., greater than 15°.

The justification for using the simple transmission function model of Eqs. (2.1) and (2.2) in the analysis of cascaded diffusers in Chapter 3 is that angular decorrelation is usually dominated by the spacing effect, not by the diffuser thickness effect. Decorrelation due to the spacing effect typically occurs for an angular change of arc minutes The angular dependence present in the ensemble averaged diffuser radiation pattern is of lesser importance in our application. The major effect, which is an increase in the diffuser roughness, and hence a spread in the radiation pattern, is discussed in the literature.[15,16]

2.2 General Illumination

The transmission function for a general diffuser must contain an angle dependence. Given the angle-dependent transmission function $t(r;k)$ for an arbitrary diffuser or optical system, we can treat non-plane-wave illumination by applying the angular-spectrum formalism.

The procedure for treating general illumination is as follows: First, the input scalar amplitude $v_1(r)$ is decomposed into an angular spectrum of plane waves by taking its 2-D Fourier transform,[17]

$$V_1(k_\perp) = \int v_1(r) \exp\left(i k_\perp \bullet r\right) d^2 r. \qquad (2.5)$$

The individual plane waves are then multiplied by the appropriate transmission function $t(\mathbf{r};\mathbf{k})$, and finally, the output that arises from each plane wave is added. Following this approach, we obtain $dv_2(\mathbf{r})$ the element of the total output that corresponds to the plane wave with wave vector $\mathbf{k}$,

$$dv_2(\mathbf{r}) = \frac{1}{(2\pi)^2} V_1(\mathbf{k}_\perp) \exp\left(-i\,\mathbf{k}_\perp \bullet \mathbf{r}\right) t(\mathbf{r};\mathbf{k})\, d^2\mathbf{k}_\perp, \tag{2.6}$$

where $d^2\mathbf{k}_\perp = dk_x dk_y$. The total output is then obtained by integrating Eq. (2.6) over the entire $k_x k_y$ plane

$$v_2(\mathbf{r}) = \frac{1}{(2\pi)^2} \int V_1(\mathbf{k}_\perp)\, t(\mathbf{r};\mathbf{k}) \exp\left(-i\,\mathbf{k}_\perp \bullet \mathbf{r}\right) d^2\mathbf{k}_\perp. \tag{2.7}$$

Equation (2.7) can be recast into the usual linear systems formalism as follows:

$$v_2(\mathbf{r}) = \int v_1(\mathbf{r}')g(\mathbf{r};\mathbf{r}')\, d^2\mathbf{r}', \tag{2.8}$$

where the impulse response $g(\mathbf{r};\mathbf{r}')$ is

$$g(\mathbf{r};\mathbf{r}') = \frac{1}{(2\pi)^2} \int t(\mathbf{r};\mathbf{k}) \exp\left[-i k_\perp \bullet \left(\mathbf{r} - \mathbf{r}'\right)\right] d^2\mathbf{k}_\perp. \tag{2.9}$$

The transmission function can be obtained in terms of the impulse response by inverting Eq. (2.9):

$$t(\mathbf{r};\mathbf{k}) = \exp\left(i\,\mathbf{k}_\perp \bullet \mathbf{r}\right) \int g(\mathbf{r};\mathbf{r}') \exp\left(-i\,\mathbf{k}_\perp \bullet \mathbf{r}'\right) d^2\mathbf{r}'. \tag{2.10}$$

Thus we see that the plane-wave transmission function $t(\mathbf{r};\mathbf{k})$ and the impulse response $g(\mathbf{r};\mathbf{r}')$ provide two alternative ways of representing the propagation of light through a linear optical system.

2.3 Angle Dependent Diffuser Models

We now derive approximate plane-wave transmission functions for two common types of diffusers: a bulk diffuser with varying index of refraction between plane parallel surfaces and a rough surface diffuser with a constant index of refraction.

2.3.1 Bulk Diffuser

We first consider a diffuser that consists of a planar slab with index-of-refraction inhomogeneities characterized by $n(\mathbf{r})$ as in Fig. 2.1. We wish to determine the complex amplitude $v_2(\mathbf{r})$ at plane II that arises from the input plane wave

$$v_1(\mathbf{r}) = \exp\left(-i\,\mathbf{k}_{0\perp}\bullet\mathbf{r}\right) \tag{2.11}$$

at plane I. If local plane-wave behavior within the medium is assumed, then at the point $\mathbf{r}$ at the input plane of the diffuser, the wave is refracted from its input angles (θ_0, ϕ_0) to the new angles (θ_1, ϕ_1) given by Snell's law:

$$n\,\sin\theta_1 = \sin\theta_0 \tag{2.12}$$

and

$$\phi_1 = \phi_0. \tag{2.13}$$

Hence the complex amplitude at $z = H$ resulting from the refracted wave is

$$v_2(\mathbf{r}) = \exp\left[-i\,k n(\mathbf{r})\sin\theta_1\left(x\cos\phi_1 + y\sin\phi_1\right)\right]\exp\left(-i\,k n(\mathbf{r})\,H\,\cos\theta_1\right), \tag{2.14}$$

where k is the free-space wave number. If reflections at the interfaces are ignored, then Eq. (2.14) gives the desired output scalar amplitude. We note that in terms of our vector notation, Snell's Law can be written as

$$n\,\mathbf{k}_{1\perp} = \mathbf{k}_{0\perp} \tag{2.15}$$

and Eq. (2.14) can be written as

$$v_2(\mathbf{r}) = \exp\left(-i\,n(\mathbf{r})\,\mathbf{k}_{1\perp}\bullet\mathbf{r}\right)\exp\left(-i\,n(\mathbf{r})\,k_{1z}H\right). \tag{2.16}$$

If Eq. (2.15) is applied to the first exponential in Eq. (2.16), then this factor can be identified as the input plane wave, and the second exponential must be the plane-wave transmission function:

$$t(\mathbf{r};\mathbf{k}_0) = \exp\left(-i\,k n(\mathbf{r})\,H\,\cos\theta_1\right) = \exp\left(-i\,n(\mathbf{r})\,k_{1z}H\right). \tag{2.17}$$

We can use the expression

$$n(\mathbf{r})\, k_{1z} = \sqrt{n^2(\mathbf{r})k^2 - |\mathbf{k}_{o\perp}|^2} \qquad (2.18)$$

to determine k_{1z} in Eq. (2.17). Note that the transmission function in Eq. (2.17) is simply the factor for propagation of the $\mathbf{k}_{o\perp}$ component of the angular spectrum a distance H along the z axis in a medium of index of refraction n.

When the angle dependence in Eq. (2.17) is ignored, i.e., when θ_1 is set equal to zero, we obtain the paraxial transmission function that we set out to improve. The importance of the angle dependence in a given situation is related to the phase difference $\Delta\phi$ between these two cases:

$$\Delta\Phi = kn H \left(1 - \cos\theta_1\right). \qquad (2.19)$$

Thus, for example, a phase error smaller than 0.1 rad can be achieved by requiring that $H/\lambda < 10.0$ and $\theta_1 < 3.2°$ or that $H/\lambda < 1.0$ and $\theta_1 < 10.2°$. However, as we now show, a large portion of the phase delay in the wide-angle transmission function is an angle-of-incidence-dependent bias term. For illumination with a single plane wave, this constant phase delay does not affect the speckle intensity, and the conditions on H and θ_1 may be relaxed. This point will be further illustrated by a computer simulation in Section 2.4.

If the index modulation $n(\mathbf{r})$ is written as the sum of the average index $<n>$ and the deviation from the mean $\Delta n(\mathbf{r})$,

$$n(\mathbf{r}) = <n> + \Delta n(\mathbf{r}), \qquad (2.20)$$

and if the condition

$$\Delta n(\mathbf{r}) << \frac{1}{2} <n> \cos^2\theta_{<n>} \qquad (2.21)$$

is satisfied, where $\theta_{<n>}$ is the propagation angle within the medium for $\Delta n = 0$,

$$<n> \cos\theta_{<n>} = \sqrt{<n>^2 - \sin^2\theta_o}, \qquad (2.22)$$

then it can be shown by factoring out the quantity $<n>k \cos\theta_{<n>}$ in the exponent of Eq. (2.17), expanding the remaining terms in a binomial series, and keeping only the first two terms, that Eq. (2.17) takes the form

$$t(\mathbf{r};\mathbf{k}_0) = \exp\left(-ik<n>H\cos\theta_{<n>}\right)\exp\left(-ik\Delta n(\mathbf{r})H/\cos\theta_{<n>}\right). \qquad (2.23)$$

This second form, Eq. (2.23), is convenient for statistical calculations since the $\mathbf{r}$ dependence has been removed from the radical and is completely contained in the second exponential. It also shows that the phase delay is largely due to the angle-of-incidence-dependent bias term for reasonable values of $\theta_{<n>}$ and Δn.

When using Eq. (2.23) it is important to consider the size of the phase difference $\Delta\Phi$ between the transmission functions of Eq. (2.17) and Eq. (2.23):

$$\Delta\Phi = kH\left[<n>\cos\theta_{<n>} - \left(<n>+\Delta n\right)\cos\theta_1 + \Delta n/\cos\theta_{<n>}\right]. \qquad (2.24)$$

In Fig. 2.3 the quantity $\Delta\Phi\lambda/(<n>H)$, is plotted on a logarithmic scale against the angle θ_1 within the medium. Figure 2.3(a) is for negative values of $\Delta n/<n>$ and Fig. 2.3(b) is for positive values. By reading the phase error for a given value of $\Delta n/<n>$ and multiplying by the thickness in terms of wavelength H/λ, the total phase error can be determined. Thus these curves are useful for deciding if Eq. (2.23) is a good approximation to Eq. (2.17) for a given situation. Note that the phase error is plotted against the internal angle θ_1 rather than the angle of incidence θ_0. Since it is assumed that the index of refraction surrounding the diffuser is unity, the internal angle will be smaller than the angle of incidence. The dashed lines indicate the maximum value that θ_1 can take for a given value of $<n>$.

2.3.2 Rough Surface Diffuser

We now consider the diffuser model of Fig. 2.4, which consists of a dielectric medium of index of refraction n bounded on the input side by a plane and on the output side by a rough surface $h(\mathbf{r})$. The mean thickness of the diffuser is denoted by H so that the expected value $<h(\mathbf{r})>$ is zero. We assume local-plane-wave behavior and ignore reflections at the surfaces in calculating the transmission function. The phase delay that results from a plane wave propagating at angle θ_1 but calculated along the dashed line between the plane surface and the rough surface at position $\mathbf{r}$ is
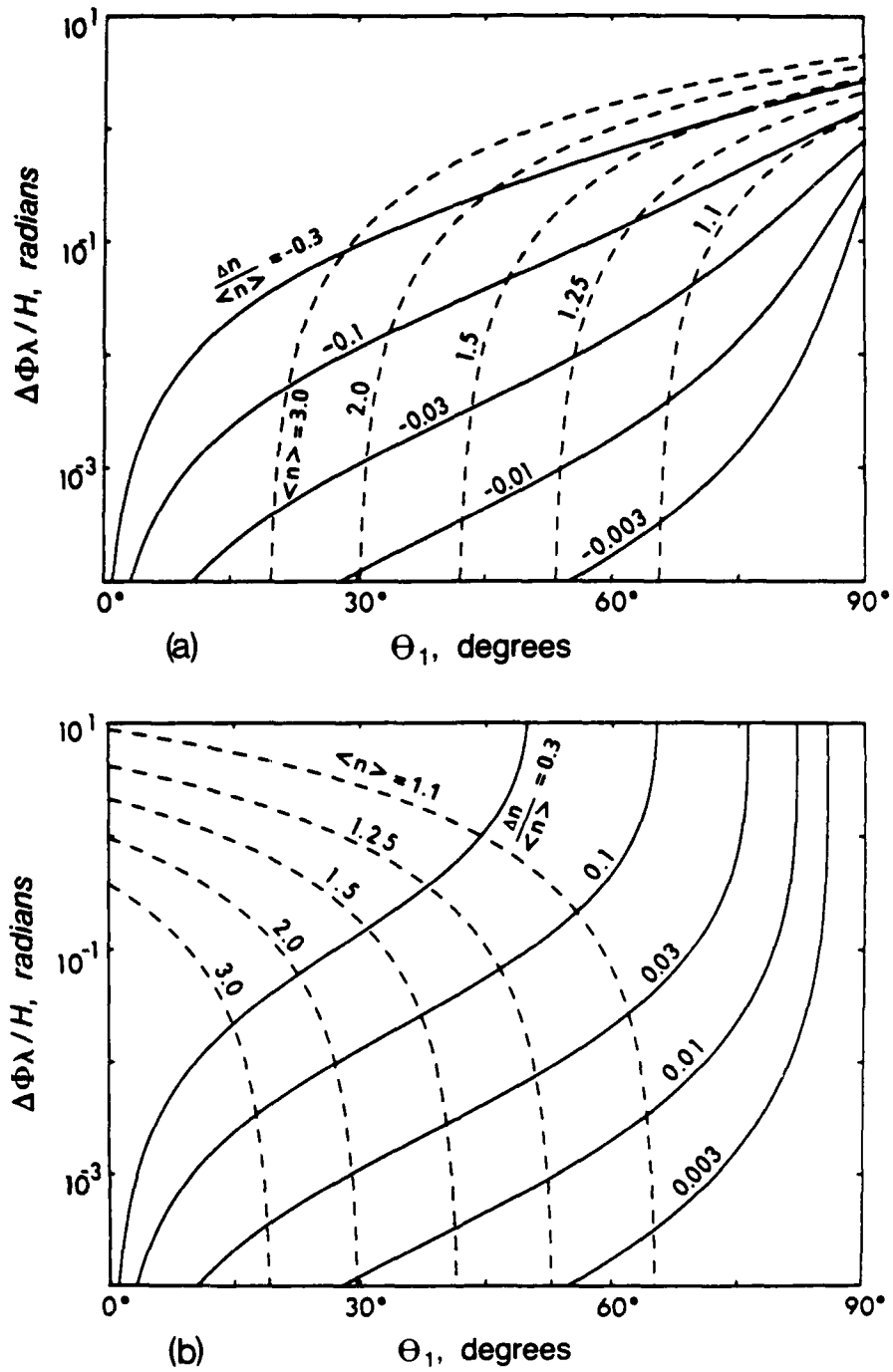
Fig. 2.3. Phase error $\Delta\phi\lambda/(<n>H)$ of Eq. (2.24) plotted against internal angle θ_1 for $\Delta n/<n>$ in the range (a) -0.3 to -0.003 and (b) 0.3 to 0.003. The dashed lines indicate the maximum internal angle θ_1 that can be obtained for a given value of $<n>$.
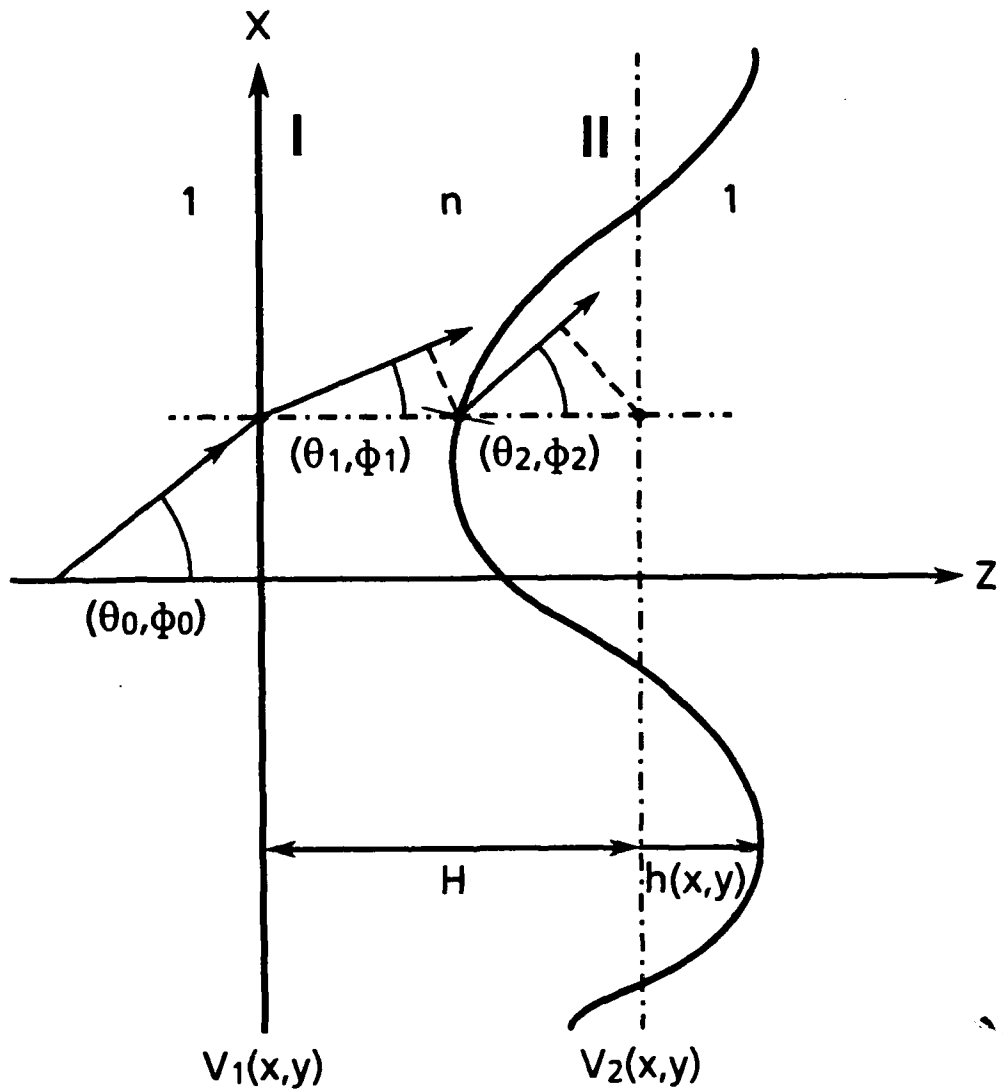
Fig. 2.4. Rough-surface diffuser of average thickness H and constant index of refraction n.

$$\Phi_1 = - kn \left[H + h(\mathbf{r}) \right] \cos\theta_1 . \tag{2.25}$$

Likewise, the phase delay that arises from a plane wave propagating at angle θ_2 but calculated in vacuum along the dashed line between the rough surface and the output plane is

$$\Phi_2 = k h(\mathbf{r}) \cos\theta_2 . \tag{2.26}$$

The resulting plane-wave transmission function is

$$t(\mathbf{r};\mathbf{k}_0) = \exp\left\{ -ik \left[H n \cos\theta_1 + h(\mathbf{r}) \left(n \cos\theta_1 - \cos\theta_2 \right) \right] \right\} . \tag{2.27}$$

The angle θ_2 is calculated by applying Snell's law while taking into account the local slope of the surface:

$$\cos\theta_2 = \frac{1}{1 + h_x^2 + h_y^2} \left[\sin\theta_0 \left(h_x \cos\phi_0 + h_y \sin\phi_0 \right) + \left(h_x^2 + h_y^2 \right) n \cos\theta_1 + \right.$$

$$\left. + \left\{ \left(1 + h_x^2 + h_y^2 \right) \left(1 - n^2 \right) + \left[\sin\theta_0 \left(h_x \cos\phi_0 + h_y \sin\phi_0 \right) - n \cos\theta_1 \right]^2 \right\}^{\frac{1}{2}} \right] , \tag{2.28}$$

where

$$h_x = \frac{\partial h(x,y)}{\partial x} , \quad h_y = \frac{\partial h(x,y)}{\partial y} , \tag{2.29}$$

and

$$\sin\theta_1 = \frac{\sin\theta_0}{n} . \tag{2.30}$$

For surfaces with small slopes, we keep only first order terms in h_x and h_y and obtain

$$\cos\theta_2 \approx \cos\theta_0 - \tan\theta_0 \left(h_x \cos\phi_0 + h_y \sin\phi_0 \right) \left(n \cos\theta_1 - \cos\theta_0 \right) . \tag{2.31}$$

The resulting transmission function is

$$t(\mathbf{r};\mathbf{k}_0) = \exp\left\{ -ik \left[H n \cos\theta_1 + h(\mathbf{r}) \left(n \cos\theta_1 - \cos\theta_0 \right) \right] \right\}$$

$$\times \exp\left\{ -ik \left[h(\mathbf{r}) \left(n \cos\theta_1 - \cos\theta_0 \right) \tan\theta_0 \left(h_x \cos\phi_0 + h_y \sin\phi_0 \right) \right] \right\} . \tag{2.32}$$

When the condition

$$\tan\theta_0 \left(h_x \cos\phi_0 + h_y \sin\phi_0 \right) h / \lambda << 1 \qquad (2.33)$$

is also satisfied the phase in the second exponential is small compared to one radian, and Eq. (2.32) simplifies to[18]

$$t(\mathbf{r};\mathbf{k}_0) = \exp\left(-i k H n \cos\theta_1 \right) \exp\left[-i k h(\mathbf{r}) \left(n \cos\theta_1 - \cos\theta_0 \right) \right] . \qquad (2.34)$$

The rough-surface transmission function of Eq. (2.34) is analogous to the bulk-diffuser transmission function of Eq. (2.23). Both forms are convenient for statistical calculations because of the linear dependence on the roughness within the exponential. Both contain a factor that accounts for the phase delay of a plane wave propagating at an angle through a medium of thickness H with constant index of refraction, and both contain a factor due to the "roughness". They suggest a diffuser model consisting of two parts: (1) a slab of index of refraction n and thickness H and (2) a thin phase screen located at the output side and having an angle-of-incidence-dependent phase delay. However, the two transmission functions do predict a slightly different angular dependence on this phase delay.

2.4 Computer Simulation of Far-Zone Speckle

We now present a computer simulation of the speckle pattern $v_R^* v_R$ that arises from plane-wave illumination of a bulk diffuser. In this simulation the diffuser index modulation $\Delta n(\mathbf{r})$ is represented by a single realization of a wide-sense stationary random process with zero mean, and Eq. (2.17) is used to obtain the plane-wave transmission function $t(\mathbf{r};\mathbf{k}_0)$ for this diffuser. The complex amplitude at the diffuser output plane for illumination of this diffuser with a plane wave having wave vector $\mathbf{k}_0$ is obtained by multiplying Eq. (2.4) by the diffuser aperture function $a(\mathbf{r})$. The far-zone complex amplitude v_R at the position $R\mathbf{s}$ in the far zone of the aperture is then

$$v_R(R\mathbf{s}) = \frac{ik}{2\pi R} \exp\left(-i k R \right) \cos\theta \int a(\mathbf{r}) t(\mathbf{r};\mathbf{k}_{0\perp}) \exp\left[-i \left(\mathbf{k}_{0\perp} - \mathbf{k}_\perp \right) \bullet \mathbf{r} \right] d^2\mathbf{r} . \qquad (2.35)$$

We assume that that the bivariate probability distribution function of the diffuser index modulation $\Delta n(\mathbf{r})$ for two diffuser coordinates is jointly normal and that its autocorrelation function is a Gaussian:

$$R_{\Delta n}(\mathbf{r}_2 - \mathbf{r}_1) = \frac{<\Delta n(\mathbf{r}_1)\,\Delta n(\mathbf{r}_2)>}{<\Delta n^2>} = \exp\left[-\frac{|\mathbf{r}_2 - \mathbf{r}_1|^2}{w^2}\right]. \qquad (2.36)$$

In the actual computer simulation, we simplify the above expressions to a one-dimensional index modulation. The method for generating the data points representing this index modulation is as follows: First, a sequence of normally distributed, uncorrelated, pseudorandom numbers is generated by the computer. These numbers are then made to correlate with their neighbors by convolving the random sequence with a narrow window function.[19,20] The autocorrelation of this window function determines the autocorrelation of the correlated sequence. For the example given here, the Gaussian autocorrelation function can be obtained by using a Gaussian window function. This is true because the autocorrelation of a Gaussian is still a Gaussian. Finally, the data are scaled to give the desired rms roughness. Since the original set of uncorrelated numbers was normally distributed, and the correlated sequence is just a linear combination of these data, the correlated sequence will also be be normally distributed.

Figure 2.5 contains computer simulations of far-zone speckle from a bulk diffuser with index variations $n(x)$. The radiation pattern is plotted against observation angle for one realization of the simulated diffuser. The same simulated diffuser is used in each plot. It has correlation length $w = 50\lambda$, average index $<n> = 1.5$, rms index modulation $<\Delta n^2>^{\frac{1}{2}} = 0.025$, and thickness $H = 80\lambda$. Hence its rms phase delay for normal incidence is $S = 4\pi$ radians. Because $S >> 1$, the direct or specular component of the radiation pattern is completely masked by the diffuse component of scattering. The effective size of the diffuser is limited by a rectangular aperture of width 1500λ attached to the output side of the diffuser. In each plot the speckle pattern is calculated both with the wide-angle transmission function of Eq. (2.17) (solid line) and with the paraxial transmission
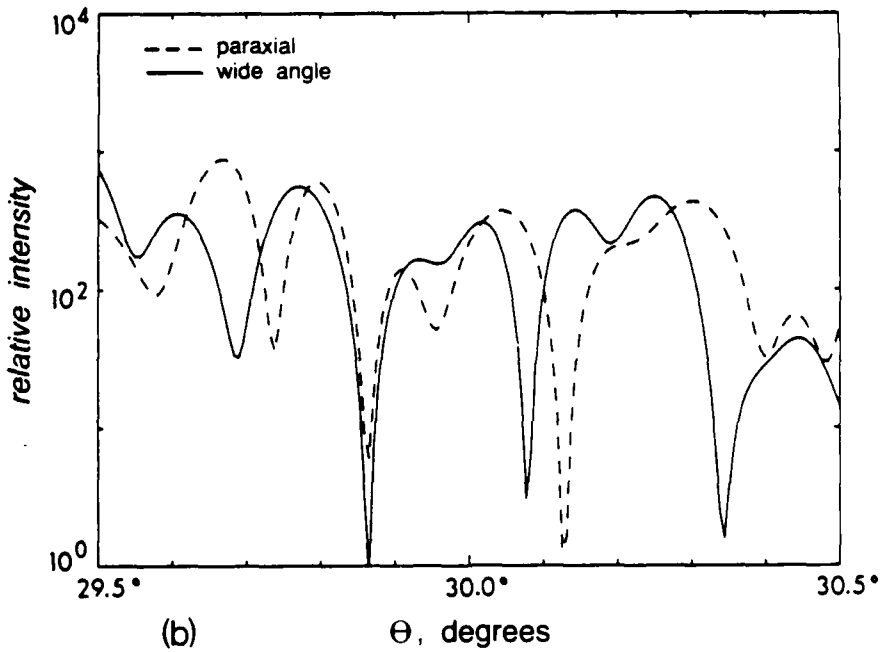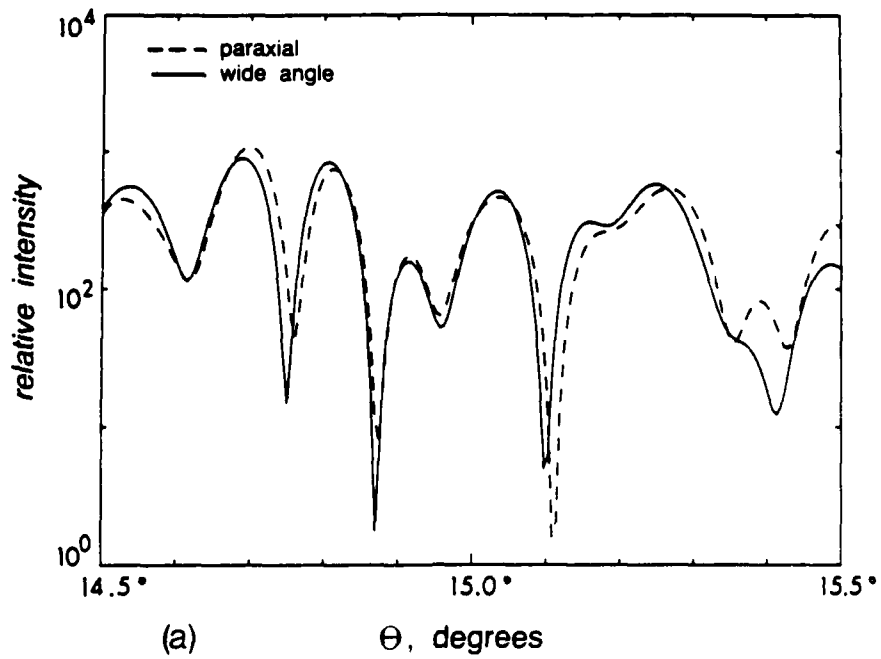
Fig. 2.5. Computer simulation of far-field speckle patterns calculated with paraxial, dashed line, and wide-angle, solid line, transmission functions for plane wave incidence at (a) 15° and (b) 30°.

function obtained by setting $\theta_1 = 0$ in Eq. (2.17) (dashed line). The speckle patterns are plotted over a 1° range of θ centered about the input angle θ_0. These curves allow us to compare the two cases and to get a feeling for the size of the angle correction.

In Figs. 2.5(a) and 2.5(b) the diffuser is illuminated with a plane wave at 15° and 30° respectively. These plots illustrate the effect of the angle dependence in the second exponential in Eq. (2.23), which is to increase the effective roughness by the factor $1/\cos\theta_{<n>}$. We see a small difference between the paraxial and wide-angle patterns when $\theta_0 = 15°$ [Fig. 2.5(a)] and a larger difference when $\theta_0 = 30°$ [Fig. 2.5(b)].

Note that if there is no input-angle dependence in the transmission function, as is assumed in the paraxial case (dashed line), then by the Fourier transform shift theorem, the speckle pattern shifts by the amount θ_0 without decorrelating. However, there is a spread in the speckle pattern because the Fourier transform is in terms of spatial frequency, which goes as $\sin\theta$ not θ. In addition, there is a drop in intensity because of the $\cos^2\theta$ obliquity factor. These effects can be seen by comparing the dashed curves of Figs. 2.5(a) and 2.5(b).

We can interpret the dashed lines in Fig. 2.5 as the speckle pattern at normal incidence but shifted by θ_0 so that it will line up with the speckle pattern for illumination at θ_0. Since these two patterns are very similar, we conclude that the angle of incidence must change by large amounts, i.e., greater than 15°, to decorrelate the speckle pattern. In Appendix B it is shown that the angle necessary for speckle decorrelation decreases as the rms roughness S increases. However, even for $S = 10,000$, the shift in the angle of incidence necessary for speckle decorrelation to occur is approximately 1°. The analysis of cascaded diffusers is greatly simplified if one can assume that the individual diffusers can be represented by the simple transmission function of Eqs. (2.1) and (2.2). In the following chapters we analyze speckle from a cascade of diffusers using the simple transmission function, and we find that the angular detuning necessary for speckle decorrelation is generally much smaller than that from the individual diffusers. For this

reason, the simple transmission function model is adequate for the analysis of speckle decorrelation from cascaded diffusers.

Chapter 2 References and Notes

1. Many authors have used a phase-changing screen to model diffraction from the ionosphere. See, for example, H. G. Booker, J. A. Ratcliffe, and D. H. Shinn, "Diffraction from an irregular screen with applications to ionospheric problems," Philos. Trans. R. Soc. London Ser. A 242, 579-607 (1950); J. A. Ratcliffe, "Some aspects of diffraction theory and their application to the ionosphere," Rep. Prog. Phys. 19, 188-218 (1956); A. Hewish, "The diffraction of radio waves in passing through a phase-changing ionosphere," Proc. R. Soc. London Ser. A 209, 81-96 (1951); R. P. Mercier, "Diffraction by a screen causing large random phase fluctuations," Proc. Cambridge Philos. Soc. 58, 382-400 (1962).

2. L. I. Goldfischer, "Autocorrelation function and power spectral density of laser-produced speckle patterns," J. Opt. Soc. Am. 55, 247-253 (1965).

3. S. Lowenthal and D. Joyeux, "Speckle removal by a slowly moving diffuser associated with a motionless diffuser," J. Opt. Soc. Am. 61, 847-851 (1971).

4. E. Jakeman and P. N. Pusey, "The statistics of light scattered by a random phase screen," J. Phys. A 6, L88-L92 (1973).

5. E. Jakeman and P. N. Pusey, "Non-Gaussian fluctuations in electromagnetic radiation scattered by a random phase screen. I. Theory," J. Phys. A 8, 369-391 (1975).

6. N. George and A. Jain, "Space and wavelength dependence of speckle intensity," Appl. Phys. 4, 201-212 (1974).

7. J. C. Dainty, ed., *Laser Speckle and Related Phenomena* (Springer-Verlag, Heidelberg, 1975).

8. A. Zardecki, "Statistical features of phase screens from scattering data," in *Inverse Scattering Problems in Optics*, H.P. Baltes, ed. (Springer-Verlag, Berlin, 1978), pp. 155-192.

9.   A. Ishimaru, Wave Propagation and Scattering in Random Media (Academic, New York, 1978), Vols. 1 and 2.

10.   W. P. Brown, Jr., "Propagation in random media--cumulative effect of weak inhomogeneities," IEEE Trans. Antennas Propag. AP-15, 81-89 (1967).

11.   P. Beckmann and A. Spizzichino, *The Scattering of Electromagnetic Waves from Rough Surfaces* (Pergamon, New York, 1963).

12.   P. Beckmann, "Scattering of light by rough surfaces," in *Progress in Optics* VI, E. Wolf, ed. (North-Holland, Amsterdam, 1967), pp.53-69.

13.   P. J. Chandley and W. T. Welford, "A re-formulation of some results of P. Beckmann for scattering from rough surfaces," Opt. Quantum Electron. 7, 393-397 (1975).

14.   M. Nieto-Vesperinas and N. Garcia, "A detailed study of the scattering of scalar waves from random rough surfaces," Opt. Acta 28, 1651-1672 (1981).

15.   L. G. Shirley and N. George, "Diffuser transmission functions and far-zone speckle patterns," in *International Conference on Speckle*, H. H. Arsenault, ed., Proc. Soc. Photo-Opt. Instrum. Eng. 556, 63-69 (1985).

16.   L. G. Shirley and N. George, "Wide-angle oiffuser transmission functions and far-zone speckle," J. Opt. Soc. Am. A 4, 734-745 (1987).

17.   Unless otherwise stated, the integrations in this thesis are over the entire r or $k_\perp$ planes. Equation (2.5) is actually an inverse Fourier transform of v_1. The sign dependence on the exponential is positive so that the wave vector $k_\perp$ will have the correct physical interpretation for the $\exp(i\omega t)$ time dependence.

18.   W. T. Welford, "Laser speckle and surface roughness," Contemp. Phys. 21, 401-412 (1980).

19.   H. Fujii, J. Uozumi, and T. Asakura, "Computer simulation study of image speckle patterns with relation to object surface profile," J. Opt. Soc. Am. 66, 1222-1236 (1976).

20.   G. M. Morris, "Serrated Apertures: Statistical Diffraction Theory and Experiments,"

Ph.D. Thesis, California Institute of Technology, CA, 1979, pp. 95-101.

Chapter 3

Decorrelation of Speckle from a Cascade of Two Thin Diffusers

3.1 Introduction

The configuration for the analysis of speckle from a cascade of two diffusers is shown in Fig. 3.1. The diffusers D_1 and D_2 in this figure are separated by the spacing H, and they are illuminated by a plane wave of wave number k that is propagating in the direction s_0. The basic quantity of interest in analyzing the speckle is the complex amplitude v in the far-zone of the aperture a. As illustrated by the photographs in Fig. 1.3, the far-zone speckle intensity pattern will decorrelate as s_0 varies. A similar phenomenon occurs for changes in wavelength. The purpose of this chapter is to provide a general analysis of the decorrelation of the far-zone speckle pattern from a cascade of two thin diffusers with respect to changes in the following parameters: the spacing H between diffuser planes, the wave number k of the incident light, the direction s_0 of the input plane wave, and the direction s of the output unit vector.

In the remainder of Section 3.1, the basic quantities necessary for relating the decorrelation of far-zone speckle to the diffuser surface statistics are introduced. Section 3.2 contains the derivation of the general expression for u_{ab}, the two-state correlation function of far-zone complex amplitude. In order to calculate u_{ab} for particular diffuser types, it is necessary to know the autocorrelation function R_{t_1} and R_{t_2} of the diffuser transmission functions t_1 and t_2. In Section 3.3 R_t is calculated for a phase-type transmission function under various conditions. The two-state correlation function of intensity is considered in Section 3.4, and an illustration of how the preceding analysis can be applied to the remote sensing of the spacing between a diffuser and an aperture is presented in Section 3.5.
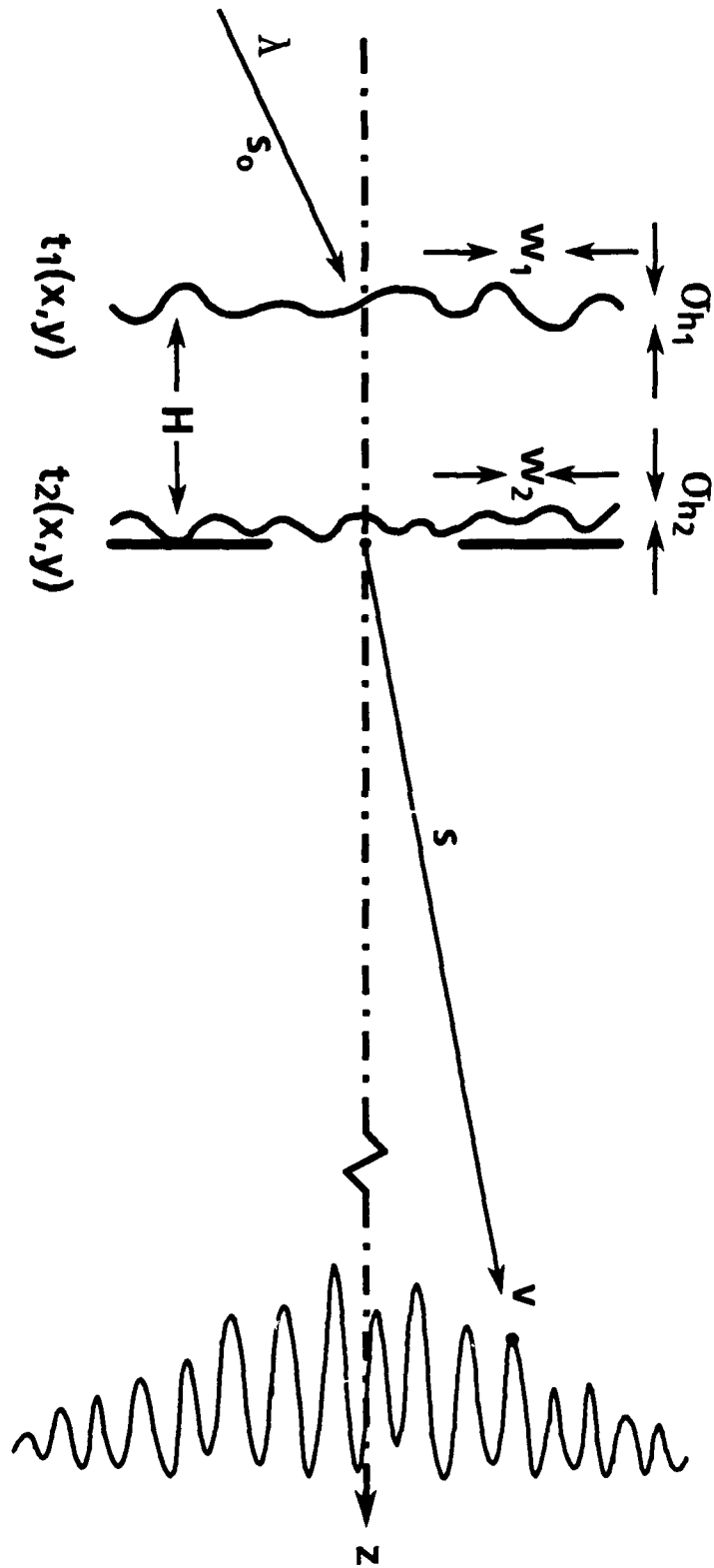
Fig. 3.1.   Configuration for the analysis of far-zone speckle from a cascade of two thin diffuser with changes in wavelength λ, input direction s_0, spacing H, and output direction s.

3.1.1 Far-Zone Speckle

The basic quantity of interest in the study of far-zone speckle from a cascade of two diffusers is the complex amplitude $v(H;\mathbf{k}_0;\mathbf{k})$ in the far-zone of the diffuser. The wave vectors $\mathbf{k}_0$ and $\mathbf{k}$ are obtained by multiplying the unit vectors $\mathbf{s}_0$ and $\mathbf{s}$ by the wave number $k=2\pi/\lambda$. We note that the unit vector $\mathbf{s}$ is related to the spherical-polar coordinates (θ,ϕ) and the cartesian unit vectors $\mathbf{x}$, $\mathbf{y}$, and $\mathbf{z}$, see Fig. 2.2, by

$$\mathbf{s} = \mathbf{x}\sin\theta\cos\phi + \mathbf{y}\sin\theta\sin\phi + \mathbf{z}\cos\theta. \tag{3.1}$$

In the statistical analysis of the decorrelation of speckle, we will calculate the following second-order moment of the complex amplitude $v(H;\mathbf{k}_0;\mathbf{k})$:

$$u_{ab} = \frac{R^2}{A_0^2} <v^*(H_a;\mathbf{k}_{oa};\mathbf{k}_a)v(H_b;\mathbf{k}_{ob};\mathbf{k}_b)> . \tag{3.2}$$

The subscripts a and b in Eq. (3.2) refer to two different states, i.e., two different sets of values of the arguments. The angle brackets denote an ensemble average over diffusers having the same statistical properties. The quantity within the angle brackets is multiplied by R^2 to account for the $1/R^2$ fall-off with distance and divided by

$$A_0^2 = \int |a(\mathbf{r})| \, d^2\mathbf{r}, \tag{3.3}$$

where $a(\mathbf{r})$ is the aperture function, to normalize by the total power passed by the aperture for the unit amplitude input plane wave. Thus, when states a and b are equal, we have

$$u_{aa} = <I_a> , \tag{3.4}$$

where $<I_a>$ is a dimensionless quantity equal to the radiant intensity in the direction specified by the unit vector $\mathbf{s}$, divided by the total incident power

$$<I_a> = \frac{dP}{d\Omega} \frac{1}{P_0} . \tag{3.5}$$

In the calculation of u_{ab}, we will model the individual diffusers by the thin-diffuser transmission functions $t_1(\mathbf{r},k)$ and $t_2(\mathbf{r},k)$, where $\mathbf{r}$ is a vector representing the diffuser coordinates (x,y). For a phase diffuser with a height profile $h(\mathbf{r})$ in a dielectric medium

with index of refraction n, we write the transmission function as

$$t(\mathbf{r},k) = \exp\left[-ik(n-1)h(\mathbf{r})\right].$$ (3.6)

As shown in Section 3.2, the autocorrelation functions R_{t_1} and R_{t_2} of the diffuser transmission functions t_1 and t_2 respectively, defined by

$$R_t(\mathbf{r}_b - \mathbf{r}_a; k_a, k_b) = <t^*(\mathbf{r}_a, k_a) t(\mathbf{r}_b, k_b)>,$$ (3.7)

appear in the calculation of u_{ab}. These functions, R_{t_1} and R_{t_2}, are particularly important because they contain all of the statistical properties of the diffusers that are necessary for the calculation of u_{ab}. The only position dependence in Eq. (3.7) is through the difference $\mathbf{r}_b$-$\mathbf{r}_a$ since the diffusers are assumed to be at least wide-sense stationary, i.e., the first and second moments of t do not depend on the choice of the origin. We will derive a general expression for u_{ab} in Section 3.2 by evaluating Eq. (3.2) in terms of R_{t_1}, R_{t_2}, and the aperture function a. In Section 3.4, we will discuss how u_{ab} is related to the second order moment of intensity $<I_a I_b>$, which is the quantity of interest in the typical experimental application.

3.1.2 Diffuser Statistics

It is not our intent to reconstruct the height profiles $h_1(\mathbf{r})$ and $h_2(\mathbf{r})$ of Fig. 3.1, but rather to characterize the diffusers in a statistical manner and to determine the spacing H or changes in this spacing. In so doing, we need to have a set of quantities that represent the statistical properties of the rough surfaces. Perhaps the most important characteristic of a rough surface $h(\mathbf{r})$ is its rms roughness

$$\sigma_h = <h^2(\mathbf{r})>^{\frac{1}{2}}.$$ (3.8)

For diffusers represented by the thin-phase-screen transmission function of Eq. (3.6), it is also convenient to define the effective roughness of the diffuser in transmission as

$$\sigma_t = (n-1)\sigma_h.$$ (3.9)

Of course, in the scattering of electromagnetic waves from rough surfaces, the overall

effective roughness is measured in terms of the wavelength λ of the incident radiation. Hence, we also define the rms phase delay in radians due to the transmission function Eq. (3.6) as

$$S = k\sigma_t = k\sigma_h(n-1). \qquad (3.10)$$

Although the roughness S is important in determining the degree of diffuse scattering, i.e., scattering out of the direction of the incident beam, surfaces having very different textures, and hence different radiation patterns, can have the same value of S. A complete statistical description of the rough surface $h(\mathbf{r})$ could be expressed formally by $P_n(h_1, h_2, \dots h_n; \mathbf{r}_1, \mathbf{r}_2, \dots \mathbf{r}_n)$, the joint probability distribution function of surface heights with respect to n arbitrary positions, where n is an arbitrary positive integer. However, since we are only considering two-state correlation function, we will not need joint probability distribution functions higher than the bivariate function P_2.

The expression for u_{ab} derived in Section 3.2 will be written in terms of R_{t_1} and R_{t_2}. However, a correlation function more closely related to the diffuser height profile is

$$R_h(\mathbf{r}_b - \mathbf{r}_a) = \frac{<h(\mathbf{r}_a)\, h(\mathbf{r}_b)>}{\sigma_h^2}. \qquad (3.11)$$

Therefore it will be important to have expressions relating R_h to R_t. This relationship will be discussed further in Section 3.3.

3.2 Two-State Correlation of Complex Amplitude

3.2.1 Far-Zone Complex Amplitude

The first step in the calculation of u_{ab} is to derive the formula for the far-zone complex amplitude $v(H; \mathbf{k}_{oa}; \mathbf{k}_a)$. We begin by listing the expressions governing propagation through each element of the system in Fig. 3.1. We write the complex amplitude at the input side of plane I, which arises from the input plane wave, as

$$v_{1-}(\mathbf{r}') = \exp\left(-i\,\mathbf{k}_{o\perp} \cdot \mathbf{r}'\right). \qquad (3.12)$$

Once again, the subscript $\perp$ in Eq. (3.12) denotes that only the components of the vector

k_0 lying in the diffuser plane, i.e., the (k_x, k_y) components, are retained. Since the diffusers are assumed to be thin, the complex amplitude at the output side of plane I is obtained by a point-by-point multiplication of the input plane wave by the transmission function:

$$v_{1+}(\mathbf{r'}) = v_{1-}(\mathbf{r'})\, t_1(\mathbf{r'};k).$$

(3.13)

As discussed in Section 2.1, a thick diffuser, or any linear optical system for that matter, could be represented by a generalized transmission function $t(\mathbf{r},\mathbf{k})$ that depends on the direction of an input plane wave in addition to the position in the diffuser plane and the wavelength.[1] Arbitrary illumination could be treated by breaking v_{1-}, the input at plane I, into an angular spectrum of plane waves and operating on each plane wave component with the appropriate transmission function.

We calculate v_{2-}, the input to the second diffuser, by performing a Fresnel-zone propagation of the complex amplitude v_{1+} along the z-axis over the distance H between diffuser planes. The impulse response for propagation between planes is

$$g_H(\mathbf{r}-\mathbf{r'}) = \frac{ik}{2nH}\, \exp(-ikH)\, \exp\!\left(-\frac{ik}{2H}|\mathbf{r}-\mathbf{r'}|^2\right).$$

(3.14)

The range of validity of Eq. (3.14) increases in the transition from deterministic to statistical calculations. One reason for this is that the effective limiting aperture decreases, owing to the finite correlation length along the diffuser plane. A quantitative discussion of the validity of Eq. (3.14), however, is beyond the scope of this thesis. We also note that Eq. (3.14) is a paraxial approximation. Therefore, we expect our results to be less accurate for wide angles. The justification for ignoring reflections between surfaces at planes I and II is that any reflected light that reaches the output point must have been reflected at least twice, and therefore its contribution to the speckle pattern will be negligible compared with the directly transmitted light.

Propagation through the second diffuser, and its associated aperture, is treated in the same manner as it was for the first diffuser, i.e., with a point-by-point multiplication

$$v_{2+}(\mathbf{r}) = v_{2-}(\mathbf{r})\, t_2(\mathbf{r};^b)\, a(\mathbf{r}). \tag{3.15}$$

The far-zone complex amplitude is then obtained by propagating v_{2+} into the far zone with the far-zone impulse response

$$g_R(\mathbf{r},R\mathbf{s}) = \cos\theta\,\frac{ik}{2\pi R}\,\exp(-ikR)\,\exp\!\left(i\,\mathbf{k}_\perp\!\bullet\mathbf{r}\right). \tag{3.16}$$

In Eq. (3.16) we choose to write the obliquity factor as $\cos\theta$ rather than as $\mathbf{s}\cdot\mathbf{z}$ or s_z. We obtain the final form of the output scalar amplitude $v(H;\mathbf{k}_0,\mathbf{k})$ by combining Eqs. (3.12) through (3.16):

$$v(H;\mathbf{k}_0;\mathbf{k}) = -\frac{k^2}{\left(2\pi\right)^2}\,\frac{\exp[-ik\,(H+R)]}{HR}\,\cos\theta\int d^2r\,a(\mathbf{r})\,t_2(\mathbf{r};k)\exp\!\left(i\,\mathbf{k}_\perp\!\bullet\mathbf{r}\right)$$

$$\times\int\exp\!\left(-i\,\mathbf{k}_{0\perp}\!\bullet\mathbf{r}'\right)t_1(\mathbf{r}';k)\,\exp\!\left(-\frac{ik}{2H}|\mathbf{r}-\mathbf{r}'|^2\right)d^2r'. \tag{3.17}$$

Unless otherwise specified, the range of integration in all integrals is over the entire x-y plane.

At this point we pause to illustrate the derivation of the plane wave transmission function for an optical system by calculating $t(\mathbf{r};\mathbf{k})$ for propagation between planes I and II of the double diffuser in Fig. 3.1, not including the aperture. Having tracked an input plane wave through this system, we can write the plane wave transmission function for the diffuser combination by taking the expression for v_{2+} and dividing it by the input plane wave given in Eq. (3.12) and by the aperture function $a(\mathbf{r})$:

$$t(\mathbf{r};\mathbf{k}_0) = \frac{ik}{2\pi}\,\frac{\exp(-ikH)}{H}\,t_2(\mathbf{r};k)$$

$$\times\int\exp\!\left[-i\!\left(\frac{k}{2H}|\mathbf{r}'|^2 + \mathbf{k}_{0\perp}\!\bullet\mathbf{r}'\right)\right]t_1(\mathbf{r}+\mathbf{r}';k)\,d^2r'. \tag{3.18}$$

The output at plane II for arbitrary illumination can be calculated by substituting the plane wave transmission function, Eq. (3.18), into Eq. (2.7) and decomposing the input at plane I into an angular spectrum of plane waves V_1. The plane-wave transmission

function representation is especially convenient for problems where the input is a plane wave, such as in the plane-wave probing of optical systems by varying the angle of incidence or the wavelength of the input plane wave. In Section 3.2.7 we will give a general form for u_{ab} in terms of $t(r;k_0)$. One could obtain u_{ab} for a cascade of two diffusers by applying the results of Section 3.2.7 to Eq. (3.18), however, in the following sections we will derive u_{ab} for a double diffuser from first principles

3.2.2 Derivation of Two-State Correlation of Complex Amplitude

We proceed with the derivation of u_{ab} by substituting Eq. (3.17), for each of the states a and b, into Eq. (3.2). We note that all of the randomness is contained in the transmission functions t_1 and t_2 through their dependence on the height profiles h_1 and h_2, and that the resulting expression for u_{ab} is just a linear combination of products involving t_1 and t_2, i.e., integrals. Therefore, the angle brackets can be moved inside the integrals so that they surround the combination of the transmission functions. Furthermore, since h_1 and h_2 are uncorrelated random processes, the angle brackets can be split into two sets: one around the t_1 dependence and the other around the t_2 dependence. We recognize the resulting functions as the transmission function autocorrelation functions R_{t_1} and R_{t_2} that are defined in Eq. (3.7). The expression that results for u_{ab} is

$$u_{ab} = \frac{k_a^2 k_b^2}{(2\pi)^4} \frac{\exp\left(-i\phi_{ab}\right)}{A_o^2 H_a H_b} \cos\theta_a \cos\theta_b \int \int d^2r\, d^2r''\, a^*(r)\, a(r'')\, R_{t_2}(r''-r;k_a,k_b)$$

$$\times \exp\left[i\left(k_{b\perp}\bullet r'' - k_{a\perp}\bullet r\right)\right] \int \int \exp\left[-i\left(k_{ob\perp}\bullet r''' - k_{oa\perp}\bullet r'\right)\right]$$

$$\times R_{t_1}(r'''-r';k_a,k_b)\exp\left[\frac{i}{2}\left(\frac{k_a}{H_a}|r-r'|^2 - \frac{k_b}{H_b}|r''-r'''|^2\right)\right] d^2r'\, d^2r''', \qquad (3.19)$$

where

$$\phi_{ab} = k_b H_b - k_a H_a + \left(k_b - k_a\right) R . \qquad (3.20)$$

By making the following change of variables, we can separate the variables in Eq. (3.19) so that four of the eight integrations can be performed without having any knowledge of the functional form of R_{t_1} and R_{t_2}:

$$\mathbf{r} = \mathbf{r}_3 - \frac{\mathbf{r}_2}{2}, \tag{3.21a}$$

$$\mathbf{r}'' = \mathbf{r}_3 + \frac{\mathbf{r}_2}{2}, \tag{3.21b}$$

$$\mathbf{r}' = \left(\mathbf{r}_3 + \mathbf{r}_4\right) - \frac{\mathbf{r}_1 + \mathbf{r}_2}{2}, \tag{3.21c}$$

and

$$\mathbf{r}''' = \left(\mathbf{r}_3 + \mathbf{r}_4\right) + \frac{\mathbf{r}_1 + \mathbf{r}_2}{2}. \tag{3.21d}$$

We note that the absolute value of the Jacobian of the transformation given by Eqs.(3.21a) through (3.21d) is unity so that the change of variables is a simple substitution. The resulting form of Eq. (3.19) is

$$u_{ab} = \frac{k_a k_b}{\left(2\pi\right)^2} \exp\left(-i\phi_{ab}\right) \cos\theta_a \cos\theta_b \int d^2\mathbf{r}_1 \; B\left(\mathbf{r}_1; \mathbf{k}_{ob\perp} - \mathbf{k}_{oa\perp}; \frac{k_a}{H_a}, \frac{k_b}{H_b}\right)$$

$$\times \exp\left[-\frac{i}{2}\left(\mathbf{k}_{oa\perp} + \mathbf{k}_{ob\perp}\right) \bullet \mathbf{r}_1\right] \int R_{t_1}(\mathbf{r}_1 + \mathbf{r}_2; k_a, k_b) \; R_{t_2}(\mathbf{r}_2; k_a, k_b)$$

$$\times \hat{A}(\mathbf{r}_2; \mathbf{k}_{a\perp} - \mathbf{k}_{oa\perp} - \mathbf{k}_{b\perp} - \mathbf{k}_{ob\perp}) \exp\left[\frac{i}{2}\left(\mathbf{k}_{a\perp} - \mathbf{k}_{oa\perp} + \mathbf{k}_{b\perp} - \mathbf{k}_{ob\perp}\right) \bullet \mathbf{r}_2\right] d^2\mathbf{r}_2, \tag{3.22}$$

where we have defined the normalized ambiguity function [2-4] of the aperture function

$$\hat{A}(\mathbf{r}; \mathbf{k}_\perp) = \frac{1}{A_0^2} \int a^*(\mathbf{r}' - \frac{\mathbf{r}}{2}) \, a(\mathbf{r}' + \frac{\mathbf{r}}{2}) \exp\left(-i\mathbf{k}_\perp \bullet \mathbf{r}'\right) d^2\mathbf{r}', \tag{3.23}$$

and the cross-ambiguity function of the Fresnel impulse response, Eq. (3.14), as

$$B(\mathbf{r}; \mathbf{k}_\perp; \frac{k_a}{H_a}, \frac{k_b}{H_b}) \approx \frac{1}{\left(2\pi\right)^2} \frac{k_a k_b}{H_a H_b}$$

$$\times \int \exp\left[\frac{i}{2}\left(\frac{k_a}{H_a} |\mathbf{r}' - \frac{\mathbf{r}}{2}|^2 - \frac{k_b}{H_b} |\mathbf{r}' + \frac{\mathbf{r}}{2}|^2\right)\right] \exp\left(-i\mathbf{k}_\perp \bullet \mathbf{r}'\right) d^2\mathbf{r}'. \tag{3.24}$$

The wave vectors that occur in the argument of $\hat{A}$ and in the exponential within the r_2 integral in Eq. (3.22) have special physical significance and will be denoted by the following symbols:

$$\Delta k_{ab\perp} = k_{a\perp} - k_{oa\perp} - k_{b\perp} + k_{ob\perp} ,\qquad(3.25)$$

and

$$k_{ab\perp} = \frac{1}{2}\left(k_{a\perp} - k_{oa\perp} + k_{b\perp} - k_{ob\perp} \right).\qquad(3.26)$$

Equations (3.25) and (3.26) are the difference and average values of the wave vectors $k_{a\perp}$-$k_{oa\perp}$ and $k_{b\perp}$-$k_{ob\perp}$, which in turn, are the differences between the input and output wave vectors for each of the two states a and b.

We explain the physical significance of $\Delta k_{ab\perp}$ and $k_{ab\perp}$ by considering the example of speckle from a single thin diffuser. In the same manner that we obtained Eq. (3.17) for the far-zone complex amplitude from a double diffuser, we can write

$$v(H;k_o,k) = \frac{ik}{2\pi R} \exp(-ik R) \cos\theta \int a(r)\,t(r;k)\exp\left[i\left(k_\perp - k_{o\perp}\right)\bullet r\right] d^2r \qquad (3.27)$$

for the far-zone complex amplitude from a single thin diffuser. Thus we see that the speckle is essentially the Fourier transform of the product of the diffuser transmission function and the aperture, and that the argument of the Fourier transform is $k_{o\perp}$. $k_\perp$, the difference between input and output wave vectors. We conclude that the speckle pattern from a single thin diffuser moves as a whole about the direction of the input plane wave, and that there is no angular decorrelation of speckle as long as the output wave vector from the second state moves in such a manner as to track the speckle, i.e., as long as $k_{a\perp}$-$k_{oa\perp} = k_{b\perp}$-$k_{ob\perp}$. For this reason, we refer to $\Delta k_{ab\perp}$ as the speckle tracking wave vector. We see that the tracking condition is satisfied when

$$\Delta k_{ab\perp} = 0 .\qquad(3.28)$$

Thus the magnitude of the offset wave vector $\Delta k_{ab\perp}$ relative to the speckle size determines the degree of decorrelation that arises from looking at different points in the

speckle pattern. In most applications, we are not interested in decorrelation arising from speckle motion, and hence most experiments would be designed so that Eq. (3.28) would be satisfied. Of course, if Eq. (3.28) holds, then Eq. (3.26) simplifies to

$$\mathbf{k}_{ab\perp} = \mathbf{k}_{a\perp} - \mathbf{k}_{oa\perp} = \mathbf{k}_{b\perp} - \mathbf{k}_{ob\perp}, \qquad (3.29)$$

and $\mathbf{k}_{ab\perp}$ is simply the difference between input and observation wave vectors for either state a or state b. We refer to $\mathbf{k}_{ab\perp}$ as the Fourier transform wave vector because it appears in the argument of the Fourier transform in Eq. (3.22).

Another observation that we make from Eq. (3.27) is that the speckle pattern spreads as k decreases, or in other words, it spreads as the wavelength λ increases. For example, if the diffuser is illuminated at normal incidence so that $\mathbf{k}_{o\perp} = 0$, and if we look at the output along the k_x-axis, then the arguments of the Fourier transform are ($k_x = k \sin\theta, k_y = 0$). Therefore, in order to stay on the same point in the speckle pattern, k_x must remain constant, i.e., $|\theta|$ must increase as k decreases. Equation (3.28) is a general expression showing the interrelationship between the input direction, output direction, and wavelength between states a and b that is necessary for tracking a speckle.

In studying speckle from a cascade of two diffusers, it is advantageous to have an intermediate function that contains all of the dependence on the diffuser correlation functions R_{t_1} and R_{t_2}, and on the aperture ambiguity function $\tilde{A}$. From inspection of Eq. (3.22), we see that the $\mathbf{r}_2$ integration provides us with such a function:

$$F(\mathbf{r}; k_a, k_b; \mathbf{k}_\perp; \Delta\mathbf{k}_\perp) = \int R_{t_1}(\mathbf{r} + \mathbf{r}'; k_a, k_b) \ R_{t_2}(\mathbf{r}'; k_a, k_b)$$

$$\times \ \tilde{A}(\mathbf{r}'; \Delta\mathbf{k}_\perp) \exp\left(i\mathbf{k}_\perp \bullet \mathbf{r}'\right) d^2\mathbf{r}' . \qquad (3.30)$$

We refer to F as the double-diffuser descriptor function. It is not to be confused with the hypergeometric function, which is also denoted by F. Through the use of Eqs. (3.26), (3.27), and (3.30), we can now rewrite Eq. (3.22) in the simplified form:

48

$$u_{ab} = \frac{k_a k_b}{(2\pi)^2} \exp\left(-i\phi_{ab}\right) \cos\theta_a \cos\theta_b \int B\left(\mathbf{r};\mathbf{k}_{ob\perp} - \mathbf{k}_{oa\perp}; \frac{k_a}{H_a}, \frac{k_b}{H_b}\right)$$

$$\times F(\mathbf{r};k_a,k_b;\mathbf{k}_{ab\perp};\Delta\mathbf{k}_{ab\perp}) \exp\left[-\frac{i}{2}\left(\mathbf{k}_{oa\perp} + \mathbf{k}_{ob\perp}\right)\bullet\mathbf{r}\right] d^2\mathbf{r}. \tag{3.31}$$

3.2.3 Aperture Ambiguity Function

Through much of the remainder of this chapter, the aperture function will be left arbitrary, and hence, the aperture ambiguity function $\tilde{A}$ will not be specified. However, we can gain insight into the effect of the aperture on the speckle decorrelation by calculating $\tilde{A}$ for some particular aperture functions. We will consider three functional forms of $a(\mathbf{r})$: a Gaussian aperture having width w_a,

$$a(\mathbf{r}) = \exp\left(-\frac{|\mathbf{r}|^2}{w_a^2}\right), \tag{3.32}$$

a rectangular aperture having full-widths w_x and w_y along the x and y axes,

$$a(\mathbf{r}) = \text{rect}\left(\frac{x}{w_x}\right)\text{rect}\left(\frac{y}{w_y}\right), \tag{3.33}$$

and a circular aperture having radius w_a,

$$a(\mathbf{r}) = \text{circ}\left(\frac{|\mathbf{r}|}{w_a}\right). \tag{3.34}$$

For the Gaussian aperture A_0^2 of Eq. (3.3), which is a measure of the total power passed by the aperture for plane wave illumination, is

$$A_0^2 = \frac{\pi}{2} w_a^2. \tag{3.35}$$

For the rectangular aperture A_0^2 is equal to the area of the rectangle

$$A_0^2 = w_x w_y, \tag{3.36}$$

and for the circular aperture it is equal to the area of the circle

$$A_0^2 = \pi w_a^2. \tag{3.37}$$

The functional form of $\tilde{A}$ is particularly convenient for the Gaussian aperture of Eq. (3.32) because $\tilde{A}$ separates into the product of a Gaussian in $\mathbf{r}$ and in $\mathbf{k}_\perp$:

$$\hat{A}(\mathbf{r};\mathbf{k}_\perp)=\exp\left(-\frac{|\mathbf{r}|^2}{2w_a^2}\right)\exp\left(-\frac{1}{8}w_a^2|\mathbf{k}_\perp|^2\right). \tag{3.38}$$

For the rectangular aperture, described by Eq. (3.33), $\hat{A}$ takes the form

$$\hat{A}(\mathbf{r};\mathbf{k}_\perp)=\frac{2}{w_x k_x}\mathrm{rect}\left(\frac{x}{2w_x}\right)\sin\left[\left(1-\frac{|x|}{w_x}\right)\frac{w_x k_x}{2}\right]$$

$$\times\frac{2}{w_y k_y}\mathrm{rect}\left(\frac{y}{2w_y}\right)\sin\left[\left(1-\frac{|y|}{w_y}\right)\frac{w_y k_y}{2}\right]. \tag{3.39}$$

It is more difficult to evaluate the ambiguity function of a circular aperture for arbitrary arguments $\mathbf{r}$ and $\mathbf{k}_\perp$.[5] However, for $\mathbf{k}_\perp=0$ the ambiguity function reduces to the autocorrelation of the circular aperture, and the solution is[6]

$$\hat{A}(\mathbf{r};0)=\frac{2}{\pi}\mathrm{circ}\left(\frac{|\mathbf{r}|}{2w_a}\right)\left\{\cos^{-1}\left(\frac{|\mathbf{r}|}{2w_a}\right)-\frac{|\mathbf{r}|}{2w_a}\left[1-\left(\frac{|\mathbf{r}|}{2w_a}\right)^2\right]^{\frac{1}{2}}\right\}. \tag{3.40}$$

Equation (3.40) is still useful because it is the speckle tracking wave vector $\Delta\mathbf{k}_{ab\perp}$ that occurs as the second argument of $\hat{A}$ in Eq. (3.22), and $\Delta\mathbf{k}_{ab\perp}=0$ in the usual application.

The dependence of Eq. (3.39) on the x and k_x variables for $y=0$ and $k_y=0$ is illustrated in Fig. 3.2. We note the following interesting features in this plot: First of all, since $\hat{A}$ contains a rectangle function in the x-variable, it is zero outside of the region $|x|\geq w_x$. In addition, $\hat{A}$ is a triangle function in x when $k_x=0$ and a sinc function in k_x when $x=0$. We also note that more and more cycles of oscillation occur along the x-axis between $\pm w_x$ as k_x increases, and that the period of the oscillations along the k_x-axis increases as $|x|$ gets closer to the cutoff value, w_x.

A general feature of aperture ambiguity functions that is illustrated in Eqs. (3.38) and (3.39) is the inverse relationship between the widths of the spatial dependence $\mathbf{r}$ and the spatial frequency dependence $\mathbf{k}_\perp$. By this we mean that as the the width of the ambiguity function increases with respect to one type of coordinate, it decreases with respect to the conjugate coordinate. The wave vector that occurs in the ambiguity function in Eq. (3.22) is $\Delta\mathbf{k}_{ab\perp}$, which we know to be related to the decorrelation of
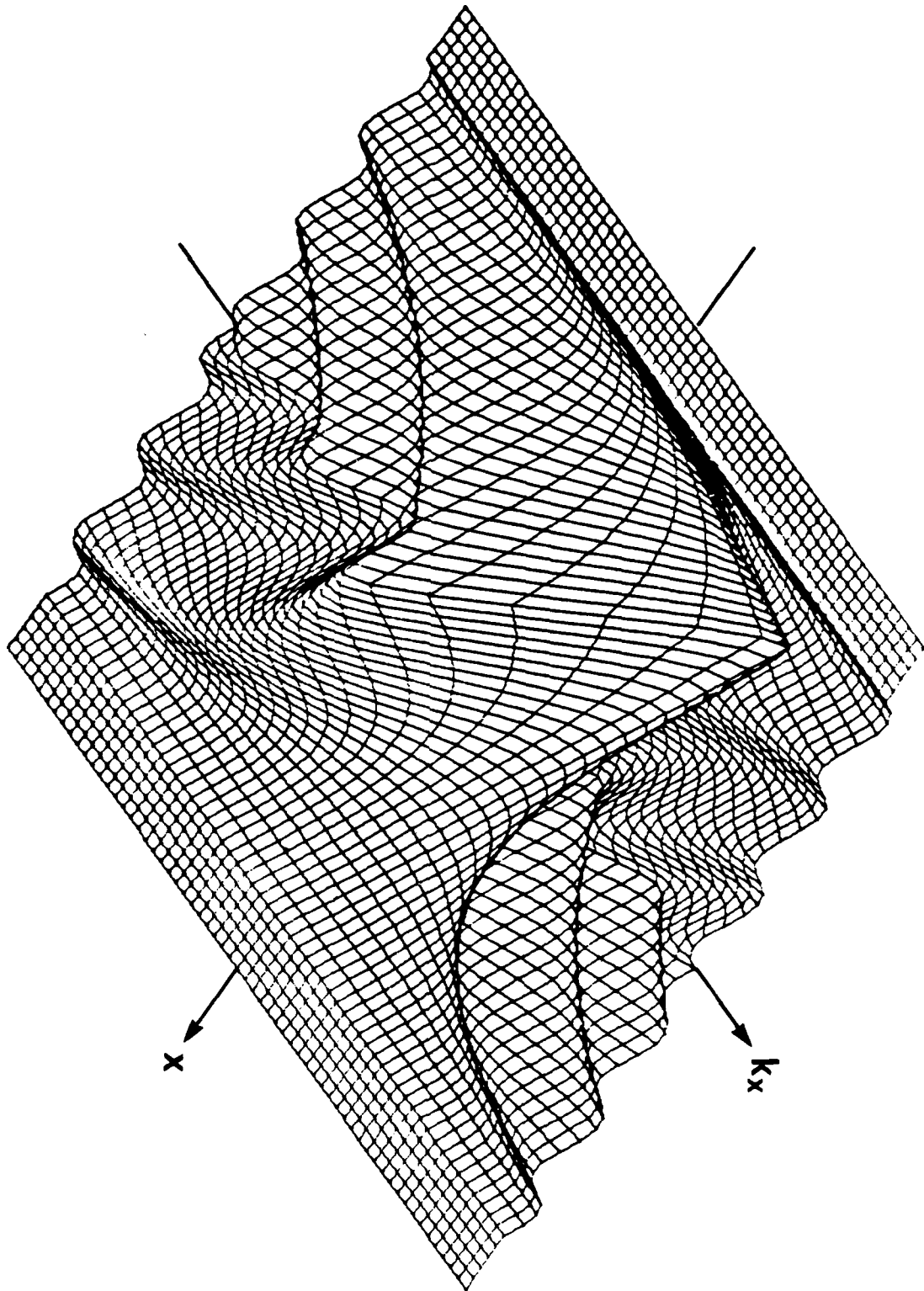
Fig. 3.2. Plot of x-k_x dependence of Eq. (3.39) for the aperture ambiguity function of a rectangular aperture.

speckle that occurs due to motion of the speckle pattern as the input angle or the wavelength is changed. In most practical applications, the aperture function, and hence the spatial dependence of the ambiguity function for $\Delta k_{ab\perp}=0$, will be wide compared to R_{t_1} and R_{t_2}. It follows from the inverse relationship between $\mathbf{r}$ and $\mathbf{k}_\perp$ that $\tilde{A}$ will be narrow with respect to $\Delta k_{ab\perp}$, i.e., that the speckle will be small in size. An advantage of making $\tilde{A}$ wide is that F can be approximated by setting the spatial argument of $\tilde{A}$ to zero in Eq. (3.30) and factoring $\tilde{A}(0;\Delta k_{ab\perp})$ out of the integral. This gives the same result as the quasihomogeneous approximation that is often used in coherence theory.[7]

3.2.4 Fresnel Cross-Ambiguity Function

Whereas Eq. (3.23) for the normalized ambiguity function $\tilde{A}$ depends on the particular function a used to represent the aperture function, the functional form of the cross-ambiguity function B is completely determined because there is no dependence on the unknown quantities R_{t_1}, R_{t_2}, or a in Eq. (3.24). We use the identity[8]

$$\int \exp\left[i\left(C|\mathbf{r}|^2 - \mathbf{k}_\perp \cdot \mathbf{r}\right)\right] d^2\mathbf{r} = \frac{i\pi}{C}\exp\left(-i\,\frac{|\mathbf{k}_\perp|^2}{4C}\right) \tag{3.41}$$

to evaluate Eq. (3.24) and obtain the solution

$$B\left(\mathbf{r};\mathbf{k}_\perp;C_a,C_b\right) = -\frac{i}{2\pi}\,\frac{C_a C_b}{C_b - C_a}$$

$$\times \exp\left\{\frac{i}{2}\,\frac{1}{C_b - C_a}\left[|\mathbf{k}_\perp|^2 + \left(C_a + C_b\right)\mathbf{k}_\perp \cdot \mathbf{r} + C_a C_b |\mathbf{r}|^2\right]\right\} \tag{3.42}$$

In Eq. (3.42) we have represented the wavelength-spacing parameters k_a/H_a and k_b/H_b by the symbols C_a and C_b respectively. In the limit as $C_a \to C_b$, Eq. (3.42) becomes a delta function:

$$B\left(\mathbf{r};\mathbf{k}_\perp;C_a,C_a\right) = \delta\left(\mathbf{r} + \frac{\mathbf{k}_\perp}{C_a}\right). \tag{3.43}$$

Equation (3.43) can be obtained by going back to Eq. (3.24) for B and noting that the

quadratic terms in the exponential cancel when $C_a = C_b$. What remains is the Fourier transform of a constant, i.e., a delta function.

In terms of the variables that occur in Eq. (3.31),

$$B\left(\mathbf{r}; \mathbf{k}_{ob\perp} - \mathbf{k}_{oa\perp}; \frac{k_a}{H_a}, \frac{k_b}{H_b}\right) = -\frac{i}{2\pi} \frac{k_a k_b}{k_b H_a - k_a H_b} \exp\left(\frac{i}{2} \frac{H_a H_b}{k_b H_a - k_a H_b} |\mathbf{k}_{ob\perp} - \mathbf{k}_{oa\perp}|^2\right)$$

$$\times \exp\left[\frac{i}{2} \frac{k_b H_a + k_a H_b}{k_b H_a - k_a H_b}\left(\mathbf{k}_{ob\perp} - \mathbf{k}_{oa\perp}\right) \cdot \mathbf{r}\right] \exp\left(\frac{i}{2} \frac{k_a k_b |\mathbf{r}|^2}{k_b H_a - k_a H_b}\right). \qquad (3.44)$$

When

$$\frac{k_a}{H_a} = \frac{k_b}{H_b}, \qquad (3.45)$$

we can use Eq. (3.43) to find the following limiting form of Eq. (3.44):

$$B\left(\mathbf{r}; \mathbf{k}_{ob\perp} - \mathbf{k}_{oa\perp}; \frac{k_a}{H_a}, \frac{k_b}{H_b} = \frac{k_a}{H_a}\right) = \delta\left(\mathbf{r} + H_b \mathbf{s}_{ob\perp} - H_a \mathbf{s}_{oa\perp}\right). \qquad (3.46)$$

We can interpret the offset vector that occurs in the argument of the delta function in Eq. (3.46) as the paraxial approximation to the lateral shift between two rays that begin at the same point on the first plane and travel in directions $\mathbf{s}_{oa}$ and $\mathbf{s}_{ob}$ to the second plane. For example, if $\mathbf{s}_{oa} = 0$, and $\phi_{ob} = 0$ so that the vector $\mathbf{s}_{ob}$ is in the x-z plane, then $H_b \mathbf{s}_{ob\perp} = H_b \sin\theta_{ob} \mathbf{x}$, which is a paraxial approximation to the actual offset $H_b \tan\theta_{ob} \mathbf{x}$.

3.2.5 General Expression for u_{ab}

Having evaluated the cross-ambiguity function B, we are now able to write the final expression for u_{ab}. In terms of the double-diffuser descriptor function F defined in Eq. (3.30) and for arbitrary values of all parameters, u_{ab} is

$$u_{ab} = -i \frac{k_a^2 k_b^2}{(2\pi)^3} \frac{\exp\left(-i\phi_{ab}\right)}{k_b H_a - k_a H_b} \exp\left(\frac{i}{2} \frac{H_a H_b}{k_b H_a - k_a H_b} |\mathbf{k}_{ob\perp} - \mathbf{k}_{oa\perp}|^2\right) \cos\theta_a \cos\theta_b$$

$$\times \int F(\mathbf{r}; k_a, k_b; \mathbf{k}_{ab\perp}; \Delta\mathbf{k}_{ab\perp}) \exp\left\{i \frac{k_a k_b}{k_b H_a - k_a H_b}\left[\frac{1}{2}|\mathbf{r}|^2 + \left(H_b \mathbf{s}_{ob\perp} - H_a \mathbf{s}_{o\perp}\right) \cdot \mathbf{r}\right]\right\} d^2\mathbf{r}. \qquad (3.47)$$

Equation (3.47) is the key expression governing the decorrelation of speckle from a cascade of two thin diffusers. For angular decorrelation only, i.e., when wavelength and spacing are fixed, or more generally, when Eq. (3.45) holds, then Eq. (3.47) simplifies: Owing to the fact that B in Eq. (3.46) is a delta function, the integral in Eq. (3.31) can be evaluated immediately yielding

$$u_{ab} = \frac{k_a k_b}{(2\pi)^2} \exp\left(-i\phi_{ab}\right) \exp\left[\frac{i}{2}\left(k_b H_b - k_a H_a\right)\right] \cos\theta_a \cos\theta_b$$

$$\times F(H_a \mathbf{s}_{oa\perp} - H_b \mathbf{s}_{ob\perp}; k_a, k_b; \mathbf{k}_{ab\perp}; \Delta \mathbf{k}_{ab\perp}). \tag{3.48}$$

Equation (3.48) is in a particularly appealing form because there are no integrations except for those implicitly involved in calculating the function F. The physical interpretation of the arguments $\Delta \mathbf{k}_{ab\perp}$ and $\mathbf{k}_{ab\perp}$ of F has been discussed in Section 3.2.2. In particular, we want to stress that the offset $H_a \mathbf{s}_{oa\perp} - H_b \mathbf{s}_{ob\perp}$, due to changing the angle of incidence, is the lateral shift in coordinates in the multiplication of R_{t_1} and R_{t_2} in Eq. (3.30). As we will see In Section 3.3.2, R_{t_1} and R_{t_2} for strong diffusers will approach zero as the offset $\mathbf{r}$ increases. Thus Eq. (3.30) for F can be made to approach zero for strong diffusers by increasing the offset so that R_{t_1} and R_{t_2} do not overlap. If F approaches zero, then u_{ab} will also approach zero by Eq. (3.48). Hence the speckle pattern will become uncorrelated.

3.2.6 Special Limiting Forms of u_{ab}

By allowing $a \to b$ in Eq. (3.48), we can also immediately determine the angular dependence of the radiation pattern $<I_a>$ from a cascade of two diffusers:

$$<I_a> = u_{aa} = \left(\frac{k_a}{2\pi}\right)^2 \cos^2\theta_a \, F(0; k_a, k_a; \mathbf{k}_{a\perp} - \mathbf{k}_{oa\perp}; 0). \tag{3.49}$$

Written in terms of R_{t_1}, R_{t_2}, and $\check{A}$, Eq. (3.49) becomes

$$<I_a> = \left(\frac{k_a}{2\pi}\right)^2 \cos^2\theta_a \int R_{t_1}(\mathbf{r}; k_a, k_a) R_{t_2}(\mathbf{r}; k_a, k_a) \, \check{A}(\mathbf{r}; 0) \exp\left[i\left(\mathbf{k}_{a\perp} - \mathbf{k}_{oa\perp}\right) \bullet \mathbf{r}\right] d^2\mathbf{r}. \tag{3.50}$$

It is significant that there is no dependence on the spacing H in Eq. (3.50). Furthermore,

by applying the convolution theorem to express the Fourier transform of a product as the convolution of the Fourier transform of the factors, we see that $<I_a>$ for two diffusers in tandem is essentially the convolution of the patterns from the individual diffusers.

We also note that if the roughness of one of the diffusers is set to zero, then R_t for that diffuser will be unity. In this case, Eq. (3.50) reduces to the radiation pattern from a single diffuser as expected:

$$<I_a> = \left(\frac{k_a}{2\pi}\right)^2 \cos^2\theta_a \int R_t(\mathbf{r};k_a,k_a) \; \check{A}(\mathbf{r};0) \; \exp\left[i\left(\mathbf{k}_{a\perp} - \mathbf{k}_{oa\perp}\right)\bullet\mathbf{r}\right] d^2\mathbf{r}. \qquad (3.51)$$

For completeness we also list the general form of u_{ab} that results from a single diffuser. This limiting form is obtained by setting $H_a = H_b = 0$ in Eq. (3.48) and setting R_t to unity for one of the diffusers. This leaves us with the angle and wavelength dependence of speckle from a single thin diffuser:

$$u_{ab} = \frac{k_a k_b}{\left(2\pi\right)^2} \exp\left(-i\phi_{ab}\right) \cos\theta_a \cos\theta_b$$

$$\times \int R_t(\mathbf{r};k_a,k_b) \; \check{A}(\mathbf{r};\Delta\mathbf{k}_{ab\perp}) \exp\left(i\,\mathbf{k}_{ab\perp}\bullet\mathbf{r}\right) d^2\mathbf{r}. \qquad (3.52)$$

3.2.7 U_{ab} for an Arbitrary Plane-Wave Transmission Function

Thus far in Section 3.2 we have calculated u_{ab} for the double-diffuser geometry shown in Fig. 3.1. In this section we derive the expression for u_{ab} for an arbitrary plane-wave transmission function $t(\mathbf{r};\mathbf{k}_0)$ that represents propagation between planes I and II in Fig. 3.1. By applying Eq. (2.4) we obtain the output complex amplitude v_{2+} at plane II, including the effect of the aperture a, that arises from an input plane wave with wave vector $\mathbf{k}_0$:

$$v_{2+}(\mathbf{r};\mathbf{k}_0) = \exp\left(-i\mathbf{k}_{0\perp}\bullet\mathbf{r}\right) t(\mathbf{r};\mathbf{k}_0) a(\mathbf{r}). \qquad (3.53)$$

The expression for the complex amplitude $v(\mathbf{k}_0;\mathbf{k})$ in the far-zone of the aperture a that corresponds to Eq. (3.17) is obtained by applying the far-zone impulse response given in Eq. (3.16):

$$v(\mathbf{k}_0;\mathbf{k}) = \frac{ik}{2\pi R} \exp\left(-ik\,R\right)\cos\theta$$

$$\times \int t(\mathbf{r};\mathbf{k}_0)\,a(\mathbf{r})\,\exp\left[-i\left(\mathbf{k}_{0\perp} - \mathbf{k}_\perp\right)\bullet\mathbf{r}\right]d^2\mathbf{r}. \tag{3.54}$$

Equation (3.54) could be generalized to include a functional dependence on one or more additional parameters of the transmission function, e.g., the H dependence of the plane-wave transmission function t given in Eq. (3.18) could be shown explicitly as $t(H;\mathbf{r};\mathbf{k}_0)$ so that decorrelation with respect to this variable could also be analyzed. The general expression for u_{ab} that corresponds to Eq. (3.19) for a cascade of two diffusers is

$$u_{ab} = \frac{k_a k_b}{\left(2\pi\right)^2}\,\frac{1}{A_0^{\,2}}\exp\left[-iR\left(k_b - k_a\right)\right]\cos\theta_a\cos\theta_b$$

$$\times \int\int R_{t_{12}}(\mathbf{r}_2 - \mathbf{r}_1;\mathbf{k}_{oa};\mathbf{k}_{ob})\,a^*(\mathbf{r}_1)\,a(\mathbf{r}_2)$$

$$\times \exp\left\{i\left[\left(\mathbf{k}_{oa\perp} - \mathbf{k}_{a\perp}\right)\bullet\mathbf{r}_1 - \left(\mathbf{k}_{ob\perp} - \mathbf{k}_{b\perp}\right)\bullet\mathbf{r}_2\right]\right\}d^2\mathbf{r}_1\,d^2\mathbf{r}_2, \tag{3.55}$$

where

$$R_{t_{12}}(\mathbf{r};\mathbf{k}_{oa};\mathbf{k}_{ob}) = \,<t^*(\mathbf{r}';\mathbf{k}_{oa})\,t(\mathbf{r}+\mathbf{r}';\mathbf{k}_{ob})>. \tag{3.56}$$

is the two-state correlation function of the plane-wave transmission function for propagation between planes I and II.

By making the substitutions

$$\mathbf{r}_1 = \mathbf{r}' - \frac{\mathbf{r}}{2} \tag{3.57a}$$

and

$$\mathbf{r}_2 = \mathbf{r}' + \frac{\mathbf{r}}{2}, \tag{3.57b}$$

and recalling the definitions of the normalized aperture ambiguity function $\bar{A}$ in Eq. (3.23), the speckle-tracking wave vector $\Delta\mathbf{k}_{ab\perp}$ in Eq. (3.25), and the Fourier-transform wave vector $\mathbf{k}_{ab\perp}$ in Eq. (3.26), we can simplify Eq. (3.55) to

$$u_{ab} = \frac{k_a k_b}{(2\pi)^2} \exp\left[-iR\left(k_b - k_a\right)\right] \cos\theta_a \cos\theta_b$$

$$\times \int R_{t_{12}}(\mathbf{r};\mathbf{k}_{oa};\mathbf{k}_{ob})\, \hat{A}(\mathbf{r};\Delta\mathbf{k}_{ab\perp})\exp\left(i\,\mathbf{k}_{ab\perp}\bullet\mathbf{r}\right)d^2\mathbf{r}. \tag{3.58}$$

Note the similarity between Eq. (3.58) for u_{ab} for a plane-wave diffuser transmission function and Eq. (3.52) for a thin diffuser transmission function. The essential difference is that the wave numbers k_a and k_b in the arguments of R_t are generalized to $\mathbf{k}_{oa}$ and $\mathbf{k}_{ob}$ in the arguments of $R_{t_{12}}$. Of course, Eq. (3.47) could also have been derived by calculating $R_{t_{12}}(H_a, H_b; \mathbf{r}; \mathbf{k}_{oa}; \mathbf{k}_{ob})$ from Eq. (3.18) for $t(H; \mathbf{r}; \mathbf{k}_o)$ and then substituting $R_{t_{12}}$ into Eq. (3.58).

3.3 Two-State Correlation of a Transmission Function

Equation (3.45) is a general expression for u_{ab} in terms of F, which in turn depends on R_{t_1} and R_{t_2}. In order to study how the decorrelation of speckle is affected by different types of diffusers, we must calculate u_{ab} for various functional forms of R_{t_1} and R_{t2}. Of course, the functions chosen for R_{t_1} and R_{t_2} must satisfy certain mathematical properties in order to be valid correlation functions.[9] For example, we know that the Fourier transform of an autocorrelation function must be non-negative. We can see that this is so by referring to Eq. (3.51) for the far-zone intensity pattern from a single diffuser: In Eq. (3.51) $k_a = k_b$ so that R_t is the autocorrelation function of the transmission function with respect to the offset $\mathbf{r}$. We can cause the aperture ambiguity function $\hat{A}(\mathbf{r};0)$ in Eq. (3.51) to be very wide compared to $R_t(\mathbf{r};k,k)$ by increasing the width of the aperture so that $\hat{A}(\mathbf{r};0)$ can be replaced by $\hat{A}(0;0) = 1$. Then the Fourier transform of R_t is essentially the far-zone intensity $<I_a>$, which, of course, is non-negative.

Equation (3.51) is very important because it provides a simple method for determining R_t for the individual diffusers.[10] For example, if R_t is circularly symmetric,

i.e., if it only depends on **r** through its magnitude $|\mathbf{r}|$, and if the illumination is normally incident, then the radiation pattern $<I_a>$ will also be circularly symmetric with respect to the z-axis. It follows that R_t can be obtained by measuring $<I_a>$ as a function of θ in one plane $\phi = \phi_0$ and then calculating the Fourier-Bessel transform numerically.

3.3.1 Phase-Type Transmission Functions

In evaluating Eq. (3.47) for u_{ab}, given the functional form of R_{t_1} and R_{t_2}, one could consider transmission functions that change both the magnitude and the phase of the incoming illumination. However, here we will be concerned with phase-only diffusers as represented by the transmission function in Eq. (3.6). By substituting Eq. (3.6) into Eq. (3.7) we obtain

$$R_t(\mathbf{r}_2 - \mathbf{r}_1; k_a, k_b) = <\exp\left[i\left(\eta_a h_1 - \eta_b h_2\right)\right]> , \qquad (3.59)$$

where

$$\eta = k\,(n-1). \qquad (3.60)$$

In Eq. (3.59) we also use the notation $\eta_a = \eta(k_a)$, $\eta_b = \eta(k_b)$, $h_1 = h(\mathbf{r}_1)$, and $h_2 = h(\mathbf{r}_2)$. Equation (3.59) is convenient for statistical calculations because the right-hand side is just the joint characteristic function of the bivariate probability distribution function $P_2(h_1, h_2; \mathbf{r}_1, \mathbf{r}_2)$ of the height profile of the diffuser surface.

3.3.2 Normally Distributed Diffuser Height Profile

For definiteness in the following analysis, we will assume that the diffuser height profile obeys a jointly normal distribution. Then evaluation of the joint characteristic function yields the following well known relationship between R_t and R_h:

$$R_t(\mathbf{r}; k_a, k_b) = \exp\left[-\frac{\sigma_h^2}{2}\left(\eta_a^2 - 2R_h(\mathbf{r})\,\eta_a\eta_b + \eta_b^2\right)\right]. \qquad (3.61)$$

It is very useful to factor this expression in the form[11]

$$R_t(\mathbf{r}; k_a, k_b) = \exp\left[-\frac{\sigma_h^2}{2}\left(\eta_b - \eta_a\right)^2\right]\exp\left[-\sigma_h^2\,\eta_a\eta_b\left(1 - R_h(\mathbf{r})\right)\right]. \qquad (3.62)$$

The first exponential in Eq. (3.62) contains the essential wavelength dependence of the

diffuser, while the second exponential contains the dependence on the correlation function R_h. Written in terms of the wave number k and the effective rms roughness σ_t, Eq. (3.62) becomes

$$R_t(\mathbf{r};k_a,k_b) = \exp\left[-\frac{\sigma_t^2}{2}\left(k_b-k_a\right)^2\right]\exp\left[-k_a k_b \sigma_t^2\left(1-R_h(\mathbf{r})\right)\right]. \qquad (3.63)$$

At this point one could substitute any valid autocorrelation function for R_h into Eq. (3.63). However, it will be instructive to consider two limiting cases that depend on the degree of roughness of the diffuser: If $k_a k_b \sigma_t^2 = S_a S_b << 1$, i.e., if the diffuser is very weak and hence passes most of the direct beam, then Eq. (3.63) reduces to

$$R_t(\mathbf{r};k_a,k_b) \approx 1 - \frac{\sigma_t^2}{2}\left(k_a^2+k_b^2\right) + k_a k_b \sigma_t^2 R_h\left(\mathbf{r}\right). \qquad (3.64)$$

In Equation (3.64) we note that R_t can drop only slightly from its initial value of unity that occurs at $\mathbf{r}=0$ and $k_a=k_b$. For example, if R_h is zero outside of a certain region, then R_t is represented by the first two terms in Eq. (3.64) in that region. In terms of the roughness parameters S_a and S_b, this drop is $(S_a^2+S_b^2)/2$, which is small compared with unity by the assumption of small roughness.

If $k_a k_b \sigma_t^2 >> 1$, i.e., if the diffuser is rough compared to the wavelength λ, and if $R_h(\mathbf{r})$ is circularly symmetric, then there are two important subcases to consider that depend on the behavior of $R_h(\mathbf{r})$ for small values of the offset parameter $|\mathbf{r}|$:[1,10]

If $R_h(\mathbf{r})$ can be expanded in a power series such that

$$R_h(\mathbf{r}) = 1 - \frac{|\mathbf{r}|}{w} + \dots, \qquad (3.65)$$

then R_h is cone shaped for small values of $|\mathbf{r}|$. Since the behavior of R_t is dominated by the functional form of R_h for small offsets when $k_a k_b \sigma_t^2 >> 1$, we can approximate R_t by substituting the first two terms of the expansion in Eq. (3.65) into Eq. (3.63). Following this procedure, we find that the $|\mathbf{r}|$ dependence is a decaying exponential:

$$R_t(\mathbf{r};k_a,k_b) = \exp\left[-\frac{\sigma_t^2}{2}\left(k_b-k_a\right)^2\right]\exp\left[-k_a k_b \sigma_t^2 \frac{|\mathbf{r}|}{w}\right]. \qquad (3.66)$$

The second subcase for very rough diffusers occurs when the linear term in Eq.

(3.65) is absent and R_h is shaped like a paraboloid for small offsets $|\mathbf{r}|$:

$$R_h(\mathbf{r}) = 1 - \left(\frac{|\mathbf{r}|}{w}\right)^2 + \ldots .$$
(3.67)

In this case R_t is approximated as a Gaussian:

$$R_t(\mathbf{r};k_a,k_b) = \exp\left[-\frac{\sigma_t^2}{2}\left(k_b - k_a\right)^2\right] \exp\left[-k_a k_b \sigma_t^2 \frac{|\mathbf{r}|^2}{w^2}\right].$$
(3.68)

Unlike Eq. (3.64), where there was little drop from the initial value of R_t, Eqs. (3.66) and (3.68) rapidly approach zero for large values of r. As a result, the decorrelation effects arising from diffuse scattering are more pronounced when the diffusers are rough compared to the wavelength of the incident light. Therefore, Eqs. (3.66) and (3.68) will be very important in the calculation of the decorrelation of speckle from cascaded diffusers. We will refer to diffusers having autocorrelation functions R_t given by Eqs. (3.66) and (3.68) as conical, C, and paraboloidal, P, diffusers, respectively.

In comparing Eq. (3.66) for the conical correlation function with Eq. (3.68) for the paraboloidal correlation function, we note that the effective correlation lengths scale differently with wave number k and roughness σ_t, i.e., for the conical correlation function, the effective correlation length is

$$w_c = \frac{w}{k_a k_b \sigma_t^2} = \frac{w}{S_{ab}^2},$$
(3.69)

but, for the paraboloidal correlation function, it is

$$w_p = \frac{w}{\sqrt{k_a k_b}\,\sigma_t} = \frac{w}{S_{ab}}.$$
(3.70)

The quantity σ_t/w in Eq. (3.70) for a paraboloidal diffuser is closely related to the rms surface slope, which can be shown to be $2\sigma_h/w$.

The texture of the rough surface controls the functional form of R_h for small offsets. For example, when Eq. (3.65) applies, the surface is very jagged, but when Eq. (3.67) applies, it is bandlimited in spatial frequency. In Chapter 5 we show that the angular distribution of intensity from ground-glass and etched-glass diffusers can be derived by using Eq. (3.65) and Eq. (3.67) to represent R_h, respectively.

3.4 Two-State Correlation of Intensity

Since one would ordinarily measure intensity rather than complex amplitude in a speckle experiment, we will now consider the correlation function

$$<I_a I_b> = \frac{R^4}{A_o^4} <v_a v_a^* v_b v_b^*> \qquad (3.71)$$

between states a and b of the output speckle intensity.

3.4.1 General Complex Gaussian Statistics

In general, one can not deduce the fourth-order moment $<I_a I_b>$ of the complex amplitude v given u_{ab}. However, if we assume that the output aperture a is large enough to contain many independent scattering cells of the transmission function t_2, then, by the central limit theorem, the real and imaginary parts of the complex amplitude v will be normally distributed. We make no assumptions about whether the complex random process is circular or whether the real and/or imaginary parts have zero means.[12-15] The conditions that must be satisfied in order to be able to make these simplifications will be established naturally in the following analysis.

We note that the fact that v obeys complex Gaussian statistics is consistent with the results of O'Donnell.[16] His conclusion, that the fluctuations of far-zone speckle intensity for doubly scattered light are stronger than those for Gaussian speckle, is valid when there are a small number of speckles incident on the second scatterer. For example, if the area of the speckle incident on the second diffuser is comparable with the area of the diffuser aperture, and the speckle pattern is dark over the region within the aperture, then the intensity of the whole output speckle pattern would drop. This phenomenon does not occur in the system shown in Fig. 3.1 because there is no limiting aperture on the input plane wave to increase the speckle size at plane II. In addition, we assume that the output aperture is large compared to the wavelength of light and to the correlation length of the diffuser.

By applying the Gaussian moment theorem for a non-circular, non-zero-mean complex Gaussian random process, see Appendix A, we arrive at the following expansion for the two-state correlation function of intensity:

$$<I_a I_b> = u_{aa}u_{bb} + |u_{ab}|^2 + |u_{ab}^\ddagger|^2 - 2\,u_a u_b,\qquad (3.72)$$

where

$$u_{ab}^\ddagger = \frac{R^2}{A_0^{\,2}} <v(H_a;\mathbf{k}_{oa};\mathbf{k}_a)v(H_b;\mathbf{k}_{ob};\mathbf{k}_b)>,\qquad (3.73)$$

and

$$u_a = \frac{R^2}{A_0^{\,2}}\, |<v(H_a;\mathbf{k}_{oa};\mathbf{k}_a)>|^2.\qquad (3.74)$$

Equations (3.73) and (3.74) are defined in analogy with Eq. (3.2) for u_{ab}. In Sections 3.4.2 through 3.4.4 we will derive expressions for the last two terms of Eq. (3.72) and find the conditions under which these terms may be neglected. When these conditions hold we have the usual result for zero-mean complex circular Gaussian speckle:

$$\frac{<I_a I_b>}{<I_a><I_b>} = 1 + \frac{|u_{ab}|^2}{u_{aa}u_{bb}}.\qquad (3.75)$$

3.4.2 Non-Circular Component

By slightly modifying the derivation of u_{ab} in Eq. (3.31), we obtain an analogous expression for the non-circular component $u_{ab}^\ddagger$ of Eq. (3.72):

$$u_{ab}^\ddagger = \frac{k_a k_b}{(2\pi)^2}\exp\left(-i\phi_{ab}^\ddagger\right)\cos\theta_a\cos\theta_b \int B\left(\mathbf{r};\mathbf{k}_{oa\perp}+\mathbf{k}_{ob\perp};-\frac{k_a}{H_a},\frac{k_b}{H_b}\right)$$

$$\times F^\ddagger(\mathbf{r};k_a,k_b;-\tfrac{1}{2}\Delta\mathbf{k}_{ab\perp};-2\mathbf{k}_{ab\perp})\exp\left[-\frac{i}{2}\left(\mathbf{k}_{ob\perp}-\mathbf{k}_{oa\perp}\right)\bullet\mathbf{r}\right]d^2\mathbf{r},\qquad (3.76)$$

where

$$\phi_{ab}^\ddagger = k_a H_a + k_b H_b + \left(k_a + k_b\right)R.\qquad (3.77)$$

In Eq. (3.76), B is as defined in Eq. (3.24). We note that the arguments of B in Eq. (3.76) are obtained from those in Eq. (3.31) by changing k_a to $-k_a$. This is a direct consequence

of not having a complex conjugate on the first Fresnel kernel for state a. In Eq. (3.76) we also define $F^{\ddagger}$ in a manner similar to F in Eq. (3.30):

$$F^{\ddagger}(\mathbf{r};k_a,k_b;\Delta\mathbf{k}_{\perp};\mathbf{k}_{\perp}) = \int R^{\ddagger}_{t_1}(\mathbf{r}+\mathbf{r}';k_a,k_b) \; R^{\ddagger}_{t_2}(\mathbf{r}';k_a,k_b)$$

$$\times \; \tilde{A}^{\ddagger}(\mathbf{r}';\mathbf{k}_{\perp}) \exp\left(i\Delta\mathbf{k}_{\perp}\bullet\mathbf{r}'\right) d^2\mathbf{r}' . \tag{3.78}$$

The $\ddagger$ symbol denotes that there is no complex conjugate on the first factor, i.e., that

$$R^{\ddagger}_{t}(\mathbf{r}_b-\mathbf{r}_a;k_a,k_b) = <t(\mathbf{r}_a,k_a)t(\mathbf{r}_b,k_b)> , \tag{3.79}$$

and

$$\tilde{A}^{\ddagger}(\mathbf{r};\mathbf{k}_{\perp}) = \frac{1}{A_0^2}\int a(\mathbf{r}'-\frac{\mathbf{r}}{2})\, a(\mathbf{r}'+\frac{\mathbf{r}}{2}) \exp\left(-i\mathbf{k}_{\perp}\bullet\mathbf{r}'\right) d^2\mathbf{r}'. \tag{3.80}$$

The general expression for $u^{\ddagger}_{ab}$ is obtained by substituting Eq. (3.44) for B into Eq. (3.76):

$$u^{\ddagger}_{ab} = -i\frac{k_a^2 k_b^2}{(2\pi)^3}\frac{\exp\left(-i\phi^{\ddagger}_{ab}\right)}{k_b H_a + k_a H_b}\exp\left(\frac{i}{2}\frac{H_a H_b}{k_b H_a + k_a H_b}\,|\mathbf{k}_{oa\perp}+\mathbf{k}_{ob\perp}|^2\right)\cos\theta_a\,\cos\theta_b$$

$$\times\int F^{\ddagger}(\mathbf{r};k_a,k_b;-\tfrac{1}{2}\Delta\mathbf{k}_{ab\perp};-2\mathbf{k}_{ab\perp})$$

$$\times\exp\left\{-i\frac{k_a k_b}{k_b H_a + k_a H_b}\left[\frac{1}{2}\,|\mathbf{r}|^2+\left(H_b\mathbf{s}_{ob\perp}-H_a\mathbf{s}_{oa\perp}\right)\bullet\mathbf{r}\right]\right\} d^2\mathbf{r}. \tag{3.81}$$

We note that the 'enominator, $k_b H_a + k_a H_b$, is non-zero unless $H_a = H_b = 0$. Therefore, there is no delta function form of B corresponding to Eq. (3.46).

We pause to compare the functions R_{t_1}, R_{t_2}, and $\tilde{A}$ in the definition of F in Eq. (3.30) with the functions $R^{\ddagger}_{t_1}$, $R^{\ddagger}_{t_2}$, and $\tilde{A}^{\ddagger}$ in the definition of $F^{\ddagger}$ in Eq. (3.78). First, we note that $\tilde{A}^{\ddagger} = \tilde{A}$ when the aperture function a is real. Similarly, $R^{\ddagger}_{t_1} = R_{t_1}$ and $R^{\ddagger}_{t_2} = R_{t_2}$ for a magnitude-only transmission function. On the other hand, if the functions a, t_1, and t_2 are complex, then the regular and the daggered functions can behave very differently.

For a phase-type transmission function, there is a simple relationship between R_t and $R^{\ddagger}_t$; it is obtained by changing the sign on the k_a variable:

$$R^{\ddagger}_t(\mathbf{r};k_a,k_b) = R_t(\mathbf{r};-k_a,k_b).$$ (3.82)

Thus, Eq. (3.63) is modified to read

$$R^{\ddagger}_t(\mathbf{r};k_a,k_b) = \exp\left[-\frac{\sigma_t^2}{2}\left(k_b+k_a\right)^2\right]\exp\left[k_a k_b \sigma_t^2\left(1-R_h(\mathbf{r})\right)\right].$$ (3.83)

Whereas R_t is an autocorrelation function, and hence drops from its maximum value of unity that occurs at zero offset and at $k_a = k_b$, the function $R^{\ddagger}_t$ is not an autocorrelation function, and it increases from an initial value that is less than unity. Furthermore, since R_h approaches zero for large values of the offset parameter, R_t and $R^{\ddagger}_t$ have the same asymptote:

$$R_t(\infty;k_a,k_b) = R^{\ddagger}_t(\infty;k_a,k_b) = \exp\left[-\frac{\sigma_t^2}{2}\left(k_a^2+k_b^2\right)\right].$$ (3.84)

In Fig. 3.3 we compare the behavior of $R_t(\mathbf{r};k,k)$ and $R^{\ddagger}_t(\mathbf{r};k,k)$ vs $\mathbf{r}$ for

$$R_h(\mathbf{r}) = \exp\left(-\frac{|\mathbf{r}|^2}{w^2}\right)$$ (3.85)

and for various values of S. We note that $R^{\ddagger}_t$ becomes negligible for all values of its offset argument as S increases. Thus $F^{\ddagger}$, and hence $u^{\ddagger}_{ab}$, can be ignored for large values of S. In Section 3.4.4 we will further discuss the relative sizes of the different terms in Eq. (3.72).

In addition to the difference in behavior between the regular and the daggered functions, we notice the following very important difference between F and $F^{\ddagger}$ as they occur in Eqs. (3.47) and (3.81), respectively: The order of $\Delta k_{ab\perp}$ and $k_{ab\perp}$ is switched in the argument list. Hence, it is $k_{ab\perp}$ rather than $\Delta k_{ab\perp}$ that occurs as the wave vector in the second argument of $\hat{A}^{\ddagger}$. Since $a(\mathbf{r})$ is ordinarily a simple aperture, and hence a real function, $\hat{A}$ and $\hat{A}^{\ddagger}$ will be equivalent in many cases. We have already identified the width of $\hat{A}$ with respect to the wave vector as the average size of the speckle, and we know that this size is the same as the size of the direct or the specular component of the
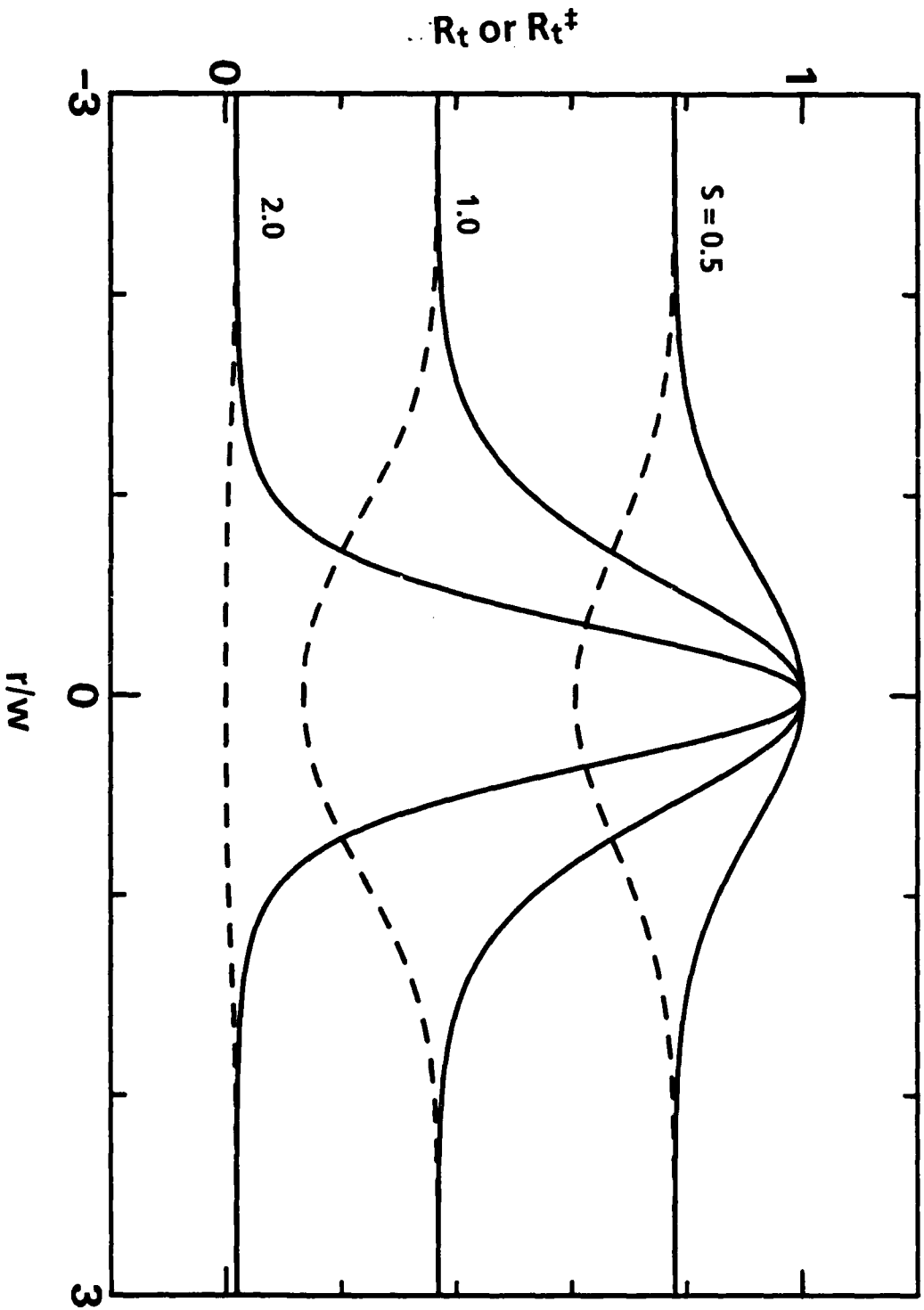
Fig 3.3. Dependence of Eq. (3.63) for R_t, solid lines, and Eq. (3.83) for $R_t^{\ddagger}$, dashed lines, on the offset r for Gaussian R_h, Eq. (3.85), and for roughness S of 0.5, 1.0, and 2.0.

radiation pattern. In Eq. (3.47) for u_{ab}, one would ordinarily set $\Delta k_{ab\perp}$ to zero to track the speckle motion at the output. However, since it is $k_{ab\perp}$ that occurs as the wave vector argument of $\tilde{A}^{\ddagger}$, and $\tilde{A}^{\ddagger}$ is usually very narrow with respect to this argument, we can cause the $u^{\ddagger}{}_{ab}$ term in Eq. (3.72) to be negligible simply by observing in a direction different from that of the input plane wave!

In the above discussion we have seen that the behavior of the function $u^{\ddagger}{}_{ab}$ is quite different from that of the correlation function u_{ab}: Whereas $|u_{ab}|/u_{aa}$ has a maximum value of unity when $a{\to}b$, the maximum value of $|u^{\ddagger}{}_{ab}|/u_{aa}$ is negligible when S is large or when we observe in a direction away from the direction of the input plane wave. In Section 3.4.4 we will see how large S must be for us to be able to observe at $k_{ab\perp}=0$ and still ignore the $u^{\ddagger}{}_{ab}$ term in Eq. (3.72).

3.4.3 Expected Value of Far-Zone Complex Amplitude

We now derive an expression for the final term in Eq. (3.72). We can write the expected value of the far-zone complex amplitude by making the following argument: Since the random processes t_1 and t_2 are stationary, the expected values $<t_1(r{:}k)>$ and $<t_2(r{:}k)>$ are independent of the position r and can be factored out of the integrals in Eq. (3.17). What remains within the r′ integral is a Fresnel-zone approximation to propagation of a plane wave between planes I and II. Instead of using this approximation, we will calculate the exact propagation by multiplying the input plane wave by the complex exponential $\exp(-ik_z H)$. Thus,

$$<v(H;k_o;k)> = \frac{ik}{2\pi R} \exp\left(-ikR\right) \exp\left(-ik_z H\right) \cos\theta$$

$$\times <t_1(0;k)> <t_2(0;k)> A(k_{o\perp} - k_{\perp}),\tag{3.86}$$

where $A(k_{\perp})$ is the two-dimensional Fourier transform of the aperture function $a(r)$:

$$A(k_{\perp}) = \int a(r)\exp\left(-i k_{\perp}\bullet r\right) d^2 r.\tag{3.37}$$

The resulting general form of u_a is

$$u_a = \frac{k_a^{\ 2}}{\left(2\pi\right)^2} \cos^2\theta_a \frac{1}{A_o^{\ 2}} \left| <t_1(0;k_a)> \ <t_2(0;k_a)> \ A(\mathbf{k}_{oa\perp} - \mathbf{k}_{a\perp}) \right|^2 . \tag{3.88}$$

Since $|A|^2$ is essentially the far-zone radiation pattern for plane wave illumination of the aperture, and the angular spread of this pattern is usually small, we see that $2u_au_b$ in Eq. (3.72), in addition to $|u^{\ddagger}_{ab}|^2$, are negligible compared to the other terms if the observation point is not in the direction of the input plane wave.

We point out that $<t(0;\mathbf{k})>$ for the phase-only transmission function defined in Eq. (3.6) can be written in terms of R_t of Eq. (3.59) by setting the offset and the first k parameter to zero. This reduces R_t from a bivariate characteristic function to a univariate characteristic function:

$$<t(0;k)> = R_t(0;0,k) . \tag{3.89}$$

3.4.4 Relative Size of Terms

As discussed in Sections 3.4.2 and 3.4.3, the terms $|u^{\ddagger}_{ab}|$ and u_au_b in Eq. (3.72) have their maximum values when $\mathbf{k}_{ab\perp} = 0$, and they fall off rapidly when $\mathbf{k}_{ab\perp}$ points in a direction that is a few speckles away from the direct beam. Thus these terms are only important over a small region centered about $\mathbf{k}_{ab\perp} = 0$. However, in some applications it is desirable to use small values of $\mathbf{k}_{ab\perp}$, e.g., the analytical expressions may be much simpler to evaluate and to use if $\mathbf{k}_{ab\perp} = 0$. We now find the conditions on how large S must be for Eq. (3.75) to hold when $\Delta\mathbf{k}_{ab\perp} = \mathbf{k}_{ab\perp} = 0$. For simplicity we let $a \rightarrow b$, and we use Eq. (3.38) for $\hat{A}(\mathbf{r};\mathbf{k}_\perp)$. In addition, we assume that $S >> 1$ so that Eq. (3.68) holds for R_t and that R_h approaches zero for large arguments so that Eq. (3.84) holds for $R^{\ddagger}_t$, outside of a small region around the origin. We will also assume that the effective correlation lengths w_p in Eq. (3.70) are the same for both diffusers. In comparing the size of the terms in Eq. (3.72) it is convenient to normalize by dividing each term by $u_{aa}u_{bb}$, the product of the average intensities for the two states. Thus, the first term will have a constant value of unity and the second term will have a maximum value of unity when

$a \rightarrow b$. The result of the calculation for the maximum values of the remaining two terms is

$$\frac{u_a^2}{u_{\alpha\alpha}^2} = \frac{|u_{\alpha a}^{\ddagger}|^2}{u_{\alpha\alpha}^2} = \left(\frac{2w_a}{w_p}\right)^4 \exp\left(-4S^2\right). \tag{3.90}$$

As a numerical example, if $w_a = 1000\,\mu$ and $w_p = 1\,\mu$, then S must be greater than or equal to 2.96 for each term to contribute less than 0.01. By comparison, the maximum value of the first two terms is 2.0. If S is increased to 4, then this error plunges to 2.6×10^{-15}. Equation (3.90) serves as a guideline for determining when Eq. (3.75) can be used at any observation position, i.e., when it can be used even at $k_{ab\perp} = 0$.

3.5 Remote Sensing of the Spacing between an Aperture and a Diffuser

The results thus far in Chapter 3 have been quite general in that we have not specified the type of diffuser or the functional form of the aperture. A calculation of $<I_a I_b>$ for a specific type of diffuser will be presented in Chapter 4, where we will gain a much better understanding of the interrelationship between the various parameters that cause decorrelation of the speckle pattern. Before closing this chapter, however, we wish to point out an interesting subcase of the analysis that does not require knowledge of the specific functional form of R_t, that of the remote sensing of the spacing between an aperture and a diffuser.

We obtain the above limit by removing diffuser D_2 in Fig. 3.1. In the theory, this is accomplished simply by setting R_{t_2} equal to unity in Eq. (3.30) for F. If diffuser D_1 is strong, i.e., if $S_1 >> 1$, then R_{t_1} approaches zero as r increases. Since the aperture function a is usually very wide compared with R_{t_1}, the spatial dependence of the aperture ambiguity function $\hat{A}$ will also be wide compared with R_{t_1}. Hence, we can evaluate $\hat{A}$ at the point $r' = -r$ where R_{t_1} is maximum and then factor $\hat{A}$ from the integral. After shifting the variable of integration to also remove r from the integral, we obtain

$$F(\mathbf{r};k_a,k_b;\mathbf{k}_{ab\perp};\Delta\mathbf{k}_{ab\perp}) \approx \dot{A}(-\mathbf{r};\Delta\mathbf{k}_{ab\perp})\exp\left(-i\,\mathbf{k}_{ab\perp}\bullet\mathbf{r}\right)$$

$$\times \int R_{t_1}(\mathbf{r}';k_a,k_b)\,\exp\left(i\,\mathbf{k}_{ab\perp}\bullet\mathbf{r}'\right)\,d^2\mathbf{r}'. \tag{3.91}$$

Equation (3.91) for F can then be substituted into Eq. (3.47) and evaluated for a given aperture function.

For angular decorrelation only, we obtain a particularly useful result. Since $k_a = k_b$ and $H_a = H_b$, we can use the simplified expression given in Eq. (3.48) for u_{ab}. Then, if Eq. (3.75) also applies, and if we require that the tracking conditon $\Delta\mathbf{k}_{ab\perp} = 0$ is satisfied, then the two-state correlation of intensity is

$$\frac{<I_a I_b>}{<I_a><I_b>} = 1 + |\dot{A}(H\mathbf{s}_{ob\perp} - H\mathbf{s}_{oa\perp};0)|^2. \tag{3.92}$$

Equation (3.92) does not contain any integrations, except for the implicit integration involved in calculating the aperture ambiguity function from the aperture function. In addition, Eq. (3.92) does not depend on the functional form of R_{t_1} but only on the fact that R_{t_1} is a narrow function compared with $\dot{A}$.

From Eq. (3.92) we see that one can determine the spacing between a diffuser and an aperture, given the aperture function $a(\mathbf{r})$, by observing the speckle pattern as the angle of illumination is changed. A practical implementation of the experiment is to illuminate the diffuser at normal incidence, $\mathbf{s}_{oa\perp} = 0$, and to observe the speckle in the same direction as the input plane wave as the diffuser and aperture rotate as a unit about the center of the aperture. In this configuration $\mathbf{k}_{ab\perp} = 0$ and the tracking condition, $\Delta\mathbf{k}_{ab\perp} = 0$, is automatically satisfied. We note, however, that Eq. (3.92) does apply for arbitrary values of $\mathbf{k}_{ab\perp}$. For a circular aperture of radius w_a, we substitute Eq. (3.40) for the autocorrelation function of the circular aperture into Eq. (3.92) and obtain the normalized two-state correlation function of intensity

$$\frac{<I_a I_b>}{<I_a><I_b>} = 1 + \frac{4}{n^2}\,\text{circ}(\xi)\left(\cos^{-1}\xi - \xi\sqrt{1-\xi^2}\right)^2. \tag{3.93}$$

We define ξ in Eq. (3.93) by the expression

$$\xi = \frac{H\sin\Delta\theta}{2w_a},$$ (3.94)

and we note that $\sin\Delta\theta = |s_{ob\perp}|$.

Equation (3.93) is plotted in Fig. 3.4. We see that the function has a maximum value of two and a minimum value of one, and that it is cone shaped for small offsets ξ. In determing H from experimental data, it is convenient to find the value of ξ in Eq. (3.93) by comparing the experimental and theroetical curves for small values of ξ. The power series expansion for Eq. (3.40) is

$$\frac{2}{\pi}\left(\cos^{-1}\xi - \xi\sqrt{1-\xi^2}\right) = 1 + \frac{4}{\pi}\left[-\xi + \frac{1}{6}\xi^3 + \sum_{n=2}^{\infty}\frac{(2n-3)!!\,\xi^{2n+1}}{2^2 n!\,(2n+1)}\right]$$ (3.95)

for $0 \leq \xi \leq 1$. In Eq. (3.95) we make use of the double-factorial notation $n!! = n\,(n-2)\,(n-4)\ldots5.3.1$. Thus we can write the first two terms of the series expansion for Eq. (3.93) as

$$\frac{<I_a I_b>}{<I_a><I_b>} = 2 - \frac{4}{\pi w_a}H\sin\Delta\theta + \ldots$$ (3.96)

Equation (3.96) is plotted as the dashed line in Fig. 3.4. It is very useful for determining H, given w_a, from the slope of the two-state correlation function near the origin with respect to angular detuning $\Delta\theta$.

3.6 Summary and Conclusions

In Chapter 3 we have analyzed the general problem of decorrelation of speckle from a cascade of two parallel diffusers. By decorrelation we mean that the two-state correlation function u_{ab} becomes small compared with its initial value u_{aa}, or that the normalized two-state correlation of intensity in Eq. (3.72) approaches unity. The setup for analyzing the speckle is illustrated in Fig. 3.1. In this figure the diffuser pair is illuminated with a plane wave of wavelength λ that points in an arbitrary input direction s_0. The two diffusers are separated by a spacing H, and there is an aperture a in contact with the second diffuser. We have written the expression for the complex amplitude in
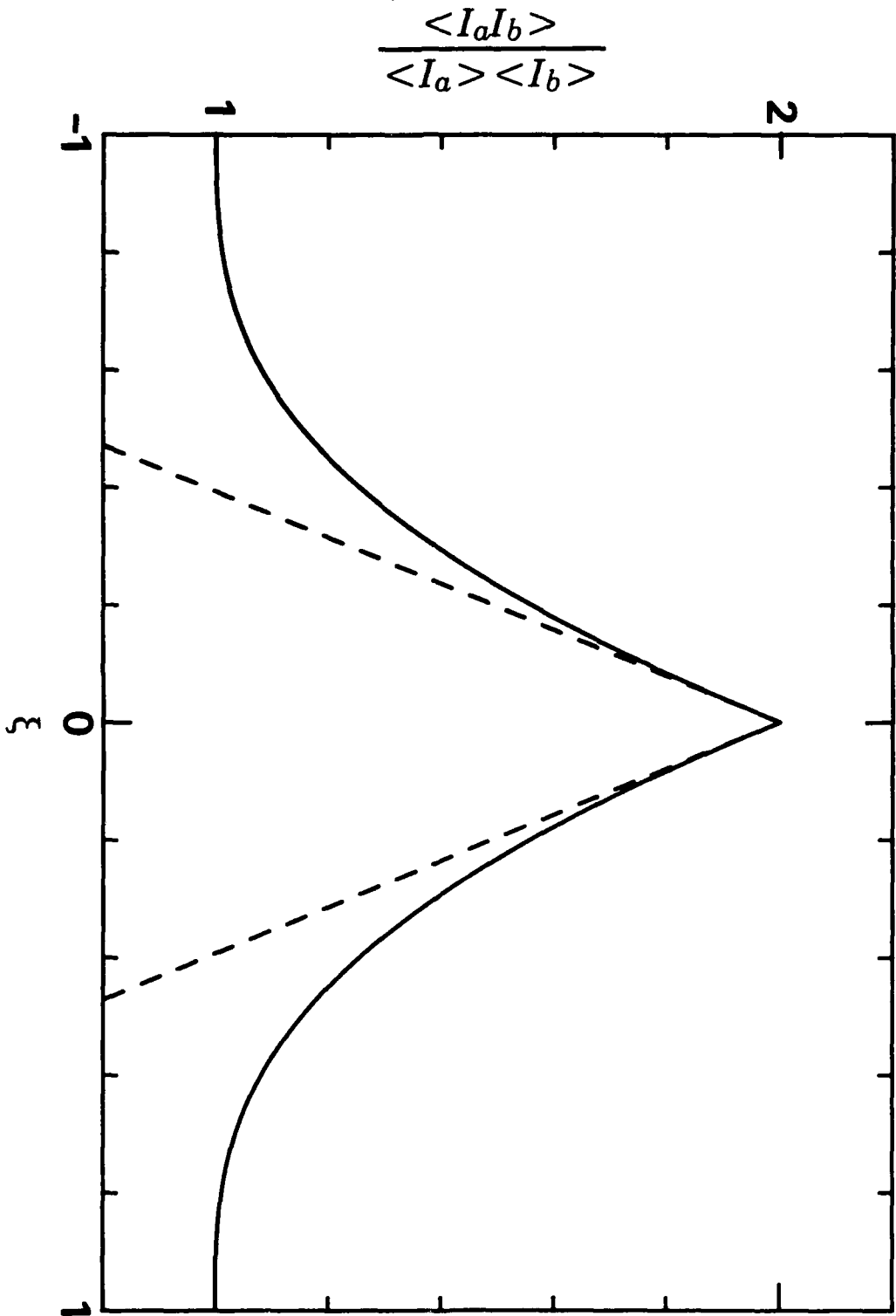
Fig. 3.4.   Plot of Eq. (3.93), solid line, and Eq. (3.96), dashed line, for the angular decorrelation of speckle arising from the spacing between a diffuser and a circular aperture.

the far-zone of this aperture in Eq. (3.17), and in Eq. (3.47) we have given a general expression for u_{ab}, the the two-state correlation function of the far-zone complex amplitude. The two states a and b represent different values of the four parameters that can be varied, i.e., the wavelength λ, the input direction s_0, the spacing H, and the observation direction s.

In Eqs. (3.25) and (3.26) we have defined the two important wave vectors $\Delta k_{ab\perp}$ and $k_{ab\perp}$. When $\Delta k_{ab\perp}$ of Eq. (3.25) is equal to zero, we have the speckle tracking condition, i.e., our observation point moves with the local speckle motion. The other vector, $k_{ab\perp}$ of Eq. (3.26), represents the average difference between the input and observation wave vectors for the two states. When $\Delta k_{ab\perp} = 0$, $k_{ab\perp}$ acts as the Fourier transform variable for the far-zone speckle pattern.

The general expression for u_{ab} given in Eq. (3.47) takes the particularly simple form given in Eq. (3.48) when k and H are constants, or more generally, when Eq. (3.45) holds. Equation (3.48) is proportional to the double-diffuser descriptor function F that is defined in Eq. (3.30). The offset vector $H_a s_{0a\perp} - H_b s_{0b\perp}$ that occurs as the first argument of F is particularly important. It can be interpreted geometrically as the lateral shift at plane II between two rays leaving plane I at the same point and traveling in directions s_{0a} and s_{0b}.

The function F contains all of the dependence on the statistics of the diffusers necessary for the calculation of u_{ab} through its dependence on the correlation functions R_{t_1} and R_{t_2} defined in Eq. (3.7). For this reason, F serves as a useful descriptor for the diffuser pair. The function F also depends on the aperture ambiguity function $\hat{A}$ that is defined in Eq. (3.23). In general, an ambiguity function depends both on a spatial and on a spatial frequency variable, and there is an inverse relationship between the width of the ambiguity function with respect to these two variables. As it appears in Eq. (3.30), $\hat{A}$ depends on r' and on the wave vector $\Delta k_{ab\perp}$. The speckle size is equal to the width of $\hat{A}$ with respect to $\Delta k_{ab\perp}$. Thus, when $\Delta k_{ab\perp}$ becomes larger than the speckle, $\hat{A}$ drops

rapidly. In most applications the experiment would be designed so that $\Delta k_{ab\perp} = 0$.
Ordinarily, the width of the aperture function is large so that $\hat{A}$ is wide spatially
compared with R_{t_2}. Therefore, $\hat{A}$ can usually be evaluated at $r' = 0$ in Eq. (3.30) and
factored out of the integral. For convenience, the ambiguity function is normalized to
unity so that $\hat{A}(0;0) = 1$. As illustrations of the functional form of $\hat{A}$ for common aperture
functions, we have evaluated $\hat{A}$ for a Gaussian aperture, Eq. (3.32), and for a rectangular
aperture, Eq. (3.33); the resulting expressions for $\hat{A}$ are given in Eqs. (3.38) and (3.39)
respectively.

Some special cases of u_{ab} are listed in Section 3.2.6. When $a \rightarrow b$ we have the
radiation pattern from a cascade of two diffuser, Eq. (3.50). This formula is reduced to
the expression for the pattern from a single diffuser in Eq. (3.51). For purposes of
comparison with the literature, u_{ab} from a single diffuser is also listed in Eq. (3.52). In
Section 3.2.7 the calculation of u_{ab} is extended to arbitrary wide-sense stationary plane-
wave transmission functions. Speckle decorrelation from double diffusers is a special
case of this more general formalism.

In order to perform calculations based on Eq. (3.47), the functional forms of R_{t_1}
and R_{t_2} must be specified. The relationship between the diffuser height profile
correlation function R_h and R_t is discussed in Section 3.3. Equation (3.63) applies for
normally distributed diffuser heights. The decaying exponential, Eq. (3.66), and the
Gaussian, Eq. (3.67), are two important limiting forms of R_t for large roughness diffusers,
i.e., for $S >> 1$. The decaying exponential applies when R_h looks like a cone, and the
Gaussian applies when R_h looks like a paraboloid for small values of the offset parameter
r.

In a typical speckle experiment, one would measure the intensity rather than the
complex amplitude. Hence it is important to calculate the moment $<I_a I_b>$. This is done
in Section 3.4 for the important case where $a(r)$ is wide compared to R_{t_2} so that the real
and imaginary parts of the complex amplitude v are normally distributed. The expansion

of $<I_a I_b>$ for non-circular non-zero-mean complex Gaussian statistics is given in Eq. (3.72). We derived expressions for the non-circular component $u\ddagger_{ab}$ in Eqs. (3.81) and for the non-zero-mean component u_a in Eq. (3.88). Although these terms may be important for some applications, they become negligible when the observation point is not on the direct beam or when $S>>1$.

The condition on S for $u\ddagger_{ab}$ and u_a to be negligible, even when observing in the direction of the direct beam, i.e., at $k_{ab\perp}=0$, is given in Eq. (3.90). Even for S as small as 3, these terms make little contribution to the total expression in Eq.(3.72).

The analysis presented in Chapter 3 is intended as a general framework for further study of speckle decorrelation from a cascade of two diffusers. The key expression, Eq. (3.47), can be used as the basis of many different remote sensing techniques. As an example of the generality of the analysis, we have given an expression, Eq. (3.92), that can be used to determine the spacing between a diffuser and an aperture by observing the angular decorrelation of the far-zone speckle pattern. Equation (3.92) is applied to a circular aperture in Eq. (3.93).

Chapter 3 References

1. L. G. Shirley and N. George, "Wide-angle diffuser transmission functions and far-zone speckle," J. Opt. Soc. Am. A **4**, 734-745 (1987).

2. P. M. Woodward, *Probability and Information Theory with Applications to Radar*, (Pergamon Press, Oxford, 1953).

3. A. Papoulis, "Ambiguity function in Fourier optics," J. Opt. Soc. Am. **64**, 779-788 (1974).

4. K. -H. Brenner and J. Ojeda-Castaneda, "Ambiguity function and Wigner distribution function applied to partially coherent imagery," Opt, Acta **31**, 213-223 (1984).

5. M. Born and E. Wolf, *Principles of Optics*, 6th ed. (Pergamon Press, New York, 1980), pp. 484-487.

6. J. W. Goodman, *Introduction to Fourier optics*, (McGraw-Hill, New York, 1968), p.120.

7. W. H. Carter and E. Wolf, "Coherence and radiometry with quasihomogeneous planar sources," J. Opt. Soc. Am. **67**, 785-796 (1977).

8. I. S. Gradshteyn and I. M. Ryzhik, *Table of Integrals, Series, and Products*, (Academic Press, New York, 1980), p. 338.

9. E. Lukacs, *Characteristic Functions*, 2nd ed. (C. Griffin, London, 1970), p. 68.

10. L. G. Shirley and N. George, "Diffuser radiation patterns over a large dynamic range. Part 1: Strong diffusers," Appl. Opt. **27**, 1850-1861 (1988).

11. N. George and A. Jain, "Space and wavelength dependence of speckle intensity," Appl. Phys. **4**, 201-212 (1974).

12. J. W. Goodman, "Dependence of image speckle on surface roughness," Opt. Commun. **14**, 324-327 (1975)..

13. H. M. Pederson, "Theory of speckle dependence on surface roughness," J. Opt. Soc. Am. **66**, 1204-1210 (1976).

14. J. Ohtsubo and T. Asakura, "Statistical properties of laser speckle produced in the diffraction field," Appl. Opt. **16**, 1742-1753 (1977).

15. J. Uozumi and T. Asakura, "First-order intensity and phase statistics of Gaussian speckle produced in the diffraction region," Appl. Opt. **20**, 1454-1466 (1981).

16. K. A. O'Donnell, "Speckle statistics of doubly scattered light," J. Opt. Soc. Am. **72**, 1459-1463 (1982).

Chapter 4

Remote Sensing of Double Diffusers

4.1 Introduction

In this chapter the analysis of Chapter 3 is applied to a specific type of diffuser cascade, and the interrelationship is discussed between the various parameters that cause the far-zone speckle pattern to decorrelate. The emphasis is on remote sensing applications, i.e., on determining the diffuser properties or the spacing between diffusers from observing the far-zone speckle. We refer to the diffuser cascade considered here by the symbol P-P because the autocorrelation functions R_{h_1} and R_{h_2} of the diffuser height profiles h_1 and h_2 are shaped like a paraboloid for small spatial offsets r. We also assume that the diffusers are strong, i.e., that the rms phase delay S is large compared to one radian. In Section 3.3.2 we have shown, that for a normally distributed diffuser height profile, these assumptions lead to the Gaussian autocorrelation function R_t, Eq. (3.68), of the diffuser transmission function t.

The P-P diffuser cascade is perhaps the most important example to consider because Eq. (3.47) for the two-state correlation function of the far-zone complex amplitude u_{ab} can be evaluated in closed form for arbitrary values of all of the decorrelation parameters. We use the resulting solution to gain a general understanding of the different speckle phenomenon that occur with double diffusers. With this understanding we will know how to configure remote sensing experiments to extract the spacing H between diffuser planes or the parameters describing the diffuser statistics.

We begin by reviewing Chapter 3; for ease of reading we will repeat the pertinent equations in Section 4.2. In Section 4.3 we present the general two-state correlation function of intensity for the P-P diffuser combination, and we discuss speckle decorrelation with respect to changes in wavelength, spacing, and angle of incidence.

We also introduce the five parameters p_0, p_1, p_2, p_3, and p_4 that one can measure by performing remote sensing experiments and that contain information about the diffuser cascade. In Section 4.4 we show how these parameters can be used to solve three classes of remote sensing problems. In Section 4.5 we discuss how the remote sensing of the P-P diffuser combination is expected to differ from the remote sensing of the other combinations of strong diffusers that are considered in Appendix E and Appendix F.

4.2 Review of Chapter 3

In Chapter 3 we obtained the general expression, Eq. (3.47), for u_{ab}, the two-state correlation function of far-zone complex amplitude from a cascade of two diffusers:

$$u_{ab} = -i \frac{k_a^2 k_b^2}{(2\pi)^3} \frac{\exp(-i\phi_{ab})}{k_b H_a - k_a H_b} \exp\left(\frac{i}{2} \frac{H_a H_b}{k_b H_a - k_a H_b} |\mathbf{k}_{ob\perp} - \mathbf{k}_{oa\perp}|^2 \right) \cos\theta_a \cos\theta_b$$

$$\times \int F(\mathbf{r}; k_a, k_b; \mathbf{k}_{ab\perp}; \Delta\mathbf{k}_{ab\perp}) \exp\left\{ i \frac{k_a k_b}{k_b H_a - k_a H_b} \left[\frac{1}{2} |\mathbf{r}|^2 + \left(H_b \mathbf{s}_{ob\perp} - H_a \mathbf{s}_{oa\perp} \right) \bullet \mathbf{r} \right] \right\} d^2\mathbf{r}. \quad (4.1)$$

The two states are represented by the subscripts a and b on the parameters that can be changed during an experiment. There are four basic quantities that we allow to vary, see Fig. 3.1. They are the wave number k, the direction $\mathbf{s}_0$ of the input plane wave, the spacing H between the diffuser planes, and the direction of observation $\mathbf{s}$. However, in Chapter 3 we showed that these parameters occur in certain combinations that have physical significance; therefore we defined the two additional wave vectors $\Delta\mathbf{k}_{ab\perp}$ and $\mathbf{k}_{ab\perp}$ in Eqs. (3.25) and (3.26):

$$\Delta\mathbf{k}_{ab\perp} = \mathbf{k}_{a\perp} - \mathbf{k}_{oa\perp} - \mathbf{k}_{b\perp} + \mathbf{k}_{ob\perp}, \quad (4.2)$$

and

$$\mathbf{k}_{ab\perp} = \frac{1}{2}\left(\mathbf{k}_{a\perp} - \mathbf{k}_{oa\perp} + \mathbf{k}_{b\perp} - \mathbf{k}_{ob\perp} \right). \quad (4.3)$$

The wave vector $\mathbf{k}$ is obtained by multiplying the unit vector $\mathbf{s}$ by the wave number k, and the subscript $\perp$ denotes that the component of $\mathbf{s}$ or $\mathbf{k}$ that lies along the z-axis has been dropped. We refer to $\Delta\mathbf{k}_{ab\perp}$ as the speckle tracking wave vector because if $\Delta\mathbf{k}_{ab\perp}=0$, then the observation point follows the speckle pattern as it shifts with changes of illumination angle or wavelength. We refer to the other wave vector, $\mathbf{k}_{ab\perp}$, as the Fourier transform wave vector because it occurs in the Fourier transform kernel. It is the average over states a and b of the difference between the input and output wave vectors. Essentially, $\mathbf{k}_{ab\perp}$ is the offset of the observation point from the input direction in the diffuser radiation pattern.

The double-diffuser descriptor function F that occurs in Eq. (4.1) is defined in Eq. (3.30):

$$F(\mathbf{r};k_a,k_b;\mathbf{k}_{ab\perp};\Delta\mathbf{k}_{ab\perp}) = \int R_{t_1}(\mathbf{r}+\mathbf{r}';k_a,k_b)\, R_{t_2}(\mathbf{r}';k_a,k_b)$$

$$\times\; \hat{A}(\mathbf{r}';\Delta\mathbf{k}_{ab\perp})\, \exp\left(i\,\mathbf{k}_{ab\perp}\bullet\mathbf{r}'\right)\, d^2\mathbf{r}' \;. \tag{4.4}$$

It depends on R_{t_1} and R_{t_2}, defined in Eq. (3.7) as the autocorrelation functions of the diffuser transmission functions t_1 and t_2, and on $\hat{A}$, defined in Eq. (3.23) as the normalized ambiguity function of the aperture function a.

The condition that must be satisfied for changes in spacing to be balanced by changes in wavelength is given in Eq. (3.45):

$$\frac{k_a}{H_a} = \frac{k_b}{H_b}\;. \tag{4.5}$$

If this condition is satisfied, then Eq. (4.1) simplifies to

$$u_{ab} = \frac{k_a k_b}{(2\pi)^2} \exp\left(-i\phi_{ab}\right) \exp\left[\frac{i}{2}\left(k_b H_b - k_a H_a\right)\right] \cos\theta_a \cos\theta_b$$

$$\times\; F(H_a \mathbf{s}_{oa\perp} - H_b \mathbf{s}_{ob\perp};k_a,k_b;\mathbf{k}_{ab\perp};\Delta\mathbf{k}_{ab\perp})\;. \tag{4.6}$$

The spatial offset vector $H_a s_{0a\perp} - H_b s_{0b\perp}$ in the argument of F is important because it is the shift between the autocorrelation functions R_{t_1} and R_{t_2} in Eq. (4.4). This offset can be interpreted geometrically as the paraxial approximation to the lateral shift between two rays that begin at plane I and propagate in the directions s_{0a} and s_{0b} to plane II.

Since it is the intensity rather than the complex amplitude that is measured in a typical remote sensing experiment, we have also given an expression, Eq. (3.72), for the two-state correlation function of far-zone intensity. Equation (3.72) applies when the speckle is Gaussian, i.e., when the real and imaginary parts of the complex amplitude are normally distributed so that the complex Gaussian moment theorem (see Appendix A) can be used to write the fourth-order moment in terms of second- and first-order moments.

Gaussian speckle occurs when the aperture function a is wide compared with R_{t_2} so that many uncorrelated diffuser cells contribute to the speckle pattern. In Section 3.4.4 we have shown that the last two terms of Eq. (3.72), which we refer to as the non-circular and non-zero-mean components respectively, are negligible for all observation points if the diffusers are very rough, i.e., if $S_1 >> 1$ and $S_2 >> 1$. In this case we have zero-mean complex circular Gaussian statistics, and Eq. (3.72) reduces to Eq. (3.75). We will use the normalization $u_{aa}(0)u_{bb}(0)$ introduced in Appendix C rather than the normalization $u_{aa}(k_{a\perp} - k_{0a\perp})u_{bb}(k_{b\perp} - k_{0b\perp})$ in this chapter. In other words, we will calculate the normalization factor as the value of the intensity in the direction of the input plane wave:

$$\frac{<I_a I_b>}{<I_a(0)> <I_b(0)>} = \frac{u_{aa} u_{bb}}{u_{aa}(0) u_{bb}(0)} + \frac{|u_{ab}|^2}{u_{aa}(0) u_{bb}(0)} . \tag{4.7}$$

In analyzing the dependence of speckle from a cascade of two strong diffusers, there are two important functional forms of the autocorrelation function R_t to consider: For diffusers that are very rough and that have a normally distributed height profile, R_t is given by the Gaussian, Eq. (3.68),

$$R_t(\mathbf{r};k_a,k_b) = \exp\left[-\frac{\sigma_t^2}{2}\left(k_b - k_a\right)^2\right]\exp\left(-k_a k_b \sigma_t^2 \frac{|\mathbf{r}|^2}{w^2}\right) \qquad (4.8)$$

if the diffuser height profile autocorrelation function R_h is shaped like a paraboloid for small spatial offsets $\mathbf{r}$, and by the decaying exponential, Eq. (3.61),

$$R_t(\mathbf{r};k_a,k_b) = \exp\left[-\frac{\sigma_t^2}{2}\left(k_b - k_a\right)^2\right]\exp\left(-k_a k_b \sigma_t^2 \frac{|\mathbf{r}|}{w}\right) \qquad (4.9)$$

if R_h is shaped like a cone for small $\mathbf{r}$. In practice, a roughness S of 3 or 4 radians will usually suffice for the diffuser to be considered strong. We designate diffusers having R_t given in Eq. (4.8) and (4.9) by the symbols P and C, respectively. Thus there are four combinations of strong diffusers to consider: We denote them by the symbols P-P, P-C, C-P, and C-C. The ordering of the letters corresponds to the ordering of the diffusers from left to right in Fig. 3.1. In this chapter we will analyze the P-P diffuser combination in detail. In order to make the analysis tractable, we assume that the aperture function a is Gaussian, Eq. (3.32), so that the aperture ambiguity function is given by Eq. (3.38):

$$\tilde{A}(\mathbf{r};\mathbf{k}_\perp) = \exp\left(-\frac{|\mathbf{r}|^2}{2w_a^2}\right)\exp\left(-\frac{1}{8}w_a^2|\mathbf{k}_\perp|^2\right). \qquad (4.10)$$

The P-C and C-P diffuser combinations are treated in Appendix E, and the C-C diffuser combination is analyzed in Appendix F.

4.3 Two Diffusers of the Paraboloidal Type

The intermediate steps in evaluating Eq. (4.1) for the P-P diffuser combination, where the output aperture is a Gaussian of arbitrary width w_a, are given in Appendix C. In most practical situations the relation

$$2k_a k_b w_a^2 >> \frac{w_2^2}{\sigma_{t2}^2} \qquad (4.11)$$

holds since the area of the aperture is large compared to the area of the diffuser correlation cells. This insures that the output speckle pattern is caused by many

uncorrelated scatterers so that Eq. (4.7) holds. Inequality (4.11) was applied in deriving the final result, Eq. (C14), in Appendix C.

In remote sensing applications we will require that the speckle tracking condition, $\Delta k_{ab\perp} = 0$, is satisfied. In practical applications the tolerance on this condition is that

$$|\Delta k_{ab\perp}| << \frac{2}{w_a}. \tag{4.12}$$

When this inequality is satisfied, the error in the speckle tracking parameter is small compared to the speckle size. Then Eq. (C14) reduces to

$$\frac{<I_a I_b>}{<I_a(0)><I_b(0)>} = \exp\left[-\frac{1}{4}\left(\frac{\sigma_{t1}^2}{w_1^2} + \frac{\sigma_{t2}^2}{w_2^2} \right)^{-1} \left(\frac{1}{k_a^2} + \frac{1}{k_b^2} \right)|k_{ab\perp}|^2 \right] +$$

$$+ \exp\left[-\left(\sigma_{t1}^2 + \sigma_{t2}^2 \right)\left(k_b - k_a \right)^2 \right] \frac{1}{1 + \beta_{pp}^2}$$

$$\times \exp\left[-2k_a k_b \left(\frac{w_1^2}{\sigma_{t1}^2} + \frac{w_2^2}{\sigma_{t2}^2} \right)^{-1} \frac{1}{1 + \beta_{pp}^2} |H_b s_{ob\perp} - H_a s_{oa\perp}|^2 \right]$$

$$\times \exp\left[-\frac{1}{2k_a k_b}\left(\frac{\sigma_{t1}^2}{w_1^2} + \frac{\sigma_{t2}^2}{w_2^2} \right)^{-1} \left(1 + \frac{\sigma_{t1}^2}{w_1^2} \frac{w_2^2}{\sigma_{t2}^2} \frac{\beta_{pp}^2}{1 + \beta_{pp}^2} \right)|k_{ab\perp}|^2 \right]$$

$$\times \exp\left[2\left(1 + \frac{w_1^2}{\sigma_{t1}^2} \frac{\sigma_{t2}^2}{w_2^2} \right)^{-1} \frac{\beta_{pp}}{1 + \beta_{pp}^2} k_{ab\perp} \bullet \left(H_b s_{ob\perp} - H_a s_{oa\perp} \right) \right], \tag{4.13}$$

where the spacing-wavelength detuning parameter β_{pp} of Eq.(C4) is now

$$\beta_{pp} = 2\left(k_b H_a - k_a H_b \right)\left(\frac{w_1^2}{\sigma_{t1}^2} + \frac{w_2^2}{\sigma_{t2}^2} \right)^{-1}. \tag{4.14}$$

Equation (4.13) is the key expression governing the decorrelation of the speckle intensity from a cascade of two paraboloidal diffusers. We will now discuss the significance of the various factors and terms making up this equation, and we will look at certain important limiting cases to gain an understanding of how Eq. (4.13) can be used to extract information about the diffuser pair. By inspection of Eq. (4.13) and Eq. (4.14)

we see that the parameters that one could hope to find, based on this equation, are the rms slope parameters σ_{t_1}/w_1 and σ_{t_2}/w_2, the spacing H, or changes ΔH in this spacing, and the sum of the squares of the roughness parameters σ_{t_1} and σ_{t_2}. In the most common application $H_a = H_b$ so that $\Delta H = 0$.

We begin by writing the degenerate from of Eq. (4.13) that results from letting $a \rightarrow b$:

$$\frac{<I_a^2>}{<I_a(0)>^2} = 2\exp\left[-\frac{1}{2}\left(\frac{\sigma_{t1}^2}{w_1^2} + \frac{\sigma_{t2}^2}{w_2^2} \right)^{-1} |s_{a\perp} - s_{oa\perp}|^2 \right]. \tag{4.15}$$

Equation (4.14) has the value two when the observation direction is equal to the input direction, and it falls off as a Gaussian in the offset $|s_{a\perp}-s_{oa\perp}|$ between these two directions. By illuminating at normal incidence, $s_{oa\perp} = 0$, and scanning the output $s_{a\perp}$, one can extract the effective slope parameter, p_0, for the diffuser combination:

$$p_0 = \left(\frac{\sigma_{t1}^2}{w_1^2} + \frac{\sigma_{t2}^2}{w_2^2} \right)^{\frac{1}{2}}. \tag{4.16}$$

In practice one can obtain p_0 more directly by fitting the radiation pattern from the diffuser pair, see Chapter 5, to

$$\frac{<I_a>}{<I_a(0)>} = \exp\left[-\frac{1}{4}\left(\frac{\sigma_{t1}^2}{w_1^2} + \frac{\sigma_{t2}^2}{w_2^2} \right)^{-1} |s_{a\perp} - s_{oa\perp}|^2 \right]. \tag{4.17}$$

Thus p_0 could be obtained by illuminating at normal incidence, $s_{oa\perp} = 0$, and finding the value of $|s_{a\perp}| = \sin\theta_a$ where $<I_a>/<I_a(0)>$ falls to its e^{-1} point. This experimental configuration is illustrated in Fig. 4.1(a). If we denote the value of θ_a where this occurs as θ_e, then $p_0 = 0.5\sin\theta_e$. Of course this method of determining p_0 can only be used for values of $p_0 < 0.5$; for larger values of p_0, one must fit the curve at angles smaller than θ_e. However, typical values of p_0 are small compared to one. For example, the etched glass diffuser described in Chapter 5 has $\sigma_t/w = 0.03$ or $\sigma_h/w = 0.06$ so that for a cascade of two of these diffusers, $p_0 = 0.04$. If the rms diffuser slope parameter σ_h/w is not small compared to unity, then we will not be able to ignore shadowing and multiple

(a)

(b)

(c)

(d)

$\Delta k_{ab\perp} = 0$

θ

$\Delta \theta$

$\Delta \lambda$

$\Delta \lambda$
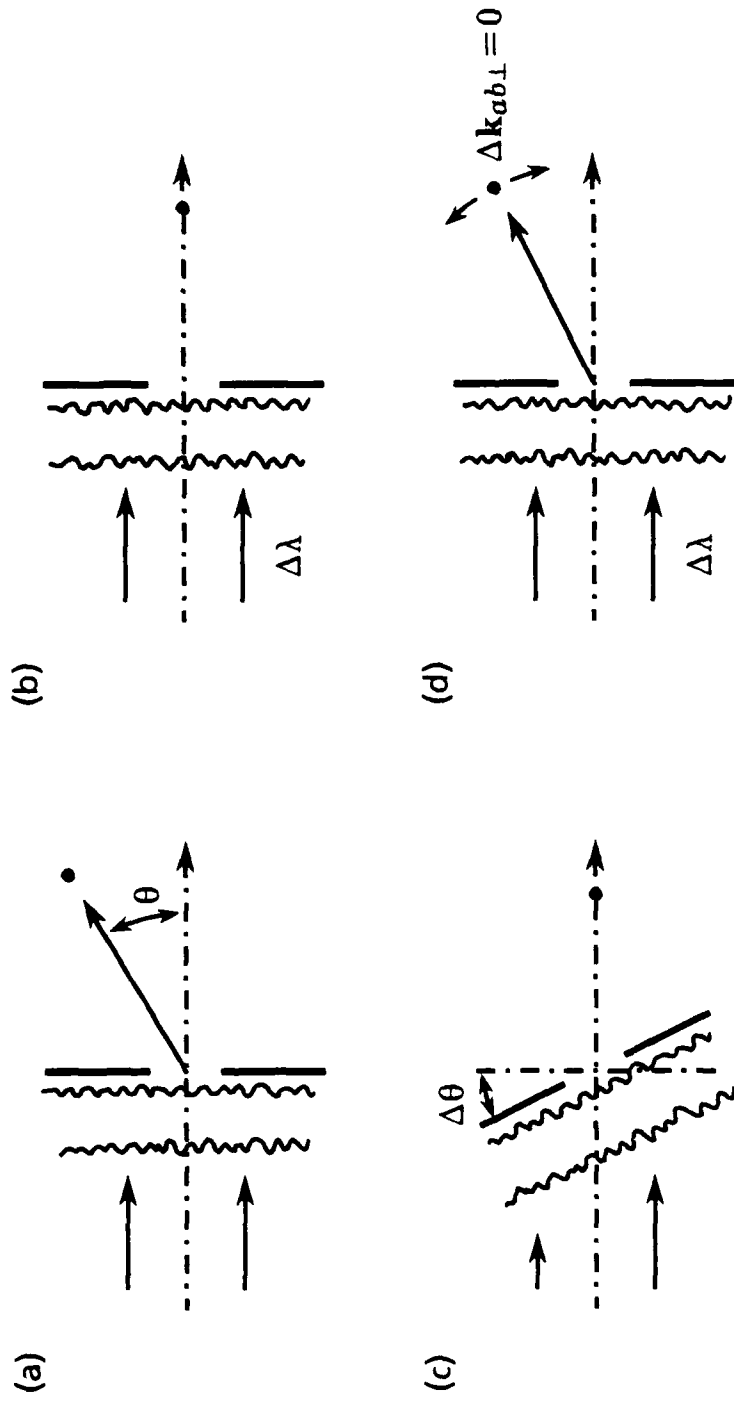
Fig. 4.1. Basic experimental configurations for the remote sensing of double diffusers through measurement of the radiation pattern(a), wavelength decorrelation (b), angular decorrelation(c), and off-axis wavelength decorrelation (d).

scattering, and the simple transmission function model given by Eqs. (2.1) and (2.2) may not adequately describe the transmission of light through the individual diffusers.

As pointed out in Section 3.2.6, the radiation pattern from a diffuser pair is essentially the convolution of the individual radiation patterns. Since the radiation patterns from the individual paraboloidal diffusers are Gaussian, the radiation pattern from the two diffusers, Eq. (4.17), is also Gaussian, but it has a larger width than either of the single diffuser patterns. In other words, p_0 is larger than σ_{t_1}/w_1 and σ_{t_2}/w_2.

In using Eq. (4.13) as the basis for remote sensing experiments, we want to find the simplest subcases that will allow us to calculate the diffuser parameters and the spacing. As we will see below, these parameters can still be obtained from the formula that results by setting $k_{ab\perp} = 0$ in Eq. (4.13):

$$\frac{<I_a I_b>}{<I_a(0)><I_b(0)>} = 1 + \exp\left[-\left(\sigma_{t1}^2 + \sigma_{t2}^2\right)\left(k_b - k_a\right)^2\right] \frac{1}{1 + \beta_{pp}^2}$$

$$\times \exp\left[-2k_a k_b \left(\frac{w_1^2}{\sigma_{t1}^2} + \frac{w_2^2}{\sigma_{t2}^2}\right)^{-1} \frac{1}{1 + \beta_{pp}^2} |H_b s_{ob\perp} - H_a s_{oa\perp}|^2\right]. \tag{4.18}$$

However, we will need to perform an additional experiment with $k_{ab\perp} \neq 0$ to determine the ordering of the diffusers. We denote the three factors in the second term of Eq. (4.18) by the symbols f_1, f_2, and f_3:

$$f_1 = \exp\left[-\left(\sigma_{t1}^2 + \sigma_{t2}^2\right)\left(k_b - k_a\right)^2\right], \tag{4.19}$$

$$f_2 = \frac{1}{1 + \beta_{pp}^2}, \tag{4.20}$$

and

$$f_3 = \exp\left[-2k_a k_b \left(\frac{w_1^2}{\sigma_{t1}^2} + \frac{w_2^2}{\sigma_{t2}^2}\right)^{-1} \frac{1}{1 + \beta_{pp}^2} |H_b s_{ob\perp} - H_a s_{oa\perp}|^2\right]. \tag{4.21}$$

We now discuss the physical significance of each of these factors and show how they can be used in remote sensing.

4.3.1 Wavelength Decorrelation

By requiring that $H_b s_{ob\perp} = H_a s_{oa\perp}$, we can eliminate f_3 from Eq. (4.18). This leaves the pure wavelength dependence of f_1 and the spacing-wavelength dependence of f_2:

$$\frac{<I_a I_b>}{<I_a(0)> <I_b(0)>} = 1 + \exp\left[-\left(\sigma_{t1}^2 + \sigma_{t2}^2\right)\left(k_b - k_a\right)^2\right] \frac{1}{1 + \beta_{pp}^2}. \qquad (4.22)$$

A simple way of eliminating f_3 is to set $s_{oa\perp} = s_{ob\perp} = 0$, i.e., to illuminate at normal incidence for both states. See Fig. 4.1(b) for a diagram of this experimental configuration. In most applications the spacing H is constant so that f_3 could also be eliminated by fixing the angle of illumination, not necessarily at normal incidence.

We first discuss the significance of the factor f_1 that occurs in Eq. (4.22). This factor arises from multiplying the wavelength dependence of the individual diffusers, see Eq. (3.63). It does not depend on the spacing between the diffusers or on the functional form of the autocorrelation functions R_{t_1} and R_{t_2}, only on the fact that h_1 and h_2 are normally distributed random variables. In order to facilitate the discussion of wavelength dependence, we will define a new parameter ρ_k as the fractional change in wave number between states a and b:

$$\rho_k = \frac{\Delta k}{k}. \qquad (4.23)$$

In Eq. (4.23) we have denoted the change $k_b - k_a$ between the wave numbers of the initial and final states by the symbol Δk, and we have dropped the subscript a on the initial wave number k in the denominator. We note that the fractional change in wave number ρ_k can range in value between negative one and infinity.

Using the above notation, we can rewrite Eq. (4.19) for f_1 in the form:

$$f_1 = \exp\left[-\left(S_1^2 + S_2^2\right)\rho_k^2\right], \qquad (4.24)$$

where we have used Eq. (3.10) to express σ_{t_1} and σ_{t_2} in terms of rms phase delays S_1 and S_2 at wave number k_a. Since we have already assumed that $S_1 >> 1$ and $S_2 >> 1$, then Eq. (4.24) implies that the wavelength dependence of the individual diffusers will cause
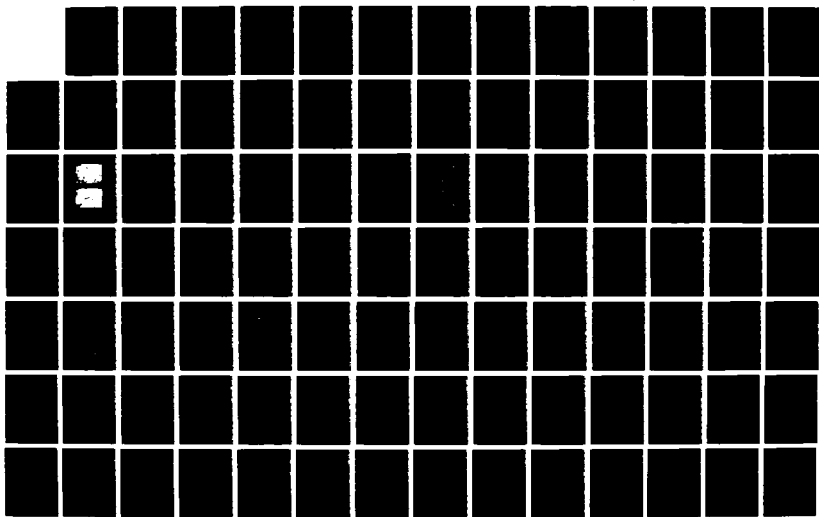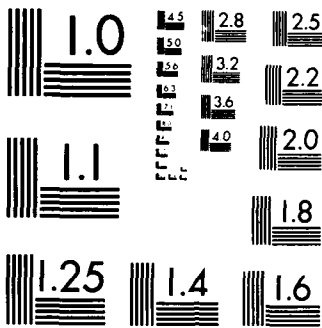
MICROCOPY RESOLUTION TEST CHART

NATIONAL BUREAU OF STANDARDS-1963-A

the speckle pattern to decorrelate unless $|\rho_k| < < 1$. If f_1 does dominate the wavelength decorrelation, then Eq. (4.19) can be used to extract the effective roughness

$$p_1 = \left(\sigma_{t1}^2 + \sigma_{t2}^2 \right)^{\frac{1}{2}} \qquad (4.25)$$

of the diffuser pair.

We now consider the spacing-wavelength decorrelation factor f_2; this factor is a Lorentzian in the parameter β_{pp}. If f_1 does not dominate the decorrelation, then by substituting Eq. (4.14) for β_{pp} into Eq. (4.20) for f_2, we see that we can find the value of the parameter

$$p_2 = 2H \left(\frac{w_1^2}{\sigma_{t1}^2} + \frac{w_2^2}{\sigma_{t2}^2} \right)^{-1}. \qquad (4.26)$$

One method of obtaining p_2 is to measure the value of Δk necessary for the factor f_2 to fall to one half of its maximum value of unity for $\Delta H = 0$, then $p_2 = \Delta k^{-1}$. We note that decorrelation arising from f_2 occurs more rapidly if the spacing H and the slope parameters σ_{t_1}/w_1 and $\sigma_{t_}/w_2$ are large. Large slopes imply a large spread in the radiation pattern and a large value of H allows the light to spread spatially between planes. Thus we see that this decorrelation phenomenon occurs more rapidly with wavelength changes if the light scattered from a point on the first diffuser illuminates a large area on the second diffuser and if the angular spread of light scattered from the second diffuser is large.

If we define ΔH as the change from the initial spacing H_a, in the same manner that we defined Δk as the change from the initial wave number k_a, and if we drop the subscript a on the initial values, then the spacing-wavelength detuning parameter that occurs in the definition of β_{pp} can be written as

$$k_b H_a - k_a H_b = H \Delta k - k \Delta H. \qquad (4.27)$$

The symmetry between decorrelation with respect to wave number k and spacing H is clearly displayed in Eq. (4.27): If the spacing is fixed and the wave number varies, then

β_{pp} is proportional to $H\Delta k$, and if the wave number is fixed and the spacing varies, then β_{pp} is proportional to $k\Delta H$. Another convenient form of Eq. (4.27) is

$$H\Delta k - k\Delta H = kH\left(\rho_k - \rho_H\right),\qquad(4.28)$$

where ρ_H is the fractional change in spacing,

$$\rho_H = \frac{\Delta H}{H}.\qquad(4.29)$$

Of course ρ_H, as well as ρ_k, can range in value between negative one and infinity. By setting

$$\rho_H = \rho_k,\qquad(4.30)$$

we see that both H and k can change without affecting the offset parameter β_{pp}. However, the range over which the speckle remains correlated by constraining ρ_k to be equal to ρ_H is limited by the factor f_1.

In wavelength experiments it is often more convenient to work in terms of wavelength λ rather than wave number k. If we define the fractional change in wavelength

$$\rho_\lambda = \frac{\Delta\lambda}{\lambda}\qquad(4.31)$$

in the same manner as we defined ρ_k in Eq. (4.23) and ρ_H in Eq. (4.29), then the expression

$$\rho_\lambda^{-1} + \rho_k^{-1} = -1\qquad(4.32)$$

may be used to convert between ρ_k and ρ_λ. For infinitesimal shifts $d\lambda$ and dH, the constraint in Eq. (4.30) becomes

$$\frac{d\lambda}{\lambda} = -\frac{dH}{H}.\qquad(4.33)$$

Equation (4.33) gives the relationship between $d\lambda$ and dH for β_{pp} to remain constant.

Thus far we have shown how one can determine the value of the parameter p_0 defined in Eq. (4.16) from the angular spread of the radiation pattern and the value of at

least one of the parameters, p_1 of Eq. (4.25) or p_2 of Eq. (4.26), from the wavelength decorrelation for normally incident illumination and on-axis observation. We can tell whether wavelength decorrelation will be dominated by the spacing effect or by the combined wavelength dependence of the individual diffusers by looking at the ratio of the width of the two factors f_1 and f_2 with respect to the fractional change of wavelength ρ_k:

$$Q = \frac{2kH\left(\dfrac{w_1^2}{\sigma_{t1}^2} + \dfrac{w_2^2}{\sigma_{t2}^2}\right)^{-1}}{\sqrt{S_1^2 + S_2^2}} . \qquad (4.34)$$

To illustrate the effect of the size of Q on our ability to determine p_1 and p_2, we have plotted Eq. (4.22) for different values of Q in Fig. 4.2. If $Q \gg 1$, then the spacing effect dominates, and the curve approaches the Lorentzian shape of the dashed line. Thus, for large Q it will only be practical to obtain p_2. On the other hand, if $Q \ll 1$, then the wavelength dependence of the individual diffusers dominates, and the curve is Gaussian shaped. For small Q it will only be practical to obtain p_1. If $Q \sim 1$, then it is likely that both p_1 and p_2 could be determined. As a numerical illustration of Eq. (4.34), we choose the following typical values for the parameters: $\sigma_{t_1}/w_1 = \sigma_{t_2}/w_2 = 0.03$, $S_1 = S_2 = 5$, $H = 5$ mm, and $\lambda = 0.5$ μm and calculate $Q = 8.0$. For this illustration we would only be able to accurately determine p_2.

In a wavelength decorrelation experiment, one is limited by the laser linewidth $\Delta \nu_{lw}$ and the range of wavelengths $\Delta \lambda_{max}$ over which the laser can be tuned. A linewidth of less than 40 GHz can be obtained with a typical tunable dye laser. This converts to $\Delta \lambda_{lw} = 0.3$ Angstoms, $\Delta k_{lw} = 8 \times 10^{-4}$ μm^{-1}, and $\rho_{k,lw} = \rho_{\lambda,lw} = 6 \times 10^{-5}$. In addition, it implies a longitudinal correlation length of 7.5 mm. The range of tunability for Rhodamine 6G dye is from 0.570 μm to 0.650 μm. Thus $|\Delta \lambda_{max}| = 0.08$ μm, $|\Delta k_{max}| = 1.5$ μm^{-1}, $|\rho_{k,max}| = 0.12$, and $|\rho_{\lambda,max}| = 0.14$. We see that there is a ratio of approximately 2000 to 1 between the range and the resolution of tunability so that one could obtain
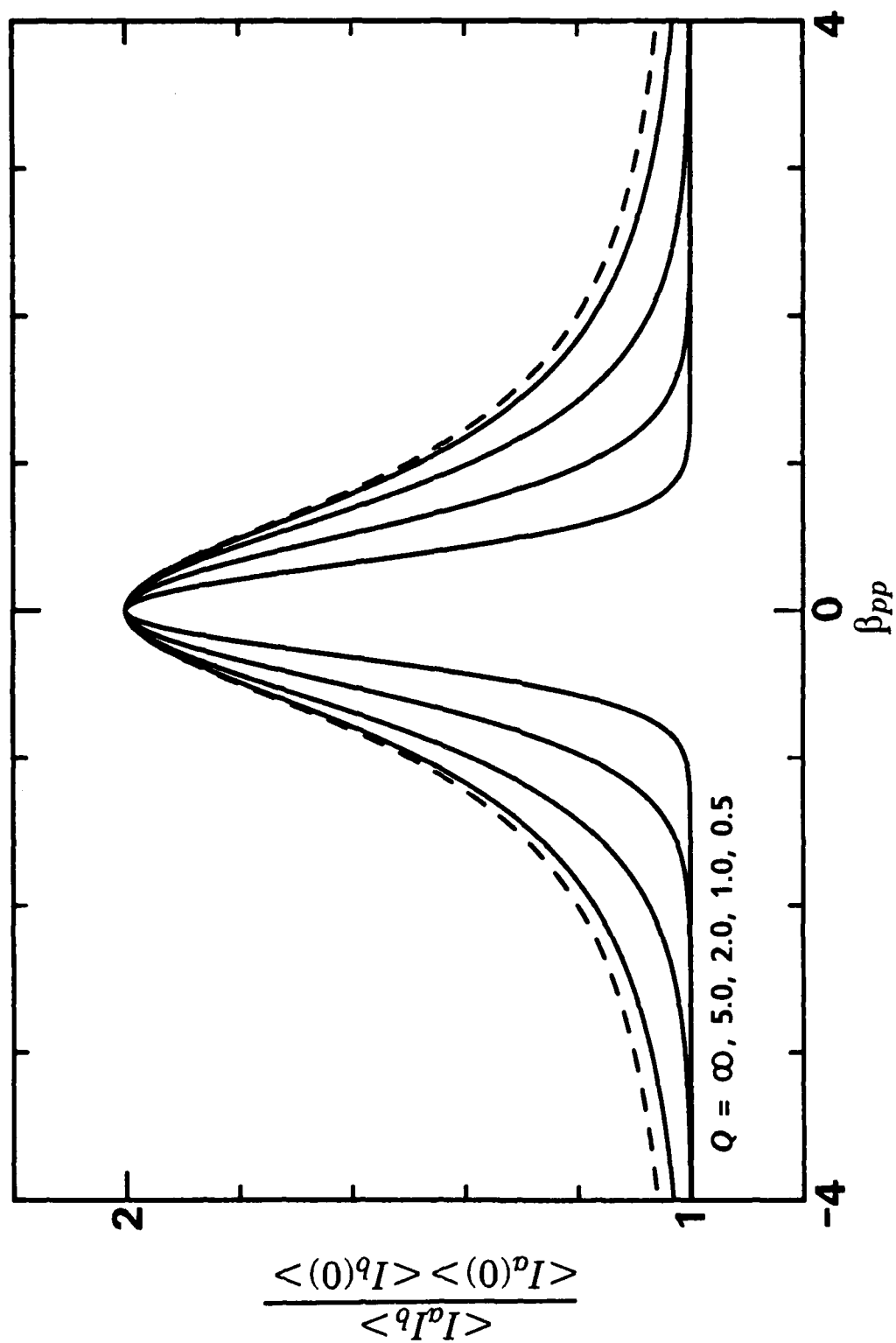
Fig. 4.2. Wavelength decorrelation of speckle from a cascade of two diffusers. Equation (4.22) is plotted against ρ_k for $Q = 0.5$, 1.0, 2.0 and 5.0 in the solid curves and for $Q = \infty$ in the dashed curve.

about 2000 nonoverlapping data points.

The laser linewidth limits the maximum value and the resolution of the distance parameters p_1 and p_2 that can be obtained with a given dye laser system. The range of tunability, on the other hand, sets the minimum values of these parameters that can be measured. If we designate the e^{-1} and the 0.5 points as the values of the factors f_1 and f_2, respectively, at which we can reliably measure the widths of f_1 and f_2, then we can write the following set of equations for the maximum and minimum values and the resolution obtainable for the parameters p_1 and p_2:

$$p_{1,max} = p_{2,max} = |\Delta k_{lw}|^{-1}, \tag{4.35}$$

$$p_{1,min} = p_{2,min} = |\Delta k_{max}|^{-1}, \tag{4.36}$$

$$p_{1,res} = p_1^2 |\Delta k_{lw}|, \tag{4.37}$$

and

$$p_{2,res} = p_2^2 |\Delta k_{lw}|. \tag{4.38}$$

We first consider the limitations imposed by the linewidth and range of tunability on our ability to measure the effective roughness p_1 of the diffuser combination. By substituting $\Delta k_{lw} = 8 \times 10^{-4}$ μm^{-1} into Eq. (4.35), we find $p_{1,max} = 1$ mm. Since 1 mm is large compared to the roughness at which one can expect the thin diffuser model to apply, it does not impose any real restrictions. We calculate the minimum value to be $p_{1,min} = 0.7$ μm by substituting $|\Delta k_{max}| = 1.5$ μm^{-1} into Eq. (4.36). The restriction on $p_{1,min}$ is more serious than the restriction on $p_{1,max}$, e.g., if both diffusers have the same roughness, then it implies that the rms phase delays S_1 and S_2 must be greater than six to be measured by wavelength decorrelation. However, Eq. (4.13) applies for values of S as small as three, e.g., the etched glass diffusers in Chapter 5. From Eq. (4.37), we calculate the resolution to be $p_{1,res} = 8$ Angstroms, 0.08 μm, and 8 μm at a roughness p_1 of 1 μm,

10 μm, and 100 μm, respectively. This resolution is very good for smaller values of p_1, but it worsens as a fraction of p_1 as p_1 increases.

From Eqs. (4.35) through (4.38), we see that the same restrictions apply for both p_1 and p_2. However, it is more meaningful to convert the conditions on p_2 to conditions on H. Thus we obtain

$$H_{max} = \frac{1}{2}\left(\frac{w_1^2}{\sigma_{t1}^2} + \frac{w_2^2}{\sigma_{t2}^2}\right)|\Delta k_{lw}|^{-1}, \tag{4.39}$$

$$H_{min} = \frac{1}{2}\left(\frac{w_1^2}{\sigma_{t1}^2} + \frac{w_2^2}{\sigma_{t2}^2}\right)|\Delta k_{max}|^{-1}, \tag{4.40}$$

and

$$H_{res} = 2H^2\left(\frac{w_1^2}{\sigma_{t1}^2} + \frac{w_2^2}{\sigma_{t2}^2}\right)^{-1}|\Delta k_{lw}|. \tag{4.41}$$

The range of σ_t/w obtainable by the etching process described in Chapter 5 is approximately 0.01 to 0.05. If we choose $\sigma_t/w = 0.03$ as a typical value, then $(w_1^2/\sigma_{t_1}^2 + w_2^2/\sigma_{t_2}^2)/2 = 1000$. Thus $H_{max} = 1$ m; however, at such large spacings, the path length differences could easily exceed the longitudinal correlation length of 7.5 mm, and the speckle contrast would be reduced. In addition, the resolution, H_{res}, arising from the finite linewidth worsens for large spacings. From Eq. (4.41) we calculate H_{res} to be 0.8 μm, 80 μm, and 8 mm at spacings H of 1 mm, 10 mm, and 100 mm, respectively.

The minimum value of H that we can measure by wavelength detuning for $\sigma_t/w = 0.03$ is calculated from Eq. (4.40) to be $H_{min} = 700$ μm. Although this is a relatively small diffuser spacing, it might be considered to be quite large if one were trying to measure the thickness of a film having rough interfaces with the surrounding medium. We note also that the value of H_{min} is very sensitive to the value of the slope parameter, e.g., if $\sigma_t/w = 0.01$, then $H_{min} = 7$ mm, and the restriction is much more severe.

4.3.2 Spacing Decorrelation

In Section 4.3.1 we have stressed the wavelength dependence of Eq. (4.22). It is also worthwhile to consider the decorrelation that occurs by keeping the wavelength constant and changing the spacing. The resulting form of Eq. (4.22) is

$$\frac{<I_a I_b>}{<I_a(0)><I_b(0)>} = 1 + \left\{1 + \left[2k\Delta H\left(\frac{w_1^2}{\sigma_{t1}^2} + \frac{w_2^2}{\sigma_{t2}^2}\right)^{-1}\right]^2\right\}^{-1} . \tag{4.42}$$

It is interesting to note that there is no dependence on the spacing H in Eq. (4.42), only on the change in spacing ΔH. If one can increment the spacing, then Eq. (4.42) provides the basis for a convenient method for measuring $w_1^2/\sigma_{t_1}^2 + w_2^2/\sigma_{t_2}^2$. If we measure ΔH at the point where the second term in Eq. (4.42) falls to 0.5, and if we assume that $\lambda = 0.5$ μm and that $\sigma_{t_1}/w_1 = \sigma_{t_2}/w_2 = 0.03$, then $\Delta H = 90$ μm. We observe that the value of ΔH necessary for decorrelation is very sensitive to the value of the slope parameters σ_{t_1}/w_1 and σ_{t_2}/w_2, e.g., if the slope is reduced by a factor of 10, so that $\sigma_{t_1}/w_1 = \sigma_{t_2}/w_2 = 0.003$, then the value of ΔH necessary for decorrelation increases by a factor of 100 to $\Delta H = 9$ mm. If one has two diffusers that are created by the same process, then it can be assumed that $\sigma_{t_1}/w_1 = \sigma_{t_2}/w_2$, and Eq. (4.42) provides a very convenient and sensitive method for determining σ_t/w for the diffusers.

4.3.3 Angular Decorrelation

Let us suppose that we can find p_2 by varying the wavelength. Since we can also evaluate p_0 from observing the radiation pattern, we need to have one more condition in order to solve for σ_{t_1}/w_1, σ_{t_2}/w_2, and H. This missing information can be provided by making use of the factor f_3 defined in Eq. (4.21). We can isolate the angular dependence in f_3 from the wavelength dependence by setting $k_a = k_b$ in Eq. (4.18). Of course, we also assume that the spacing is constant for the present discussion, i.e., that $H_a = H_b$ so that $\beta_{pp} = 0$. Equation (4.18) then reduces to

$$\frac{<I_a I_b>}{<I_a(0)><I_b(0)>} = 1 + \exp\left[-2\left(\frac{w_1^2}{\sigma_{t1}^2} + \frac{w_2^2}{\sigma_{t2}^2}\right)^{-1}\left(kH|s_{\alpha b\perp} - s_{\alpha a\perp}'|\right)^2\right] \tag{4.43}$$

From Eq. (4.43) we can deduce the value of

$$p_3 = \sqrt{2}\, H \left(\frac{w_1^2}{\sigma_{t1}^2} + \frac{w_2^2}{\sigma_{t2}^2} \right)^{-\frac{1}{2}} .$$

(4.44)

The parameter p_3 can be obtained experimentally by setting $s_{oa\perp} = 0$ and finding the value of θ_{ob} such that f_3 falls to its $1/e$ point. If we denote this angle as $\Delta\theta_e$, then $p_3 = (k \sin\Delta\theta_e)^{-1}$. The practical implementation of this experiment is to illuminate the diffuser pair at normal incidence and to observe on axis as the diffuser pair is rotated as a whole about a line lying in the output diffuser plane and passing through the center of the output aperture, see Fig. 4.1(c). In this configuration the conditions $k_{ab\perp} = 0$ and $\Delta k_{ab\perp} = 0$ are automatically satisfied as the diffuser pair is rotated.

Since it is $w_1^2/\sigma_{t_1}^2 + w_2^2/\sigma_{t_2}^2$ that occurs in the wavelength detuning parameter p_2, and it is the square-root of this quantity that occurs in the angular detuning parameter p_3, Eq. (4.44) is the third equation necessary for solution of the three quantities w_1/σ_{t_1}, w_2/σ_{t_2}, and H. As with wavelength decorrelation, angular decorrelation occurs more rapidly for larger values of the spacing H. In addition, both phenomenon rely on their being an angular spread in the radiation pattern, and decorrelation occurs more rapidly if this spread is large.

Just as we calculated the limitations imposed by a finite laser linewidth and a finite tuning range on our ability to measure the parameters p_1 and p_2, we can determine the corresponding conditions on the maximum and minimum values and on the resolution obtainable for p_3 that arise from the finite angular resolution $\Delta\theta_{res}$ and the maximum angular range $\Delta\theta_{max}$. The equations corresponding to Eqs. (4.35) through (4.38) are:

$$p_{3,max} = |k\Delta\theta_{res}|^{-1} ,$$

(4.45)

$$p_{3,min} = |k \sin\Delta\theta_{max}|^{-1} ,$$

(4.46)

and

$$p_{3,res} = k\,p_3^2\,|\Delta\theta_{res}|\ .\tag{4.47}$$

We write Eqs. (4.45) through (4.47) in terms of conditions on H as:

$$H_{max} = \frac{1}{\sqrt{2}}\left(\frac{w_1^2}{\sigma_{t1}^2}+\frac{w_2^2}{\sigma_{t2}^2}\right)^{\frac{1}{4}}|k\Delta\theta_{res}|^{-1},\tag{4.48}$$

$$H_{min} = \frac{1}{\sqrt{2}}\left(\frac{w_1^2}{\sigma_{t1}^2}+\frac{w_2^2}{\sigma_{t2}^2}\right)^{\frac{1}{4}}|k\sin\Delta\theta_{max}|^{-1},\tag{4.49}$$

and

$$H_{res} = \sqrt{2}\,H^2\left(\frac{w_1^2}{\sigma_{t1}^2}+\frac{w_2^2}{\sigma_{t2}^2}\right)^{-1}k|\Delta\theta_{res}|.\tag{4.50}$$

To illustrate Eqs. (4.48) through (4.50), we assume that the angular resolution is one arc second and that the range over which one can change the input angle without causing decorrelation due to thickness effects from the individual diffusers is $30°$. This implies that $\sin\Delta\theta_{res}=5\times10^{-6}$ and $\sin\Delta\theta_{max}=0.5$. We see that one could resolve about 10^5 individual data points over this $30°$ range. If $\sigma_{t_1}/w_1=\sigma_{t_2}/w_2=0.03$, then $H_{max}=150$ mm. Although this value of H_{max} is smaller than it was for wavelength decorrelation in Section 4.3.1, it is still large enough to cover the likely range of applications. The resolution H_{res} is $1.8\ \mu m$, $180\ \mu m$, and 5 mm for spacings H of 1 mm, 10 mm, and 50 mm, respectively. The minimum spacing that one can measure is $H_{min}=5\ \mu m$; this is much smaller than it was for wavelength decorrelation. Thus there is an advantage to angular decorrelation over wavelength decorrelation for small values of H. In addition, for wavelength decorrelation, one had to be concerned with the competition of wavelength decorrelation from the individual diffusers. However, the angular decorrelation from a typical single diffuser is small compared to the decorrelation from the effect of the spacing between the diffusers.

4.3.4 Unequal Input and Observation Directions

In Eq. (4.18) we note that the slope parameters σ_{t_1}/w_1 and σ_{t_2}/w_2 occur symmetrically in the factors f_0, f_2, and f_3, i.e., Eq. (4.18) is not altered if the subscripts 1 and 2 are interchanged. Therefore we can not distinguish between the two diffusers, given only the values of the parameters p_0, p_2, and p_3. This ambiguity in the ordering arises mathematically from the arbitrary choice of the sign in the solution of a quadratic equation, see Section 4.4.3.

In order to resolve this ambiguity, we need to perform one more experiment. Recall that Eq. (4.18) is the reduced form of Eq. (4.13) that resulted from setting $k_{ab\perp} = 0$. This caused the first term and the last two exponential factors in the second term to reduce to unity. By performing an experiment where $k_{ab\perp} \neq 0$, i.e., where the input and observation direction are not equal, we can extract the information contained in the last two factors. Continuing with our numbering system for the factors in Eq. (4.13), we will refer to these two factors as

$$f_4 = \exp\left[-\frac{1}{2k_a k_b}\left(\frac{\sigma_{t1}^2}{w_1^2} + \frac{\sigma_{t2}^2}{w_2^2} \right)^{-1} \left(1 + \frac{\sigma_{t1}^2}{w_1^2} \frac{w_2^2}{\sigma_{t2}^2} \frac{\beta_{pp}^2}{1+\beta_{pp}^2} \right) |k_{ab\perp}|^2 \right] \tag{4.51}$$

and

$$f_5 = \exp\left[2\left(1 + \frac{w_1^2}{\sigma_{t1}^2} \frac{\sigma_{t2}^2}{w_2^2} \right)^{-1} \frac{\beta_{pp}}{1+\beta_{pp}^2} \, k_{ab\perp} \bullet \left(H_b s_{ob\perp} - H_a s_{oa\perp} \right) \right]. \tag{4.52}$$

We note that neither f_4 nor f_5 is symmetric with respect to the subscripts 1 and 2, and that one can obtain the value of a fourth parameter,

$$p_4 = \frac{\sigma_{t1}}{w_1} \frac{w_2}{\sigma_{t2}}, \tag{4.53}$$

the ratio of the effective slope parameters of the two diffusers, from either Eq. (4.51) or Eq. (4.52).

We can emphasize f_4 in Eq. (4.13) by illuminating at normal incidence, $s_{oa\perp} = s_{ob\perp} = 0$, so that f_3 and f_5 reduce to unity, see Fig. 4.1(d). The resulting simplified form of Eq. (4.13) is

$$\frac{<I_a I_b>}{<I_a(0)> <I_b(0)>} = \exp\left[-\frac{1}{4}\left(\frac{\sigma_{t1}^2}{w_1^2} + \frac{\sigma_{t2}^2}{w_2^2}\right)^{-1}\left(1 + \frac{k_a^2}{k_b^2}\right)|s_{a\perp}|^2 \right]$$

$$\times \left\{ 1 + \frac{1}{1+\beta_{pp}^2} \exp\left[-\frac{k_a}{2k_b}\left(\frac{\sigma_{t1}^2}{w_1^2} + \frac{\sigma_{t2}^2}{w_2^2}\right)^{-1} \frac{\sigma_{t1}^2}{w_1^2} \frac{w_2^2}{\sigma_{t2}^2} \frac{\beta_{pp}^2}{1+\beta_{pp}^2} |s_{a\perp}|^2 \right] \right\}. \qquad (4.54)$$

In Eq. (4.54) we have assumed that $Q >> 1$ so that f_2 dominates f_1, and we have used the speckle tracking condition $\Delta k_{ab\perp} = 0$ to write $s_{b\perp}$ in terms of $s_{a\perp}$:

$$s_{b\perp} = \frac{k_a}{k_b} s_{a\perp}. \qquad (4.55)$$

By invoking the condition $|\rho_k| << 1$, we see that replacing k_b by k_a in the two places where k_b appears explicitly in Eq. (4.54) will have an insignificant effect on the overall equation. The resulting form of Eq. (4.54) is

$$\frac{<I_a I_b>}{<I_a(0)> <I_b(0)>} = \exp\left[-\frac{1}{2}\left(\frac{\sigma_{t1}^2}{w_1^2} + \frac{\sigma_{t2}^2}{w_2^2}\right)^{-1}|s_{a\perp}|^2 \right]$$

$$\times \left\{ 1 + \frac{1}{1+\beta_{pp}^2} \exp\left[-\frac{1}{2}\left(\frac{\sigma_{t1}^2}{w_1^2} + \frac{\sigma_{t2}^2}{w_2^2}\right)^{-1} \frac{\sigma_{t1}^2}{w_1^2} \frac{w_2^2}{\sigma_{t2}^2} \frac{\beta_{pp}^2}{1+\beta_{pp}^2} |s_{a\perp}|^2 \right] \right\}. \qquad (4.56)$$

A difficulty in evaluating p_4 based on Eq. (4.54) or Eq. (4.56) is that the speckle tracking condition is not automatically satisfied when $k_{ab\perp} \neq 0$. It is important, therefore, to determine the conditions under which this tracking condition can be ignored by keeping the observation angle fixed as the wavelength changes: For normal incidence we set $k_{oa\perp} = k_{ob\perp} = 0$ in Eq. (4.2) for $\Delta k_{ab\perp}$. Then by substituting $k_a s_{a\perp}$ for $k_{a\perp}$ and $k_b s_{b\perp}$ for $k_{b\perp}$, setting $s_{b\perp}$ equal to $s_{a\perp}$, substituting the resulting expression for $\Delta k_{ab\perp}$ into Eq. (4.12), and converting k_b-k_a to ρ_k, we obtain

$$|\rho_k| << \frac{2}{kw_a\sin\theta_a} \qquad (4.57)$$

as the condition on ρ_k that must be satisfied for speckle motion to be negligible. The above inequality is expressed in terms of the initial angle of observation θ_a through $|s_{a\perp}| = \sin\theta_a$. As a numerical illustration of Eq. (4.57), we set $\theta_a = 10°$, $w_a = 1$ mm, and $\lambda = 0.5$ μm and find that $|\rho_k| << 0.001$, or else speckle motion can not be ignored. For $\lambda = 0.5$ μm, this corresponds to a change in wavelength $|\Delta\lambda|$ that is small compared to 5 Angstoms! Thus we see that it is important to configure the experiment so that the tracking condition is satisfied.

In Fig. 4.3, Eq. (4.56) is plotted against β_{pp} for different values of p_4 and $\sin\theta_a/p_0$. As $\sin\theta_a/p_0$ increases, the maximum value of the curves, which occurs at $\beta_{pp} = 0$, decreases. However, the ratio between this maximum value and the minimum value, i.e., the asymptote at large β_{pp}, is always two. For a given value of $\sin\theta_a/p_0$, the curves become more narrow as p_4 increases, but as p_4 decreases, the curves approach the Lorentzian shape represented by the dashed lines. If $\sin\theta_a/p_0 = 0$, then Eq. (4.56) reduces to the large Q form of Eq. (4.22), and there is no p_4 dependence. For a given value of p_4, the curves become narrower as $\sin\theta_a/p_0$ increases. Thus, the sensitivity to p_4 increases as $\sin\theta_a/p_0$ increases. We see that one could distinguish between diffusers by illuminating on-axis and observing the off-axis wavelength decorrelation of speckle, see Fig. 4.1(d). This decorrelation occurs more rapidly if $p_4 > 1$, i.e., if the diffuser having the larger spread in its radiation pattern occurs first in the cascade.

We note that β_{pp}, in addition to $|k_{ab\perp}|$, must be nonzero for either f_4 or f_5 to affect Eq. (4.13). Since f_4 and f_5 are the only components of Eq. (4.13) that contain information about the ordering of the diffusers, we conclude that two conditions must be satisfied for us to distinguish between the diffusers: The input and observation directions must be different, and the wavelength must be tunable. One can not determine the order of the diffusers by angular detuning alone.
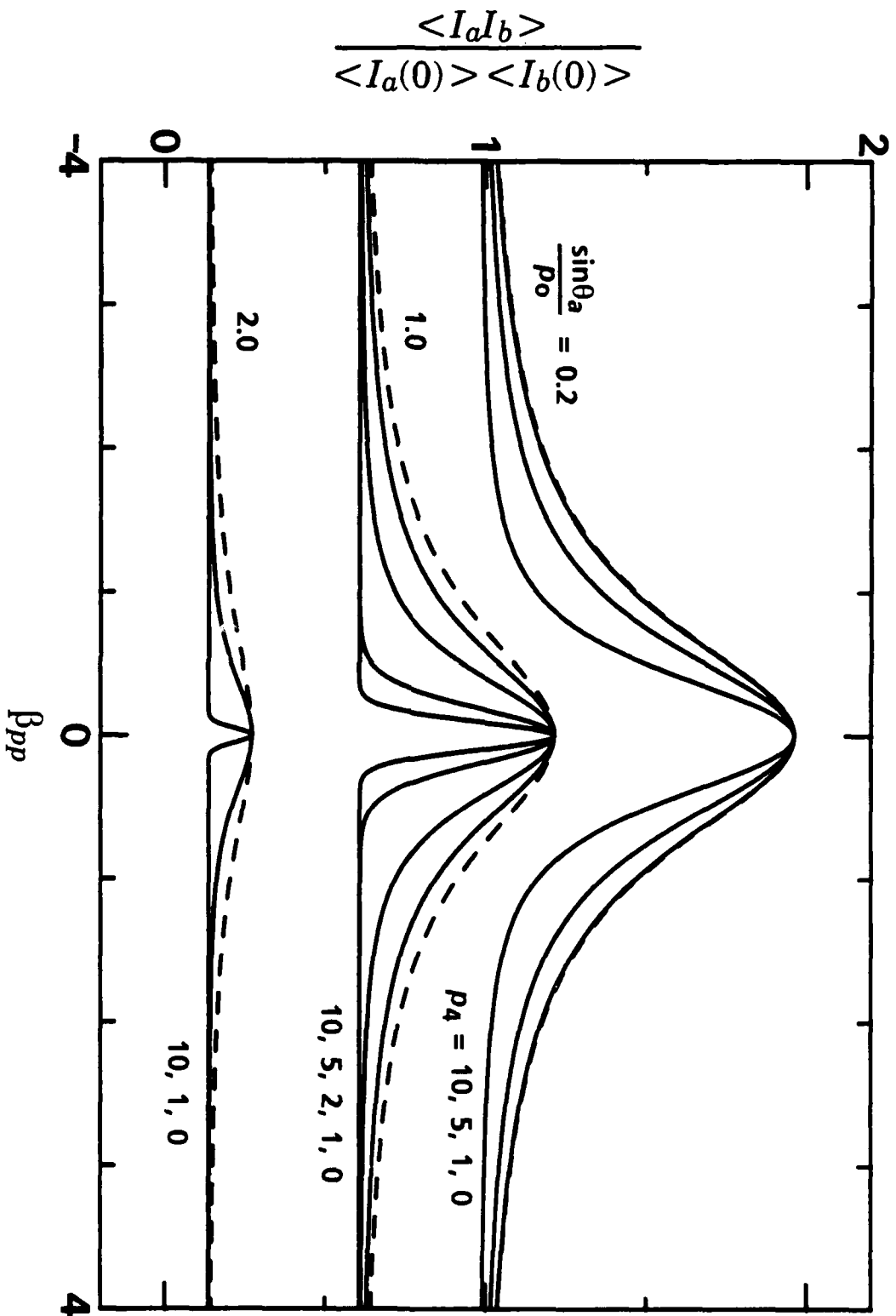
Fig. 4.3. Effect of the ratio parameter p_4 on wavelength decorrelation for off-axis illumination of a cascade of two diffusers. Equation (4.56) is plotted against β_{pp} for different values of p_4 and $\sin\theta_a/p_0$. The dashed lines are the limiting curves for $p_4 = 0$.

One could also determine p_4 from f_5, however, f_5 is the most difficult to use of all the factors since $|\mathbf{k}_{ab\perp}|$ must be nonzero, and since both angular and wavelength detuning must be present simultaneously for it to contribute. Hence f_5 is also the easiest factor to eliminate from Eq. (4.13). We note that f_5 is the only factor that curves upwards about the origin, but that it does not increase indefinitely with β_{pp} because $\beta_{pp}/(1+\beta_{pp}^2)$ has a maximum value of 0.5 at $\beta_{pp}=1$.

In optimizing the accuracy of a measurement system, it may be desirable to measure the parameters p_0, p_2, p_3, and p_4 in several different ways to check for consistency and to average measurement errors. In such a system f_5 may be of some value, however, f_5 is not important in most practical applications, and there are no new parameters to be obtained from it.

4.4 Determination of Spacing and Diffuser Slope Parameters

In Section 4.3 we have introduced the five parameters p_0, p_1, p_2, p_3, and p_4 in Eqs. (4.16), (4.25), (4.26), (4.44), and (4.53), respectively. These parameters represent the information that one can obtain from different remote sensing measurements based on Eq. (4.13). In applying the analysis to the remote sensing of a cascade of two thin diffusers, there are three experimental configurations that are particularly useful, and that should be treated in more detail.

In the first application it is desired to measure the thickness H of a layer of material or a film that has rough interfaces with the surrounding medium. Perhaps it is not possible to measure this thickness directly without destroying either the sample or the surrounding medium, or perhaps the sample is immersed in the surrounding medium in such a way that one can not measure the thickness mechanically. We will refer to this configuration by the symbol (H). In the second application one can measure the surface properties of diffuser D_2 directly because it is on the observation side of the diffuser combination. Given this information, it is desired to find the surface slope statistics of

the input surface, D_1, and the spacing between surfaces. We shall denote this problem by the symbol $(H,D_1|D_2)$ because we are to determine σ_{t_1}/w_1 for D_1 and H given σ_{t_2}/w_2 for D_2. In the third problem, denoted as (H,D_1,D_2), we have no prior knowledge of H, σ_{t_1}/w_1, or σ_{t_2}/w_2, and it is necessary to determine all three parameters remotely.

In solving these three remote sensing problems, we will assume that we can perform experiments to obtain the parameters p_0, p_1, p_2, p_3, and p_4. In this section we will determine which parameters must be evaluated, or in other words, what types of experiments must be performed, for the solution of each remote sensing problem. For convenience we list the definitions of all five parameters together in one location:

$$p_0 = \left(\frac{\sigma_{t1}^2}{w_1^2} + \frac{\sigma_{t2}^2}{w_2^2} \right)^{\frac{1}{2}}, \qquad [(4.16)]$$

$$p_1 = \left(\sigma_{t1}^2 + \sigma_{t2}^2 \right)^{\frac{1}{2}}, \qquad [(4.25)]$$

$$p_2 = 2H \left(\frac{w_1^2}{\sigma_{t1}^2} + \frac{w_2^2}{\sigma_{t2}^2} \right)^{-1}, \qquad [(4.26)]$$

$$p_3 = \sqrt{2}\, H \left(\frac{w_1^2}{\sigma_{t1}^2} + \frac{w_2^2}{\sigma_{t2}^2} \right)^{-\frac{1}{2}}, \qquad [(4.44)]$$

and

$$p_4 = \frac{\sigma_{t1}}{w_1} \frac{w_2}{\sigma_{t2}}. \qquad [(4.53)]$$

The parameter p_1 is in class by itself because it involves the rms roughness, not the rms slope. Unless we are given more information, we cannot solve for σ_{t_1} and σ_{t_2} separately. Hence we will concentrate on the evaluation of σ_{t_1}/w_1, σ_{t_2}/w_2, and H given one or more of the parameters p_0, p_2, p_3, and p_4. Since there are four remaining equations and only three unknowns, these four parameters are obviously not independent; in fact, they are related by the expression

$$2\,p_0^{\,2}p_3^{\,2} = p_2^{\,2}\left(2 + p_4^{\,2} + p_4^{\,-2}\right). \tag{4.58}$$

This dependence implies that there will be more than one method for obtaining a given diffuser parameter.

We have described the following three basic experiments in Section 4.3: measurement of the angular distribution of the radiation pattern for determination of p_0, measurement of the decorrelation of the far-zone speckle pattern with respect to the wavelength for determination of p_1 and p_2, and decorrelation with respect to the angle of incidence for determination of p_3. In addition we have described an auxiliary experiment for distinguishing between the input and output diffusers by measuring whether p_4 is greater than or less than one. Since both parameters p_1 and p_2 are measured through wavelength decorrelation, it may not be possible to accurately determine both parameters experimentally if the ratio Q, Eq. (4.34), is either very large or very small compared to one. In the remainder of Section 4.4, we will assume that $Q >> 1$ or that $Q \approx 1$ so that we can at least determine the spacing-wavelength parameter p_2.

4.4.1 Spacing

In the first class of problems, denoted by the symbol (H), we are to determine the spacing H between diffuser planes. By comparing Eq. (4.26) for p_2 with Eq. (4.44) for p_3, we see that we can obtain H given p_2 and p_3 by the expression

$$H = \frac{p_3^{\,2}}{p_2}. \tag{4.59}$$

Thus H can be found by performing a wavelength and an angle of incidence experiment. Once H has been evaluated, one can use either Eq. (4.26) or Eq. (4.44) to determine $w_1^2/\sigma_{t_1}^{\,2} + w_2^2/\sigma_{t_2}^{\,2}$. In many applications, this quantity is constant so that one would need only a wavelength experiment or an angle of incidence experiment to determine new values of H. Another possibility is that one is only interested in the ratio of two spacings.

This ratio can also be determined by performing either a wavelength or an angle of incidence experiment for the two spacings.

Using Eq. (4.58), we can eliminate either p_2 or p_3 from Eq. (4.59), however, the resulting expressions also require knowledge of p_0 and p_4:

$$H = \frac{p_2}{2 p_0^2}\left(2 + p_4^2 + p_4^{-2}\right)$$

(4.60)

and

$$H = \frac{p_3}{\sqrt{2}\, p_0}\sqrt{2 + p_4^2 + p_4^{-2}}\,.$$

(4.61)

If the rough interfaces are produced by the same process, then one may assume that $\sigma_{t_1}/w_1 = \sigma_{t_2}/w_2$, i.e., that $p_4 = 1$. Then Eqs. (4.60) and (4.61) are particularly useful because H can be determined by finding p_0 from a radiation pattern measurement and either p_2 from a wavelength experiment,

$$H = 2\,\frac{p_2}{p_0^2}\,,$$

(4.62)

or p_3 from an angle of incidence experiment

$$H = \sqrt{2}\,\frac{p_3}{p_0}\,.$$

(4.63)

4.4.2 Depth and rms Slope of a Buried Rough Surface

In the second class of problems, denoted by the symbol $(H, D_1 | D_2)$, one wishes to determine the slope parameter σ_{t_1}/w_1 of a hidden surface D_1 and the depth H of this surface below an outer diffusing surface D_2. Since the outer surface can be observed directly, we assume that its slope parameter σ_{t_2}/w_2 is known.

There are five methods for determining the two unknown parameters H and σ_{t_1}/w_1, each of which requires knowledge of two of the parameters p_0, p_2, p_3, or p_4. The sixth combination, (p_0, p_4), of the four parameters does not allow for evaluation of H. In the first method, which we refer to by the symbol (p_2, p_3), we obtain p_2 through a wavelength experiment and p_3 through an angle of incidence experiment. We have

already shown how one obtains H from these measurements, see Eq. (4.59). The solution for the other parameter σ_{t_1}/w_1 is found by substituting Eq (4.59) for H into either Eq. (4.26) or Eq. (4.44):

$$\frac{\sigma_{t1}}{w_1} = \left(\frac{2 p_3^2}{p_2^2} - \frac{w_2^2}{\sigma_{t2}^2} \right)^{-\frac{1}{2}} . \tag{4.64}$$

In the second and third methods, denoted by (p_0, p_2) and (p_0, p_3), we determine p_0 from the radiation pattern. When Eq. (4.16) for p_0 is solved for the unknown, σ_{t_1}/w_1, we obtain

$$\frac{\sigma_{t1}}{w_1} = \left(p_0^2 - \frac{\sigma_{t2}^2}{w_2^2} \right)^{\frac{1}{2}} . \tag{4.65}$$

We can determine the other unknown, H, from either a wavelength experiment to find p_2, or an angle of incidence experiment to find p_3. We calculate H for the (p_0, p_2) method by substituting Eq. (4.65) for σ_{t_1}/w_1 into Eq. (4.26):

$$H = \frac{p_2}{2} \frac{w_2^2}{\sigma_{t2}^2} \left(1 - \frac{\sigma_{t2}^2}{p_0^2 w_2^2} \right)^{-1} . \tag{4.66}$$

Likewise, we calculate H for the (p_0, p_3) method by substituting Eq. (4.65) into Eq. (4.44):

$$H = \frac{p_3}{\sqrt{2}} \frac{w_2}{\sigma_{t2}} \left(1 - \frac{\sigma_{t2}^2}{p_0^2 w_2^2} \right)^{-\frac{1}{2}} . \tag{4.67}$$

For completeness, we have included the fourth and fifth methods, (p_4, p_2) and (p_4, p_3), even though they require knowledge of p_4, the most difficult of all the parameters to measure. The solution of σ_{t_1}/w_1 follows immediately from the definition of p_4:

$$\frac{\sigma_{t1}}{w_1} = p_4 \frac{\sigma_{t2}}{w_{t2}} . \tag{4.68}$$

The spacing H is determined by substituting Eq. (4.68) into Eq. (4.26) for the (p_4, p_2) method or into Eq. (4.44) for (p_4, p_3) method:

$$H = \frac{p_2}{2} \frac{w_2^2}{\sigma_{t2}^2} \left(1 + p_4^{-2} \right) \tag{4.69}$$

and

$$H = \frac{p_3}{\sqrt{2}} \frac{w_2}{\sigma_{t2}} \left(1 + p_4^{-2}\right)^{\frac{1}{2}}. \tag{4.70}$$

If we can assume that both surfaces are created by the same process so that $p_4 = 1$, then Eqs. (4.69) and (4.70) are more useful. Then it is only necessary to perform a wavelength or an angle of incidence decorrelation experiment to evaluate H.

4.4.3 Spacing and Diffuser Slope Parameters for Both Diffusers

In the final class of problems, (H, D_1, D_2), one wishes to determine all three parameters, H, σ_{t_1}/w_1, and σ_{t_2}/w_2, remotely. Since we have already shown how to obtain H in Section 4.4.1, we will emphasize the evaluation of σ_{t_1}/w_1 and σ_{t_2}/w_2 in this section. For the solution of the present problem we need to determine at least three of the parameters p_0, p_2, p_3, and p_4 by remote sensing experiments since we are to solve for all three parameters H, σ_{t_1}/w_1, and σ_{t_2}/w_2. There are four possible combinations of these parameters taken three at a time. In the preferred experimental method, we use the combination (p_0, p_2, p_3) because p_4 is more difficult to measure. First, we use Eq. (4.59) to determine H, and then we obtain the solution for σ_{t_1}/w_1 and σ_{t_2}/w_2 as follows: We use Eq. (4.59) to eliminate H from Eq. (4.26), solve the resulting equation for $\sigma_{t_2}^2/w_2^2$ and substitute this solution into Eq. (4.16). This yields a quadratic equation for $\sigma_{t_1}^2/w_1^2$:

$$\frac{1}{p_0^2} \frac{\sigma_{t1}^4}{w_1^4} - \frac{\sigma_{t1}^2}{w_1^2} + \frac{p_2^2}{2 p_3^2} = 0. \tag{4.71}$$

The solution of Eq. (4.71) for σ_{t_1}/w_1 is

$$\frac{\sigma_{t1}}{w_1} = \frac{p_0}{\sqrt{2}} \left[1 \pm \left(1 - \frac{2 p_2^2}{p_0^2 p_3^2} \right)^{\frac{1}{2}} \right]^{\frac{1}{2}}. \tag{4.72}$$

By substituting this solution back into Eq. (4.16) and solving for σ_{t_2}/w_2, we obtain the corresponding solution,

$$\frac{\sigma_{t2}}{w_2} = \frac{p_0}{\sqrt{2}} \left[1 \mp \left(1 - \frac{2 p_2^2}{p_0^2 p_3^2} \right)^{\frac{1}{2}} \right]^{\frac{1}{2}}, \tag{4.73}$$

for diffuser D_2. In comparing Eqs. (4.72) and (4.73), we note that the $\pm$ sign has been

replaced by $\mp$ in Eq. (4.73). In other words, we must use opposite signs in the two solutions. We point out that we are unable to tell whether the upper or lower choice of signs is correct without having more information. This sign ambiguity results from the symmetry with respect to σ_{t_1}/w_1 and σ_{t_2}/w_2 in the definitions of p_0, p_2, and p_3. As discussed in Section 4.3.4, we can resolve this ambiguity by measuring whether p_4 is greater than or less than unity.

If the quantity $2p_2^2/(p_0^2 p_3^2)$ in Eqs. (4.72) and (4.73) were greater than one, then we would have the square-root of a negative number. However, this is not allowed to happen, as we see by writing this quantity in terms of p_4 via Eq. (4.58): Even though p_4 ranges between zero and infinity, the condition

$$0 \leq \frac{2 p_2^2}{p_0^2 p_3^2} = \frac{4}{2 + p_4^2 + p_4^{-2}} \leq 1 \tag{4.74}$$

always holds. Owing to the uncertainty in experimental measurements of p_0, p_2, and p_3, the condition in Eq. (4.74) could be violated. However, this is most likely to occur near $p_4 = 1$ where the inequality has its maximum value. Hence, if the condition is violated, one can assume that $p_4 = 1$ to within the resolution of the measurements.

For completeness we also list the equations for the other three methods. In the (p_0, p_2, p_4) and (p_0, p_3, p_4) methods, one uses Eqs. (4.60) and (4.61) respectively to find H. For both methods, one then determines σ_{t_1}/w_1 and σ_{t_2}/w_2 via

$$\frac{\sigma_{t1}}{w_1} = p_0 \left(\frac{1 + p_4^2}{2 + p_4^2 + p_4^{-2}} \right)^{\frac{1}{2}} \tag{4.75}$$

and

$$\frac{\sigma_{t2}}{w_2} = p_0 \left(\frac{1 + p_4^{-2}}{2 + p_4^2 + p_4^{-2}} \right)^{\frac{1}{2}} . \tag{4.76}$$

Equations (4.75) and (4.76) are obtained from Eqs. (4.72) and (4.73) by using Eq. (4.58) to eliminate p_2 and p_3 and choosing the signs to agree with the definition of p_4 in Eq. (4.53).

If both rough surfaces are caused by the same random process, then $p_4 = 1$, and we have the simple result $\sigma_{t_1}/w_1 = \sigma_{t_2}/w_2 = p_0/2^{\frac{1}{2}}$.

In the final method of determining H, σ_{t_1}/w_1, and σ_{t_2}/w_2, referred to as the (p_2, p_3, p_4) method, H is determined from Eq. (4.59), and σ_{t_1}/w_1 and σ_{t_2}/w_2 are given by

$$\frac{\sigma_{t1}}{w_1} = \frac{p_2}{\sqrt{2}\, p_3} \sqrt{1 + p_4^2} \tag{4.77}$$

and

$$\frac{\sigma_{t2}}{w_2} = \frac{p_2}{\sqrt{2}\, p_3} \sqrt{1 + p_4^{-2}} \,. \tag{4.78}$$

Equations (4.77) and (4.78) are obtained from Eqs. (4.75) and (4.76) by using Eq. (4.58) to eliminate p_0.

4.5 Discussion

The analysis of the paraboloidal-paraboloidal diffuser combination presented in Chapter 4 has been important to our understanding of the remote sensing of double diffusers because we were able to obtain the general expression given in Eq. (4.13) for the two-state correlation of far-zone intensity for arbitrary values of all the input parameters and then to study the significance of each of the factors f_1, f_2, f_3, f_4, and f_5. Through this analysis we learned that H, σ_{t_1}/w_1, and σ_{t_2}/w_2 could be obtained by performing simple experiments with equal input and observation directions, $k_{ab\perp} = 0$. It was only necessary to have $k_{ab\perp} \neq 0$ to distinguish between the two diffusers, i.e., to tell the order in which the diffusers appear in Fig. 3.1.

In Chapter 4 we have been able to classify the different speckle phenomenon that occur in double-diffuser decorrelation experiments by analyzing the P-P diffuser combination. However, we point out that there is one major difference between speckle from the P-P and from other diffuser combinations. The unique property of u_{ab} for the P-P combination is that the shape of the decorrelation curves do no depend on the

diffuser parameters σ_{t_1}/w_1 and σ_{t_2}/w_2, i.e., the widths of the curves are scaled by changing these parameters, but Eq. (4.13) remains a combination of Lorentzian and Gaussian functions. For this reason, we are only able to extract one parameter from each of the three experiments depicted in Fig. 4.1(a) through 4.1(c), i.e., the width of the functions f_0, f_2, and f_3.

However, by inspection of the results in Appendix E for the P-C and C-P combinations and in Appendix F for the C-C combinations, we see that one can extract two parameters from each experiment. For example, by comparing Eq. (E10) for the two-state correlation function of intensity for the P-C diffuser combination with the corresponding function, Eq. (4.22), for the spacing-wavelength dependence of the P-P combination, we see that the factor corresponding to f_2 defined in Eq. (4.20) is

$$f_{2,pc} = \frac{|D(\gamma_{pc}\sqrt{k_a k_b}\sqrt{1+i\beta_{pc}})|^2}{D(\gamma_{pc}k_a)\,D(\gamma_{pc}k_b)}\,, \tag{4.79}$$

where D is defined in Eq. (E4). In addition, the spacing-wavelength detuning parameter β_{pc} is

$$\beta_{pc} = 2\,H\,\Delta k\,\frac{\sigma_{t1}^2}{w_1^2}\,, \tag{4.80}$$

and ratio parameter γ_{pc} is

$$\gamma_{pc} = \frac{w_1}{\sigma_{t1}}\,\frac{\sigma_{t2}^2}{\sqrt{2}\,w_2}\,. \tag{4.81}$$

We see that γ_{pc} determines the shape of the function $f_{2,pc}$ plotted against β_{pc}. By fitting the experimental data to Eq. (4.79), one could determine the ratio parameter γ_{pc} from matching the curve shape and the product $H\sigma_{t_1}^2/w_1^2$ from matching the curve width. We also note that one could determine both σ_{t_1}/w_1 and $\sigma_{t_2}^2/w_2$ from measuring the angular distribution of the radiation pattern, see Fig. 4.1(a), and both γ_{pc} and $H\sigma_{t_1}/w_1$ from performing an angular decorrelation experiment on the P-C diffuser combination, see Fig. 4.1(b).

By inspection of the results for the C-P and C-C combinations, we see that one can also determine two parameters from each type of experiment. Thus we have much more freedom in choosing our experiments in the remote sensing of the P-C, C-P, and C-C diffuser combinations. We also note that the diffuser parameters that one can determine are different for each of the four combinations, i.e., σ_{t_1}/w_1 and σ_{t_2}/w_2 for P-P, σ_{t_1}/w_1 and $\sigma_{t_2}^2/w_2$ for P-C, $\sigma_{t_1}^2/w_1$ and σ_{t_2}/w_2 for C-P, and $\sigma_{t_1}^2/w_1$ and $\sigma_{t_2}^2/w_2$ for C-C.

For the P-P combination, it was necessary to perform and auxiliary experiment with $k_{ab\perp} \neq 0$ to determine the order in which the diffusers occur. This also appears to be true for other diffuser combinations. For example, Eq. (E10) for the P-C and Eq. (E20) for the C-P diffuser combinations are identical except that the numbering on the rms roughnesses σ_{t_1} and σ_{t_2} and on the correlation lengths w_1 and w_2 has been switched. In other words, β is defined in terms of σ_t/w for the paraboloidal diffuser for both cases, and γ is defined as the ratio of $\sigma_t^2/(2\ell w)$ for the conical diffuser and σ_t/w for the paraboloidal diffuser for both cases. Thus, we are able to find the appropriate parameter for the conical and paraboloidal diffusers, but we must have some other method of determining whether the combination is P-C or C-P. In conclusion, we note that there is also an ambiguity in the ordering of the diffusers for the C-C combination, e.g., Eq. (F15) is defined in terms of the absolute value of the difference between the parameters $\sigma_{t_1}^2/w_1$ and $\sigma_{t_2}^2/w_2$.

Chapter 5

Experiments: Radiation Patterns from Strong Diffusers

5.1 Introduction

The relationship between the characteristics of a rough surface and the angular distribution of light scattered from the surface is a subject of considerable interest. Applications include designing rough surfaces or diffusers with a desired angular distribution, predicting the radiation patterns from a given surface, and providing a noncontact method for characterizing surfaces.[1-18] Diffuser radiation patterns are also of interest in the analysis of the decorrelation of speckle from a cascade of diffusers. As discussed in Section 3.3, one can determine the autocorrelation function R_t of the diffuser transmission function t by measuring the radiation pattern and then performing a Fourier transform, see Eq. (3.51). Given R_t for the individual diffusers, one can then predict the speckle decorrelation properties for the diffuser cascade.

In this chapter we study the radiation patterns from paraboloidal and conical diffusers, which were defined in Section 3.3.2 as strong diffusers having a circularly symmetric autocorrelation function, a normally distributed height profile, and height profile autocorrelation functions that are paraboloidal or conical, respectively, for small spatial offsets. We also extend the analysis of these single-scale diffusers to diffusers having two scales of roughness and present measured radiation patterns over a large dynamic range. For ease of reading, and to make Chapter 5 self contained, we will reintroduce the basic quantities. Because of the applied nature of Chapter 5, the formulas will be written in terms of input and output angles rather than direction vectors. In addition, the arguments will be written in terms of the x-y coordinates of the diffuser planes rather than the vector r or simply as r when there is circular symmetry.

109

We define a strong diffuser as one whose rms phase delay

$$S = k\sigma_h (n-1) \tag{5.1}$$

caused by the surface roughness is much greater than one radian. In Eq. (5.1), n is the index of refraction of the diffuser, σ_h is the rms diffuser height, and $k = 2\pi/\lambda$, where λ is the wavelength of illumination. In general, the functional form of the radiation pattern depends both on the value of S and on the form of the normalized autocorrelation function of the surface profile

$$R_h(x_2 - x_1, y_2 - y_1) = \frac{< h(x_1, y_1)\, h(x_2, y_2) >}{\sigma_h^2} , \tag{5.2}$$

where the angle brackets denote an ensemble average. However, for $S >> 1$, the effect of R_h on the radiation pattern is determined by the behavior of R_h for small spatial offsets.

We consider diffusers where the surface profile $h(x,y)$ is normally distributed and the autocorrelation function depends on the offset $r = [(x_2-x_1)^2 + (y_2-y_1)^2]^{\frac{1}{2}}$ between points (x_1, y_1) and (x_2, y_2), but not on the direction of this offset. When the latter property holds, the envelope of the radiation pattern for normal incidence will be circularly symmetric. If the autocorrelation function can be represented by a power series in r, then one of the two classes will arise depending on whether the linear term in r is present or missing. If this term is present, then the autocorrelation function will be cone shaped near the origin,

$$R_h(r) = 1 - \frac{r}{w} + \ldots , \tag{5.3}$$

and the shape of the radiation patterns will depend on the quantity w/S^2, where w is the correlation length of the diffuser roughness. If the linear term is missing, then the autocorrelation function will be paraboloidal near the origin

$$R_h(r) = 1 - \left(\frac{r}{w}\right)^2 + \ldots , \tag{5.4}$$

and the shape of the radiation pattern will depend on the ratio w/S.

We use the terms conical and paraboloidal only to refer to the shape of R_h for small offsets. A cone and a paraboloid, defined respectively by the first two terms of Eq. (5.3) and Eq. (5.4) for $r \leq w$ and as zero otherwise, would not be valid autocorrelation functions since their Fourier transforms are negative in certain regions. Equation (5.3) is characteristic of surfaces having discontinuities and high slopes. An example of a rapidly falling autocorrelation function in one dimension is the triangle function which results as the autocorrelation of a rectangle function. Equation (5.4), on the other hand, is characteristic of smooth surfaces that are bandlimited in spatial frequency.

We present radiation patterns from a ground-glass diffuser and a specially fabricated etched-glass diffuser measured over an output angle θ of nearly $\pm 90°$ and over a dynamic range of six and eight orders of magnitude, respectively. In these measurements the solid angle subtended by the detector is large enough to include many speckles but small enough so as not to have a significant effect on the angular resolution of the measurement. Thus, the measured intensity is a good approximation to the expected envelope of intensity that is calculated in the statistical analysis.

There is very good agreement between the ground-glass radiation patterns and curves of the first type, which depend on the value of w/S^2, and between the etched-glass radiation patterns and curves of the second type, which depend on the value of w/S. The etched-glass radiation patterns can be fit over about three orders of magnitude, i.e., at small angles, with a simple paraboloidal autocorrelation function. However, due to the microstructure of the surface, it is necessary to use a composite diffuser model containing two scales of roughness to fit the radiation pattern over all angles. The model for the surface profile then consists of a large roughness paraboloidal component with a small roughness exponential component superimposed. The small roughness component has a negligible effect on the upper two or three orders of magnitude of the radiation pattern, but it dominates at wide angles.

The first diffuser was made by grinding glass, and the second diffuser was made by chemically etching preroughened glass surfaces. Photographs of the surfaces of both types of diffuser, as taken with a scanning electron microscope, are shown in Fig. 5.1. The ground-glass surface of Fig. 5.1(a) has the discontinuities and the high spatial frequency content characteristic of Eq. (5.3). The etched-glass surface of Fig. 5.1(b), on the other hand, is smooth on a wavelength scale and has gentle slopes, except for the ridges, as is characteristic of Eq. (5.4).

Much has been written on the scattering of light from ground glass.[19-26] For example, it has been demonstrated that the height profile is approximately normally distributed.[19-23] In previous attempts to calculate the angular distribution of the radiation from ground glass, it has been assumed, for simplicity, that the autocorrelation function of heights is Gaussian. However, as pointed out by Chandley,[22] the autocorrelation function is not Gaussian. Hence, these predictions of the angular distribution of light have failed. Since ground glass does not fit the analysis, other authors have gone to considerable effort to prepare this type of Gaussian diffuser.[27-29] However, the interest in modeling actual diffusers that are widely used ll exists.

Another common assumption in theoretical derivations is that the rms phase delay produced by the diffuser is large compared to one radian, i.e., $S >> 1$. For such a diffuser, it is not the exact shape of the autocorrelation function that is important, but its behavior for small offsets. Therefore, the type of etched-glass diffuser studied below, which has a normally distributed height profile, a paraboloidal or Gaussian like autocorrelation function, and a large rms phase deviation, should be useful for testing theories based on these assumptions.

In Section 5.2 we present the equations governing the angular dependence of the intensity scattered from single-scale diffusers having $S >> 1$ and behaving like Eq. (5.3) or Eq. (5.4) for small offsets. We develop a composite diffuser model consisting of two scales of roughness in Section 5.3 and describe the experimental configuration for

20 μm ――――――――

(a)

20 μm ――――――――
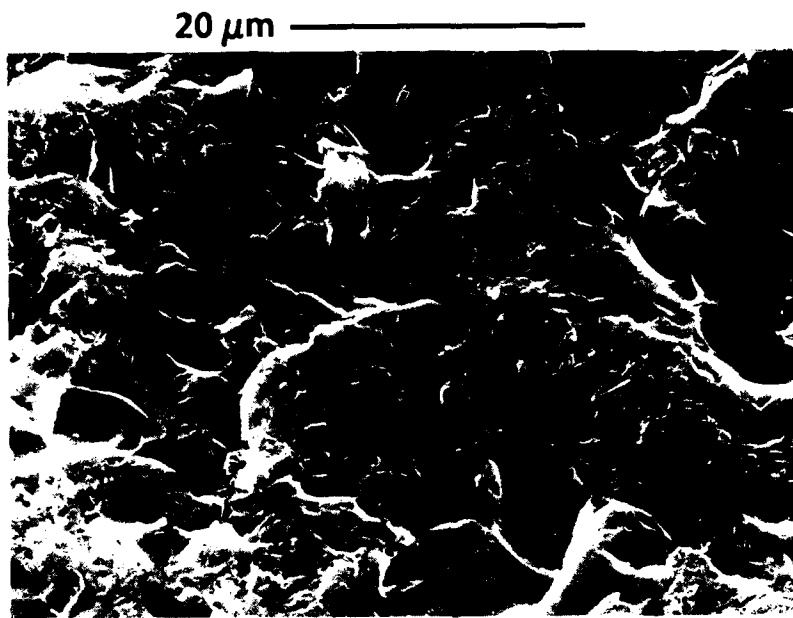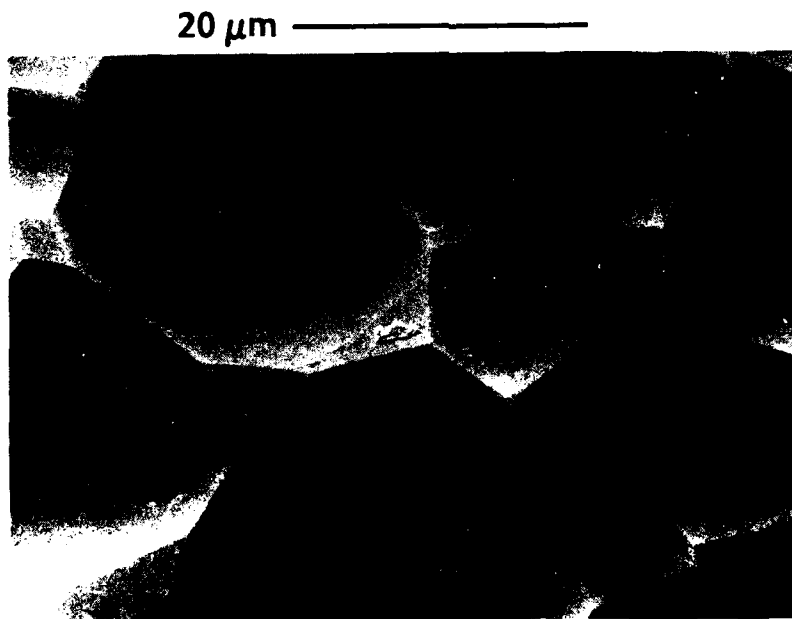
(b)

Fig. 5.1.   SEMs of glass surfaces (a) ground with 820 grit and (b) preroughened for 60
minutes with Armour Etch and etched for 45 minutes in BOE.

measuring the radiation patterns in Section 5.4. In Section 5.5 experimentally measured radiation patterns are presented for ground-glass and etched-glass diffusers. These results are found to be in excellent agreement with the theoretical predictions. By varying the etching process, paraboloidal diffusers with $w/(\lambda S)$ ranging between 3 and 13 are obtained. There is also excellent agreement between values of $w/(\lambda S)$ for the various etched-glass diffusers as obtained by fitting the radiation patterns to the theoretical curves and by measuring the surface profile with a stylus profilometer.

5.2 Envelope of Far-Zone Intensity

The physical quantity of interest in the study of radiation patterns is the power per unit solid angle received by a detector, i.e., the radiant intensity

$$I = \frac{dP}{d\Omega} .$$ (5.5)

When laser light is used to illuminate the sample, a speckle pattern will appear in the scattered light. However, we are not interested in the microscopic detail of this speckle pattern, but rather in the angular distribution of the envelope of intensity I_e. Since any practical detector system will subtend a finite solid angle $\Delta\Omega$, we will be able to smooth out these rapid intensity variations by choosing a detector that is large compared to the size of a speckle, yet small enough so as not to have a significant effect on the angular resolution of the measurement. Furthermore, to standardize the radiation patterns so that they can be compared to one another, we will plot all radiation patterns relative to the incident power P_0. Therefore, we will use the normalized envelope of intensity I_{en} defined by[30]

$$I_{en} = \frac{\Delta P}{\Delta\Omega\ P_0} .$$ (5.6)

The coordinate system used for both the experiments and the analysis is the same as in Fig. 2.2. The diffuser is located at the x-y plane with illumination incident at angles (θ_0,ϕ_0). Scattered radiation is measured at observation angles (θ,ϕ). If the azimuthal angles ϕ_0 and ϕ are equal, then the measurement is in the plane of incidence.

In the analysis the diffuser height profile will be represented by a normally distributed, zero mean, wide-sense stationary, random process $h(x,y)$ having a normalized autocorrelation function $R_h(r)$, defined in Eq. (5.2), and an arbitrary roughness σ_h. The expected value, or the ensemble average, of the normalized intensity will be denoted by $<I_n>$. The general form for $<I_n>$ arising from a diffuser with a normally distributed height profile is

$$<I_n> = \cos^n\theta \frac{2\pi}{\lambda^2} \int_0^\infty rJ_0\left(2\pi\frac{r}{\lambda}\sqrt{\sin^2\theta - 2\cos(\phi - \phi_0)\sin\theta\sin\theta_0 + \sin^2\theta_0}\right)$$

$$\times \exp\left\{-S^2\left[1 - R_h(r)\right]\right\} dr. \tag{5.7}$$

Equation (5.7) is obtained by substituting Eq. (3.62) for R_t into Eq. (3.51), setting $k_a = k_b$, replacing $\bar{A}$ by its initial value of unity, converting from wave vectors to angles through Eq. (2.3), and converting the circularly symmetric Fourier transform to a Fourier-Bessel transform. The $\cos^2\theta$ obliquity factor is also generalized to $\cos^n\theta$. Of course, the angle dependence within the argument of the Bessel function in Eq. (5.7) simplifies to $\sin\theta$ for normal incidence $\theta_0 = 0$ and to $\sin\theta$-$\sin\theta_0$ for measurements in the plane of incidence $\phi_0 = \phi$. From the theoretical model, the $\cos^n\theta$ in Eq. (5.7) should be $\cos^2\theta$. However, the theory neglects multiple bounce effects in the surface structure of the diffuser and shadowing as well. Hence, the precision of fit at angles $\theta > 75°$ is uncertain. We prefer to keep the coefficient n general at this point. Empirically, we have found that better experimental fit to the data is obtained by setting $n = 1$. Thus, we will set $n = 1$ in expressions for $<I_n>$ throughout the remainder of this chapter.

If S is not large compared with unity, then Eq. (5.7) may contain a direct component, as represented by a delta function. This delta function should be replaced by the functional form of the aperture radiation pattern. We see that this direct component becomes insignificant for large S, e.g., if $R_h(r)$ falls to zero as r increases, then the magnitude of the delta function will be $\exp(-S^2)$.

5.2.1 Strong Diffusers (S>>1)

We will now briefly describe how the two classes of radiation patterns arise for single scale diffusers with $S>>1$. By inspection of Eq. (5.7), we see that the major contributions to the integral for large values of S occur near the origin $r=0$. Therefore, the shape of the radiation pattern is determined by the behavior of R_h for small values of r. This leads us to consider the beginning terms of power series expansions of R_h. The first term will be unity for any choice of R_h since R_h is normalized to unity at the origin. This term drops out of Eq. (5.7) because it is $1-R_h$ that appears in the exponent. The second term will be of the form r^a, where a is the lowest nonzero power of r with a nonzero coefficient; this term will control R_h for small r. With the exception of a constant autocorrelation function where a is infinite, the highest possible value of a is two.[31] We will only consider autocorrelation functions where $a=1$ or $a=2$. However, autocorrelation functions do exist where a is a noninteger less than two. In general, for single scale diffusers with $S>>1$, $<I_n>$ will depend on w and S through the single dimensionless shape parameter $w/(\lambda S^{2/a})$.

We can see the relative importance of the different terms in a power series expansion of R_h by writing the exponent in Eq. (5.7) as

$$\exp\left[-S^2\left(1-R_h(r)\right)\right] = \exp\left[\frac{C_1 S^2}{w}|r| + \frac{C_2 S^2}{w^2}r^2 + \frac{C_3 S^2}{w^3}|r|^3 + \ldots\right]. \qquad (5.8)$$

If $C_1=-1$, then R_h is conical, Eq. (5.3), and if $C_1=0$ and $C_2=-1$, then R_h is paraboloidal, Eq. (5.4). We consider conical autocorrelation functions first. For $S>>1$, the linear term will determine the behavior of Eq. (5.8) as illustrated by the following numerical example: In Eq. (5.8) we have $C_1=-1$ for the conical autocorrelation function; let us also suppose $C_2=-1$ and $S=10$. The $1/e^2$ point for the decaying exponential, arising from the first term, is $r=w/50$. However, at this value of r the Gaussian, arising from the second term, has only dropped from unity to 0.96. Higher order terms will be even less significant. By keeping only the first term in Eq. (5.8), setting $n=1$ as discussed, and

evaluating the integral in Eq. (5.7), we see that the expected value of the normalized radiant intensity $<I_n>$ for a strong diffuser of the conical type is

$$<I_n> = \cos\theta \, 2\pi \left(\frac{w}{\lambda S^2} \right)^2$$

$$\times \left[1 + \left(\frac{2\pi w}{\lambda S^2} \right)^2 \left(\sin^2\theta - 2 \cos(\phi - \phi_0) \sin\theta \sin\theta_0 + \sin^2\theta_0 \right) \right]^{-3/2} . \qquad (5.9)$$

In Eq. (5.9) the shape parameter is $w/(\lambda S^2) = w\lambda/(2\pi\sigma_t)^2$. For paraboloidal diffusers, the quadratic term will dominate the higher order terms for $S >> 1$. By keeping only the second term in Eq. (5.8) and again evaluating Eq. (5.7), we obtain

$$<I_n> = \cos\theta \, \pi \left(\frac{w}{\lambda S} \right)^2$$

$$\times \exp\left[-\left(\frac{\pi w}{\lambda S} \right)^2 \left(\sin^2\theta - 2 \cos(\phi - \phi_0) \sin\theta \sin\theta_0 + \sin^2\theta_0 \right) \right]. \qquad (5.10)$$

The shape parameter in Eq. (5.10) is $w/(\lambda S) = w/(2\pi\sigma_t)$.

Equations (5.9) and (5.10) were derived for diffusers having a single scale of roughness. In Section 5.3 we will extend these results to diffusers with two scales of roughness by assuming that the surface profile is the sum of two functions having autocorrelation functions R_{h_1} and R_{h_2}, normalized roughness S_1 and S_2, and correlation lengths w_1 and w_2. Depending on the choices of these autocorrelation functions and parameters, more than one term in Eq. (5.8) can be significant in determining $<I_n>$, even if $S_1 >> 1$ or $S_2 >> 1$ and especially at large angles θ.

It is useful to compare Eqs. (5.9) and (5.10) with the radiation pattern of an idealized Lambertian diffuser for which

$$<I_n> = \frac{\cos\theta}{\pi} . \qquad (5.11)$$

We note that Eq. (5.11) is not a large roughness limiting form of either Eq. (5.9) or (5.10). As described in Section 5.4, a Lambertian diffuser may be used to perform the system calibration.

It is also of interest to integrate the intensities in Eqs. (5.9) and (5.10) over the output hemisphere for normal incidence to obtain the total integrated power. This yields

$$P = P_0 \left\{ 1 - \left[1 + \left(\frac{2\pi w}{\lambda S^2} \right)^2 \right]^{-\frac{1}{2}} \right\} \tag{5.12}$$

for the conical diffuser of Eq. (5.9) and

$$P = P_0 \left\{ 1 - \exp\left[-\left(\frac{\pi w}{\lambda S} \right)^2 \right] \right\} \tag{5.13}$$

for the paraboloidal diffuser of Eq. (5.10). Equations (5.12) and (5.13) show that according to the diffuser model considered here, the total integrated power approaches P_0 for large values of $w/(\lambda S^2)$ and $w/(\lambda S)$. Most interestingly, we notice that P approaches zero as the roughness S increases. This same effect is noted for $<I_n>$ at $\theta = 0$ in the literature.[18]

We illustrate the behavior of Eqs. (5.9) and (5.10) with plots. In Fig. 5.2, $<I_n>$ is plotted from Eq. (5.9) as a function of output angle θ, for $\theta_0 = 0$, and for various values of $w/(\lambda S^2)$ ranging from 1/32 to 8. The intensity is displayed on a logarithmic scale over six orders of magnitude to stress the wide-angle behavior of the radiation patterns. In this family of curves we see how the maximum value $<I_n>_{max}$ for normal incidence increases as $w/(\lambda S^2)$ increases according to

$$<I_n>_{max} = 2\pi \left(\frac{w}{\lambda S^2} \right)^2 \tag{5.14}$$

and how the width of the curves goes as $\lambda S^2/w$. We also observe that, except for very small values, i.e., $w/(\lambda S^2) < 1/4$, the shape of these curves is the same for angles larger than about 45°. We can readily understand why the shape is the same by comparing the size of the two terms within the square brackets in Eq. (5.9). If $[2\pi w/(\lambda S)]^2 >> 1$, then the second term will dominate the first term for large angles. Thus, the large-angle normal-
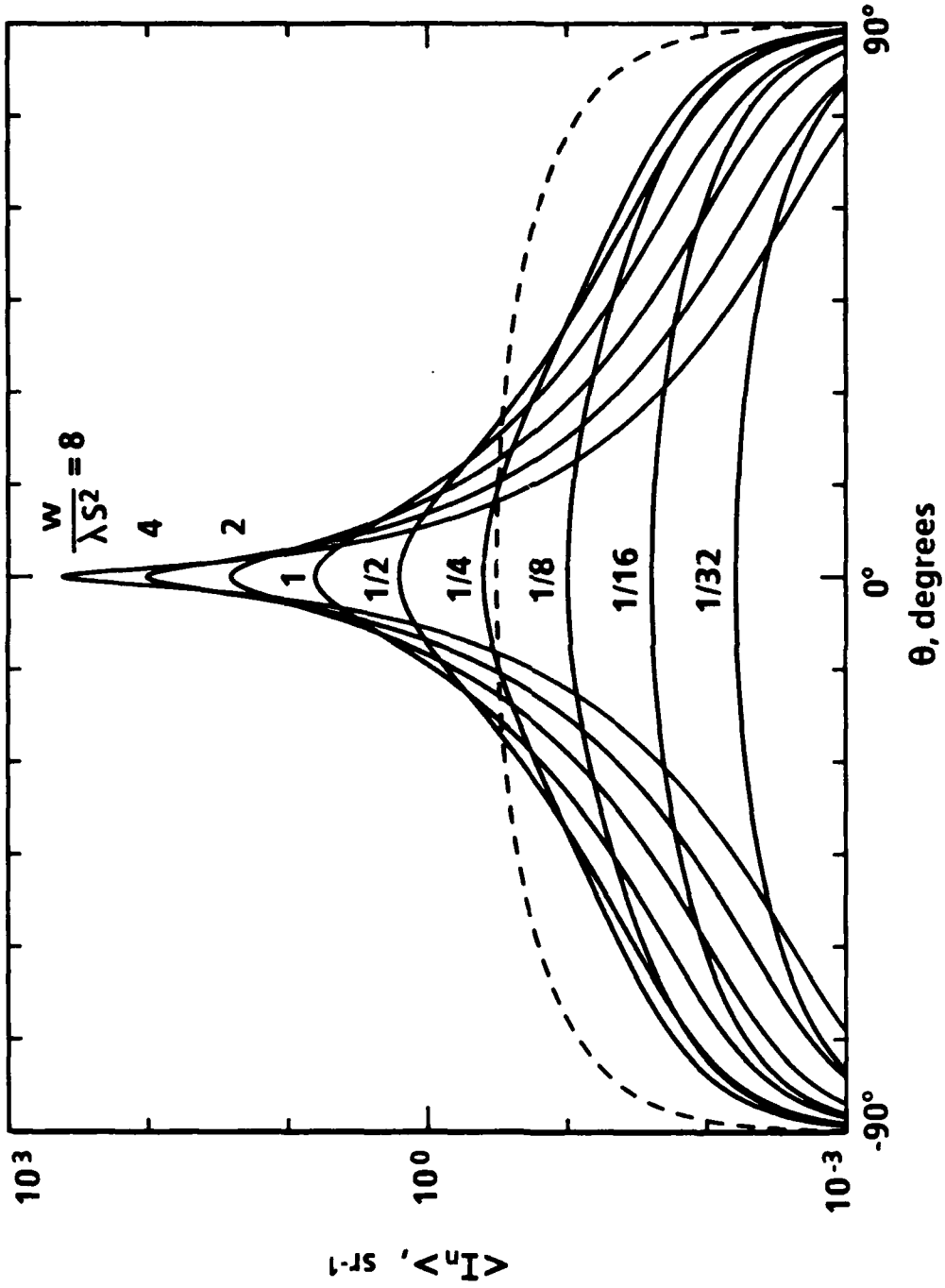
Fig. 5.2. $\langle I_n \rangle$ vs θ for the conical diffuser of Eq. (5.9) with $\theta_0 = 0$ and for various values of $w/(\lambda S^2)$. The dashed line represents an idealized Lambertian diffuser.

incidence form of Eq. (5.9) that is valid when $w/(\lambda S^2)$ is large is

$$<I_n> \approx \frac{\cos\theta}{(2\pi)^2} \frac{\lambda S^2}{w \sin^3\theta} \quad . \tag{5.15}$$

For the purpose of comparison, Eq. (5.11) for an idealized Lambertian diffuser is also plotted as a dashed line.

The family of curves shown in Fig. 5.3 is calculated from Eq. (5.10) with $\theta_0 = 0$ and with $w/(\lambda S)$ also ranging from 1/32 to 8. We see that $<I_n>_{max}$ increases as $w/(\lambda S)$ increases according to

$$<I_n>_{max} = \pi \left(\frac{w}{\lambda S} \right)^2 \tag{5.16}$$

and that the widths of these curves now go as $\lambda S/w$. There is no large-angle approximation of Eq. (5.10) analogous to Eq. (5.15). Except for the $\cos\theta$ factor, the curves in Fig. 5.3 are Gaussian in $\sin\theta$, or parabolic on a logarithmic intensity scale.

Since experimental radiation patterns are most easily observed near the intensity peak, it is useful to compare the effect that the shape parameters $w/(\lambda S^2)$ in Fig. 5.2 and $w/(\lambda S)$ in Fig. 5.3 have in determining the behavior of $<I_n>$ near its maximum for normal incidence, $\theta_0 = 0$. For example, from Eqs. (5.14) and (5.16) we see immediately that the on axis intensity of the conical diffuser is twice as great as that of the paraboloidal diffuser for the same values of the appropriate shape parameter. Also from Eqs. (5.9) and (5.10) at normal incidence, the curvature κ of $<I_n>/(<I_n>_{max}\cos\theta)$ as a function of $\sin\theta$ at the peak is calculated to be $12\pi^2[w/(\lambda S^2)]^2$ for the conical diffuser and $2\pi^2[w/(\lambda S)]^2$ for the paraboloidal diffuser. Thus the radius of curvature, $\rho = 1/\kappa$, is 6 times greater for the paraboloidal diffuser as for the conical diffuser for the same value of the appropriate shape parameter $w/(\lambda S^2)$ or $w/(\lambda S)$. Another observation that we make from Figs. 5.2 and 5.3 is the decrease in total integrated power P of Eqs. (5.12) and (5.13) that occurs as $w/(\lambda S^2)$ or $w/(\lambda S)$ becomes small.

We would like to point out that there are important applications, both in transmission and reflection, of non-normal incidence for Eqs. (5.9) and (5.10) and for the
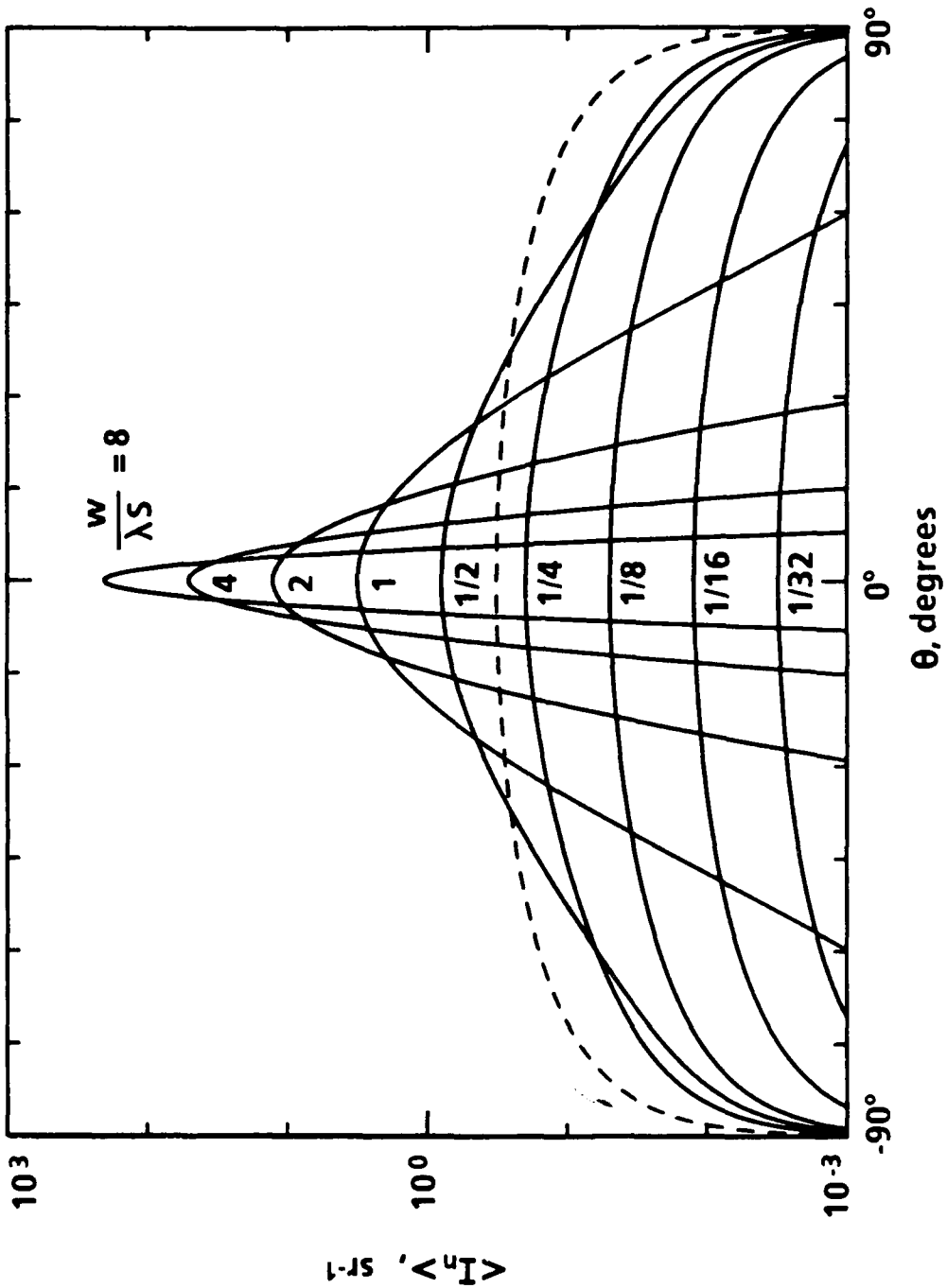
Fig 5.3. $<I_n>$ vs θ for the paraboloidal diffuser of Eq. (5.10) with $\theta_0 = 0$ and for various values of $w/(\lambda S)$. The dashed line represents an idealized Lambertian diffuser.

other expressions for $<I_n>$ that will follow. For example, arbitrary input angles (θ_0,ϕ_0) and output angles (θ,ϕ) are useful in robot vision and in computer generation of realistic looking images of rotating diffuse objects. We note that these equations are also applicable to reflection, in which case

$$S(\theta_0)=4\pi\,\frac{\sigma_h}{\lambda}\cos\theta_0 \;,\tag{5.17}$$

and θ goes to $180° -\theta$. Actually, the effective value of S for transmission in Eq (5.1) also depends on the angle of illumination θ_0:[6]

$$S(\theta_0)=2\pi\,\frac{\sigma_h}{\lambda}\left(\sqrt{n^2-\sin^2\theta_0}\,-\cos\theta_0\right)\;.\tag{5.18}$$

Besides using Eqs. (5.9) and (5.10) to find the values of $w/(\lambda S^2)$ or $w/(\lambda S)$ for strong diffusers by fitting the shapes of the experimental curves, we can approximate these quantities in an experiment with simple methods suggested by Eqs. (5.9) and (5.10) and (5.14) through (5.16). The first method is to use Eq. (5.9) or Eq. (5.10) by measuring the intensity at $\theta=0$ and then to change the angle θ until the intensity level falls to a certain fraction of this value. In the second method, $w/(\lambda S^2)$ or $w/(\lambda S)$ can be read by measuring $<I_n>_{max}$ and solving Eq. (5.14) or Eq. (5.16). A similar single point measurement could be done using Eq. (5.15) at an angle of, say, $60°$, to find $w/(\lambda S^2)$. However, both of these latter methods require that the detector system is calibrated and that the insertion loss is accounted for.

5.3 Diffusers with Two Scales of Roughness

As stated in Section 5.1, it is necessary to use a diffuser model with two scales of roughness to describe the wide-angle scattering from the etched-glass diffuser.[32] A simple way of accounting for this wide-angle component is to assume that the random variable $h(x,y)$ representing the diffuser surface profile is the sum of two normally distributed zero-mean components $h_1(x,y)$ and $h_2(x,y)$ that are uncorrelated with each other

$$h(x,y) = h_1(x,y) + h_2(x,y) \; . \tag{5.19}$$

Then $h(x,y)$ is also normally distributed and its autocorrelation function is given by

$$\sigma_h^2 R_h(r) = \sigma_{h_1}^2 R_{h_1}(r) + \sigma_{h_2}^2 R_{h_2}(r) \; , \tag{5.20}$$

where R_h, R_{h_1}, and R_{h_2} are the normalized autocorrelation functions of h, h_1, and h_2, respectively, and the variance $\sigma_h{}^2$ is related to S^2 through Eq. (5.1). Similar expressions hold for $S_1{}^2$ and $S_2{}^2$. Thus the exponential in Eq. (5.8) becomes

$$\exp\left[-S^2 \Big(1 - R_h(r) \Big) \right] = \exp\left[-S_1^2 \Big(1 - R_{h_1}(r) \Big) \right] \exp\left[-S_2^2 \Big(1 - R_{h_2}(r) \Big) \right] \; . \tag{5.21}$$

We will use Eq. (5.21) as the basis for categorizing the different types of composite diffuser. Any valid autocorrelation functions R_{h_1} and R_{h_2} and any values S_1 and S_2 could be used. However, in this discussion we are interested in strong diffusers and assume that $S_1 >> 1$. Having made this assumption, we need only specify whether the behavior of R_{h_1} for small offsets is conical as in Eq. (5.3) or paraboloidal as in Eq. (5.4).

5.3.1 Large Roughnesses S_1 and S_2

Besides assuming that $S_1 >> 1$, let us also assume for the moment that $S_2 >> 1$, then when each exponential on the right-hand side of Eq. (5.21) is expressed in terms of the series in Eq. (5.8), it will only be necessary to keep the lowest order term. This leaves us with three possibilities that we will denote by (C,C), (P,P), and (C,P) according to whether R_{h_1} and R_{h_2} are conical, paraboloidal, or mixed. For the (C,C) combination, Eq. (5.9) will still hold. But, of course, the effective parameter will be different:

$$\frac{w}{\lambda S^2} = \left(\frac{\lambda S_1^2}{w_1} + \frac{\lambda S_2^2}{w_2} \right)^{-1} \; . \tag{5.22}$$

Likewise, for the (P,P) combination, Eq. (5.10) will hold with the effective parameter

$$\frac{w}{\lambda S} = \left[\left(\frac{\lambda S_1}{w_1} \right)^2 + \left(\frac{\lambda S_2}{w_2} \right)^2 \right]^{-\frac{1}{2}} \; . \tag{5.23}$$

For the remaining (C,P) combination, Eq. (5.7), again with the selection $n = 1$, becomes

$$<I_n> = \cos\theta \frac{2\pi}{\lambda^2} \int_0^\infty rJ_0\left(2\pi\frac{r}{\lambda}\sqrt{\sin^2\theta - 2\cos(\phi - \phi_o)\sin\theta\sin\theta_o + \sin^2\theta_o}\right)\right] dr$$

$$\times \exp\left[-\frac{rS_1^2}{w_1^2} - \frac{r^2S_z^2}{w_2^2}\right] dr. \qquad (5.24)$$

One can readily understand the behavior of Eq. (5.24) by applying the convolution theorem, i.e., since $<I_n>/\cos\theta$ in Eq. (5.24) is the two-dimensional Fourier transform of the product of an exponential and a Gaussian, then it is also the convolution of $<I_n>/\cos\theta$ of Eqs. (5.9) and (5.10). We define β as the ratio of the two components:

$$\beta = \frac{w_2/S_2}{w_1/S_1^2} \qquad (5.25)$$

so that for β of zero and infinity Eq. (5.24) reduces to Eqs. (5.9) and (5.10), respectively. Equation (5.24), without the obliquity factor, is illustrated in the universal plots of Fig. 5.4 for various values of β ranging between 0 and 4. Because of the way Eq. (5.24) is plotted in Fig. 5.4, the curve for $\beta=0$ looks the same for any choice of $w_1/(\lambda S_1^2)$. As β increases, the top of the curve becomes more rounded and the intensity level drops. As β increases more, the curve begins to behave like Eq. (5.10) over a larger and larger dynamic range, but the wide-angle values of this convolution cannot drop below the $\beta=0$ curve.

5.3.2 Large S_1 and Arbitrary S_2

If $S_1 >> 1$ and S_2 is arbitrary, then we have one of two general expressions depending on whether R_{h_1} is conical or paraboloidal for small offsets. If R_{h_1} is conical, then the first factor on the right-hand side of Eq. (5.21) can be replaced by a decaying exponential, i.e., by Eq. (5.8) with $C_1 = -1$ and with all other coefficients set to zero. If we write the second factor in Eq. (5.21) as

$$\exp\left[-S_2^2\left(1 - R_{h_2}(r)\right)\right] = \exp(-S_2^2)\left\{1 + \left[\exp\left(S_2^2 R_{h_2}(r)\right) - 1\right]\right\}, \qquad (5.26)$$

then Eq. (5.7) can be broken into two parts:
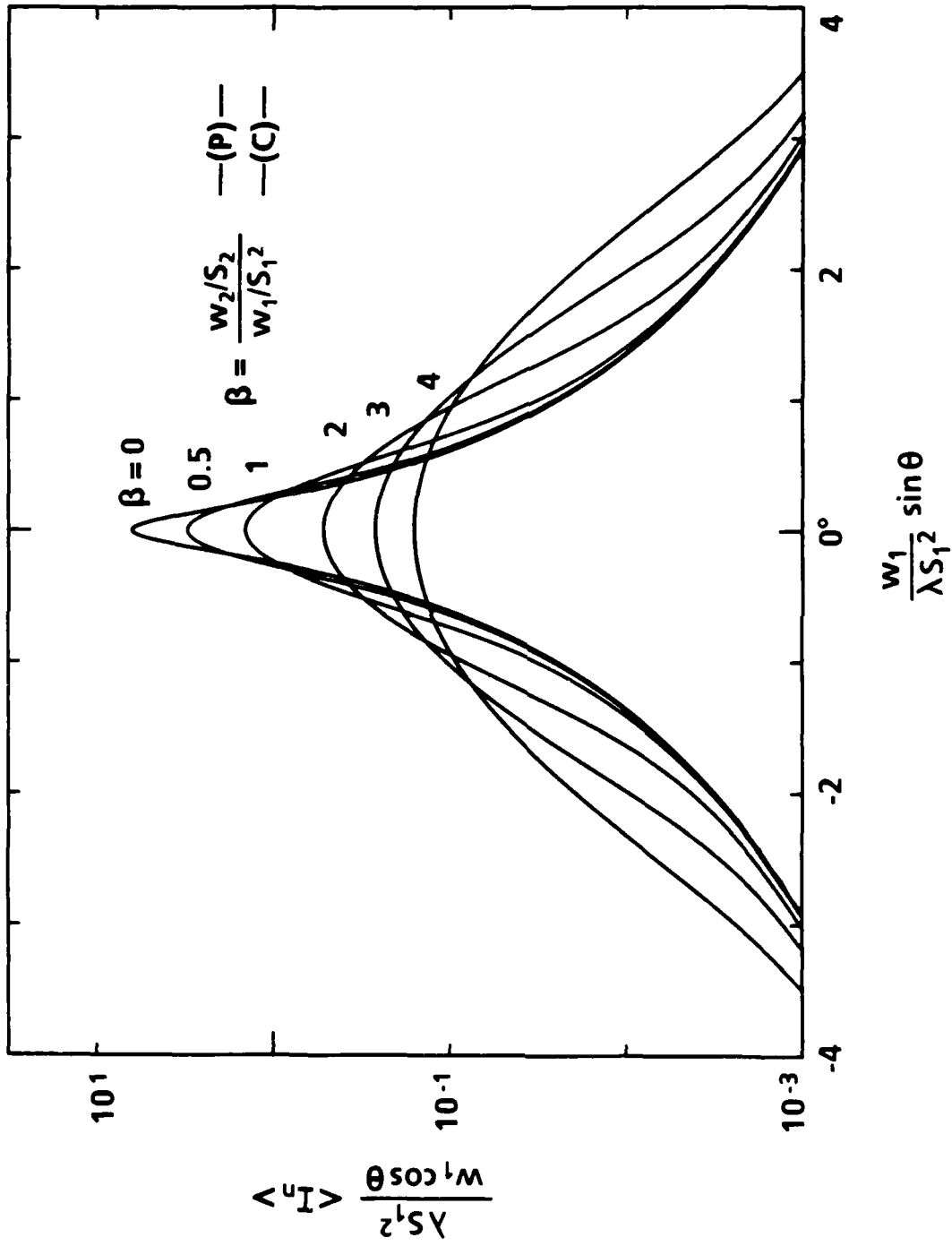
Fig. 5.4.   Universal plots of Eq. (5.24) with β of Eq. (5.25) ranging between 0 and 4.

$$<I_n> = \cos\theta \, 2\pi \exp(-S_2^2)$$

$$\times \left\{ \left(\frac{w_1}{\lambda S_1^2}\right)^2 \left[1 + \left(\frac{2\pi w_1}{\lambda S_1^2}\right)^2 \left(\sin^2\theta - 2\cos(\phi-\phi_0)\sin\theta\sin\theta_0 + \sin^2\theta_0\right)\right]^{-3/2} \right.$$

$$+ \frac{1}{\lambda^2} \int_0^\infty r J_0\left(2\pi\frac{r}{\lambda}\sqrt{\sin^2\theta - 2\cos(\phi-\phi_0)\sin\theta\sin\theta_0 + \sin^2\theta_0}\right)$$

$$\left. \times \exp\left(-\frac{rS_1^2}{w_1}\right)\left[\exp\left(S_2^2 R_{h_2}(r)\right) - 1\right] dr \right\}. \tag{5.27}$$

Likewise, if R_{h_1} is paraboloidal, then the first factor in Eq. (5.21) can be replaced by a Gaussian. Again using Eq. (5.26) for the second factor, we obtain the expression

$$<I_n> = \cos\theta \, \pi \, \exp(-S_2^2)$$

$$\times \left\{ \left(\frac{w_1}{\lambda S_1}\right)^2 \exp\left[-\left(\frac{\pi w_1}{\lambda S_1}\right)^2 \left(\sin^2\theta - 2\cos(\phi-\phi_0)\sin\theta\sin\theta_0 + \sin^2\theta_0\right)\right] \right.$$

$$+ \frac{2}{\lambda^2} \int_0^\infty r J_0\left(2\pi\frac{r}{\lambda}\sqrt{\sin^2\theta - 2\cos(\phi-\phi_0)\sin\theta\sin\theta_0 + \sin^2\theta_0}\right)$$

$$\left. \times \exp\left[-\left(\frac{rS_1}{w_1}\right)^2\right]\left[\exp\left(S_2^2 R_{h_2}(r)\right) - 1\right] dr \right\}. \tag{5.28}$$

5.3.3 Large S_1 and Small S_2

If we assume that $S_2 << 1$, then it is only necessary to keep the first term in the power series expansion

$$\exp\left[S_2^2 R_{h_2}(r)\right] - 1 = S_2^2 R_{h_2}(r) + \ldots \tag{5.29}$$

The choice of R_{h_2} is arbitrary, but for definiteness, we will use either an exponential autocorrelation function

$$R_h(r) = \exp\left(-\frac{r}{w}\right) \tag{5.30}$$

or a Gaussian autocorrelation function

$$R_h(r) = \exp\left(-\frac{r^2}{w^2}\right).$$ (5.31)

We note that Eqs. (5.30) and (5.31) have the expansions given in Eqs. (5.3) and (5.4), respectively. After choosing the above two types of autocorrelation function for R_{h_2}, we have four possible combinations. We will denote them as (C,E), (C,G), (P,E), and (P,G). The first letter in each pair corresponds to the choice of a conical or a paraboloidal autocorrelation function for the large roughness component, and the second letter indicates whether an exponential or a Gaussian autocorrelation function is used for the second component. The (C,E) and the (C,G) expressions for $S_2 < < 1$ can both be derived from Eq. (5.27) by keeping only the first term in the expansion given in Eq. (5.29). For the (C,E) combination Eq. (5.30) is used for R_{h_2}, and we obtain

$$<I_n> = \cos\theta\, 2\pi \exp\left(-S_2^2\right)$$

$$\times \left\{ \left(\frac{w_1}{\lambda S_1^2}\right)^2 \left[1 + \left(\frac{2\pi w_1}{\lambda S_1^2}\right)^2 \left(\sin^2\theta - 2\cos(\phi - \phi_0)\sin\theta\sin\theta_0 + \sin^2\theta_0\right)\right]^{-3/2} \right.$$

$$+ \left(\frac{S_2}{\lambda/w_2 + \lambda S_1^2/w_1}\right)^2$$

$$\left. \times \left[1 + \frac{4\pi^2\left(\sin^2\theta - 2\cos(\phi - \phi_0)\sin\theta\sin\theta_0 + \sin^2\theta_0\right)}{\left(\lambda/w_2 + \lambda S_1/w_1\right)^2}\right]^{-3/2}\right\}.$$ (5.32)

For the (C,G) combination, R_{h_2} is given by Eq. (5.31). Then the Fourier-Bessel transform in Eq. (5.27) is of the same form as Eq. (5.24), which has already been plotted in Fig. 5.4. If we assume that R_{h_2} is a narrow function of r compared to the exponential, i.e.,

$$w_2 < < w_1/S_1^2,$$ (5.33)

then the exponential can be replaced by its $r=0$ value of unity. Equation (5.27) for the (C,G) combination then simplifies to

$$<I_n> = \cos\theta \; \pi \; \exp(-S_2^2)$$

$$\times \left\{ 2\left(\frac{w_1}{\lambda S_1^2}\right)^2 \left[1 + \left(\frac{2\pi w_1}{\lambda S_1^2}\right)^2 \left(\sin^2\theta - 2\cos(\phi - \phi_0)\sin\theta\sin\theta_0 + \sin^2\theta_0\right)\right]^{-3/2}\right.$$

$$\left. + \left(\frac{S_2 w_2}{\lambda}\right)^2 \exp\left[-\left(\frac{\pi w_2}{\lambda}\right)^2\left(\sin^2\theta - 2\cos(\phi - \phi_0)\sin\theta\sin\theta_0 + \sin^2\theta_0\right)\right]\right\} . \qquad (5.34)$$

Equation (5.34) must be used with care because, as illustrated in Fig. 5.4, the second term is only a valid approximation to the integral over a certain dynamic range, i.e., for large enough values along the abscissa the curves will approach the $\beta=0$ curve unless β is infinite. We note, however, that this (C,G) combination is of little practical interest because the conical component will dominate at both large and small angles.

The (P,E) and the (P,G) expressions for $S_2 << 1$ can both be derived from Eq. (5.28) by keeping only the first term in the expansion given in Eq. (5.29). The (P,E) expression is obtained by using Eq. (5.30) for R_{h_2}. Once again, the second term has the same form as Eq. (5.24). However, a very good approximation for our purposes is obtained by assuming that

$$w_2 << w_1 / S_1 , \qquad (5.35)$$

so that the Gaussian in Eq. (5.28) can be replaced by its $r=0$ value of unity. Then the expression for $<I_n>$ simplifies to

$$<I_n> = \cos\theta \; \pi \; \exp(-S_2^2)$$

$$\times \left\{ \left(\frac{w_1}{\lambda S_1}\right)^2 \exp\left[-\left(\frac{\pi w_1}{\lambda S_1}\right)^2\left(\sin^2\theta - 2\cos(\phi - \phi_0)\sin\theta\sin\theta_0 + \sin^2\theta_0\right)\right]\right.$$

$$\left. + 2\left(\frac{S_2 w_2}{\lambda}\right)^2 \left[1 + \left(\frac{2\pi w_2}{\lambda}\right)^2\left(\sin^2\theta - 2\cos(\phi - \phi_0)\sin\theta\sin\theta_0 + \sin^2\theta_0\right)\right]^{-3/2}\right\} . \qquad (5.36)$$

The approximation in Eq. (5.35) corresponds to having $\beta << 1$ in Fig. 5.4. We see that Eq. (5.36) is a very good approximation because for $\beta < 1$ the major effect of the convolution appears at small angles where the first term in Eq. (5.36) dominates anyway.

Finally, for the (P,G) case, R_{h_2} is given by Eq. (5.31), and Eq. (5.28) becomes

$$<I_n> \, = \cos\theta \, \pi \exp{(-S_2^2)}$$

$$\times \left\{ \left(\frac{w_1}{\lambda S_1} \right)^2 \exp\left[-\left(\frac{\pi w_1}{\lambda S_1} \right)^2 \left(\sin^2\theta - 2\cos(\phi - \phi_o)\sin\theta\sin\theta_o + \sin^2\theta_o \right) \right] \right.$$

$$\left. + \frac{S_2^2}{(\lambda/w_2)^2 + (\lambda S_1/w_1)^2} \, \exp\left[\frac{-\pi^2 \left(\sin^2\theta - 2\cos(\phi-\phi_o)\sin\theta\sin\theta_o + \sin^2\theta_o \right)}{(\lambda/w_2)^2 + (\lambda S_1/w_1)^2} \right] \right\} . \quad (5.37)$$

Equations (5.36) and (5.37) for the composite diffuser model are illustrated in Fig. 5.5. In these plots $w_1/(\lambda S_1) = 5$. Thus, the small-angle behavior that is dominated by the first term in Eqs. (5.36) and (5.37) is the same in each case. Since Eqs. (5.36) and (5.37) are even in θ, we will display Eq. (5.36) for negative angles and Eq. (5.37) for positive angles. Equation (5.36) will be emphasized in this discussion because the (P,E) combination fits the etched-glass radiation patterns. The second term in Eq. (5.36), which controls the wide angle behavior, has the same shape as Eq. (5.9). However, the width is λ/w_2 rather than $\lambda S^2/w$, and the weighting factor has changed. From a first look at Eq. (5.36), it appears that the shape of the wide-angle wings can be controlled by varying w_2/λ, and that the intensity level of these wings is proportional to $(S_2 w_2/\lambda)^2$. However, by referring back to Fig. 5.2 and Eq. (5.15), we see that, except for very small values of $w/(\lambda S^2)$, the wide-angle portions of the curves all had the same shapes. The same thing occurs in Eq. (5.36); the expression for the wide-angle component of Eq. (5.36) analogous to Eq. (5.15) is

$$<I_n> \, \approx \frac{\cos\theta}{(2\pi)^2} \frac{\lambda S_2^2}{w_2 \sin^3\theta} . \quad (5.38)$$

Equations (5.15) and (5.38) are identical except that S^2/w has been replaced by S_2^2/w_2.
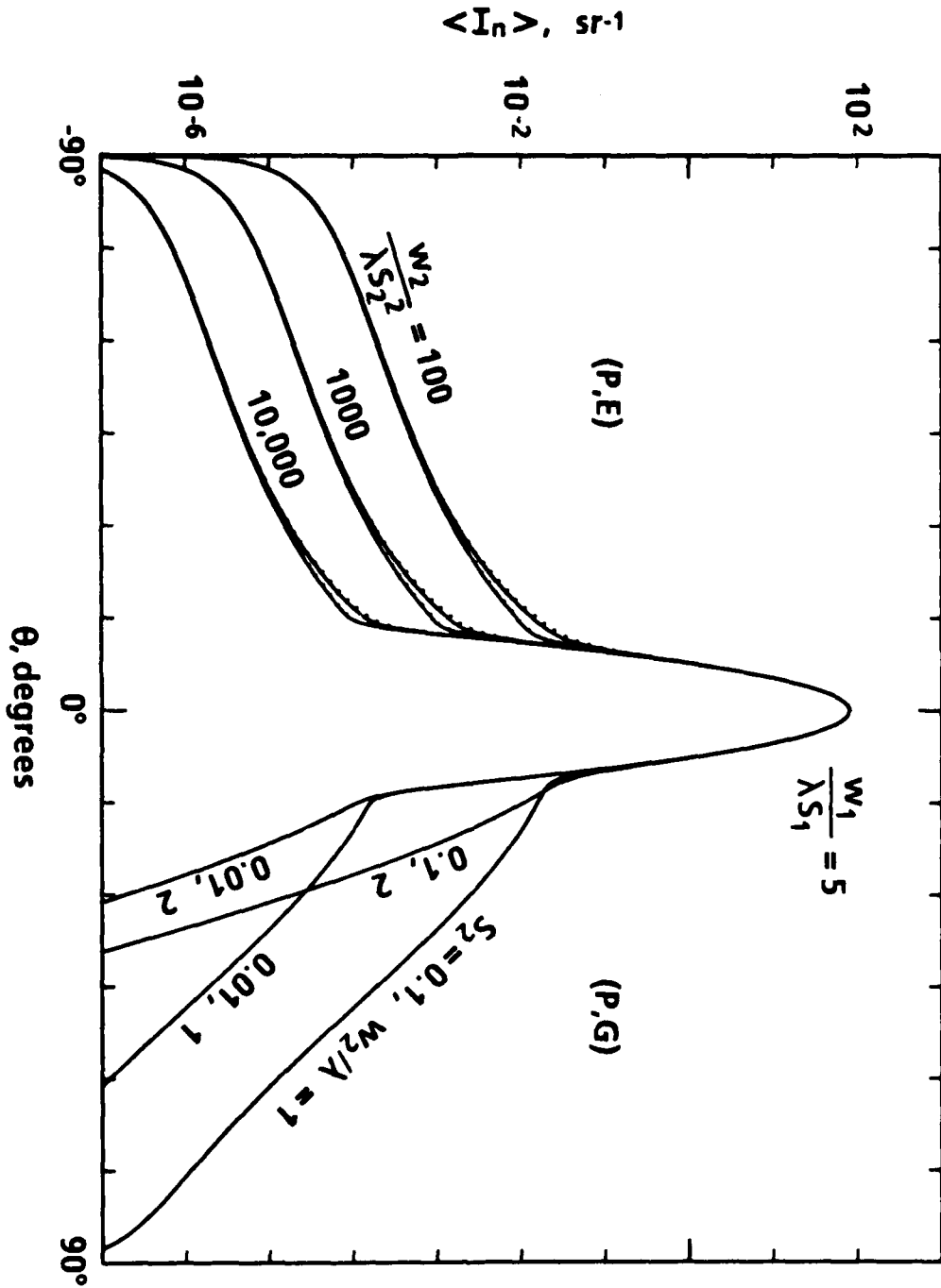
Fig. 5.5. $\langle I_n \rangle$ vs θ for the composite diffusers of Eq. (5.36), negative angles, and of Eq. (5.37), positive angles.

Therefore, although Eq. (5.36) appears to have the three independent parameters, $w_1/(\lambda S_1)$, w_2, and S_2, there are actually only two important parameters: $\lambda S_1/w_1$ sets the width of the central Gaussian and $\lambda S_2^2/w_2$ sets the intensity level of the wings. However, the choice of w_2 and S_2 does give us some latitude in controlling how smoothly the two regions of the curve join. This is illustrated on the left-hand side of Fig. 5.5 where curves for $w_2/(\lambda S_2^2)$ of 100 in the upper curve, 1000 in the middle curve, and 10,000 in the lower curve are shown. Each of these curves breaks into two curves at the transition region according to two choices of w_2 and S_2 used to obtain this ratio. In the lower set of curves $w_2/\lambda = 1$, and in the upper set of curves $w_2/\lambda = 4$. The curves look the same for $w_2/\lambda > 4$ as long as $S_2 << 1$ and Eq. (5.35) holds. The dotted lines correspond to a numerical integration of Eq. (5.28) with an exponential autocorrelation function for R_{h_2}; they show that the error introduced by the approximate form, Eq. (5.36), is very small.

Equation (5.37) is plotted on the right-hand side of Fig. 5.5 for $w_1/(\lambda S_1) = 5$ and for various values of w_2 and S_2. There is no wide-angle expression analogous to Eq. (5.38) for Eq. (5.37). Therefore, w_2 and S_2 have independent effects. By assuming that Eq. (5.35) holds, we see that the width of the wings is λ/w_2 and that the intensity level is proportional to $(w_2 S_2/\lambda)^2$.

5.4 Experimental Configuration

A scatterometer was constructed for measuring diffuser radiation patterns. Because of its high dynamic range, this instrument gives one the capability of measuring these patterns over output angles of nearly $\pm 90°$. Although transmission measurements will be described here, reflection measurements are also possible since the arm could rotate completely around the sample. Scattered intensity is measured in the plane of incidence with the angle of incidence being set by rotating the diffuser about the axis of detector arm motion. The system is operated under computer control to improve

performance and for the purpose of automation. A block diagram of the entire system is shown in Fig. 5.6.

5.4.1 Input Optics

The light source is an argon-ion laser operating at 0.4880 μm and modulated at 930 Hz by a rotating mechanical chopper. A small fraction of the light is directed by a beam splitter to a reference photodiode to measure fluctuation of the input power. The direct beam is sent through a broadband polarization rotator and then to a Glan-Thompson polarizer to ensure that the input to the diffuser has the desired polarization. Although experiments were performed with both p- and s- polarized light, in most experiments we used s polarization, i.e., the electric field is polarized perpendicular to the plane of incidence.

The light passed through an iris as it entered the blackened chamber. This chamber, measuring about 1.5 m on each side, had its walls, ceiling, and floor covered with black velvet, which was very effective in reducing scattered light within the chamber. There was also an opening in the wall opposite the input iris so that the direct beam, if it were not extinguished by the diffuser, would leave the blackened chamber. The size of this opening could be adjusted according to the angular spread of the radiation pattern of the diffuser being tested so that most of the scattered transmitted light left the chamber.

5.4.2 Diffuser Preparation and Mounting

The diffuser or rough surface is mounted on a rotation stage that is located in the center of the chamber and used for setting the input angle θ_0 in the plane of incidence. The diffuser mount was designed to allow for angles of incidence between ±75°. Some care was necessary in designing the mount and in preparing the diffuser for illumination. The diffuser mount served as an opaque wall so that the only light reaching the detector passed through a small aperture on the diffuser. This mount was long enough to block light scattered from the input iris that would otherwise be in the field of view of the
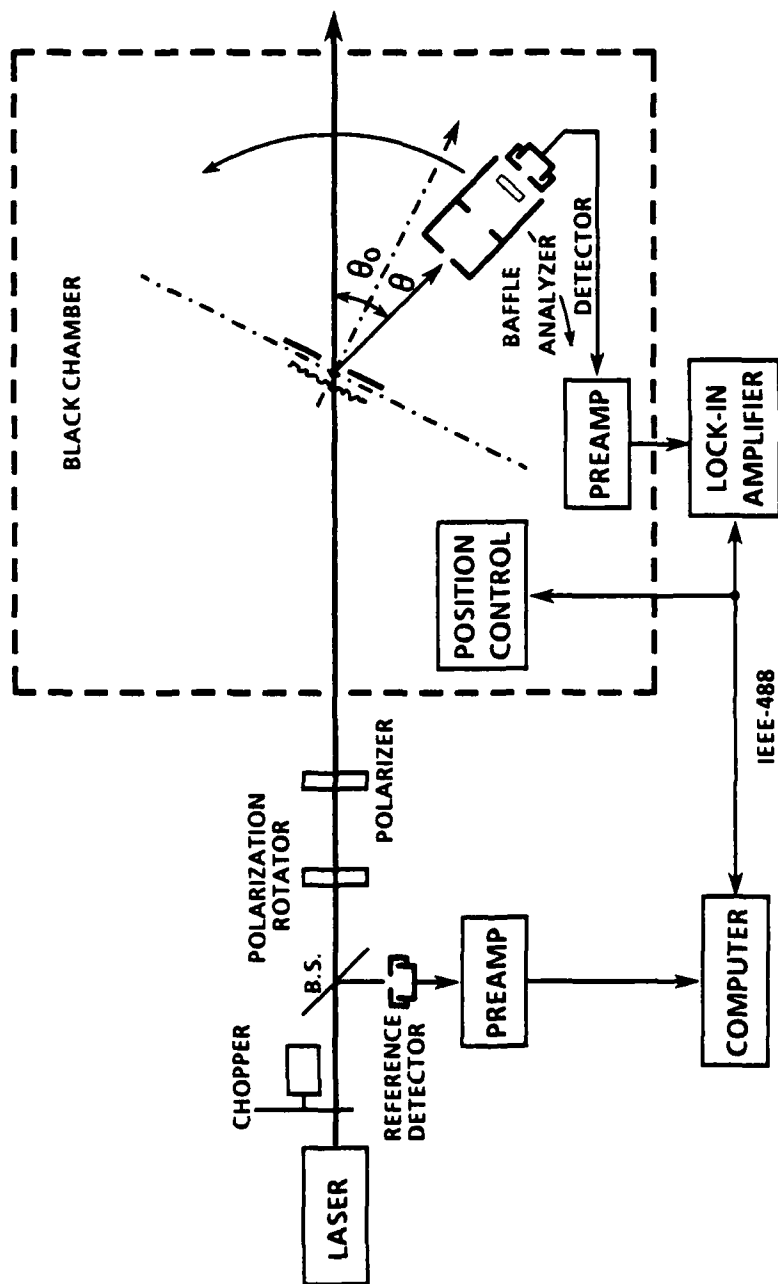
Fig. 5.6.   Block diagram of the scatterometer for measuring angular dependence of radiation patterns I_{en}.

detector as it scanned the radiation pattern, even for an angle of incidence of 75° At observation angles near ±90°, light scattered from the backside of the diffuser or its mount was prevented from reaching the detector by side pieces on the diffuser holder.

The diffusers were made by grinding or etching one side of $\frac{1}{4}$" x 2" x 3" pieces of float glass that had been cut from a single sheet. The ground-glass diffuser was ground with 820 grit. The etched-glass diffusers were prepared in a manner similar to that used by Dyson.[33,34] His method was to preroughen the glass by grinding and then to expose the preroughened surface to hydrofluoric acid for various lengths of time. We obtained better results by preroughening the glass with Armour Etch[35] etching cream. For short exposures to the etching cream, the surface texture of the glass goes through various stages that are critically dependent on time; however, after an etch time of 45 minutes the texture does not seem to change. Nine diffuser blanks were preroughened on one side with Armour Etch for 60 min and then exposed to BOE[36] (4-1) etchant for times of 2, 5, 10, 20, 30, 45, 60, 90, and 120 min. As the BOE etch time increases, the cell size or the size of the scallops in Fig. 5.1 also increases. However, the rms height stays nearly constant at about 1 μm. The limiting etch time is about 2 hrs. For longer times the surface develops smaller scale structure and large splotches. For etch times up to 5 min, the major effect of the BOE is to smooth out the high spatial frequency detail of the preroughened surface, not to increase the cell size.

The diffusers were then painted black on the four sides and on the diffuser surface, except for an opening about 4 mm wide by 7 mm high. The light is incident from the smooth side of the diffuser, and the effects on the radiation pattern of reflections between this surface and the rough surface, which can be significant at high observation angles, are reduced by keeping the ratio of aperture width to glass thickness small. The aperture was made somewhat larger than the size of the laser beam, which had a $1/e^2$ intensity point of $w_a = 0.59$ mm, to reduce scattering from its edges. There were certain advantages to forming the aperture with paint over placing an aperture in

contact with the surface. For example, when a metal aperture with a thickness of about 30 μm was attached to the surface, the scattering from its edges dominated the scattering from the diffuser itself at large observation angles. On the other hand, the edge formed by the paint could be made to be very thin at the border and to increase in thickness with distance so that the edge scattering was reduced. It was necessary to use an aperture on the diffuser, otherwise, unilluminated areas of the diffuser would light up through multiple scattering and increase the light scattered at high angles. Since the paint was in contact with the rough surface and partially index matched the glass, reflections and multiple scattering were reduced in the painted regions.

The diffuser could be positioned through micrometers on three translation stages and on a tilt stage. The translation stages are used to center the diffuser in the input beam and to control its longitudinal position so that the area to be illuminated with the laser was at the center of rotation. The tilt stage was used to achieve retroreflection off of the polished input surface of the diffuser. For illumination with non-normal incidence, this position served as the zero degree mark for the diffuser rotation stage. To account for beam displacement that occurred when the 12 mm thick glass diffusers were illuminated at an angle, the whole diffuser detector assembly was translated laterally to bring the beam back into the center of the diffuser aperture.

5.4.3 Detection System

The detector was mounted on an arm that could rotate completely around the sample, and that had the same axis of rotation as the diffuser. Both the diffuser rotation and the arm rotation were computer controlled. The step size of the arm between intensity measurements for most applications was 0.20°. However, a step size as small as 0.01° could be obtained with the system.

The distance from the center of rotation to the detector, a silicon PIN photodiode operated in the photovoltaic mode with no bias voltage, was 65 cm. The field of view of this detector is restricted to a half angle of 3.2° by a baffle. Also at the entrance to the

detector is a polarization analyzer mounted in a rotation stage. The effective diameter of the detector is 2.5 mm so that it subtends a solid angle Ω of 1.16×10^{-5} sr or a half-angle of $0.11°$.

The signal from the detector went to a PAR Model 181 Current Sensitive Preamp. For detection of the low light levels that occurred at high angles, the sensitivity of the preamp was set at 10^{-7} A/V. However, in the region around the intensity peak, it was necessary to switch to a lower sensitivity, 10^{-4} A/V in most cases, to avoid saturation. To measure the intensity spike that occurred from diffusers that passed the direct beam, it was also necessary to reduce the intensity of this spike with neutral density filters. The signal from the preamp was input into a PAR Model 5301 Lock-In Amplifier that was controlled by the host computer over the IEEE-488 interface bus. Since the signal strength changed by many orders of magnitude as the arm moved between the different regions of the radiation pattern, the autoranging capability of the lock-in amplifier w is used to maintain its sensitivity at the appropriate level.

5.4.4 Linearity and Calibration

Since the radiation patterns were measured over many orders of magnitude, and the preamp sensitivity was switched within a single measurement run, it was important to test the linearity of the system and the consistency of the preamp at the sensitivity settings of 10^{-7} and 10^{-4} A/V used for most applications. To check this range switch, the power incident on the detector was set at the level where the range would be switched in an actual radiation pattern measurement. The average difference between readings taken before and after this 10^3 range switch was less than 1%.

The linearity of the detector system was checked over a wide range of input powers, ranging from direct illumination of the detector with a He-Ne laser to six orders of magnitude below this level by using neutral density filters. One neutral density filter, having a density of 0.3, was mounted so that it could be removed from the beam path and then reinserted to the same position. It served as a repeatable attenuator for

showing that the attenuation measured by the system was the same at different power levels. The attenuation agreed to within 1% over the six decade range.

The system was calibrated using both a direct and an indirect method. In the direct method there was no test diffuser. The laser beam was attenuated with neutral density filters placed before the beam splitter in Fig. 5.6, and the total energy within the direct beam that entered the blackened chamber was incident on the detector. The preamp was set at 10^{-4} A/V, and the ratio of the signal voltage V_{so} out of this preamp to the voltage V_{ro} from the reference detector was calculated as

$$g = \frac{V_{so}}{V_{ro}} . \tag{5.39}$$

The product gV_r became the indicator of the power level incident on the diffuser for a given reference voltage V_r. It was not necessary to perform an absolute calibration of these detectors in watts per volt because the quantity of interest I_{en} is normalized by the incident illumination and hence does not depend on the input power. However, to facilitate the discussion, we assume that we do have a calibration factor a such that the total power P_0 entering the chamber is

$$P_0 = a\, g\, V_r , \tag{5.40}$$

and the power scattered from the diffuser and received by the detector is

$$\Delta P = a\, V_s . \tag{5.41}$$

Then by Eq. (5.6),

$$I_{en} = \frac{V_s}{\Delta \Omega\, g\, V_r} . \tag{5.42}$$

In the indirect calibration method, a barium sulfate disk was used to approximate an idealized Lambertian scatterer, and the radiation pattern in reflection was measured with the scatterometer. The calibration factor Ωg of Eq. (5.42) was calculated by comparing the resulting radiation pattern with Eq. (5.11). Since the indirect method was

more repeatable, and the signal levels V_s and V_r for this method were in the range used for actual measurements, it was the preferred method of calibration. The calibration was performed for wavelengths of 0.4880 µm and 0.6328 µm. The minimum detectable I_{en} is 4.0 × 10^{-7} sr^{-1} for an average input power of 30 mW at 0.4880 µm and 1.3 × 10^{-5} sr^{-1} for an average input power of 1.2 mW at 0.6328 µm. This corresponds to a minimum detectable power for the receiver of about 1.5 × 10^{-13} W.

5.5 Measured Radiation Patterns

5.5.1 Ground Glass

The radiation pattern from a ground-glass diffuser is presented for comparison with the theory of Section 5.2 Since this type of surface is made by an abrasive grinding process, it has sharp edges and abrupt discontinuities as illustrated in Fig. 5.1(a). Hence, one would expect that the resulting autocorrelation function would drop immediately, i.e., be better represented by a conical shape than by a paraboloidal shape for small offsets. Hence, Eq. (5.9), and correspondingly Fig. 5.2, are expected to provide a theoretical basis for the prediction of the radiation pattern.

Before presenting the experimental data from the ground-glass diffuser, we will present the calibration curve from the barium sulfate scatterer used to approximate an idealized Lambertian surface. In the two curves labeled (a) in Fig. 5.7, the radiation pattern in reflection resulting from illumination of this surface at normal incidence is plotted, solid line, and compared with Eq. (5.11), dashed line. There is a break in the experimental data around $\theta = 0°$ where the detector assembly blocked the input beam. The calibration factor was obtained by adjusting the experimental curve vertically until the solid line and the dashed line overlapped.

In curves (b) of Fig. 5.7, we see the experimental results from the ground-glass diffuser, solid line, together with Eq. (5.9), dashed line, plotted for $w/(\lambda S^2) = 1.4$. A very good fit has been obtained at all angles and over five orders of magnitude. We did not
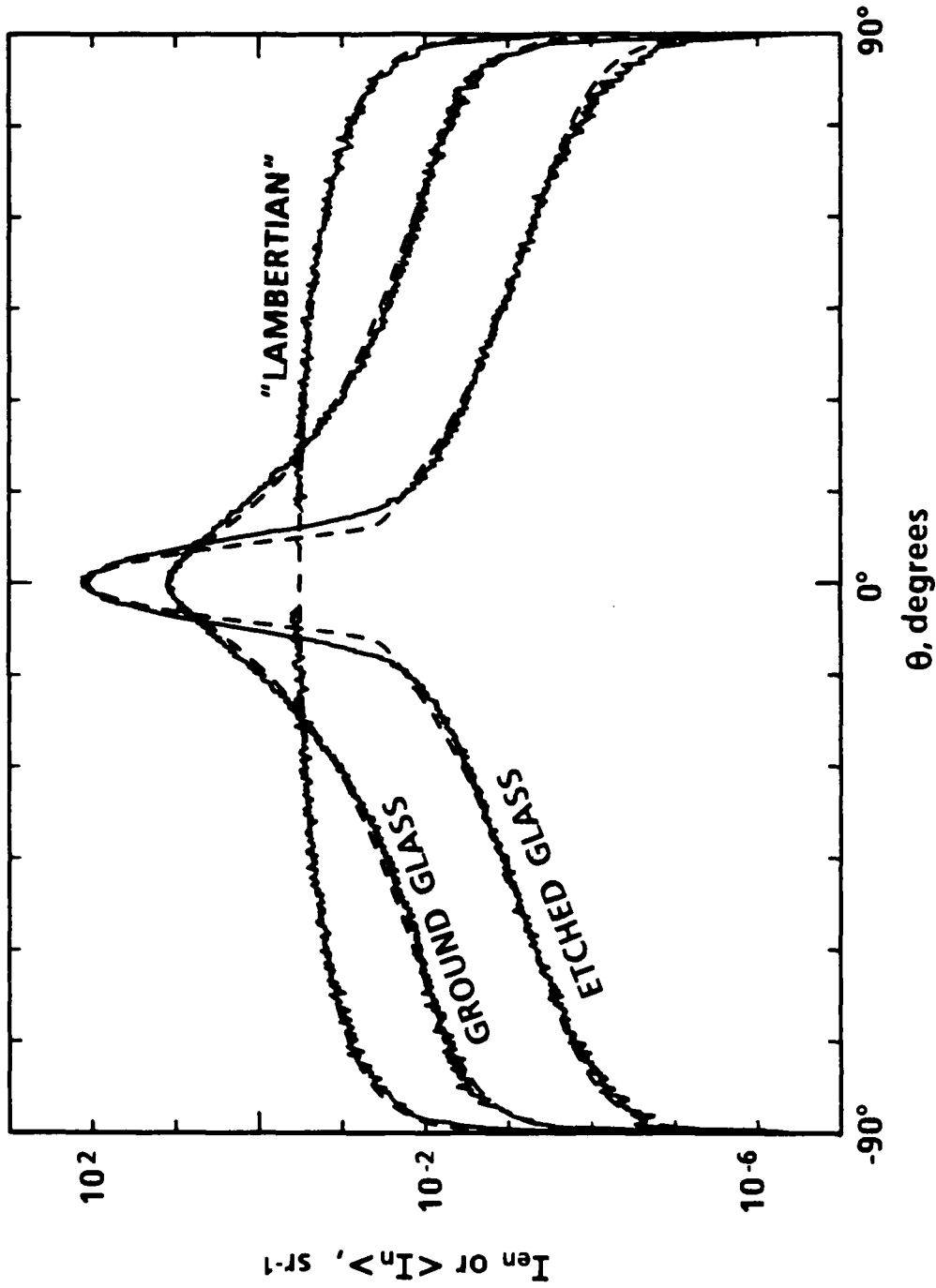
Fig. 5.7. Measured radiation patterns I_{en}, solid lines, and theoretical radiation patterns $<I_n>$, dashed lines, for the "Lambertian" surface compared to Eq. (5.10), the ground-glass diffuser compared to Eq. (5.9) with $w/(\lambda S^2) = 1.4$, and the etched-glass diffuser compared to Eq. (5.36) with $w_1/(\lambda S_1) = 6$, $w_2/\lambda = 0.75$, and $S_2 = 0.14$.

observe a significant difference when the radiation pattern measurement was repeated

for p polarization, i.e., when both the polarizer and the analyzer were rotated by 90°.

5.5.2 Etched Glass

As illustrated in Fig. 5.1(b), the surface of the etched-glass diffusers are smooth on

a wavelength scale and have slowly changing slopes except at the ridges. Hence, we

would expect the radiation patterns to be quite different from those of ground glass. In

curves (c) of Fig. 5.7 we compare the theoretical prediction, using the composite diffuser

model of Eq. (5.36), with the measured patte. from an etched-glass diffuser

(AE 60 min, BOE 45 min). Very good agreement is seen at all angles and over eight orders

of magnitude. This fit is obtained by choosing $w_1/(\lambda S_1) = 6.0$ to set the height of the

central Gaussian intensity profile and by choosing $w_2/(\lambda S_2^2) = 38$ to set the height of the

wide-angle wings. Alternatively, we could have chosen $w_1/(\lambda S_1) = 5.0$ to obtain better

agreement between the widths of the two curves in the central region, but then the

height of the dashed line at $\theta = 0$ would have fallen by 30% or by 0.16 units on the

logarithmic scale. The transition region between the central Gaussian and the wings is

dependent on the values of w_2 and S_2 used to produce the above ratio. For the curve

shown, $w_2/\lambda = 0.75$ so that $S_2 = 0.14$. The fitting of the wings is consistent with the

presence of microstructure on the surface having the discontinuities that are

characteristic of an autocorrelation function that isconical for small offsets. With

reference to Fig. 5.5, we review the curve fitting procedure as follows. As explained

directly above, (1) the parameter $w_1/(\lambda S_1)$ is obtained by intensities I_{en} at small angles

and (2) $w_2/(\lambda S_2^2)$ is obtained from I_{en} for $\theta \sim 60°$. Finally, (3) the parameter w_2/λ is obtained

from the transition region between the central Gaussian and the wings.

In Fig. 5.8 we see the radiation patterns for the same etched-glass diffuser

(AE 60 min, BOE 45 min) as measured for input angles $\theta_0 = -60°$, $-30°$, $0°$, $30°$, and $60°$.

Similar curves for ground-glass diffusers are in the literature.[26] The measurements in

Fig. 5.8 were made with the detector arm sweeping out a half circle in the plane of
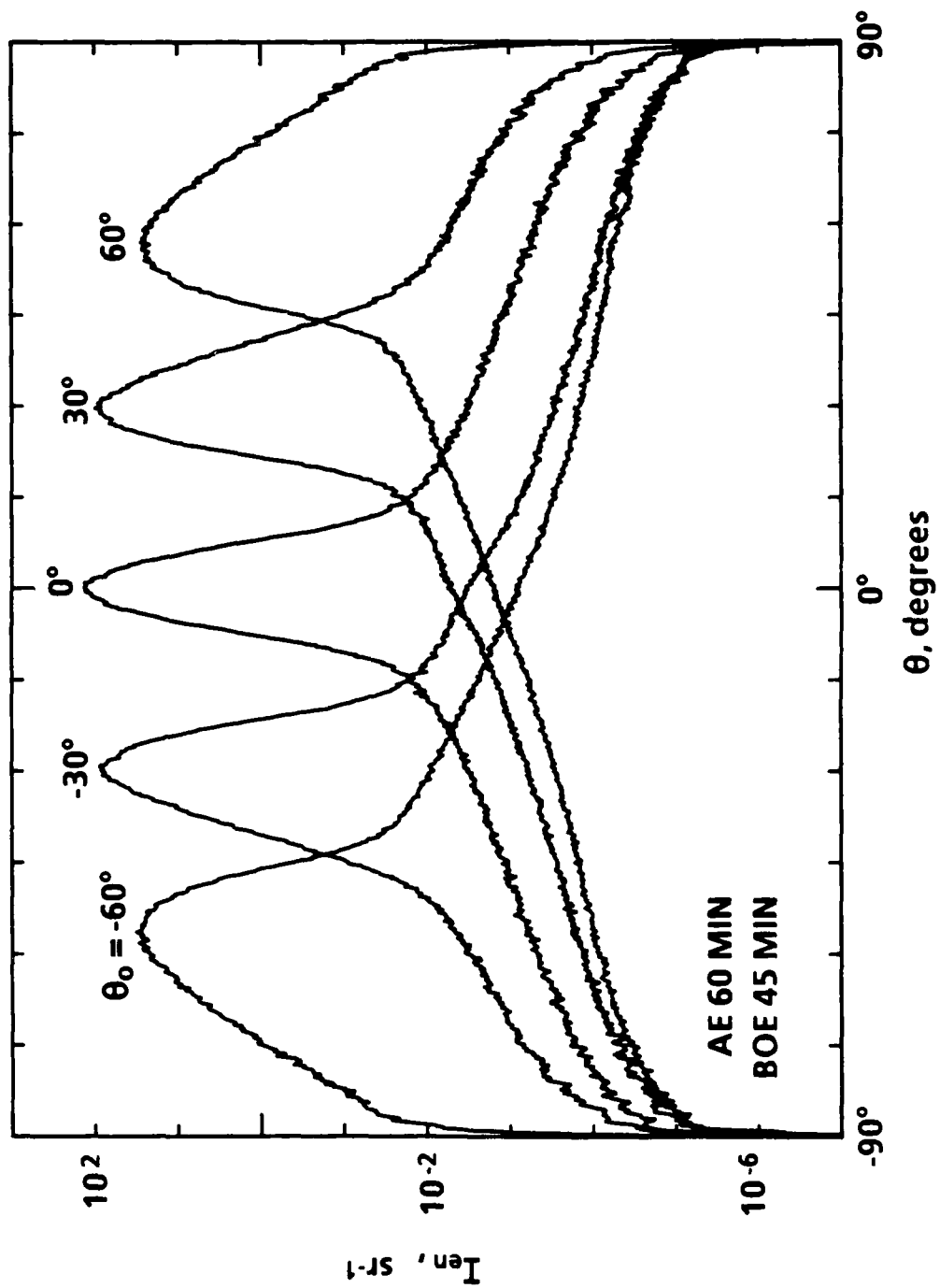
Fig. 5.8.   Measured radiation patterns I_{en} from the etched-glass diffuser for various angles of incidence θ_o.

incidence for s polarization. In these curves we observe that the position of the maximum of each radiation pattern slides according to the illumination direction θ_0 but that this peak is displaced toward smaller angles, the displacement increasing with increasing angles of incidence. Some of this displacement arises from the fact that the obliquity factor is stronger on the high-angle side of the curve, which tends to shift the maximum value of the curve inward.

We also observe that the radiation patterns widen and that the maximum values decrease as the input angle θ_0 increases. Part of this widening is due to the effective value of S increasing as θ_0 increases in Eq. (5.18). However, most of it arises from the fact that we are observing the radiation pattern as a function of the angle θ, not as a function of the spatial frequency, which goes as $\sin\theta$.

In Fig. 5.9 we have used Eq. (5.36) to plot a family of radiation patterns in the plane of incidence for the same values of θ_0 as in Fig. 5.8 and for $w_1/(\lambda S_1) = 6$, $w_2/\lambda = 0.75$, and $S_2 = 0.14$. We observe very good agreement between Figs. 5.8 and 5.9, especially in the angular dependence of the wings. In plotting Eq. (5.36) we have used Eq. (5.18) for the dependence of S on input angle θ_0. The etched-glass radiation pattern measurements were repeated for p polarization. The only observed difference between these patterns was that the intensity level of the wings dropped on the long side of the patterns for oblique incidence.

Figure 5.10 contains plots of the radiation patterns for three of the nine etched glass diffusers for normally incident illumination. From these radiation patterns we see the large range in the widths and maximum values of the intensity curves that can be obtained by varying the BOE etch time between 2 min and 120 min. By fitting these radiation patterns to Eq. (5.10), we can obtain the values of the shape parameter $w/(\lambda S)$ for the paraboloidal component. We use a linear rather than a logarithmic intensity axis for this fitting procedure because the angular distribution of intensity in the wings is insignificant on a linear scale. In Fig. 5.11 the values of $w/(\lambda S)$ as so obtained are
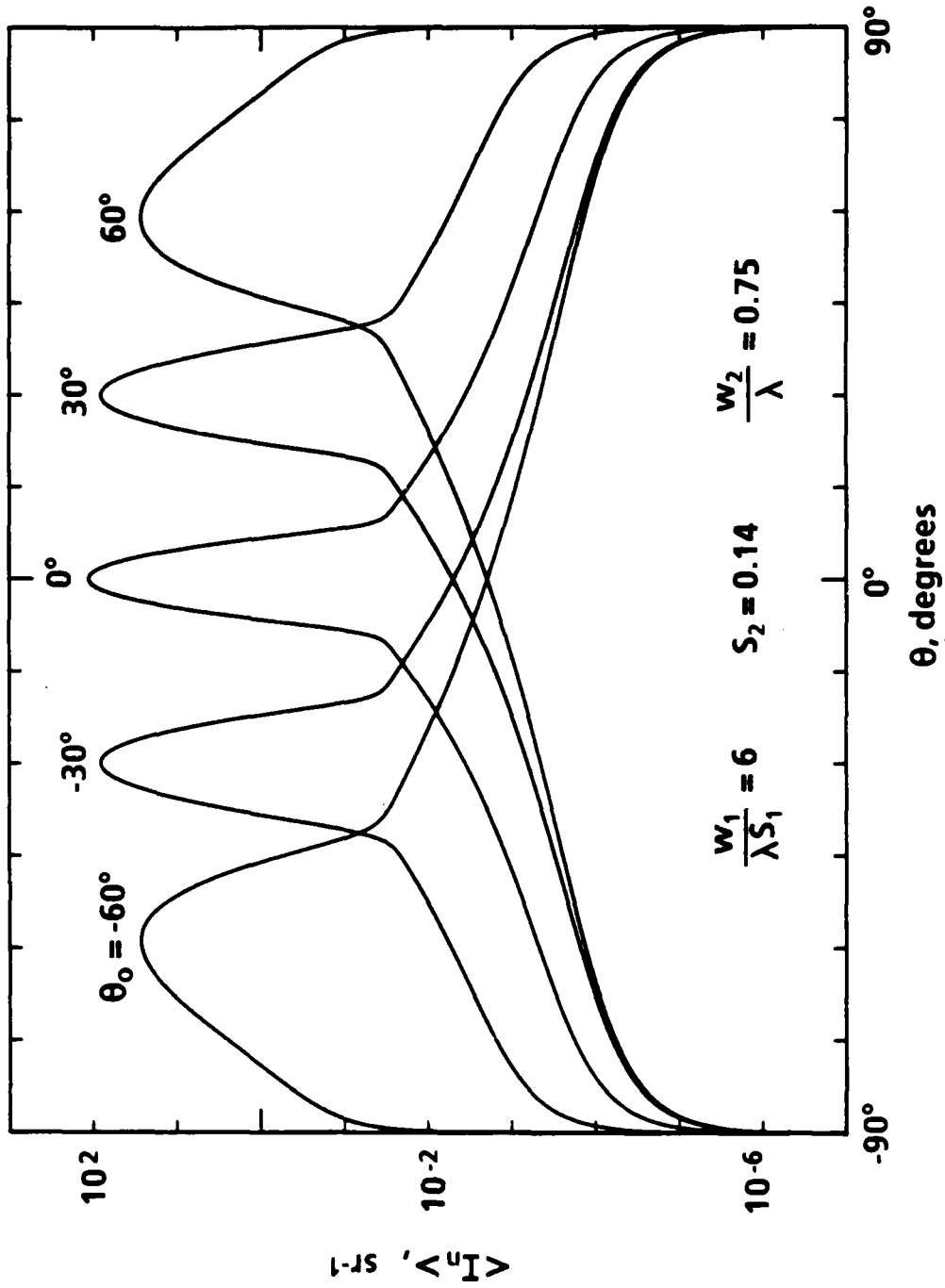
Fig. 5.9. $\langle I_n \rangle$ vs θ as calculated by Eq. (5.36) for various angles of incidence θ_0 and for $w_1/(\lambda S_1) = 6$, $w_2/\lambda = 0.75$, and $S_2 = 0.14$.
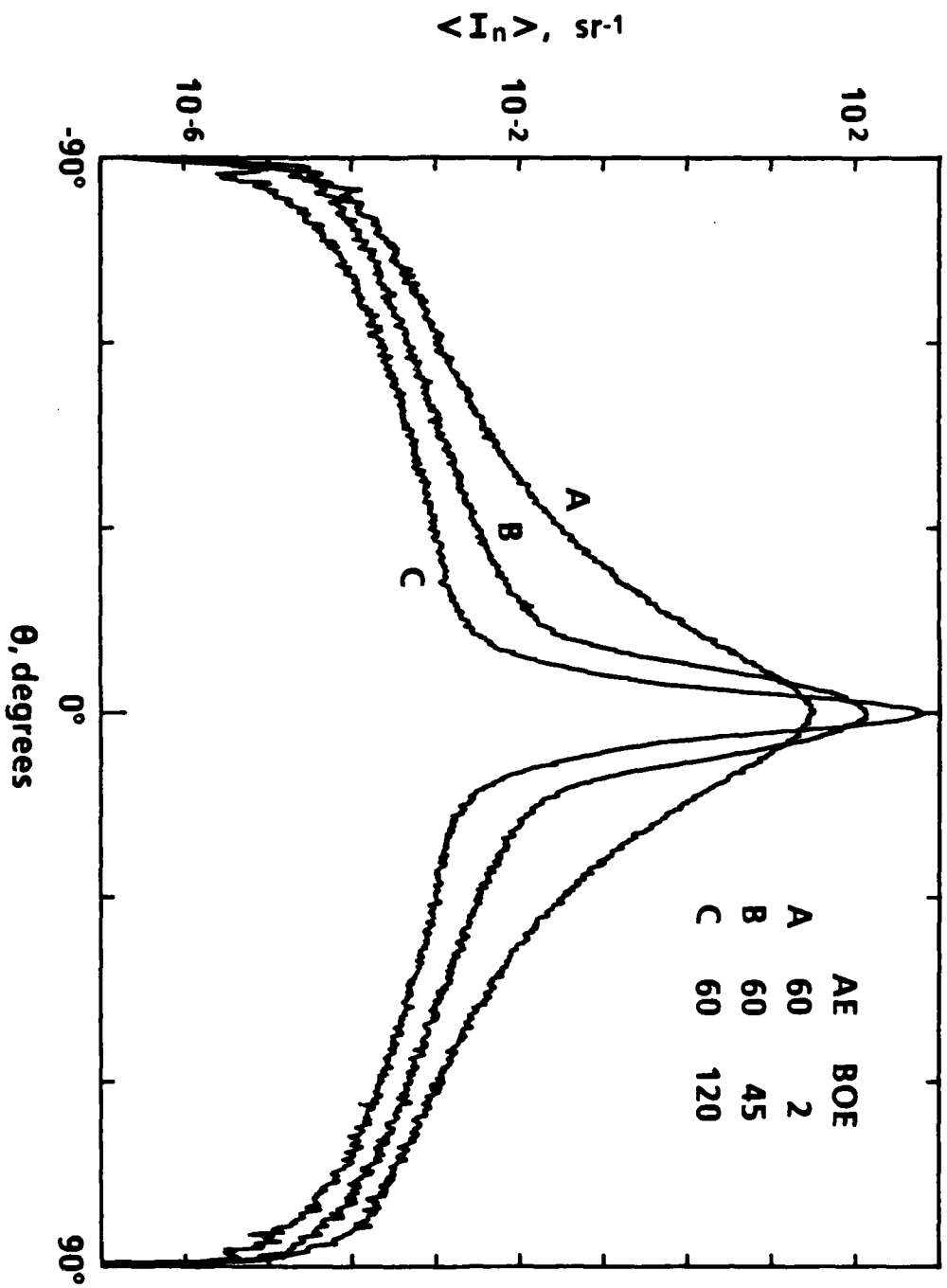
Fig. 5.10. Measured radiation patterns I_{en} for etched-glass diffusers preroughened 60 min with Armour Etch and etched 2 min (A), 45 min (B), and 120 min (C) with BOE.
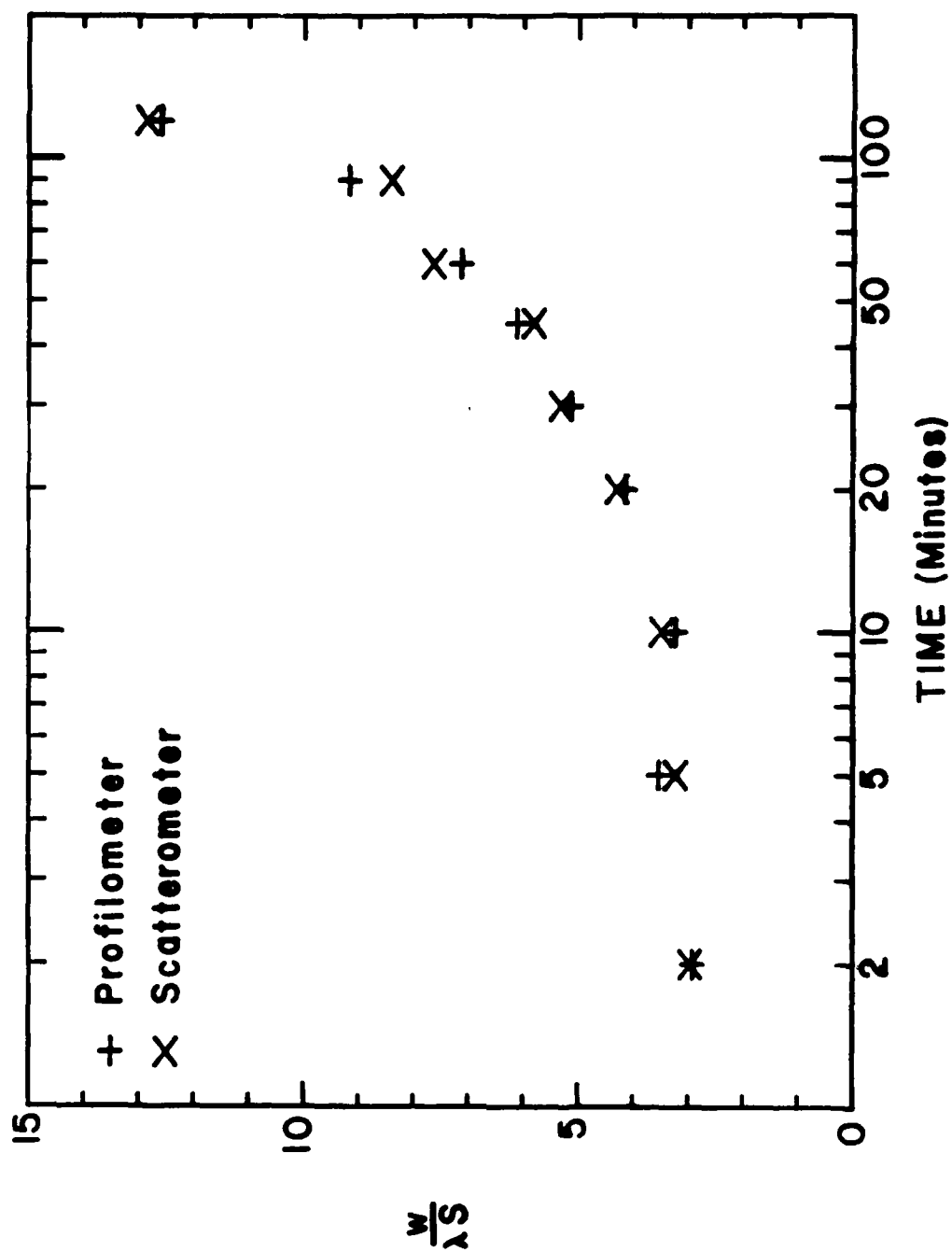
Fig. 5.11. Comparison between profilometer (+) and Scatterometer (X) measurements of the shape parameter $w/(\lambda S)$ for etched-glass diffusers with BOE etch times ranging between 2 to 120 minutes.

compared with direct measurements from a stylus profilometer. In the profilometer method, 1 mm scans consisting of 2048 data points are taken for each diffuser. Autocorrelation functions from each scan are calculated and fit to a Gaussian to obtain w and S. The excellent agreement between these two methods of measuring $w/(\lambda S)$ establishes measurement of the radiation pattern as a useful and accurate noncontact method for characterizing paraboloidal surfaces.

5.6 Summary

A theoretical formulation for the far-zone radiation pattern resulting when a diffuser with a normally distributed surface height profile is monochromatically illuminated is presented in detail and compared to experiments. In the theory, which is extended from an earlier publication,[6] we emphasize predictions of the expected value of the normalized intensity $<I_n>$, and we stress that this corresponds to the envelope of the speckle pattern I_{en}. First, in the theory for the case of normalized roughness S in Eq. (5.1) much greater than one, we present two important limiting forms of $<I_n>$, Eqs. (5.9) and (5.10), which correspond, respectively, to autocorrelation functions that are Eq. (5.3) conical and Eq. (5.4) paraboloidal for small offsets. Second, we present forms for $<I_n>$ from a diffuser with two scales of roughness where the first component has large roughness $S_1>>1$ and the roughness S_2 of the second component is in one of three categories: If $S_2>>1$, and the autocorrelation functions of the first and second components are conical and paraboloidal, respectively, then we denote this combination by the symbol (C,P) and Eq. (5.24) applies. For arbitrary S_2, Eq. (5.27) will apply if the first component is conical and Eq. (5.28) will apply if the first component is paraboloidal. If $S_2<<1$ then Eqs. (5.27) and (5.28) simplify. We illustrated this case with four examples, denoted by the symbols (C,E), (C,G), (P,E), and (P,G), that correspond to Eqs. (5.32), (5.34), (5.36), and (5.37), respectively. The second letter in each pair symbolizes either an exponential or a Gaussian autocorrelation function for the small roughness component.

In Fig. 5.7 excellent agreement is obtained between Eq. (5.9) and the ground-glass radiation pattern by adjusting the single parameter $w/(\lambda S^2)$ and between Eq. (5.36) and the etched-glass radiation pattern by choosing the three parameters $w_1/(\lambda S_1)$, w_2/λ, and S_2 properly. As illustrated in Fig. 5.11, the values of $w_1/(\lambda S_1)$ obtained by measuring the angular distribution of the radiation pattern agree well with stylus profilometer measurements of diffuser surfaces.

Chapter 5 References and Notes

1. C. N. Kurtz, "Transmittance characteristics of surface diffusers and the design of nearly band-limited binary diffusers," J. Opt. Soc. Am. **62**, 982-989 (1972).

2. C. N. Kurtz, H. O. Hoadley, and J. J. DePalma, "Design and synthesis of random phase diffusers," J. Opt. Soc. Am. **63**, 1080-1092 (1973).

3. R. C. Waag and K. T. Knox, "Power-spectrum analysis of exponential diffusers," J. Opt. Soc. Am. **62**, 877-881 (1972).

4. Y. Nakayama and M. Kato, "Diffuser with pseudorandom phase sequence," J. Opt. Soc. Am. **69**, 1367-1372 (1979).

5. M. Kowalczyk, "Spectral and imaging properties of uniform diffusers," J. Opt. Soc. Am. A **1**, 192-200 (1984).

6. L. G. Shirley and N. George, "Wide-angle diffuser transmission functions and far-zone speckle," J. Opt. Soc. Am. A **4**, 734-745 (1987).

7. C. Pask, "Derivation of source-field coherence properties from radiation angular distribution," Opt. Acta. **24**, 235-240 (1977).

8. E. Wolf, "Coherence and radiometry," J. Opt. Soc. Am. **68**, 6-17 (1978).

9. E. Wolf and W. H. Carter, "Fields generated by homogeneous and by quasi-homogeneous planar secondary sources," Opt. Commun. **50**, 131-136 (1984).

10. M. V. Berry, "Diffractals," J. Phys. A **12**, 781-797 (1979).

11. D. L. Jordan, R. C. Hollins, and E. Jakeman, "Experimental measurements of non-Gaussian scattering by a fractal diffuser," Appl. Phys. B **31**, 179-186 (1983).

12. E. Jakeman, "Fraunhofer scattering by a sub-fractal diffuser," Opt. Acta **30**, 1207-1212 (1983).

13. D. L. Jaggard and Y. Kim, "Diffraction by band-limited fractal screens," J. Opt. Soc. Am. A **4**, 1055-1062 (1987).

14. W. T. Welford, "Review-Optical estimation of statistics of surface roughness from light scattering measurements," Opt. Quantum Electron. **9**, 269-287 (1977).

15. J. M. Elson and J. M. Bennett, "Relation between the angular dependence of scattering and the statistical properties of optical surfaces," J. Opt. Soc. Am. **69**, 31-47 (1979).

16. Y. Wang and W. L. Wolfe, "Scattering from microrough surfaces: comparison of theory and experiment," J. Opt. Soc. Am. **73** 1596-1602 (1983).

17. P. Roche and E. Pelletier, "Characterizations of optical surfaces by measurement of scattering distribution," Appl. Opt. **23**, 3561-3566 (1984).

18. K. J. Allardyce and N. George, "Diffraction analysis of rough reflective surfaces," Appl. Opt. **26**, 2364-2375 (1987).

19. H. E. Bennett, "Specular reflectance of aluminized ground glass and the height distribution of surface irregularities," J. Opt. Soc. Am. **53**, 1389-1394 (1963).

20. M. R. Latta, "The scattering of 10.6 micron radiation from ground glass surfaces," M.S. Thesis, U. Rochester, Rochester, NY, 1968.

21. R. I. Hamaguchi, "Transmission characteristics of ground glass," M.S. Thesis, U. Rochester, NY, 1970.

22. P. J. Chandley, "Surface roughness measurements from coherent light scattering," Opt. Quantum Electron. **8**, 323-327 (1976).

23. P. J. Chandley, "Determination of the probability density function of height on a rough surface from far-field coherent light scattering," Opt. Quantum Electron. **11**, 413-418 (1979).

24. N. G. Gaggioli and M. L. Roblin, "Etudes des etats de surface par les properties de diffusion a l'infini en lumiere transmise," Opt. Commun. **32**, 209-213 (1980).

25. P. Croce and L. Prod'Homme, "Contribution of immersion technique to light scattering analysis of very rough surfaces," J. Opt. **11**, 319-327 (1980).

26. L. G. Shirley and N. George, "Diffuser transmission functions and far-zone speckle patterns," in *International Conference on Speckle*, H. H. Arsenault, ed., Proc. Soc. Photo-Opt. Instrum. Eng. **556**, 63-69 (1985).

150

27. P. F. Gray, "A method of forming optical diffusers of simple known statistical properties," Opt. Acta **25**, 765-775 (1978).

28. B. M. Levine and J. C. Dainty, "Non-Gaussian image plane speckle: measurements from diffusers of known statistics," Opt. Commun. **45**, 252-257 (1983).

29. E. R. Mendez and K. A. O'Donnell, "Observation of depolarization and backscattering enhancement in light scattering from Gaussian random surfaces," Opt. Commun. **61**, 91-95 (1987).

30. We use I_{en} instead of the BRDF because I_{en} is proportional to the power at the detector. The BRDF can be obtained from I_{en} by dividing I_{en} by $\cos\theta$. See F. E. Nicodemus, "Reflectance nomenclature and directional reflectance and emissivity," Appl. Opt. **9**, 1474-1475 (1970).

31. E. Lukacs, *Characteristic Functions*, 2nd ed. (C. Griffin, London, 1970), p. 68.

32. P. Beckmann, "Scattering by composite rough surfaces," Proc. IEEE **53**, 1012-1015 (1965).

33. J. Dyson, "Optical diffusing screens of high efficiency," J. Opt. Soc. Am. **50**, 519-520 (1960).

34. E. G. Rawson, A. B. Nafarrate, and R. E. Norton, "Speckle-free rear-projection screen using two close screens in slow relative motion," J. Opt. Soc. Am. **66**, 1290-1294 (1976).

35. Armour Products, Midland Park, NJ 07432.

36. Allied Chemical, Allied Corp., Morristown, NJ 07960.

SUMMARY

In this thesis the scattering of laser light from single thin diffusers and from a cascade of two thin diffusers is analyzed with particular emphasis on remote sensing. In both scattering configurations, the diffusers are probed with a monochromatic plane wave, see Fig. 1.1. For single diffusers, the angular distribution of the radiation pattern, i.e, the slowly varying envelope of intensity, is related to the statistical properties of the diffuser surface. For double diffusers, decorrelation of the far-zone speckle pattern with respect to changes in the wavelength and/or angle of incidence of the input plane wave is related to the diffuser surface properties and to the spacing H between diffusers. It is shown that these two problems are very closely related in that one can predict the decorrelation behavior from a cascade of two diffusers given the angular distribution of the radiation patterns from the single diffusers that make up the cascade.

The propagation of light through single diffusers is treated in Chapter 2. Of particular interest is the validity of Eq. (2.1) for obtaining the complex amplitude $v_2(\mathbf{r})$ at the output plane of a diffuser by multiplying the complex amplitude $v_1(\mathbf{r})$ at the input plane, point-by-point, by a diffuser transmission function $t(\mathbf{r};k)$. This simple transmission function approach is limited because it does not account for diffuser thickness effects. For comparison, a generalized transmission function $t(\mathbf{r};\mathbf{k})$ is introduced that does account for thickness effects through its additional dependence on the angle of incidence of an input plane wave. Hence, $t(\mathbf{r};\mathbf{k})$ is denoted as the plane-wave transmission function for the plane wave with wave vector $\mathbf{k}$. For general illumination, the input $v_1(\mathbf{r})$ is decomposing into an angular spectrum of plane waves, and Eq. (2.7) is used to calculate the output $v_2(\mathbf{r})$. As is evident from Eqs. (2.9) and (2.10), the plane-wave transmission function $t(\mathbf{r};\mathbf{k})$ is an alternative to the impulse response $g(\mathbf{r};\mathbf{r}')$ for treating the propagation of light through an arbitrary linear system.

151

Approximate plane-wave transmission functions are given in Eq. (2.23) for a bulk diffuser and in Eq. (2.34) for a rough surface diffuser. Through computer simulations of far-zone speckle patterns (see Fig. 2.5) and through analytical calculations of the speckle decorrelation (see Appendix B) it is shown that the angular dependence of the generalized transmission function is not important for typical thin diffusers illuminated at small input angles. Hence, the simple transmission function is adequate for treating the individual thin diffusers in a cascade. This is important because it makes the resulting expressions for the cascade manageable.

In Chapter 3 the decorrelation of speckle from double diffusers is analyzed with respect to changes in wavelength, angle of incidence, angle of observation, and spacing. The diffuser pair, see Fig. 3.1, is illuminated with a plane wave of wave number k that points in an arbitrary input direction s_0. The two diffusers are separated by a spacing H, and there is an aperture a in contact with the second diffuser. The expression for the complex amplitude in the far-zone of this aperture is given by Eq. (3.17).

Equation (3.47) is a general expression for u_{ab}, the two-state correlation function of the far-zone complex amplitude. The subscripts a and b represent the initial and final states of the four parameters that can be varied during an experiment, i.e., the wave number k, the input direction s_0, the spacing H, and the observation direction s. In a typical speckle experiment, one would measure the intensity rather than the complex amplitude. Hence, it is important to also calculate the two-state correlation function of intensity $<I_aI_b>$. The expansion of $<I_aI_b>$ in terms u_{ab} for circular complex Gaussian statistics is given in Eq. (3.75). The two-state correlation functions u_{ab} and $<I_aI_b>$ are measures of the correlation between the initial and final speckle patterns. A speckle pattern is said to be decorrelated if u_{ab} is small compared to its initial value u_{aa} or if the normalized two-state correlation of intensity in Eq. (3.75) approaches unity.

The general expression for u_{ab} given in Eq. (3.47) takes the especially simple form given in Eq. (3.48) when k and H are constant, or more generally, when Eq. (3.45) holds.

Equation (3.48) is proportional to the double-diffuser descriptor function F that is defined in Eq. (3.30). The offset vector $H_a s_{oa\perp} - H_b s_{ob\perp}$ that occurs as the first argument of F is particularly important. It can be interpreted geometrically as the lateral shift at plane II between two rays leaving plane I at the same point and traveling in directions s_{oa} and s_{ob}. Some special cases of u_{ab} listed in Section 3.2.6 are the radiation pattern from a cascade of two diffusers in Eq. (3.50), the radiation pattern from a single diffuser in Eq. (3.51), and u_{ab} for a single diffuser in Eq. (3.52). Equation (3.58) is a general form of u_{ab} for a diffuser with an arbitrary plane-wave transmission function. It includes the double diffuser as a special case.

The analysis in Chapter 3 applies to general diffusers; however, in order to perform calculations based on Eq. (3.47), the functional forms of the autocorrelation functions R_{t_1} and R_{t_2} of the diffuser transmission function t_1 and t_2 must be specified. For diffusers whose height profile h is normally distributed, there is a particularly simple relationship, Eq. (3.63), between the autocorrelation functions R_t of the transmission function and R_h of the height profile. The decaying exponential, Eq. (3.66), and the Gaussian, Eq. (3.67), are two important large roughness limiting forms of Eq. (3.63) for R_t. The decaying exponential applies when R_h looks like a cone, and the Gaussian applies when R_h looks like a paraboloid for small values of the offset parameter $\mathbf{r}$. These diffusers are designated as conical, C, and paraboloidal, P, respectively. For paraboloidal diffusers, the slope parameter σ_h/w, where σ_h is the rms surface roughness and w is the lateral correlation length, determines the angular spread of the radiation pattern. For conical diffusers, the corresponding parameter is σ_h^2/w.

Chapter 3 provides a framework for further analysis of speckle decorrelation from a cascade of two diffusers. The general expression in Eq. (3.47) for u_{ab} can be used as the basis for many different remote sensing techniques. An important special case of the analysis is the remote sensing of the spacing between a large roughness diffuser and a

circular aperture by observing the angular decorrelation of the far-zone speckle pattern, see Eq. (3.93).

In Chapter 4 the analysis of speckle decorrelation is applied to the remote sensing of a P-P diffuser cascade. The advantage of analyzing this combination first is that the two-state correlation function of intensity can be calculated in closed form for arbitrary values of the state variables. The resulting solution, Eq. (4.13), is used in categorizing the different speckle decorrelation phenomenon and in configuring remote sensing experiments. Equation (4.18) is the simplified version of Eq. (4.13) that results by setting $k_{ab\perp} = 0$, i.e., by using equal input and observation angles. Based on Eq. (4.18), it is shown that the three parameters σ_{h_1}/w_1, σ_{h_2}/w_2, and H of the diffuser cascade can be determined remotely by performing three experiments. These experiments are measurement of the decorrelation of the speckle pattern with changes of wavelength and spacing and measurement of the angular distribution of the radiation pattern. However, it is also necessary to perform a wavelength decorrelation experiment with $k_{ab\perp} \neq 0$ to distinguish between the diffusers, i.e., to determine the ordering of the diffusers in the cascade. This additional experiment is based on the fact that the wavelength decorrelation for $k_{ab\perp} \neq 0$ is enhanced if $p_4 > 1$, i.e., if the diffuser having the larger spread in its radiation pattern occurs first in the cascade.

The analysis is presented in Appendix E for the P-C and C-P diffuser cascades and in Appendix F for the C-C cascade. It is shown that one can determine the values of the appropriate diffuser parameter σ_h/w or σ_h^2/w for each diffuser, together with the spacing, by performing simple remote sensing experiments. The major difference between these diffuser combinations and the P-P combination is that two unknowns, instead of one, can be obtained from each experiment, see Section 4.5. This implies that there is more freedom in choosing the types of experiments used in the remote sensing of the P-C, C-P, and C-C diffuser combinations.

In Chapter 5 theoretical radiation patterns are compared with measured radiation patterns from ground-glass and acid-etched diffusers. First, the theoretical radiation patterns from conical and paraboloidal diffusers are given in Eqs. (5.9) and (5.10), respectively. Then diffusers with two scales of roughness are also analyzed. Of particular importance is Eq. (5.36) for the (P,E) diffuser, where the letter P denotes a large roughness paraboloidal component as usual, and the letter E denotes a small roughness component having an exponential autocorrelation function.

Measured radiation patterns over a dynamic range of about 6 orders of magnitude are presented for ground-glass diffusers and about 8 orders of magnitude for acid-etched diffusers. For ground glass, excellent agreement is obtained using an autocorrelation function that is conical for small spatial offsets; this is consistent with our physical expectation based on the need for a rapid fall-off in surface correlation due to the jagged nature of the surface relief. For etched glass, excellent agreement is obtained with the (P,E) diffuser. The upper two or three orders of magnitude of the radiation pattern is dominated by the large roughness paraboloidal component, and the scattering at wide angles is predicted by the small roughness component having a decaying exponential autocorrelation function. The values of $w/(\lambda S) = w/(2\pi\sigma_l)$ for the paraboloidal component of etched-glass diffusers made with BOE etch times ranging between 2 and 120 min are obtained from the measured radiation patterns. These values of $w/(\lambda S)$ range between 3 and 13 and compare well with those obtained by direct measurement of the surface profile with a stylus profilometer.

REFERENCES

M. Abramowitz and I. A. Stegun, *Handbook of Mathematical Functions*, (Dover, New York, 1965).

K. J. Allardyce and N. George, "Diffraction analysis of rough reflective surfaces," Appl. Opt. **26**, 2364-2375 (1987).

H. H. Arsenault, ed., *International Conference on Speckle*, Proc. SPIE 556 (1985).

H. P. Baltes, H. A. Ferwerda, A. S. Glass, and B. Steinle, "Retrieval of structural information from far-zone intensity and coherence of scattered radiation," Opt. Acta **28**, 11-28 (1981).

N. Barakat, T. El Dessouki, M. El Nicklawy, and M. Abdel Sadek, "Interference from two identical diffusers," Acta Phys. Acad. Scientiarum Hungaricae **51**, 341-347 (1981).

R. Barakat, "The brightness distribution of the product of two partially correlated speckle patterns," Opt. Commun. **52**, 1-4 (1984).

R. Barakat and R. J. Salawitch, "Second- and fourth-order statistics of double scattered speckle," Opt. Acta **33**, 79-89 (1986).

P. Beckmann and A. Spizzichino, *The Scattering of Electromagnetic Waves from Rough Surfaces* (Pergamon Press, New York, 1962).

P. Beckmann, "Scattering by composite rough surfaces," Proc. IEEE **53**, 1012-1015 (1965).

P. Beckmann, "Scattering of light by rough surfaces," in *Progress in Optics VI*, E. Wolf, ed. (North-Holland, Amsterdam, 1967), pp. 53-69.

H. E. Bennett, "Specular reflectance of aluminized ground glass and the height distribution of surface irregularities," J. Opt. Soc. Am. **53**, 1389-1394 (1963).

M. V. Berry, "Diffractals," J. Phys. A **12**, 781-797 (1979).

H. G. Booker, J. A. Ratcliffe, and D. H. Shinn, "Diffraction from an irregular screen with applications to ionospheric problems," Philos. Trans. R. Soc. London Ser. A **242**, 579-607 (1950).

M. Born and E. Wolf, *Principles of Optics*, 6th ed. (Pergamon Press, New York, 1980).

K. -H. Brenner and J. Ojeda-Castaneda, "Ambiguity function and Wigner distribution function applied to partially coherent imagery," Opt. Acta **31**, 213-223 (1984).

W. P. Brown, Jr., "Propagation in random media--cumulative effect of weak inhomogeneities," IEEE Trans. Antennas Propag. AP-**15**, 81-89 (1967).

C. B. Burckhardt, "Laser speckle pattern---A narrowband noise model." Bell System Tech. J. **49**, 309-316 (1970).

W. H. Carter and E. Wolf, "Coherence and radiometry with quasihomogeneous planar sources," J. Opt. Soc. Am. **67**, 785-796 (1977).

W. H. Carter, ed., *Applications of Speckle Phenomena*, Proc. SPIE 243 (1980).

P. J. Chandley and W. T. Welford, "A re-formulation of some results of P. Beckmann for scattering from rough surfaces," Opt. Quantum Electron. **7**, 393-397 (1975).

P. J. Chandley, "Surface roughness measurements from coherent light scattering," Opt. Quantum Electron. **8**, 323-327 (1976).

P. J. Chandley, "Determination of the probability density function of height on a rough surface from far-field coherent light scattering," Opt. Quantum Electron. **11**, 413-418 (1979).

P. Croce and L. Prod'Homme, "Contribution of immersion technique to light scattering analysis of very rough surfaces," J. Opt. **11**,319-327 (1980).

J. C. Dainty, "Some statistical properties of random speckle patterns in coherent and partially coherent illumination," Optica Acta **17**, 761-772 (1970).

J. C. Dainty, ed., *Laser Speckle and Related Phenomenon* (Springer-Verlag, Berlin, 1975).

J. C. Dainty and D. Newman, "Detection of gratings hidden by diffusers using photon-correlation techniques," Opt. Lett. **8**, 608-610 (1983).

J. Dyson, "Optical diffusing screens of high efficiency," J. Opt. Soc. Am. **50**, 519-520 (1960).

J. M. Elson and J. M. Bennett, "Relation between the angular dependence of scattering and the statistical properties of optical surfaces," J. Opt. Soc. Am. **69**, 31-47 (1979).

L. H. Enloe, "Noise-like structure in the image of diffusely reflecting objects in coherent illumination,"Bell System Tech. J. **46**, 1479-1489 (1967).

A. E. Ennos, "Speckle Interferometry," in *Progress in Optics* XVI, 235-288, E. Wolf, ed. (North-Holland, Amsterdam, 1978).

R. K. Erf, ed., *Speckle Metrology* (Academic Press, New York, 1979).

M. Francon, *Laser Speckle and Applications in Optics* (Academic Press, New York, 1979).

D. L. Fried, "Laser eye safety: the implications of ordinary speckle statistics and of speckled-speckle statistics," J. Opt. Soc. Am. **71**, 914-916 (1981).

H. Fujii, J. Uozumi, and T. Asakura, "Computer simulation study of image speckle patterns with relation to object surface profile," J. Opt. Soc. Am. **66**, 1222-1236 (1976).

N. G. Gaggioli and M. L. Roblin, "Etudes des etats de surface par les properties de diffusion a l'infini en lumiere transmise," Opt. Commun. **32**, 209-213 (1980).

W. Gautschi, "Complex error function," Commun. ACM **12**, 635 (1969).

W. Gautschi, " Efficient computation of the complex error function," SIAM J. Numer. Anal. **7**, 187-198 (1970).

N. George and A. Jain, "Speckle reduction using multiple tones of illumination," Appl. Opt. **12**, 1202-1212 (1973).

N. George and A. Jain, "Space and wavelength dependence of speckle intensity," Appl. Phys. **4**, 201-212 (1974).

N. George, A. Jain, and R. D. S. Melville, Jr., "Experiments on the space and wavelength dependence of speckle," Appl. Phys. **7**, 157-169 (1975).

N. George and A. Jain, "Speckle from a cascade of two diffusers," Opt. Commun. **15**, 71-75 (1975).

N. George and D. C. Sinclair, "Editorial---Topical issue on laser speckle" J. Opt. Soc. AM. **66**, 1316 (1976).

L. I. Goldfischer, "Autocorrelation function and power spectral density of laser-produced speckle patterns," J. Opt. Soc. Am. **55**, 247-253 (1965).

J. W. Goodman, "Statistical properties of Laser sparkle patterns," Stanford Electronics Laboratories TR2303-1 (SEL-63-140) (1963).

J. W. Goodman, *Introduction to Fourier optics*, (McGraw-Hill, New York, 1968).

J. W. Goodman, "Dependence of image speckle on surface roughness," Opt. Commun. **14**, 324-327 (1975)..

I. S. Gradshteyn and I. M. Ryzhik, *Table of Integrals, Series, and Products*, (Academic Press, New York, 1980).

P. F. Gray, "A method of forming optical diffusers of simple known statistical properties," Opt. Acta **25**, 765-775 (1978) .

R. I. Hamaguchi, "Transmission characteristics of ground glass," M.S. Thesis, U. Rochester, NY, 1970.

A. Hewish, "The diffraction of radio waves in passing through a phase-changing ionosphere," Proc. R. Soc. London Ser. A **209**, 81-96 (1951).

A. Ishimaru, Wave Propagation and Scattering in Random Media (Academic, New York, 1978), Vols. 1 and 2.

D. L. Jaggard and Y. Kim, "Diffraction by band-limited fractal screens," J. Opt. Soc. Am. A **4**, 1055-1062 (1987).

E. Jakeman and P. N. Pusey, "The statistics of light scattered by a random phase screen," J. Phys. A **6**, L88-L92 (1973).

E. Jakeman and P. N. Pusey, "Non-Gaussian fluctuations in electromagnetic radiation scattered by a random phase screen. I. Theory," J. Phys. A **8**, 369-391 (1975).

E. Jakeman, "Fraunhofer scattering by a sub-fractal diffuser," Opt. Acta **30**, 1207-1212 (1983).

R. Jones and C. Wykes, *Holographic and Speckle Interferometry* (Cambridge University Press, Cambridge, 1983).

D. L. Jordan, R. C. Hollins, and E. Jakeman, "Experimental measurements of non-Gaussian scattering by a fractal diffuser," Appl. Phys. B **31**, 179-186 (1983).

M. Kowalczyk, "Spectral and imaging properties of uniform diffusers," J. Opt. Soc. Am. A **1**, 192-200 (1984).

C. N. Kurtz, "Transmittance characteristics of surface diffusers and the design of nearly band-limited binary diffusers," J. Opt. Soc. Am. **62**, 982-989 (1972).

C. N. Kurtz, H. O. Hoadley, and J. J. DePalma, "Design and synthesis of random phase diffusers," J. Opt. Soc. Am. **63**, 1080-1092 (1973).

R. V. Langmuir, "Scattering of Laser light," Appl. Phys. Lett. **2**, 29-30 (1963).

M. R. Latta, "The scattering of 10.6 micron radiation from ground glass surfaces," M.S. Thesis, U. Rochester, NY, 1968.

M. von Laue, Sitzungsber. K. Preuss. Akad. Wiss. **47**,1144 (1914).

R. W. Lee and J. C. Harp, "Weak scattering in random media, with applications to remote probing," Proc. IEEE **57**, 375-406 (1969).

B. M. Levine and J. C. Dainty, "Non-Gaussian image plane speckle: measurements from diffusers of known statistics," Opt. Commun. **45**, 252-257 (1983).

I. Liefer, C. J. D. Spencer, and W. T. Welford, "Grainless screens for projection microscopy," J. Opt. Soc. Am. **51**, 1422-1423 (1961).

S. Lowenthal and H. Arsenault, "Image formation for coherent diffuse objects: Statistical properties," J. Opt. Soc. Am. **60**, 1478-1483 (1970).

S. Lowenthal and D. Joyeux, "Speckle removal by a slowly moving diffuser associated with a motionless diffuser," J. Opt. Soc. Am. **61**, 847-851 (1971).

E. Lukacs , *Characteristic Functions*, 2nd ed. (C. Griffin, London, 1970).

L. Mandel, "Fluctuations of light beams," in *Progress in Optics* II, E. Wolf, ed. (North-Holland, Amersterdam, 1963), pp.181-248 .

W. F. McGee, "Complex Gaussian noise moments," IEEE Trans. Inf. Theory **IT-17**, 149-157 (1971).

C. L. Mehta, "Coherence and statistics of radiation," in *Lectures in Theoretical Physics* VIIC, W. E. Brittin, ed. (University of Colorado, Boulder, 1964), pp. 345-401.

E. R. Mendez and K. A. O'Donnell, "Observation of depolarization and backscattering enhancement in light scattering from Gaussian random surfaces," Opt. Commun. **61**, 91-95 (1987).

R. P. Mercier, "Diffraction by a screen causing large random phase fluctuations," Proc. Cambridge Philos. Soc. **58**, 382-400 (1962).

K. S. Miller, "Complex Gaussian processes," SIAM Rev. **11**, 544-567 (1969).

G. M. Morris, "Serrated Apertures: Statistical Diffraction Theory and Experiments," Ph.D. Thesis, California Institute of Technology, CA, 1979.

Y. Nakayama and M. Kato, "Diffuser with pseudorandom phase sequence," J. Opt. Soc. Am. **69**, 1367-1372 (1979).

F. E. Nicodemus, "Reflectance nomenclature and directional reflectance and emissivity," Appl. Opt. **9**, 1474-1475 (1970).

M. Nieto-Vesperinas and N. Garcia, "A detailed study of the scattering of scalar waves from random rough surfaces," Opt. Acta **28**, 1651-1672 (1981).

D. Newman, "K distributions from doubly scattered light," J. Opt. Soc. Am. A **2**, 22-26 (1985).

K. A. O'Donnell, "Speckle statistics of doubly scattered light," J. Opt. Soc. Am. **72**, 1459-1463 (1982).

J. Ohtsubo and T. Asakura, "Statistical properties of laser speckle produced in the diffraction field," Appl. Opt. **16**, 1742-1753 (1977).

B. M. Oliver, "Sparkling spots and random diffraction," Proc. IEEE **5**, 220-221 (1963).

A. Papoulis, "Ambiguity function in Fourier optics," J. Opt. Soc. Am. **64**, 779-788 (1974).

C. Pask, "Derivation of source-field coherence properties from radiation angular distribution," Opt. Acta. **24**, 235-240 (1977).

H. M. Pederson, "Theory of speckle dependence on surface roughness," J. Opt. Soc. Am. **66**, 1204-1210 (1976).

J. A. Ratcliffe, "Some aspects of diffraction theory and their application to the ionosphere," Rep. Prog. Phys. **19**, 188-218 (1956).

E. G. Rawson, A. B. Nafarrate, and R. E. Norton, "Speckle-free rear-projection screen using two close screens in slow relative motion," J. Opt. Soc. Am. **66**, 1290-1294 (1976).

Lord Rayleigh, "On the resultant of a large number of vibrations of the same pitch and of arbitrary phase," Phil. Mag. **10**, 73-78 (1880).

I. S. Reed, "On a moment theorem for complex Gaussian processes," IRE Trans. Inf. Theory **IT-8**, 194-195 (1962).

J. D. Rigden and E. I. Gordon, "The granularity of scattered optical maser light," Proc. IRE **50**, 2367-2368 (1962).

P. Roche and E. Pelletier, "Characterizations of optical surfaces by measurement of scattering distribution," Appl. Opt. **23**, 3561-3566 (1984).

F. Roddier, "The effects of atmospheric turbulence in optical astronomy," in *Progress in Optics* XIX, E. Wolf, ed. (North-Holland, Amsterdam, 1981), pp.281-376.

F. Roddier, J. M. Gilli, and J. Vernin, " On the isoplanatic patch size in stellar speckle interferometry," J. Optics. 13, 63-70 (1982).

F. Roddier, J. M. Gilli, and G. Lund, "On the origin of speckle boiling and its effects in stellar speckle interferometry," J. Optics 13, 263-271 (1982).

H. E. Salzer, " Formulas for calculating the error function of a complex variable," Math. Tables Aids Comp. 5, 67-70 (1951).

L. G. Shirley and N. George, "Diffuser transmission functions and far-zone speckle patterns," in *International Conference on Speckle*, H. H. Arsenault, ed., Proc. Soc. Photo-Opt. Instrum. Eng. 556, 63-69 (1985).

L. G. Shirley and N. George, "Speckle from a thick diffuser," J. Opt. Soc. Am. A 3, P121 (1986).

L. G. Shirley and N. George, "Wide-angle diffuser transmission functions and far-zone speckle," J. Opt. Soc. Am. A 4, 734-745 (1987).

L. G. Shirley and N. George, "Diffuser radiation patterns over a large dynamic range," J. Opt. Soc. Am. A 5, P64 (1988).

L. G. Shirley and N. George, "Diffuser radiation patterns over a large dynamic range. Part I: Strong diffusers," Appl. Opt. 27, 1850-1861 (1988).

J. Uozumi and T. Asakura, "First-order intensity and phase statistics of Gaussian speckle produced in the diffraction region," Appl. Opt. 20, 1454-1466 (1981).

R. C. Waag and K. T. Knox, "Power-spectrum analysis of exponential diffusers," J. Opt. Soc. Am. 62, 877-881 (1972).

Y. Wang and W. L. Wolfe, "Scattering from microrough surfaces: comparison of theory and experiment," J. Opt. Soc. Am. 73 1596-1602 (1983).

W. T. Welford, "Review-Optical estimation of statistics of surface roughness from light scattering measurements," Opt. Quantum Electron. 9, 269-287 (1977).

W. T. Welford, "Laser speckle and surface roughness," Contemp. Phys. 21, 401-412 (1980).

E. Wolf, "Coherence and radiometry," J. Opt. Soc. Am. 68, 6-17 (1978).

E. Wolf and W. H. Carter, "Fields generated by homogeneous and by quasi-homogeneous planar secondary sources," Opt. Commun. 50, 131-136 (1984).

P. M. Woodward, *Probability and Information Theory with Applications to Radar*, (Pergamon Press, Oxford, 1953).

A. Zardecki, "Statistical features of phase screens from scattering data," in *Inverse Scattering Problems in Optics*, H.P. Baltes, ed. (Springer-Verlag, Berlin, 1978), pp.155-192.

Appendix A

Fourth-Order Moment of a Non-Circular, Non-Zero mean,

Complex Gaussian Random Process

The complex Gaussian random process z is defined as

$$z = x + iy,$$ (A1)

where x and y are arbitrary real Gaussian random variables. In much of what is written on the subject it is assumed that z has zero mean, i.e., that $<x> = <y> = 0$, and that z is circular.[1-5] Circularity is defined below in Eq. (A11). There seems to be a lack of written material on the general case of, non-circular, non-zero-mean complex Gaussian random processes. There is sometimes confusion in the literature because the results for zero-mean circular-complex random processes are applied to general complex Gaussian random processes. The results of this appendix are used in obtaining Eq. (3.72) for the two-state correlation function of intensity.

We begin calculation of the general fourth-order moment of a complex Gaussian random process by first considering real Gaussian random variables. Let x_1, x_2, x_3, and x_4 be four Gaussian distributed random variables, each having a mean value of zero. Then by the Gaussian moment theorem,[3,4] we can write the fourth-order moment in terms of the second-order moments as

$$<x_1 x_2 x_3 x_4> = <x_1 x_2><x_3 x_4> + <x_1 x_3><x_2 x_4> + <x_1 x_4><x_2 x_3> .$$ (A2)

Since all odd-order moments are equal to zero, we also have

$$<x_1 x_2 x_3> = 0 .$$ (A3)

The random variables in Eqs. (A2) and (A3) could be interpreted as arising from distinct random processes, which may or may not be correlated with each other. However, in the

162

usual application x_i represents a single random process where the subscript denotes a certain argument, i.e., $x_i = x(t_i)$, where $i = 1,2,3$, or 4.

We generalize Eq. (A3) to include non-zero-mean statistics by substituting the zero-mean random process $x_i - <x_i>$ for each of the variables and then expanding. The resulting expression for the third-order moment is

$$<x_1 x_2 x_3> = <x_2 x_3><x_1> + <x_1 x_3><x_2> + <x_1 x_2><x_3>$$

$$-2<x_1><x_2><x_3> . \tag{A4}$$

By following the same procedure for Eq. (A2) and using Eq. (A4) to reduce the resulting terms containing third-order moments to second- and first-order moments, we obtain

$$<x_1 x_2 x_3 x_4> = <x_1 x_2><x_3 x_4> + <x_1 x_3><x_2 x_4> + <x_1 x_4><x_2 x_3>$$

$$-2<x_1><x_2><x_3><x_4> \tag{A5}$$

for the expansion of the fourth-order moment when the random variables have non-zero means.

When $<x_i> = 0$ and $<y_i> = 0$, the expansions for complex random variables corresponding to Eqs. (A2) and (A3) are

$$<z_1 z_2 z_3 z_4> = <z_1 z_2><z_3 z_4> + <z_1 z_3><z_2 z_4> + <z_1 z_4><z_2 z_3> \tag{A6}$$

and

$$<z_1 z_2 z_3> = 0 . \tag{A7}$$

The validity of Eqs. (A6) and (A7) can be checked by writing z_i in terms of the real variables x_i and y_i, expanding, and using Eq. (A2) to reduce the real fourth-order moments to second order moments and Eq. (A3) to show that the real third-order moments are zero. Equations (A4) and (A5) also generalize to complex variables yielding

$$<z_1 z_2 z_3> = <z_2 z_3><z_1> + <z_1 z_3><z_2> + <z_1 z_2><z_3>$$

$$-2<z_1><z_2><z_3> \qquad \text{(A8)}$$

and

$$<z_1 z_2 z_3 z_4> = <z_1 z_2><z_3 z_4> + <z_1 z_3><z_2 z_4> + <z_1 z_4><z_2 z_3>$$

$$-2<z_1><z_2><z_3><z_4> \qquad \text{(A9)}$$

for the expansion of the third- and fourth-order moments of non-zero mean complex Gaussian random variables. The steps in obtaining Eqs. (A8) and (A9) from Eq. (A6) and (A7) are exactly the same as those used to obtain Eqs. (A4) and (A5) from Eqs. (A2) and (A3).

The usual complex fourth-order moment that one encounters in random processes has complex conjugates on two of the four z variables, and z is interpreted as a single random process, i.e., $z_i = z(t_i)$. Thus we rewrite Eq. (A9) as

$$<z(t_1) z(t_2) z^*(t_3) z^*(t_4)> = <z(t_1) z(t_2)><z^*(t_3) z^*(t_4)>$$

$$+ <z(t_1) z^*(t_3)><z(t_2) z^*(t_4)> + <z(t_1) z^*(t_4)><z(t_2) z^*(t_3)>$$

$$-2<z(t_1)><z(t_2)><z^*(t_3)><z^*(t_4)>. \qquad \text{(A10)}$$

In many cases, e.g., when $z(t)$ is an analytic signal representation of the real function $x(t)$, the random process will be circular.[5] The definition of circularity is that

$$<z(t_1) z(t_2)> = <z(t_1)><z(t_2)> \qquad \text{(A11)}$$

for any values of t_1 and t_2. Equation (A11) implies that the real and imaginary parts of z will obey the following two relationships:

$$<x(t_1) x(t_2)> - <x(t_1)><x(t_2)> = <y(t_1) y(t_2)> - <y(t_1)><y(t_2)> \qquad \text{(A12)}$$

and

$$<x(t_1) y(t_2)> - <x(t_1)><x(t_2)> = - <x(t_2) y(t_1)> - <y(t_1)><y(t_2)>. \qquad \text{(A13)}$$

For circularity, Eq. (A10) reduces to

$$<z(t_1)\,z(t_2)\,z^*(t_3)\,z^*(t_4)> = <z(t_1)\,z^*(t_3)><z(t_2)\,z^*(t_4)>$$

$$+ <z(t_1)\,z^*(t_4)><z(t_2)\,z^*(t_3)> - <z(t_1)><z(t_2)><z^*(t_3)><z^*(t_4)> . \qquad \text{(A14)}$$

Appendix A References

1. K. S. Miller, "Complex Gaussian processes," SIAM Rev. 11, 544-567 (1969).

2. W. F. McGee, "Complex Gaussian noise moments," IEEE Trans. Inf. Theory IT-17, 149-157 (1971).

3. I. S. Reed, "On a moment theorem for complex Gaussian processes," IRE Trans. Inf. Theory IT-8, 194-195 (1962).

4. C. L. Mehta, "Coherence and statistics of radiation," in *Lectures in Theoretical Physics VII* C, W. E. Brittin, ed. (University of Colorado, Boulder, 1964), pp. 345-401.

5. L. Mandel, "Fluctuations of light beams," in *Progress in Optics* II, E. Wolf, ed. (North-Holland, Amersterdam, 1963), pp.181-248 .

Appendix B

Plane-Wave Probing of Single Diffusers

Approximate plane-wave transmission functions for bulk diffusers and rough-surface diffusers are given in Eqs. (2.23) and (2.34), respectively. In this appendix these transmission functions are used to evaluate the two-state correlation function $R_{t_{12}}(\mathbf{r};\mathbf{k}_{oa};\mathbf{k}_{ob})$ defined in Eq. (3.56). The two-state correlation function u_{ab} of far-zone complex amplitude is then obtained by substituting $R_{t_{12}}$ into Eq. (3.58), and Eq. (3.75) is applied to calculate the two-state correlation function of far-zone intensity. This appendix is useful for showing that the wavelength and angular decorrelation of speckle from single diffusers generally occurs slowly compared with decorrelation from cascaded diffusers.

F.1 Bulk Diffusers

Upon substituting Eq. (2.23) into Eq. (3.56) and using Eq. (2.22) to write $\cos\theta_{<n>}$ in terms of $\sin\theta_0$, we obtain

$$R_{t_{12}}(\mathbf{r};\mathbf{k}_{oa};\mathbf{k}_{ob}) = \exp\left[iH\left(k_a\sqrt{\overline{<n>^2 - \sin^2\theta_{oa}}} - k_b\sqrt{\overline{<n>^2 - \sin^2\theta_{ob}}} \right) \right]$$

$$\times \left< \exp\left[iH<n>\left(\frac{k_a\,\overline{\Delta n(\mathbf{r}')}}{\sqrt{<n>^2 - \sin^2\theta_{oa}}} - \frac{k_b\,\overline{\Delta n(\mathbf{r} + \mathbf{r}')}}{\sqrt{<n>^2 - \sin^2\theta_{ob}}} \right) \right] \right> \quad (B1)$$

as the two-state correlation function for the plane-wave transmission function of a bulk diffuser. Following Section 3.3, we identify the ensemble average of the exponential in Eq. (B1) as the joint characteristic function[1] of the random process Δn with respect to the variables η_a and η_b, where

$$\eta_a = \frac{H k_a <n>}{\sqrt{<n>^2 - \sin^2\theta_{oa}}} \quad (B2)$$

167

and

$$\eta_b = -\frac{H k_b <n>}{\sqrt{<n>^2 - \sin^2\theta_{ob}}} \, .$$

(B3)

For a normally distributed wide-sense stationary random process, see Eq. (3.62),

$$< \exp\left[i\eta_a \Delta n(\mathbf{r}') + i\eta_b \Delta n(\mathbf{r}+\mathbf{r}')\right] > = \exp\left[-\frac{1}{2}\sigma_{\Delta n}^2 \left(\eta_b - \eta_a\right)^2\right]$$

$$\times \exp\left[-\sigma_{\Delta n}^2 \eta_a \eta_b \left(1 - R_{\Delta n}(\mathbf{r})\right)\right] .$$

(B4)

In Eq. (B4)

$$\sigma_{\Delta n} = <\Delta n(r)>^{\frac{1}{2}}$$

(B5)

and

$$R_{\Delta n}(\mathbf{r}) = \frac{<\Delta n(\mathbf{r}') \, \Delta n(\mathbf{r}+\mathbf{r}')>}{\sigma_{\Delta n}^2} \, .$$

(B6)

Through its dependence on the difference $\eta_b - \eta_a$, the first exponential on the right-hand side of Eq. (B4) controls decorrelation with respect to changes in the wavelength and the angle of incidence of the input plane wave. The second exponential is relatively insensitive to small changes in wavelength or angle of incidence because η_a and η_b occur as a product. We also note that the first exponential can be factored out of the integral in calculating u_{ab} from Eq. (3.58). Hence, it is not the precise functional form of $R_{\Delta n}$ that is important in determining the decorrelation properties of a single bulk diffuser, but rather the magnitude of the normal incidence rms phase delay

$$S_o = k H \sigma_{\Delta n} \, .$$

(B7)

A good approximation to Eq. (3.58) for u_{ab} is obtained by setting $\eta_b = \eta_a$ within the second exponential in Eq. (B4):

$$u_{ab} = \frac{k_a k_b}{\left(2\pi\right)^2} \exp\left[-iR\left(k_b - k_a\right)\right] \cos\theta_a \cos\theta_b$$

$$\times \exp\left[iH\left(k_a \sqrt{\overline{<n>^2 - \sin^2\theta_{oa}}} - k_b \sqrt{\overline{<n>^2 - \sin^2\theta_{ob}}}\right)\right] \exp\left[-\frac{1}{2}\sigma_{\Delta n}^2\left(\eta_b - \eta_a\right)^2\right]$$

$$\times \int \exp\left[-\sigma_{\Delta n}^2 \eta_a^2\left(1 - R_{\Delta n}(\mathbf{r})\right)\right] \tilde{A}(\mathbf{r}; \Delta\mathbf{k}_{ab\perp}) \exp\left(i\,\mathbf{k}_{ab\perp} \bullet \mathbf{r}\right) d^2\mathbf{r}. \tag{B8}$$

We use Eq. (3.75) to calculate the two-state correlation function of far-zone intensity from a strong diffuser whose limiting aperture is large compared to the diffuser correlation length. By requiring that the speckle tracking condition holds, i.e., that $\Delta k_{ab\perp} = 0$, the integral in Eq. (B8) will have the same value for u_{ab}, u_{aa}, and u_{bb}, and Eq. (3.75) will take the simple form

$$\frac{<I_a I_b>}{<I_a><I_b>} = 1 + \exp\left[-\sigma_{\Delta n}^2\left(\eta_b - \eta_a\right)^2\right]. \tag{B9}$$

Equation (B9) governs the wavelength and the angular dependence of speckle from a single bulk diffuser. We emphasize the wavelength dependence by applying Eq. (B9) to normally incident illumination and note that the wavelength dependence reduces to that of a single diffuser in a cascade, see Eq. (4.24):

$$\frac{<I_a I_b>}{<I_a><I_b>} = 1 + \exp\left(-S_o^2 \rho_k^2\right). \tag{B10}$$

In Eq. (B10) we have used the fractional change in wavenumber ρ_k defined in Eq. (4.23), and S_o is calculated for the initial wavenumber k_a. The angular dependence in Eq. (B9) is emphasized by assuming $k_a = k_b$:

$$\frac{<I_a I_b>}{<I_a><I_b>} = 1 + \exp\left\{-S_o^2\left[\left(1 - \frac{\sin^2\theta_{oa}}{<n>^2}\right)^{-\frac{1}{2}} - \left(1 - \frac{\sin^2\theta_{ob}}{<n>^2}\right)^{-\frac{1}{2}}\right]^2\right\}. \tag{B11}$$

In many applications $\theta_{oa} = 0$, i.e., the input plane wave is initially normally incident. Then for small angular detuning, Eq. (B11) reduces to

$$\frac{<I_a I_b>}{<I_a><I_b>} = 1 + \exp\left(-\frac{S_o^2 \theta_{ob}^4}{4<n>^4}\right). \tag{B12}$$

If we say that angular decorrelation has occurred when the exponential in Eq. (B12) falls to its $1/e$ point, then the value of θ_{ob} necessary for decorrelation is

$$\theta_{ob} = <n> \sqrt{2/S_o} . \tag{B13}$$

For the speckle pattern from a thin bulk diffuser to decorrelate with a change of angle of incidence of $\theta_{ob} \leq 1°$, S_o must be very large, i.e., $S_o \geq 15{,}000$ rad. Even for $\theta_{ob} \leq 10°$, $S_o \geq 150$ rad for the speckle pattern to decorrelate. As illustrated in Fig. 1.3, changes in the angle of incidence required to decorrelate speckle from a cascade of two diffusers are typically of the order of arc minutes. Thus angular decorrelation arising from the individual diffusers is usually insignificant compared to angular decorrelation arising from the spacing between diffusers.

F.2 Rough-Surface Diffuser

The two-state correlation function for the plane-wave transmission function of a rough-surface diffuser is obtained by substituting Eq. (2.34) for t into Eq. (3.56) for $R_{t_{12}}$ and using Eq. (2.30) to express θ_1 in terms of the input angle θ_0:

$$R_{t_{12}}(\mathbf{r};\mathbf{k}_{oa};\mathbf{k}_{ob}) = \exp\left[iH\left(k_a \sqrt{n^2 - \sin^2\theta_{oa}} - k_b \sqrt{n^2 - \sin^2\theta_{ob}} \right) \right]$$

$$\times <\exp\left[ik_a h(\mathbf{r}')\left(\sqrt{n^2 - \sin^2\theta_{oa}} - \cos\theta_{oa} \right) - ik_b h(\mathbf{r}+\mathbf{r}')\left(\sqrt{n^2 - \sin^2\theta_{ob}} - \cos\theta_{ob} \right) \right]> . \tag{B14}$$

Once again, the ensemble average of the exponential is a joint characteristic function, this time of the random process $h(\mathbf{r})$ with respect to the variables

$$\eta_a = k_a \left(\sqrt{n^2 - \sin^2\theta_{oa}} - \cos\theta_{oa} \right) \tag{B15}$$

and

$$\eta_b = -k_b \left(\sqrt{n^2 - \sin^2\theta_{ob}} - \cos\theta_{ob} \right) . \tag{B16}$$

The normal incidence rms phase delay corresponding to Eq. (B7) is

$$S_o = k \sigma_h (n-1) . \tag{B17}$$

Equation (B17) is identical to Eq. (3.10) except there is a subscript on S in Eq. (B17) to emphasize that the phase delay is for normal incidence.

The expression analogous to Eq. (B9) for the two-state correlation function of far-zone intensity is

$$\frac{<I_a I_b>}{<I_a><I_b>} = 1 + \exp\left[-\sigma_h^2\left(\eta_b - \eta_a\right)^2\right]. \tag{B18}$$

Equation (B10) also applies for the wavelength dependence of a rough-surface diffuser, but S_0 is now given by Eq. (B17) rather than Eq. (B7). The expression corresponding to Eq. (B11) for the angular decorrelation at constant wavelength is

$$\frac{<I_a I_b>}{<I_a><I_b>} = 1$$

$$+ \exp\left\{-S_0^2\left[\frac{1}{n-1}\left(\sqrt{n^2-\sin^2\theta_{oa}} -\cos\theta_{oa} - \sqrt{n^2-\sin^2\theta_{ob}} + \cos\theta_{ob}\right)\right]^2\right\}. \tag{B19}$$

For $\theta_{oa} = 0$ and small values of θ_{ob}, Eq. (B19) simplifies to

$$\frac{<I_a I_b>}{<I_a><I_b>} = 1 + \exp\left(-\frac{S_0^2\theta_{ob}^4}{4n^2}\right). \tag{B20}$$

Except for the difference between the way S_0 is defined for a rough-surface diffuser and the difference in the way the index of refraction occurs in the denominator, i.e., n^2 instead of $<n>^4$, Eq. (B20) is identical to Eq. (B12) for a bulk diffuser. The rough-surface analog of Eq. (B13) is

$$\theta_{ob} = \sqrt{2n/S_0}. \tag{B21}$$

From Eq. (B21) we see that $S_0 \geq 10,000$ rad and $S_0 \geq 100$ rad for the speckle pattern from a rough-surface diffuser to decorrelate with changes of angle of incidence of $\theta_{ob} \leq 1°$ and $\theta_{ob} \leq 10°$, respectively. Once again, these decorrelation angles are large compared to typical decorrelation angles arising from the spacing between diffusers.

Appendix B Reference

1. N. George and A. Jain, "Space and wavelength dependence of speckle intensity,"

    Appl. Phys. 4, 201-212 (1974).

Appendix C

Paraboloidal-Paraboloidal Diffuser Combination

In this appendix we present the results of the intermediate steps in the calculation of Eq. (4.7) for the two-state correlation of far-zone intensity from a cascade of two thin diffusers. The diffusers are assumed to be strong, i.e., S_1 and S_2 are much larger than one, and Eq. (4.8) applies for both R_{t_1} and R_{t_2} so that both diffusers are paraboloidal. We denote this diffuser combination by the symbol P-P. The subscripts 1 and 2 on the diffuser parameters σ_t and w refer to the planes I and II of Fig. 3.1. We proceed by first evaluating Eq. (4.4) for F while keeping all of its arguments arbitrary. Using the identity[1]

$$\int \exp\left[-\left(a^2|\mathbf{r}|^2 + i\mathbf{k}_\perp \bullet \mathbf{r}\right)\right] d^2r = \frac{\pi}{a^2}\exp\left(-\frac{|\mathbf{k}_\perp|^2}{4a^2}\right), \tag{C1}$$

where $\mathrm{Re}(a) \neq 0$, to evaluate the integral, we arrive at

$$F(\mathbf{r};k_a,k_b;\mathbf{k}_{ab\perp};\Delta\mathbf{k}_{ab\perp}) = \frac{\pi}{k_a k_b}\left(\frac{\sigma_{t1}^2}{w_1^2} + \frac{\sigma_{t2}^2}{w_2^2} + \frac{1}{2k_a k_b w_a^2}\right)^{-1}$$

$$\times \exp\left(-\frac{1}{8}w_a^2|\Delta\mathbf{k}_{ab\perp}|^2\right)\exp\left[-\frac{1}{2}\left(\sigma_{t1}^2 + \sigma_{t2}^2\right)\left(k_b - k_a\right)^2\right]$$

$$\times \exp\left[-\frac{1}{4k_a k_b}\left(\frac{\sigma_{t1}^2}{w_1^2} + \frac{\sigma_{t2}^2}{w_2^2} + \frac{1}{2k_a k_b w_a^2}\right)^{-1}|\mathbf{k}_{ab\perp}|^2\right]$$

$$\times \exp\left\{-\left[\frac{w_1^2}{\sigma_{t1}^2} + \left(\frac{\sigma_{t2}^2}{w_2^2} + \frac{1}{2k_a k_b w_a^2}\right)^{-1}\right]^{-1}\left[k_a k_b |\mathbf{r}|^2 + \right.\right.$$

$$\left.\left. + i\left(\frac{\sigma_{t2}^2}{w_2^2} + \frac{1}{2k_a k_b w_a^2}\right)^{-1}\mathbf{k}_{ab\perp}\bullet\mathbf{r}\right]\right\}. \tag{C2}$$

173

When we substitute Eq. (C2) into Eq. (4.1) and evaluate the integral, again using Eq. (C1), we obtain the following general expression for u_{ab}:

$$u_{ab} = \frac{1}{4\pi} \exp\left(-i\phi_{ab}\right) \exp\left(\frac{i}{2} \frac{H_a H_b}{k_b H_a - k_a H_b} |\mathbf{k}_{ob\perp} - \mathbf{k}_{oa\perp}|^2\right)$$

$$\times \cos\theta_a \cos\theta_b \left(\frac{\sigma_{t1}^2}{w_1^2} + \frac{\sigma_{t2}^2}{w_2^2} + \frac{1}{2k_a k_b w_a^2}\right)^{-1} \exp\left(-\frac{1}{8} w_a^2 |\Delta\mathbf{k}_{ab\perp}|^2\right)$$

$$\times \exp\left[-\frac{1}{2}\left(\sigma_{t1}^2 + \sigma_{t2}^2\right)\left(k_b - k_a\right)^2\right] \frac{1}{1 + i\beta_{pp}}$$

$$\times \exp\left\{-k_a k_b \left[\frac{w_1^2}{\sigma_{t1}^2} + \left(\frac{\sigma_{t2}^2}{w_2^2} + \frac{1}{2k_a k_b w_a^2}\right)^{-1}\right]^{-1} \frac{1 + i\beta_{pp}^{-1}}{1 + \beta_{pp}^2} |H_b \mathbf{s}_{ob\perp} - H_a \mathbf{s}_{oa\perp}|^2\right\}$$

$$\times \exp\left\{-\frac{1}{4k_a k_b} \left(\frac{\sigma_{t1}^2}{w_1^2} + \frac{\sigma_{t2}^2}{w_2^2} + \frac{1}{2k_a k_b w_a^2}\right)^{-1} \left[1 + \right.\right.$$

$$\left.\left. + \frac{\sigma_{t1}^2}{w_1^2} \left(\frac{\sigma_{t2}^2}{w_2^2} + \frac{1}{2k_a k_b w_a^2}\right)^{-1} \frac{\beta_{pp}}{1 + \beta_{pp}^2} \left(\beta_{pp} + i\right)\right] |\mathbf{k}_{ab\perp}|^2\right\}$$

$$\times \exp\left\{\left[1 + \frac{w_1^2}{\sigma_{t1}^2} \left(\frac{\sigma_{t2}^2}{w_2^2} + \frac{1}{2k_a k_b w_a^2}\right)\right]^{-1} \frac{\beta_{pp} + i}{1 + \beta_{pp}^2} \mathbf{k}_{ab\perp} \cdot \left(H_b \mathbf{s}_{ob\perp} - H_a \mathbf{s}_{oa\perp}\right)\right\}, \quad \text{(C3)}$$

where β_{pp} is a wavelength-spacing detuning parameter defined as

$$\beta_{pp} = 2\left(k_b H_a - k_a H_b\right)\left[\frac{w_1^2}{\sigma_{t1}^2} + \left(\frac{\sigma_{t2}^2}{w_2^2} + \frac{1}{2k_a k_b w_a^2}\right)^{-1}\right]^{-1}. \quad \text{(C4)}$$

We note that β_{pp} is zero when the condition in Eq. (3.45) is satisfied, i.e., when $k_b H_a = k_a H_b$. We point out that there is an inherent difference between the parameters $\Delta\mathbf{k}_{ab\perp}$, $k_b - k_a$, μ_{pp}, and $H_b \mathbf{s}_{ob\perp} - H_a \mathbf{s}_{oa\perp}$ and the parameter $\mathbf{k}_{ab\perp}$ that occur in Eq. (C3). The parameters in the first set all vanish when the states a and b are equal, but $\mathbf{k}_{ab\perp}$ can be non-zero. For example, when we calculate u_{aa} from Eq. (C3), most of the factors reduce

to unity, but we are left with a function of the offset between input and output wave vectors:

$$u_{aa}(\mathbf{k}_{a\perp}-\mathbf{k}_{oa\perp}) = <I_a(\mathbf{k}_{a\perp}-\mathbf{k}_{oa\perp})> = \frac{1}{4\pi}\cos^2\theta_a \left(\frac{\sigma_{t1}^2}{w_1^2} + \frac{\sigma_{t2}^2}{w_2^2} + \frac{1}{2k_a k_b w_a^2}\right)$$

$$\times \exp\left[-\frac{1}{4k_a^2}\left(\frac{\sigma_{t1}^2}{w_1^2} + \frac{\sigma_{t2}^2}{w_2^2} + \frac{1}{2k_a k_b w_a^2}\right)^{-1}|\mathbf{k}_{a\perp}-\mathbf{k}_{oa\perp}|^2\right]. \tag{C5}$$

Of course, $\mathbf{k}_{a\perp}\text{-}\mathbf{k}_{oa\perp}=\mathbf{k}_{ab\perp}$ by Eq. (3.29) since $\Delta\mathbf{k}_{ab\perp}=0$. When we write u_{aa} without an argument, we mean that the argument is $\mathbf{k}_{a\perp}\text{-}\mathbf{k}_{oa\perp}$ as given in Eq. (C5). When we write $u_{aa}(0)$, we mean that $\mathbf{k}_{a\perp}=\mathbf{k}_{oa\perp}$, i.e., that the observation point lies in the same direction as the input plane wave. As we will see below, there is an advantage to using $u_{aa}(0)$ and $u_{bb}(0)$ instead of u_{aa} and u_{bb} as the normalization factors.

We need to know $|u_{ab}|^2$ in order to obtain the two-state correlation of intensity from Eq. (4.7). In calculating $|u_{ab}|^2$ from Eq. (C3), the real components of the arguments of the exponentials double and the imaginary parts disappear since they are just phase factors. We begin by using the normalization factors u_{aa} and u_{bb}. The resulting expression for the normalized magnitude squared of u_{ab} is:

$$\frac{|u_{ab}|^2}{u_{aa}u_{bb}} = \left(\frac{\sigma_{t1}^2}{w_1^2} + \frac{\sigma_{t2}^2}{w_2^2} + \frac{1}{2w_a^2 k_a^2} \right)\left(\frac{\sigma_{t1}^2}{w_1^2} + \frac{\sigma_{t2}^2}{w_2^2} + \frac{1}{2w_a^2 k_b^2} \right)\left(\frac{\sigma_{t1}^2}{w_1^2} + \frac{\sigma_{t2}^2}{w_2^2} + \frac{1}{2k_a k_b w_a^2} \right)^{-2}$$

$$\times \exp\left(-\frac{1}{4} w_a^2 |\Delta \mathbf{k}_{ab\perp}|^2 \right) \exp\left[-\left(\sigma_{t1}^2 + \sigma_{t2}^2 \right)\left(k_b - k_a \right)^2 \right] \frac{1}{1 + \beta_{pp}^2}$$

$$\times \exp\left\{ -2k_a k_b \left| \frac{w_1^2}{\sigma_{t1}^2} + \left(\frac{\sigma_{t2}^2}{w_2^2} + \frac{1}{2k_a k_b w_a^2} \right)^{-1} \right|^{-1} \frac{1}{1 + \beta_{pp}^2} |H_b \mathbf{s}_{ob\perp} - H_a \mathbf{s}_{oa\perp}|^2 \right\},$$

$$\times \exp\left\{ -\frac{1}{2k_a k_b}\left(\frac{\sigma_{t1}^2}{w_1^2} + \frac{\sigma_{t2}^2}{w_2^2} + \frac{1}{2k_a k_b w_a^2} \right)^{-1} \left| 1 + \right.\right.$$

$$\left. + \frac{\sigma_{t1}^2}{w_1^2}\left(\frac{\sigma_{t2}^2}{w_2^2} + \frac{1}{2k_a k_b w_a^2} \right)^{-1} \frac{\beta_{pp}^2}{1 + \beta_{pp}^2} \right| |\mathbf{k}_{ab\perp}|^2 \right\}$$

$$\times \exp\left| \frac{1}{4k_a^2}\left(\frac{\sigma_{t1}^2}{w_1^2} + \frac{\sigma_{t2}^2}{w_2^2} + \frac{1}{2k_a^2 w_a^2} \right)^{-1} |\mathbf{k}_{ab\perp} + \frac{1}{2}\Delta \mathbf{k}_{ab\perp}|^2 \right|$$

$$\times \exp\left| \frac{1}{4k_b^2}\left(\frac{\sigma_{t1}^2}{w_1^2} + \frac{\sigma_{t2}^2}{w_2^2} + \frac{1}{2k_b^2 w_a^2} \right)^{-1} |\mathbf{k}_{ab\perp} - \frac{1}{2}\Delta \mathbf{k}_{ab\perp}|^2 \right|$$

$$\times \exp\left\{ 2 \left| 1 + \frac{w_1^2}{\sigma_{t1}^2}\left(\frac{\sigma_{t2}^2}{w_2^2} + \frac{1}{2k_a k_b w_a^2} \right) \right|^{-1} \frac{\beta_{pp}}{1 + \beta_{pp}^2} \mathbf{k}_{ab\perp} \bullet \left(H_b \mathbf{s}_{ob\perp} - H_a \mathbf{s}_{oa\perp} \right) \right\}. \tag{C6}$$

In Eq. (C6) we have used

$$\mathbf{k}_{a\perp} - \mathbf{k}_{oa\perp} = \mathbf{k}_{ab\perp} + \frac{1}{2}\Delta \mathbf{k}_{ab\perp} \tag{C7}$$

and

$$\mathbf{k}_{b\perp} - \mathbf{k}_{ob\perp} = \mathbf{k}_{ab\perp} - \frac{1}{2}\Delta \mathbf{k}_{ab\perp} \tag{C8}$$

to express the normalization exponentials in terms of $\Delta \mathbf{k}_{ab\perp}$ and $\mathbf{k}_{ab\perp}$.

We have left the width w_a of the Gaussian aperture arbitrary in order to see how it enters into the equations. It is evident from Eqs. (C3) and (C4) that the aperture can be accounted for implicitly within the rms slope parameter σ_t/w_2 of diffuser D_2 by not

writing the w_a dependence and letting

$$\frac{\sigma_{t2}^2}{w_2^2} \to \frac{\sigma_{t2}^2}{w_2^2} + \frac{1}{2k_a k_b w_a^2} . \tag{C9}$$

In most practical applications, the aperture contains many diffuser correlation cells so that the condition

$$2k_a k_b w_a^2 >> \frac{w_2^2}{\sigma_{t2}^2} \tag{C10}$$

is satisfied. Then the first two factors in Eq. (C6) cancel with the third factor and the w_a dependence within the exponentials in Eq. (C6) and within the definition of β_{pp} can be dropped. The resulting expression corresponding to Eq. (C6) is:

$$\frac{|u_{ab}|^2}{u_{aa} u_{bb}} = \exp\left(-\frac{1}{4} w_a^2 |\Delta \mathbf{k}_{ab\perp}|^2 \right) \exp\left[-\left(\sigma_{t1}^2 + \sigma_{t2}^2 \right)\left(k_b - k_a \right)^2 \right] \frac{1}{1 + \beta_{pp}^2}$$

$$\times \exp\left[-2k_a k_b \left(\frac{w_1^2}{\sigma_{t1}^2} + \frac{w_2^2}{\sigma_{t2}^2} \right)^{-1} \frac{1}{1 + \beta_{pp}^2} |H_b \mathbf{s}_{ob\perp} - H_a \mathbf{s}_{oa\perp}|^2 \right]$$

$$\times \exp\left[-\frac{1}{2k_a k_b} \left(\frac{\sigma_{t1}^2}{w_1^2} + \frac{\sigma_{t2}^2}{w_2^2} \right)^{-1} \left(1 + \frac{\sigma_{t1}^2}{w_1^2} \frac{w_2^2}{\sigma_{t2}^2} \frac{\beta_{pp}^2}{1 + \beta_{pp}^2} \right) |\mathbf{k}_{ab\perp}|^2 \right]$$

$$\times \exp\left[\frac{1}{4} \left(\frac{\sigma_{t1}^2}{w_1^2} + \frac{\sigma_{t2}^2}{w_2^2} \right)^{-1} \left(\frac{1}{k_a^2} |\mathbf{k}_{ab\perp} + \Delta \mathbf{k}_{ab\perp}|^2 + \frac{1}{k_b^2} |\mathbf{k}_{ab\perp} - \Delta \mathbf{k}_{ab\perp}|^2 \right) \right]$$

$$\times \exp\left[2 \left(1 + \frac{w_1^2}{\sigma_{t1}^2} \frac{\sigma_{t2}^2}{w_2^2} \right)^{-1} \frac{\beta_{pp}}{1 + \beta_{pp}^2} \mathbf{k}_{ab\perp} \bullet \left(H_b \mathbf{s}_{ob\perp} - H_a \mathbf{s}_{oa\perp} \right) \right] . \tag{C11}$$

We show why the normalization $u_{aa}(0) u_{bb}(0)$ is preferred to $u_{aa} u_{bb}$ by evaluating Eq. (C11) for the limiting values of the arguments $\Delta \mathbf{k}_{ab\perp} = 0$, $\beta_{pp} = 0$, and $\mathbf{s}_{oa\perp} = \mathbf{s}_{ob\perp}$:

$$\frac{|u_{ab}|^2}{u_{aa}u_{bb}} = \exp\left[-\left(\sigma_{t1}^2+\sigma_{t2}^2\right)\left(k_b-k_a\right)^2\right]$$

$$\times \exp\left[\frac{1}{4}\left(\frac{\sigma_{t1}^2}{w_1^2}+\frac{\sigma_{t2}^2}{w_2^2}\right)^{-1}\frac{\left(k_b-k_a\right)^2}{k_a^2 k_b^2}|\mathbf{k}_{ab\perp}|^2\right]. \tag{C12}$$

Since we have assumed that S_1 and S_2 are much larger than one, the first exponential will have damped to a small value unless $(k_b-k_a)/k_a$ is small compared with unity. However, the argument of the second exponential is positive and there is no restriction on how small the slope parameters σ_{t_1}/w_1 and σ_{t_2}/w_2 can be; Therefore, this exponential will increase as k_b-k_a increases and it can dominate the first exponential so that the product increases as a function of of the wavelength offset k_b-k_a. The reason that Eq. (C12) increases about the origin is that we are dividing by normalization factors that fall off rapidly as $|\mathbf{k}_{ab\perp}|$ increases. Since we would like our normalized $|u_{ab}|^2$ to behave like an autocorrelation function, i.e., drop as k_b-k_a increases, we will use $u_{aa}(0)$ and $u_{bb}(0)$ as the normalization factors. The corresponding form of Eq. (3.75) is

$$\frac{<I_a I_b>}{<I_a(0)><I_b(0)>} = \frac{u_{aa}u_{bb}}{u_{aa}(0)u_{bb}(0)} + \frac{|u_{ab}|^2}{u_{aa}(0)u_{bb}(0)}. \tag{C13}$$

For the *P-P* diffuser combination, Eq. (C13) takes the form

$$\frac{<I_a I_b>}{<I_a(0)><I_b(0)>} =$$

$$\exp\left[-\frac{1}{4}\left(\frac{\sigma_{t1}^2}{w_1^2}+\frac{\sigma_{t2}^2}{w_2^2}\right)^{-1}\left(\frac{1}{k_a^2}|\mathbf{k}_{ab\perp}+\Delta\mathbf{k}_{ab\perp}|^2+\frac{1}{k_b^2}|\mathbf{k}_{ab\perp}-\Delta\mathbf{k}_{ab\perp}|^2\right)\right]$$

$$+\exp\left(-\frac{1}{4}w_a^2|\Delta\mathbf{k}_{ab\perp}|^2\right)\exp\left[-\left(\sigma_{t1}^2+\sigma_{t2}^2\right)\left(k_b-k_a\right)^2\right]\frac{1}{1+\beta_{pp}^2}$$

$$\times\exp\left[-2k_a k_b\left(\frac{w_1^2}{\sigma_{t1}^2}+\frac{w_2^2}{\sigma_{t2}^2}\right)^{-1}\frac{1}{1+\beta_{pp}^2}\,|H_b\mathbf{s}_{ob\perp}-H_a\mathbf{s}_{oa\perp}|^2\right]$$

$$\times\exp\left[-\frac{1}{2k_a k_b}\left(\frac{\sigma_{t1}^2}{w_1^2}+\frac{\sigma_{t2}^2}{w_2^2}\right)^{-1}\left(1+\frac{\sigma_{t1}^2}{w_1^2}\frac{w_2^2}{\sigma_{t2}^2}\frac{\beta_{pp}^2}{1+\beta_{pp}^2}\right)|\mathbf{k}_{ab\perp}|^2\right]$$

$$\times\exp\left[2\left(1+\frac{w_1^2}{\sigma_{t1}^2}\frac{\sigma_{t2}^2}{w_2^2}\right)^{-1}\frac{\beta_{pp}}{1+\beta_{pp}^2}\,\mathbf{k}_{ab\perp}\bullet\left(H_b\mathbf{s}_{ob\perp}-H_a\mathbf{s}_{oa\perp}\right)\right]. \tag{C14}$$

Appendix C Reference

1.   I. S. Gradshteyn and I. M. Ryzhik, *Table of Integrals, Series, and Products*, (Academic Press, New York, 1980), p. 338.

Appendix D

Circular Symmetry and Two-State Correlation Functions

With the exception of certain special cases, the general expression for u_{ab}, the two-state correlation function of the far-zone complex amplitude from a cascade of two diffusers is very difficult to evaluate analytically. In this appendix we derive the reduced form of Eq. (3.47) for u_{ab} that results for wavelength and spacing dependence by assuming normal incidence, on-axis observation, and that the correlation functions R_{t_1} and R_{t_2}, along with the aperture ambiguity function $\hat{A}$, are circularly symmetric, i.e., that they depend on $\mathbf{r}$ only through its magnitude $|\mathbf{r}|$. Appendix D is used in the calculation of u_{ab} for the P-C and C-P diffuser combinations in Appendix E. For convenience, we repeat Eq. (3.47) here:

$$u_{ab} = -i \frac{k_a^2 k_b^2}{(2\pi)^3} \frac{\exp(-i\phi_{ab})}{k_b H_a - k_a H_b} \exp\left(\frac{i}{2} \frac{H_a H_b}{k_b H_a - k_a H_b} |\mathbf{k}_{ob\perp} - \mathbf{k}_{oa\perp}|^2 \right) \cos\theta_a \cos\theta_b$$

$$\times \int F(\mathbf{r}; k_a, k_b; \mathbf{k}_{ab\perp}; \Delta\mathbf{k}_{ab\perp}) \exp\left\{ i \frac{k_a k_b}{k_b H_a - k_a H_b} \left[\frac{1}{2} |\mathbf{r}|^2 + \left(H_b \mathbf{s}_{ob\perp} - H_a \mathbf{s}_{oa\perp} \right) \bullet \mathbf{r} \right] \right\} d^2\mathbf{r}, \tag{D1}$$

The above assumptions imply that $\mathbf{k}_{ab\perp} = \Delta\mathbf{k}_{ab\perp} = 0$, and that $F(\mathbf{r}; k_a, k_b; 0; 0)$ is also circularly symmetric. If we convert the $\mathbf{r}$ integral to the polar coordinates r and θ, then we can evaluate the θ integration immediately. The resulting expression for u_{ab} is

$$u_{ab} = -i \left(\frac{k_a k_b}{2\pi} \right)^2 \frac{\exp(-i\phi_{ab})}{k_b H_a - k_a H_b}$$

$$\times \int_0^\infty r F(\mathbf{r}; k_a, k_b; 0; 0) \exp\left(\frac{i}{2} \frac{k_a k_b}{k_b H_a - k_a H_b} r^2 \right) dr. \tag{D2}$$

Equation (D2) is only useful as long as we can evaluate the functional form of F.

181
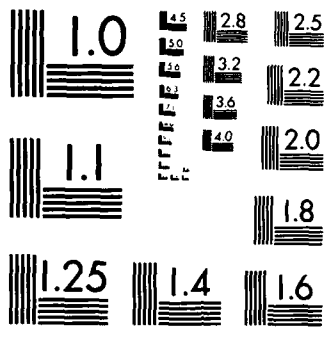
MICROCOPY RESOLUTION TEST CHART

NATIONAL BUREAU OF STANDARDS-1963-A

In some instances, we can not evaluate F directly, however, it may still be possible to find a closed form solution for u_{ab}. Given the same assumptions used to arrive at Eq. (D2), we can alternatively write Eq. (D1) as

$$u_{ab} = -i \frac{k_a^2 k_b^2}{(2\pi)^3} \frac{\exp(-i\phi_{ab})}{k_b H_a - k_a H_b} \int \int R_{t_1}(\mathbf{r}; k_a, k_b) \, R_{t_2}(\mathbf{r}'; k_a, k_b) \, \tilde{A}(\mathbf{r}'; 0)$$

$$\times \exp\left(\frac{i}{2} \frac{k_a k_b}{k_b H_a - k_a H_b} |\mathbf{r} - \mathbf{r}'|^2 \right) d^2\mathbf{r} \, d^2\mathbf{r}' . \tag{D3}$$

By converting both the $\mathbf{r}$ and the $\mathbf{r}'$ integrals to polar coordinates and evaluating the θ and θ' integrals using

$$\int_0^{2\pi} \int_0^{2\pi} \exp\left[-iC \cos(\theta - \theta') \right] d\theta \, d\theta' = (2\pi)^2 J_0(C) , \tag{D4}$$

we obtain the solution

$$u_{ab} = -i \frac{k_a^2 k_b^2}{2\pi} \frac{\exp(-i\phi_{ab})}{k_b H_a - k_a H_b} \int_0^\infty \int_0^\infty r r' J_0\left(\frac{k_a k_b}{k_b H_a - k_a H_b} r r' \right) R_{t_1}(\mathbf{r}; k_a, k_b)$$

$$\times R_{t_2}(\mathbf{r}'; k_a, k_b) \, \tilde{A}(\mathbf{r}'; 0) \exp\left[\frac{i}{2} \frac{k_a k_b}{k_b H_a - k_a H_b} \left(r^2 + r'^2 \right) \right] dr \, dr' . \tag{D5}$$

Since the number of integrations has been reduced from four to two, Eq. (D5) is useful for numerical or analytical evaluation of u_{ab} for circular symmetry.

Appendix E

Mixed Diffuser Combination: Paraboloidal and Conical

In Appendix E we calculate the wavelength and spacing dependence of the two-state correlation of intensity, Eq. (4.7), for the P-C and C-P combinations of strong diffusers. The letters P and C stand for paraboloidal and conical and represent the autocorrelation functions R_t given by Eqs. (4.8) and (4.9), respectively. The first letter of the pair corresponds to R_{t_1} and the second letter to R_{t_2}. In this appendix the output aperture is a Gaussian of arbitrary width w_a. Hence the aperture ambiguity function is given by Eq. (4.10).

E.1 Paraboloidal-Conical

We calculate u_{ab} for the P-C diffuser combination directly from the equation that results from substituting Eq. (4.8) for R_{t_1}, Eq. (4.9) for R_{t_2}, and Eq. (4.10) for $\tilde{A}$ into Eq. (D5):

$$u_{ab} = -i\,\frac{k_a^2 k_b^2}{2\pi}\,\frac{\exp\left(-i\phi_{ab}\right)}{k_b H_a - k_a H_b}\exp\left[-\frac{1}{2}\left(\sigma_{t1}^2 + \sigma_{t2}^2\right)\left(k_b - k_a\right)^2\right]$$

$$\times \int_0^\infty \int_0^\infty r\,r'\,J_0\!\left(\frac{k_a k_b}{k_b H_a - k_a H_b}\,r\,r'\right)\exp\left|-k_a k_b\left(\sigma_{t1}^2\frac{|\mathbf{r}|^2}{w_1^2} + \sigma_{t2}^2\frac{|\mathbf{r}|}{w_2}\right)\right|$$

$$\times \exp\left(-\frac{|\mathbf{r'}|^2}{2w_a^2}\right)\exp\left[\frac{i}{2}\,\frac{k_a k_b}{k_b H_a - k_a H_b}\left(r^2 + r'^2\right)\right]\,dr\,dr'. \tag{E1}$$

Since the r integral in Eq. (E1) is $(2\pi)^{-1}$ times the Fourier-Bessel transform of a complex Gaussian, Eq. (D1) can be used to evaluate the equivalent two-dimensional Fourier transform:

$$u_{ab} = \frac{k_a k_b}{2\pi} \exp\left(-i\phi_{ab}\right) \left[1 + i2\left(k_b H_a - k_a H_b\right) \frac{\sigma_{t1}^2}{w_1^2}\right]^{-1} \exp\left[-\frac{1}{2}\left(\sigma_{t1}^2 + \sigma_{t2}^2\right)\left(k_b - k_a\right)^2\right]$$

$$\times \int_0^\infty r \exp\left(-k_a k_b \sigma_{t2}^2 \frac{r}{w_2}\right) \exp\left\{-\left[\frac{k_a k_b \sigma_{t1}^2/w_1^2}{1 + i2\left(k_b H_a - k_a H_b\right)\sigma_{t1}^2/w_1^2} + \frac{1}{2w_a^2}\right]r^2\right\} dr . \tag{E2}$$

The remaining integral in Eq. (E2) can be evaluated using[1]

$$\int_0^\infty r \exp\left[-\left(ar^2 + br\right)\right] dr = \frac{1}{2a} D\left(\frac{b}{2\sqrt{a}}\right). \tag{E3}$$

In Eq. (E3) we have introduced the decorrelation function

$$D\left(z\right) = 1 - \sqrt{\pi}\, z \exp\left(z^2\right) \mathrm{erfc}\left(z\right). \tag{E4}$$

Methods for evaluating the complimentary error function of a complex argument are given in the literature[2-5]. Upon evaluating the integral in Eq. (E2), we obtain the final form of u_{ab}:

$$u_{ab} = \frac{1}{4\pi} \exp\left(-i\phi_{ab}\right) \left[\frac{1}{2w_a^2 k_a k_b} + \frac{\sigma_{t1}^2}{w_1^2}\left(1 + i\frac{k_b H_a - k_a H_b}{w_a^2 k_a k_b}\right)\right]^{-1}$$

$$\times \exp\left[-\frac{1}{2}\left(\sigma_{t1}^2 + \sigma_{t2}^2\right)\left(k_b - k_a\right)^2\right] D\left(\gamma_{pc}\sqrt{k_a k_b}\sqrt{1 + i\beta_{pc}}\right), \tag{E5}$$

where

$$\beta_{pc} = 2\left(k_b H_a - k_a H_b\right)\frac{\sigma_{t1}^2}{w_1^2}\xi_{pc} \tag{E6}$$

is the spacing-wavelength detuning parameter,

$$\gamma_{pc} = \frac{w_1}{\sigma_{t1}}\frac{\sigma_{t2}^2}{\sqrt{2}\,w_2}\left[\frac{\xi_{pc}^2 + \beta_{pc}^2}{\xi_{pc}\left(1 + \beta_{pc}^2\right)}\right]^{\frac{1}{2}} \tag{E7}$$

is the effective ratio of diffuser shape parameters, and

$$\xi_{pc} = \left[1 + \frac{1 + 4\left(k_b H_a - k_a H_b\right)^2 \sigma_{t1}^2/w_1^2}{2w_a^2 k_a k_b \sigma_{t1}/w_1}\right]^{-1} \tag{E8}$$

is the output aperture discombobulation factor. The expression for the normalized square of the magnitude of u_{ab} is

$$\frac{|u_{ab}|^2}{u_{aa}u_{bb}} = \left(\frac{1}{2w_a^2 k_a^2} + \frac{\sigma_{t1}^2}{w_1^2}\right)\left(\frac{1}{2w_a^2 k_b^2} + \frac{\sigma_{t1}^2}{w_1^2}\right)$$

$$\times \left[\left(\frac{1}{2w_a^2 k_a k_b} + \frac{\sigma_{t1}^2}{w_1^2}\right)^2 + \left(\frac{k_b H_a - k_a H_b}{w_a^2 k_a k_b}\right)^2 \frac{\sigma_{t1}^4}{w_1^4}\right]^{-1}$$

$$\times \exp\left[-\left(\sigma_{t1}^2 + \sigma_{t2}^2\right)\left(k_b - k_a\right)^2\right] \frac{|D\left(\gamma_{pc}\sqrt{k_a k_b}\sqrt{1 + i\beta_{pc}}\right)|^2}{D\left(\gamma_{pc} k_a\right) D\left(\gamma_{pc} k_b\right)}. \qquad (E9)$$

For large apertures, we can use Eq. (3.75) to express the two-state correlation function of intensity in terms of the normalized square of the magnitude of u_{ab} given in Eq. (E9). Equations (E5) through (E9) also simplify for large apertures, e.g., ξ_{pc} approaches unity so that the expression within the square-root in Eq. (E7) reduces to unity, and the product of the first three factors in Eq. (E9) approaches unity. The resulting expression for the wavelength and spacing dependence of the normalized two-state correlation function of far-zone intensity for the P-C diffuser combination is

$$\frac{<I_a I_b>}{<I_a><I_b>} = 1 + \exp\left[-\left(\sigma_{t1}^2 + \sigma_{t2}^2\right)\left(k_b - k_a\right)^2\right] \frac{|D\left(\gamma_{pc}\sqrt{k_a k_b}\sqrt{1 + i\beta_{pc}}\right)|^2}{D\left(\gamma_{pc} k_a\right) D\left(\gamma_{pc} k_b\right)}, \qquad (E10)$$

where

$$\beta_{pc} = 2\left(k_b H_a - k_a H_b\right)\frac{\sigma_{t1}^2}{w_1^2}, \qquad (E11)$$

and

$$\gamma_{pc} = \frac{w_1}{\sigma_{t1}}\frac{\sigma_{t2}^2}{\sqrt{2}\,w_2}. \qquad (E12)$$

F.2 Conical-Paraboloidal

We can also calculate u_{ab} for the C-P diffuser combination directly from Eq. (D5).

In this case R_{t_1} and R_{t_2} are of the form of Eqs. (4.9) and (4.8) respectively:

$$u_{ab} = -i \frac{k_a^2 k_b^2}{2\pi} \frac{\exp(-i\phi_{ab})}{k_b H_a - k_a H_b} \exp\left[-\frac{1}{2}\left(\sigma_{t1}^2 + \sigma_{t2}^2 \right)\left(k_b - k_a \right)^2 \right]$$

$$\times \int_0^\infty \int_0^\infty r r' J_0\left(\frac{k_a k_b}{k_b H_a - k_a H_b} r r' \right) \exp\left[-k_a k_b \left(\sigma_{t1}^2 \frac{|\mathbf{r}|}{w_1} + \sigma_{t2}^2 \frac{|\mathbf{r}'|^2}{w_2^2} \right) \right]$$

$$\times \exp\left(-\frac{|\mathbf{r}'|^2}{2w_a^2} \right) \exp\left[\frac{i}{2} \frac{k_a k_b}{k_b H_a - k_a H_b} \left(r^2 + r'^2 \right) \right] dr \, dr' . \tag{E13}$$

This time we evaluate the dr' integral first:

$$u_{ab} = -i \frac{k_a k_b}{4\pi} \frac{\exp(-i\phi_{ab})}{k_b H_a - k_a H_b} \left[\frac{\sigma_{t2}^2}{w_2^2} + \frac{1}{2w_a^2 k_a k_b} - \frac{i}{2}\left(k_b H_a - k_a H_b \right)^{-1} \right]^{-1}$$

$$\times \exp\left[-\frac{1}{2}\left(\sigma_{t1}^2 + \sigma_{t2}^2 \right)\left(k_b - k_a \right)^2 \right] \int_0^\infty r \exp\left(-k_a k_b \sigma_{t1}^2 \frac{r}{w_1} \right)$$

$$\times \exp\left\{ -k_a k_b \left[\left(\frac{\sigma_{t2}^2}{w_2^2} + \frac{1}{2w_a^2 k_a k_b} \right)^{-1} + i\, 2\left(k_b H_a - k_a H_b \right) \right]^{-1} r^2 \right\} dr . \tag{E14}$$

Once again, Eq. (E3) is used to evaluate the remaining integral:

$$u_{ab} = \frac{1}{4\pi} \exp(-i\phi_{ab}) \left(\frac{\sigma_{t2}^2}{w_2^2} + \frac{1}{2w_a^2 k_a k_b} \right)^{-1}$$

$$\times \exp\left[-\frac{1}{2}\left(\sigma_{t1}^2 + \sigma_{t2}^2 \right)\left(k_b - k_a \right)^2 \right] D\left(\gamma_{cp} \sqrt{k_a k_b} \sqrt{1 + i\beta_{cp}} \right), \tag{E15}$$

where the offset parameter is now

$$\beta_{cp} = 2\left(k_b H_a - k_a H_b \right)\left(\frac{\sigma_{t2}^2}{w_2^2} + \frac{1}{2w_a^2 k_a k_b} \right), \tag{E16}$$

and the effective ratio of diffuser shape parameters is

$$\gamma_{cp} = \frac{\sigma_{t1}^2}{\sqrt{2}\,w_1} \left(\frac{\sigma_{t2}^2}{w_2^2} + \frac{1}{2w_a^2 k_a k_b}\right)^{-\frac{1}{4}}. \qquad (E17)$$

The normalized square of the magnitude of u_{ab} is now

$$\frac{|u_{ab}|^2}{u_{aa}u_{bb}} = \left(\frac{\sigma_{t2}^2}{w_2^2} + \frac{1}{2w_a^2 k_a^2}\right)\left(\frac{\sigma_{t2}^2}{w_2^2} + \frac{1}{2w_a^2 k_b^2}\right)\left(\frac{\sigma_{t2}^2}{w_2^2} + \frac{1}{2w_a^2 k_a k_b}\right)^{-2}$$

$$\times \exp\left[-\left(\sigma_{t1}^2 + \sigma_{t2}^2\right)\left(k_b - k_a\right)^2\right] \frac{|D\left(\gamma_{cp}\sqrt{k_a k_b}\,\sqrt{1+i\beta_{cp}}\right)|^2}{D\left(\gamma_{cp}k_a\right)D\left(\gamma_{cp}k_b\right)}. \qquad (E18)$$

In practical applications the condition

$$2w_a^2 k_a k_b >> \frac{w_2^2}{\sigma_{t2}^2} \qquad (E19)$$

is usually satisfied, i.e., the aperture is large compared to the effective diffuser correlation length, so that Eq. (E18) simplifies, and Eq. (3.75) applies. The resulting form for the wavelength and spacing dependence of the normalized two-state correlation function of far-zone intensity for the C-P diffuser combination is identical to Eq. (E10), except that the detuning parameter β and the ratio parameter γ are redefined to account for the switch in the order of the diffusers:

$$\frac{<I_a I_b>}{<I_a><I_b>} = 1 + \exp\left[-\left(\sigma_{t1}^2 + \sigma_{t2}^2\right)\left(k_b - k_a\right)^2\right] \frac{|D\left(\gamma_{cp}\sqrt{k_a k_b}\,\sqrt{1+i\beta_{cp}}\right)|^2}{D\left(\gamma_{cp}k_a\right)D\left(\gamma_{cp}k_b\right)}, \qquad (E20)$$

where

$$\beta_{cp} = 2\left(k_b H_a - k_a H_b\right)\frac{\sigma_{t2}^2}{w_2^2}, \qquad (E21)$$

and

$$\gamma_{cp} = \frac{\sigma_{t1}^2}{\sqrt{2}\,w_1}\frac{w_2}{\sigma_{t1}}. \qquad (E22)$$

Appendix E References

1. I. S. Gradshteyn and I. M. Ryzhik, *Table of Integrals, Series, and Products,* (Academic Press, New York, 1980), p. 337.

2. H. E. Salzer, " Formulas for calculating the error function of a complex variable," Math. Tables Aids Comp. **5**, 67-70 (1951).

3. W. Gautschi, "Complex error function," Commun. ACM **12**, 635 (1969).

4. W. Gautschi, " Efficient computation of the complex error function," SIAM J. Numer. Anal. **7**, 187-198 (1970).

5. M. Abramowitz and I. A. Stegun, *Handbook of Mathematical Functions,* (Dover, New York, 1965), p. 299.

Appendix F

Conical-Conical Diffuser Combination

In Appendix F we evaluate the two-state correlation function of intensity given in Eq. (4.7) for the C-C combination of strong diffusers. This is the most difficult of the four diffuser combinations, P-P, P-C, C-P, and C-C, to analyze. By assuming that the input and observation angles are equal, i.e., $\mathbf{k}_{ab\perp} = 0$, that the speckle tracking condition is satisfied, i.e., $\Delta\mathbf{k}_{ab\perp} = 0$, and that the aperture function a is wide spatially compared to R_{t_2}, so that $\hat{A}(\mathbf{r};0)$ can be replaced by $\hat{A}(0;0) = 1$, we can evaluate the double-diffuser descriptor function $F(\mathbf{r};k_a,k_b;0;0)$ defined in Eq. (4.4). In Section F.1 we evaluate F by assuming that the diffusers have equal shape parameters, i.e., that $w_1/\sigma_{t_1}{}^2 = w_2/\sigma_{t_2}{}^2$. Given F we then find closed form solutions for the angular dependence and for the spacing-wavelength dependence of u_{ab}. In Section F.2 we give the functional form of F for arbitrary shape parameters. This allows us to write the angular dependence of u_{ab} immediately, and to reduce to one, the number of integrations necessary in evaluating the spacing-wavelength dependence of u_{ab}.

F.1 Equal Shape Parameters

Since R_{t_1} and R_{t_2} are circularly symmetric, and the aperture ambiguity function $\hat{A}$ has been removed, we can write F as the convolution of R_{t_1} and R_{t_2}:

$$F(\mathbf{r};k_a,k_b;0;0) = \int R_{t_1}(\mathbf{r}';k_a,k_b)\, R_{t_2}(\mathbf{r}-\mathbf{r}';k_a,k_b)\, d^2r' . \tag{F1}$$

Then by the convolution theorem, F is the inverse Fourier transform of the product of the Fourier transforms of R_{t_1} and R_{t_2}. The two-dimensional Fourier transform of a decaying circularly symmetric exponential of width w is the Fourier-Bessel transform[1]

$$2\pi \int_0^\infty r\, J_0(kr)\exp\left(-\frac{r}{w}\right) dr = 2\pi w^2 \left| 1 + \left(2\pi k w\right)^2 \right|^{-3/2} . \tag{F2}$$

Since R_{t_1} and R_{t_2} are identical functions, the product of the Fourier transforms is the square of Eq. (F2). The inverse Fourier transform of this product is the Fourier-Bessel transform[2]

$$2\pi \int_0^\infty x\, J_0\!\left(cx\right)\left(1+x^2\right)^{-3} dx = 2\pi\, \frac{c^2}{8}\, K_2(c).$$ (F3)

Hence

$$F(\mathbf{r};k_a,k_b;0;0) = \frac{\pi}{4}\exp\!\left[-\frac{1}{2}\left(\sigma_{t1}^2+\sigma_{t2}^2\right)\left(k_b-k_a\right)^2\right] r^2\, K_2\!\left(k_a k_b \sigma_t^2 \frac{r}{w}\right).$$ (F4)

In Eqs. (F3) and (F4), K_2 is the modified Bessel function of the second kind of order two. For small arguments

$$K_2(z) \sim 2\, z^{-2},$$ (F5)

so that

$$F(0;k,k;0,0) = \frac{\pi}{2}\, \frac{w^2}{k^4 \sigma_t^4}.$$ (F6)

We calculate the angular dependence of the two-state correlation function of intensity by substituting Eq. (F4) for F into Eq. (4.6) for u_{ab} and then substituting the resulting expression for u_{ab} into Eq. (4.7):

$$\frac{\langle I_a I_b\rangle}{\langle I_a\rangle\langle I_b\rangle} = 1 + \frac{\zeta_c^4}{4}\, K_2^2\!\left(\zeta_c\right).$$ (F7)

The angular detuning variable ζ_c in Eq. (F7) is defined as

$$\zeta_c = k_a^2 \sigma_t^2\, \frac{H}{w}\, \left|\mathbf{s}_{oa\perp}-\mathbf{s}_{ob\perp}\right|.$$ (F8)

The arguments on the intensity normalization factors in the denominator in Eq. (4.7) have been dropped in going from Eq. (4.7) to Eq. (F7) since we have already assumed that $\mathbf{k}_{ab\perp}=0$.

We calculate the spacing-wavelength dependence of u_{ab} by substituting Eq. (F4) for F into Eq. (4.1), setting $\mathbf{s}_{oa\perp}=\mathbf{s}_{ob\perp}=0$, and using the identity[3]

$$\int_0^\infty x^3 \exp\!\left(-ax^2\right) K_2\!\left(bx\right) dx = \frac{1}{a^2 b}\left[1-\frac{b^2}{4a}-\left(\frac{b^2}{4a}\right)^2\exp\!\left(\frac{b^2}{4a}\right)\mathrm{Ei}\!\left(-\frac{b^2}{4a}\right)\right],$$ (F9)

where $\text{Re}(a) > 0$, to evaluate the integral. The resulting expression for u_{ab} is

$$u_{ab} = \frac{1}{8\pi} \frac{w^2}{k_a k_b \sigma_t^4} \exp\left(-i\phi_{ab}\right) \exp\left[-\frac{1}{2}\left(\sigma_{t1}^2 + \sigma_{t2}^2\right)\left(k_b - k_a\right)^2\right]$$

$$\times \left[1 - i\beta_c + \beta_c^2 \exp(i\beta_c)\,\text{Ei}(-i\beta_c)\right]. \tag{F10}$$

The single subscript on the spacing-wavelength detuning parameter,

$$\beta_c = \left(k_b H_a - k_a H_b\right) \frac{k_a k_b \sigma_t^4}{2w^2}, \tag{F11}$$

indicates that R_{t_1} and R_{t_2} are identical functions. Finally, the two-state correlation function of intensity, obtained by substituting Eq. (F10) for u_{ab} into Eq. (4.7) and writing the complex exponential in terms of a sine and a cosine and the exponential integral Ei in terms of a sine integral si and a cosine integral ci, is

$$\frac{<I_a I_b>}{<I_a><I_b>} = 1 + \exp\left[-\left(\sigma_{t1}^2 + \sigma_{t2}^2\right)\left(k_b - k_a\right)^2\right]$$

$$\times \left\{ \left[1 + \beta_c^2\left(\cos\beta_c\,\text{ci}\beta_c + \sin\beta_c\,\text{si}\beta_c\right)\right]^2 + \beta_c^2\left[1 + \beta_c\left(\cos\beta_c\,\text{si}\beta_c - \sin\beta_c\,\text{ci}\beta_c\right)\right]^2 \right\}. \tag{F12}$$

F.2 Arbitrary Shape Parameters

When the shape parameters $w_1/\sigma_{t_1}^2$ and $w_2/\sigma_{t_2}^2$ are arbitrary, it can be shown that

$$F(\mathbf{r};k_a,k_b;0,0) = \frac{\pi}{4}\exp\left[-\frac{1}{2}\left(\sigma_{t1}^2 + \sigma_{t2}^2\right)\left(k_b - k_a\right)^2\right]$$

$$\times r^2 \left[I_0\left(\frac{r}{w_-}\right) K_2\left(\frac{r}{w_+}\right) - I_2\left(\frac{r}{w_-}\right) K_0\left(\frac{r}{w_+}\right)\right], \tag{F13}$$

where

$$\frac{1}{w_+} = \frac{k_a k_b}{2}\left(\frac{\sigma_{t1}^2}{w_1} + \frac{\sigma_{t2}^2}{w_2}\right), \tag{F14}$$

and

$$\frac{1}{w_-} = \frac{k_a k_b}{2} \left| \frac{o_{t1}^2}{w_1} - \frac{o_{t2}^2}{w_2} \right|. \tag{F15}$$

We note that $1/w_-$ is zero when the shape parameters are equal; thus Eq. (F13) reduces to Eq. (F4). We also note that

$$F(0;k,k;0;0) = \frac{n}{2} w_+^2, \tag{F16}$$

which reduces to Eq. (F6) for equal shape parameters.

Given Eq. (F13) for F, we can now generalize Eq. (F7) for the angular dependence of the two-state correlation function of intensity to arbitrary shape parameters:

$$\frac{\langle I_a I_b \rangle}{\langle I_a \rangle \langle I_b \rangle} = 1 + \frac{\zeta_{cc}^4}{4} \left| I_0 \left(\gamma_{cc} \zeta_{cc} \right) K_2 \left(\zeta_{cc} \right) - I_2 \left(\gamma_{cc} \zeta_{cc} \right) K_0 \left(\zeta_{cc} \right) \right|^2. \tag{F17}$$

In Eq. (F17) we have also generalized the angular detuning parameter ζ for equal shape parameters to

$$\zeta_{cc} = \frac{H}{w_+} |\mathbf{s}_{oa\perp} - \mathbf{s}_{ob\perp}| \tag{F18}$$

for arbitrary shape parameters, and we have introduced the ratio parameter

$$\gamma_{cc} = \frac{w_+}{w_-}. \tag{F19}$$

We note that γ_{cc} is zero when $w_1/o_{t_1}^2 = w_2/o_{t_2}^2$, and that it approaches unity when $w_1/o_{t_1}^2 >> w_2/o_{t_2}^2$ or when $w_1/o_{t_1}^2 << w_2/o_{t_2}^2$.

By substituting Eq. (F13) for F into Eq. (4.1) and setting $\mathbf{s}_{oa\perp} = \mathbf{s}_{ob\perp} = 0$, we obtain the spacing-wavelength dependence of u_{ab}:

$$u_{ab} = -i \frac{k_a k_b w_+^2}{8n} \exp\left(-i\phi_{ab} \right) \exp\left[-\frac{1}{2} \left(o_{t1}^2 + o_{t2}^2 \right) \left(k_b - k_a \right)^2 \right] G\left(\beta_{cc}, \gamma_{cc} \right), \tag{F20}$$

where the spacing-wavelength decorrelation function G is defined as

$$G\left(\beta_{cc}, \gamma_{cc} \right) = \frac{1}{4\beta_{cc}} \int_0^\infty x^3 \left[I_0 \left(\gamma_{cc} x \right) K_2(x) - I_2 \left(\gamma_{cc} x \right) K_0(x) \right] \exp\left(i \frac{x^2}{4\beta_{cc}} \right) dx, \tag{F21}$$

and the spacing-wavelength detuning parameter β_{cc} is

$$\beta_{cc} = \frac{k_b H_a - k_a H_b}{2 w_+^2 k_a k_b}. \tag{F22}$$

When β_{cc} is zero,

$$G\left(0, \gamma_{cc}\right) = i.$$
(F23)

Hence the normalized two-state correlation function of intensity is

$$\frac{<I_a I_b>}{<I_a><I_b>} = 1 + \exp\left[-\left(\sigma_{t1}^2 + \sigma_{t2}^2\right)\left(k_b - k_a\right)^2\right] |G\left(\beta_{cc}, \gamma_{cc}\right)|^2.$$
(F24)

In evaluating Eq. (F24) numerically, it is convenient to rewrite Eq. (F2) for G as a one-sided

Fourier transform:

$$G\left(\beta_{cc}, \gamma_{cc}\right) = \frac{1}{4\beta_{cc}} \int_0^\infty x \left| I_0\left(\gamma_{cc} \sqrt{x}\right) K_2\left(\sqrt{x}\right) + \right.$$

$$\left. - I_2\left(\gamma_{cc} \sqrt{x}\right) K_0\left(\sqrt{x}\right) \right| \exp\left(i \frac{x}{4\beta_{cc}}\right) dx.$$
(F25)

Appendix F References

1. I. S. Gradshteyn and I. M. Ryzhik, *Table of Integrals, Series, and Products*, (Academic Press, New York, 1980), p. 712.

2. *Ibid.*, p. 686.

3. *Ibid.*, p. 717.

HRR 77 036

REPORT DOCUMENTATION PAGE

1a. REPORT SECURITY CLASSIFICATION Unclassified	1b. RESTRICTIVE MARKINGS
2a. SECURITY CLASSIFICATION AUTHORITY	3. DISTRIBUTION / AVAILABILITY OF REPORT Approved for public release; distribution unlimited.
2b. DECLASSIFICATION / DOWNGRADING SCHEDULE	
4. PERFORMING ORGANIZATION REPORT NUMBER(S)	5. MONITORING ORGANIZATION REPORT NUMBER(S)

6a. NAME OF PERFORMING ORGANIZATION University of Rochester	6b. OFFICE SYMBOL (If applicable)	7a. NAME OF MONITORING ORGANIZATION U. S. Army Research Office
6c. ADDRESS (City, State, and ZIP Code) Institute of Optics Rochester, New York 14627		7b. ADDRESS (City, State, and ZIP Code) P. O. Box 12211 Research Triangle Park, NC 27709-2211

8a. NAME OF FUNDING / SPONSORING ORGANIZATION U. S. Army Research Office	8b. OFFICE SYMBOL (If applicable)	9. PROCUREMENT INSTRUMENT IDENTIFICATION NUMBER Reporting Numbers: 24626-PH-UIR 24749-PH

8c. ADDRESS (City, State, and ZIP Code) P. O. Box 12211 Research Triangle Park, NC 27709-2211	10. SOURCE OF FUNDING NUMBERS			
	PROGRAM ELEMENT NO.	PROJECT NO.	TASK NO.	WORK UNIT ACCESSION NO.

11. TITLE (Include Security Classification)
Laser Speckle from Thin and Cascaded Diffusers

12. PERSONAL AUTHOR(S)
Lyle G. Shirley

13a. TYPE OF REPORT Interim Technical	13b. TIME COVERED FROM ___ TO ___	14. DATE OF REPORT (Year, Month, Day) May 1988	15. PAGE COUNT 194

16. SUPPLEMENTARY NOTATION The view, opinions and/or findings contained in this report are those of the author(s) and should not be construed as an official Department of the Army position, policy, or decision, unless so designated by other documentation.

17.	COSATI CODES		18. SUBJECT TERMS (Continue on reverse if necessary and identify by block number)
FIELD	GROUP	SUB-GROUP	Laser speckle; double diffusers; plane-wave probing; wave-
			length decorrelation; remote sensing; transmission functions;
			radiation patterns; rough surface scattering; ground glass

19. ABSTRACT (Continue on reverse if necessary and identify by block number)

The scattering of laser light from a single diffuser and from a cascade of two diffusers is analyzed with particular emphasis on remote sensing. It is shown that diffuser surface properties and the spacing between diffuser planes can be determined remotely by measuring the angular distribution of the radiation pattern or the decorrelation of the far-zone speckle pattern with respect to changes in the wavelength or the angle of incidence of an input plane wave.

A general expression is derived for the two-state correlation function of far-zone complex amplitude from a cascade of two diffusers, where the two states are the initial and final values of the wavelength, angle of incidence, angle of observation, and spacing. This function is then related to the two-state correlation function of intensity, which is a measure of the correlation between the initial and final speckle patterns. The two-state correlation function of intensity is evaluated for various double diffuser combinations.

The effect of surface height profiles on the radiation pattern is studied. Of particular interest are strong diffusers that have a normally distributed height profile and whose surface height autocorrelation functions are paraboloidal or conical for small spatial offsets. Excellent agreement is obtained between theoretical radiation patterns calculated with conical and paraboloidal autocorrelation functions and experimental radiation patterns measured from ground-glass and acid-etched diffusers, respectively. —

20. DISTRIBUTION / AVAILABILITY OF ABSTRACT ☐ UNCLASSIFIED/UNLIMITED ☐ SAME AS RPT. ☐ DTIC USERS	21. ABSTRACT SECURITY CLASSIFICATION Unclassified
22a. NAME OF RESPONSIBLE INDIVIDUAL Nicholas George	22b. TELEPHONE (Include Area Code) 716-275-2417	22c. OFFICE SYMBOL